ROBERTA CASTRO MARTINS

AMPEROMETRIC SENSOR MODIFIED WITH NANOMATERIALS FOR DETERMINATION OF HYDROQUINONE IN PHARMACEUTICAL SAMPLES

LAVRAS - MG

2023

ROBERTA CASTRO MARTINS

AMPEROMETRIC SENSOR MODIFIED WITH NANOMATERIALS FOR DETERMINATION OF HYDROQUINONE IN PHARMACEUTICAL SAMPLES

Dissertação apresentada à Universidade Federal de Lavras, como parte das exigências do Programa de Pós-Graduação de Engenharia de Biomateriais, para a obtenção do título de Mestre.

Profª. Dra. Fabiana da Silva Felix

Orientadora

Dra. Tássia Regina de Oliveira

Coorientadora

LAVRAS - MG

2023

Ficha catalográfica elaborada pelo Sistema de Geração de Ficha Catalográfica da Biblioteca Universitária da UFLA, com dados informados pelo(a) próprio(a) autor(a).

Martins, Roberta Castro.
Amperometric sensor modified with nanomaterials fordetermination of hydroquinone in pharmaceutical samples / Roberta Castro Martins. - 2023.
238 p.

Orientador(a): Fabiana da Silva Felix.
Coorientador(a): Tássia Regina de Oliveira.
Dissertação (mestrado acadêmico) - Universidade Federal de Lavras, 2023.
Bibliografia.

1. Amperometry. 2. Modified sensor. 3. FIA. I. Felix, Fabiana da Silva. II. Oliveira, Tássia Regina de. III. Título.

ROBERTA CASTRO MARTINS

AMPEROMETRIC SENSOR MODIFIED WITH NANOMATERIALS FOR DETERMINATION OF HYDROQUINONE IN PHARMACEUTICAL SAMPLES

SENSOR AMPEROMÉTRICO MODIFICADO COM NANOMATERIAIS PARA DETERMINAÇÃO DE HIDROQUINONA EM AMOSTRAS FARMACÊUTICAS

Dissertação apresentada à Universidade Federal de Lavras, como parte das exigências do Programa de Pós-Graduação de Engenharia de Biomateriais, para a obtenção do título de Mestre.

APROVADA em 29 de junho de 2023.

Dra. Fabiana da Silva Felix UFLA

Dra. Maiara Oliveira Salles UFRJ

Dr. Eduardo Mathias Richter UFU

Profª. Dra. Fabiana da Silva Felix
Orientadora

Dra. Tássia Regina de Oliveira
Coorientadora

LAVRAS - MG
2023

AGRADECIMENTOS

Agradeço primeiramente aos meus pais, Roberto Martins e Claudia Castro, que sempre me incentivaram nos estudos. Em especial à minha mãe, que desde os meus primeiros passos na universidade sempre me orientou e mostrou o melhor caminho na minha trajetória. Ao meu padrasto Felipe Jesus e os irmãos caninos Max e Bob que contribuem nos momentos de descontração e convívio familiar.

Agradeço também à *abuelita*, Deidamia Sanhueza, que sempre esteve do meu lado me apoiando nos melhores e nos piores momentos da minha trajetória acadêmica.

Aos meus amigos que me acompanham desde a graduação, Luiz Capucho, Natânia Rodrigues e Maria Augusta Marques, deixo meu muito obrigada por sempre estarem comigo também.

Em especial aos meus novos laços de amizade, meu querido e mais animado grupo do Pocs Vôlei Clube. Foi demais conhecer todos vocês e ter tido a oportunidade de criar memórias que ficarão para sempre comigo. Esse clubinho foi a dose de alegria e descontração para os momentos que eu precisava. Deixo aqui representado o meu carinho por todos vocês.

Agradeço também a minha orientadora, Professora Dra. Fabiana Felix, que desde o início acreditou em mim e nas minhas ideias. Sempre me auxiliou com muito carinho e parceria.

Em especial, agradeço ao professor Lúcio Angnes e seus alunos por todo o auxílio e disponibilidade no desenvolvimento deste trabalho. Me senti muito bem recebida e acolhida quando os visitei na USP.

Deixo, também, meus agradecimentos aos colegas de laboratório pela troca de conhecimento.

Agradeço à Professora Dra. Adelir Saczk, à Professora Dra. Zuy Magriotis, ao Professor Dr. Gustavo Tonoli, ao Professor Dr. Teodorico Castro Ramalho, ao Dr. Mateus Aquino e ao grupo de pesquisa do Complexo BIOMAT, que de alguma forma contribuíram com o desenvolvimento deste trabalho, seja com doação de materiais, disponibilização de laboratório, parcerias ou verba financeira.

Agradeço à minha coorientadora Dra. Tássia Regina de Oliveira por toda a atenção.

À minha banca de qualificação composta pela Dra. Jéssica Stefano e pelo Professor Dr. Diego Rocha, deixo meu agradecimento pelas contribuições feitas para o trabalho, bem como

à banca de defesa, composta pela Professora Dra. Maiara Salles pelo Professor Dr. Eduardo Richter.

À FAPEMIG (Fundação de Amparo à Pesquisa do Estado de Minas Gerais), pela bolsa de estudos, auxílio financeiro que possibilitou meus estudos.

Ao DQI (Departamento de Química), pela estrutura oferecida para o desenvolvimento da pesquisa.

À coordenação do programa que sempre esteve disponível para sanar dúvidas e auxiliar no que fosse necessário.

A todos os professores que contribuíram para a minha formação.

À ESAL (Escola de Ciências Agrárias) e ao DCF (Departamento de Engenharia Florestal), onde está lotado o Programa de Pós-Graduação em Engenharia de Biomateriais.

À UFLA (Universidade Federal de Lavras), pelas oportunidades oferecidas e pelas experiências vividas, que sempre me lembrarei com muito carinho.

“A tarefa não é tanto ver aquilo que ninguém viu, mas pensar o que ninguém ainda pensou sobre aquilo que todo mundo vê.” (Arthur Schopenhauer)

RESUMO

Os sensores eletroquímicos, dispositivos capazes de analisar o comportamento eletroquímico de um sistema, surgem como uma alternativa às técnicas analíticas instrumentais convencionais. Através das alterações do meio em que estão inseridos, esses sensores irão transformar o sinal elétrico gerado em um sinal mensurável proporcional à concentração do analito em solução. Esse sinal gerado pode ser avaliado através de algumas técnicas eletroquímicas, como voltametria, amperometria, impedimetria, condutometria e potenciometria. A fim de melhorar o desempenho dos sensores eletroquímicos, processos de modificação da superfície dos mesmos são realizados. Assim, na primeira parte, foi realizada uma revisão teórica a fim de elucidar conceitos da área de eletroquímica, bem como propriedades dos materiais utilizados como modificadores e seus meios de síntese e tratamentos. Na segunda parte, o objetivo foi desenvolver um sensor amperométrico modificado com nanotubos de carbono (NTC) e zeólita do tipo HY (ZEO-HY) para análise de hidroquinona (HQ) em produtos farmacêuticos. Na segunda parte do trabalho, foram realizados, primeiramente, estudos de otimização voltamétrica quanto à composição da pasta de carbono modificada, chegando a valores mais favoráveis de 20% de óleo mineral, 30% de pós de grafite, 30% de ZEO-HY e 20% de NTC. Estudos práticos e teóricos foram feitos em relação à contribuição dos modificadores utilizados, bem como a caracterização do material desenvolvido. Para as análises das amostras comerciais contendo HQ, a amperometria em associação com análise de injeção em fluxo (FIA – do inglês, *flow injection analysis*) foi escolhida por apresentar maior sensibilidade e melhores limite de detecção (LD) e limite de quantificação (LQ), repetibilidade e frequência analítica. Para a etapa de otimização de amperometria-FIA, os parâmetros de potencial de trabalho, vazão e volume de alça de amostragem foram variados, e as melhores condições foram de 0,1 V *vs.* Ag/AgCl, 4,69 mL min^{-1} e 65,0 µL, respectivamente. A curva de calibração, construída nas melhores condições operacionais, apresentou equação de regressão linear de $i = 4{,}87925 \times 10^{-8} + 0{,}00597 * C$, com $R = 0{,}997$. Uma frequência de amostragem de 100 injeções por hora foi alcançada. O LD calculado foi de $2{,}69 \times 10^{-7}$ mol L^{-1} e o LQ de $8{,}99 \times 10^{-7}$ mol L^{-1}. Para o estudo de repetibilidade (n=15), utilizando uma solução de $6{,}0 \times 10^{-5}$ mol L^{-1} de HQ, o desvio padrão relativo (DPR) foi de 1,44 %. As amostras farmacêuticas analisadas apresentaram resultados em concordância com aqueles valores encontrados nos rótulos dos cremes, bem como a cromatografia líquida de alta eficiência (técnica comparativa).

Palavras-chave: Amperometria. Sensor modificado. Nanotubos de carbono. Zeólita. FIA. Creme.

ABSTRACT

Electrochemical sensors, devices capable of analyzing the electrochemical behavior of a system, appear as an alternative to conventional instrumental analytical techniques. Through changes in the environment in which they are inserted, these sensors will transform the electrical signal generated into a measurable signal proportional to the concentration of the analyte in solution. This generated signal can be evaluated through some electrochemical techniques, such as voltammetry, amperometry, impedimetry, conductometry and potentiometry. In order to improve the performance of electrochemical sensors, surface modification processes are carried out. Thus, in the first part, a theoretical review was carried out in order to elucidate concepts in the field of electrochemistry, as well as properties of the materials used as modifiers and their means of synthesis and treatments. In the second part, the objective was to develop an amperometric sensor modified with carbon nanotubes (CNT) and HY-type zeolite (ZEO-HY) for analysis of hydroquinone (HQ) in pharmaceutical products. In the second part of the work, first, voltammetric optimization studies were carried out regarding the composition of the modified carbon paste, reaching more favorable values of 20% of mineral oil, 30% of graphite powders, 30% of ZEO-HY and 20% NTC. Practical and theoretical studies were carried out regarding the contribution of the modifiers used, as well as the characterization of the developed material. For the analyzes of commercial samples containing HQ, amperometry in association with flow injection analysis (FIA) was chosen due to its greater sensitivity and better limit of detection (LD) and limit of quantification (LQ), repeatability and analytical frequency. For the amperometry-FIA optimization step, the parameters of work potential, flow rate and sampling loop volume were varied, and the best conditions were 0.1 V vs. Ag/AgCl, 4.69 mL min^{-1} and 65.0 µL, respectively. The calibration curve, constructed under the best operating conditions, presented a linear regression equation of $i = 4.87925 \times 10^{-8} + 0.00597 * C$, with $R = 0.997$. A sampling rate of 100 injections per hour was achieved. The calculated LD was 2.69×10^{-7} mol L^{-1} and the LQ 8.99×10^{-7} mol L^{-1}. For the repeatability study (n=15), using a solution of 6.0×10^{-5} mol L^{-1} HQ, the relative standard deviation (RSD) was 1.44%. The pharmaceutical samples analyzed showed results in agreement with those values found on the labels of the creams, as well as the High-Performance Liquid Chromatography (comparative technique).

Keywords: Amperometry. Modified sensor. Carbon nanotubes. Zeolite. FIA. Cream.

SUMÁRIO

PRIMEIRA PARTE

1. INTRODUÇÃO

A hidroquinona (HQ) é uma substância química utilizada em processos como revelador fotográfico, inibidor de polimerização, antioxidante e agente despigmentante. O uso da HQ em cremes e géis não provoca reações adversas quando em concentrações de 2 a 4% (m/m), contudo, quando utilizado em concentrações superiores e em uso prolongado pode ocasionar irritação ou até mesmo erupções na pele do consumidor. Desta forma, visando a segurança do consumidor, bem como o controle de qualidade dos produtos, é importante se estabelecer métodos analíticos para a determinação de hidroquinona em diversos produtos, para que os mesmos estejam de acordo com a legislação vigente (SAKODINSKAYA et al., 1992; COROMINAS et al., 2004; OLIVEIRA & VIEIRA, 2006).

A identificação e quantificação da HQ pode ser feita no espectro de absorção no infravermelho ou no espectro de absorção no ultravioleta (ANVISA, 2019), além da possibilidade de utilizar a técnica de cromatografia líquida de alta eficiência (CUNHA *et al*., 2013). Contudo, essas técnicas convencionais são mais trabalhosas, caras, necessitam de operadores com habilidades avançadas e são de mais difícil implementação devido ao tamanho dos equipamentos. Desta forma, as técnicas eletroquímicas surgem como uma alternativa (TAJIK *et. al*., 2021; LIANG *et. al*., 2022).

A eletroquímica, de forma geral, estuda reações de transferência de carga elétrica, que ocorrem devido à aplicação de potencial eletroquímico. Essa transferência pode ocorrer homogeneamente, em solução, ou heterogeneamente na superfície de um eletrodo. A medição da transferência de carga elétrica é possível, pois muitas espécies químicas têm a capacidade de sofrer reações de oxirredução. As técnicas eletroquímicas podem ser aplicadas em diferentes áreas das ciências, sendo associadas à identificação e determinação de interesse biológico, farmacêutico e industrial (COSTA, 2016). Contudo, a resposta eletroquímica coletada está diretamente ligada ao eletrodo de trabalho, o sensor eletroquímico que fará o monitoramento das mudanças do meio reacional (HAN *et al*., 2022).

Os eletrodos de trabalho ou sensores podem reconhecer um ou mais analitos por meio de reações químicas na interface eletrodo-solução. A mudança química resultante será traduzida pelo elemento de transdução em sinal elétrico (COSTA, 2016). Apesar das técnicas

eletroquímicas já apresentarem uma série de vantagens como simples operação, baixo custo e equipamento de tamanho reduzido em alternativa aos meios instrumentais convencionas, há uma crescente gama de estudos que visam melhorar o desempenho dos sensores eletroquímicos utilizando materiais para modificação da superfície dos mesmos (HAN *et al*., 2022).

Diante do exposto, nesta primeira etapa da dissertação objetivou-se realizar uma revisão teórica sobre conceitos da área de eletroquímica e as propriedades dos materiais utilizados como modificadores e seus meios de síntese e tratamentos na primeira parte de sua estrutura. Na segunda parte serão apresentados os estudos experimentais realizados com o objetivo de desenvolver um sensor amperométrico modificado com nanomateriais para análise em fluxo de hidroquinona em cremes farmacêuticos. Objetivos específicos como otimização da pasta de carbono modificada, estudo prático e teórico da contribuição dos modificadores, caracterização do material desenvolvido com técnicas de microscopia eletrônica de varredura, espectroscopia vibracional na região do infravermelho, espectroscopia de impedância eletroquímica, estudo da influência do pH do meio reacional, estudos no sistema amperometria-FIA e estudos comparativos com a cromatografia líquida de alta eficiência serão também apresentados e discutidos.

2. REFERENCIAL TEÓRICO

2.1.Técnicas eletroquímicas

É importante destacar que as técnicas eletroquímicas podem ser interfaciais ou não-interfaciais, ainda podendo ser classificadas entre métodos estático ou dinâmico, quando interfaciais. Adicionalmente, com os métodos dinâmicos têm-se a possibilidade de se trabalhar com potencial controlado ou com corrente constante (ALEIXO, 2018).

No geral, os sensores eletroquímicos podem ser classificados, no que se diz respeito ao princípio de detecção do transdutor eletroquímico, em impedimétricos, condutométricos, potenciométricos, voltamétricos e amperométricos (LAKHERA *et al*., 2022).

A fim de realizar caracterização da superfície do eletrodo, a espectroscopia de impedância eletroquímica (EIS – do inglês, *electrochemical impedance spectrosco*py) pode ser utilizada. Além disso, avaliações da interface eletrodo/eletrólito e da cinética de reação entre o eletrodo e os analitos podem ser realizadas (LAKHERA *et al*., 2022).

Na condutometria, observa-se a relação entre a condutância de diferentes íons em solução e o evento de reconhecimento e, desta forma, apresenta baixa seletividade. Por fim, na potenciometria, mede-se a diferença de potencial (DDP) entre o eletrodo de trabalho e o eletrodo de referência, porém sua detectabilidade é menor quando comparada com as demais técnicas devido à pequena DDP durante a reação (LAKHERA *et al*., 2022).

A técnica voltamétrica proporciona uma boa sensibilidade e seu princípio está em medir a relação corrente-potencial, ou seja, a medição da corrente é feita em diferentes potenciais. Sendo assim, mede-se a corrente com variadas formas de aplicação de potencial, sendo elas de varredura, de onda, de incremento e de rampa. Desta forma, alguns agrupamentos ainda podem ser feitos, sendo eles voltametria cíclica (CV – do inglês, *cyclic voltammetry*), voltametria de pulso diferencial (DPV – do inglês, *diferencial pulse voltammetry*), voltametria de varredura linear (LSV – do inglês, *linear sweep voltammetry*) e voltametria de onda quadrada (SWV – do inglês, *square wave voltammetry*) (LAKHERA *et al*., 2022; TAJIK *et al*., 2021).

Na amperometria também se observa a relação corrente-potencial em função do tempo. Contudo, ao contrário da voltametria, nesta técnica a corrente é medida a um potencial constante. Neste sentido, a cronoamperometria é uma técnica amperométrica em que um potencial constante é aplicado ao eletrodo de trabalho e a corrente é medida em função do tempo (LAKHERA *et al*., 2022). Devido à crescente demanda no número de análises, esta técnica ainda pode ser associada com o sistema de análise por injeção em fluxo (FIA – do inglês, *flow injection analysis*) (FELIX & ANGNES, 2010).

FIA é uma técnica analítica parcialmente automatizada utilizada em análises químicas e processamento de amostras. O princípio básico de FIA envolve a injeção controlada de uma amostra em um fluxo de transporte, a solução carreadora, que então passa por um detector para análise. A amostra, geralmente em estado líquido, pode ser injetada manualmente ou automaticamente utilizando uma bomba injetora. Os detectores podem ser diferentes tipos de instrumentos analíticos, dependendo-se da natureza da análise, como espectrofotômetros, fluorímetros, potenciostatos ou outros equipamentos específicos. A depender do sensor utilizado, a resposta do sinal medido poderá ser física ou química. Por fim, o sinal gerado pode ser analisado de forma quali ou quantitativa usando sistemas computadorizados (CERDÀ *et. al*., 1999; OTEEF & IDRIS, 2023).

A aplicação de FIA em associação a diferentes detectores proporciona algumas vantagens em relação a outros métodos de análise em batelada, pois proporciona o desenvolvimento de análises rápidas e automatizadas, tornando-a adequada para aplicações de alto rendimento, já que esses sistemas em FIA podem analisar várias amostras (acima de 100 determinações/hora) em um curto período de tempo. Além disso, o consumo de reagentes se torna menor, já que volumes pequenos são necessários para a realização das análises, se tornando um método atrativo em relação à economia de recursos (MELCHERT *et. al*., 2012).

Quando a cronoamperometria é combinada com a FIA, se torna possível a medição de respostas de corrente dependentes do tempo em uma solução fluida. Nesta configuração, a célula eletroquímica é integrada ao sistema de fluxo e um eletrodo de trabalho é colocado dentro da célula. A amostra que flui é colocada em contato com o eletrodo de trabalho e um potencial é aplicado para iniciar uma reação eletroquímica. Essa técnica fornece informações sobre os processos eletroquímicos que ocorrem na superfície do eletrodo de trabalho, como a cinética de uma reação do eletrodo ou a concentração de um analito na amostra (BAZZANA *et. al*., 2023).

No geral, a cronoamperometria associada à FIA combina as vantagens de análise rápida, automação, sensibilidade e versatilidade, tornando-a uma ferramenta valiosa na análise eletroquímica para uma ampla gama de aplicações, como monitoramento ambiental, análise farmacêutica e ensaios bioquímicos (BAZZANA *et. al*., 2023).

As técnicas eletroquímicas surgem como uma alternativa às técnicas analíticas instrumentais que necessitam de equipamentos mais sofisticados, como cromatografia gasosa/espectrometria de massas, espectroscopia de absorção atômica, cromatografia líquida de alta eficiência, espectrofluorimetria, eletroforese capilar e quimiluminescência. Essas técnicas convencionais são mais trabalhosas, caras, necessitam de operadores com algumas habilidades avançadas e, ademais, têm difícil implantação devido ao tamanho dos equipamentos. Contudo, apesar dessas técnicas apresentarem vantagens como simples operação, baixo custo e equipamento de tamanho reduzido, a sensibilidade da técnica depende diretamente do sensor eletroquímico utilizado (HAN *et al*., 2022).

2.2.Sensores eletroquímicos

Entende-se por sensor eletroquímico, um dispositivo que é capaz de analisar o comportamento eletroquímico de um sistema, gerando informações mensuráveis, que podem ser quantitativas ou semi-quantitativas, por meio de um transdutor (LAKHERA *et al*., 2022).

O sensor eletroquímico é composto por um transdutor eletroquímico, ou seja, esses sensores funcionam, basicamente, monitorando uma reação redox. Isso significa dizer que ao se adicionar o analito estudado no eletrólito do sistema, o sensor eletroquímico irá monitorar a reação que está ocorrendo na interface eletrodo/eletrólito. Através das alterações do meio, um sinal elétrico será gerado proporcional à concentração o analito em solução, na qual pode ser analisado por meio de técnicas eletroquímicas (TAJIK *et al*., 2021).

Desde a sua introdução na eletroquímica, o eletrodo de pasta de carbono (EPC) tem sido amplamente utilizado em diversas aplicações, como análises ambientais, farmacêuticas, de alimentos, eletrocatálise e outras (SUN; GAO & JIAO, 2007; AFKHAMI *et al*., 2014; GAUTAM; SINGH & YADAV, 2018; BEITOLLAHI; IVARI & TORKZADEH-MAHANI, 2018; AGLAN; HAMED; SALEH, 2019). Sua forma mais simples requer apenas pó de carbono e um aglutinante (pasta de carbono não modificada) (KALCHER *et al*., 1995). A utilização do EPC tem crescido e se tornado cada vez mais comum em laboratórios pelo fato de poder ser preparado simplesmente misturando manualmente, podendo o próprio analista escolher as proporções e quais materiais serão incorporados à pasta de carbono (ŠVANCARA *et al*., 2009). Essa característica é interessante quando se prepara uma pasta de carbono modificada.

2.3.Sensores eletroquímicos modificados

A fim de melhorar o desempenho dos sensores eletroquímicos, processos de modificação da superfície dos mesmos são realizados. A pesquisa de novos materiais para tal é um campo de estudo ascendente, tendo crescido rapidamente (HAN *et al*., 2022).

A primeira modificação da pasta de carbono é datada entre 1964 e 1965 (ŠVANCARA *et al*., 2001). Sua base continuou sendo a mistura de pó de grafite e líquido orgânico, mas aqui foi adicionado um agente modificador (ŠVANCARA *et al*., 2009). Como recomendação, 10 a 30% (m/m) do agente modificador pode ser incorporado à mistura, podendo ser feito dissolvendo-o no ligante ou misturando-o mecanicamente à pasta (ŠVANCARA *et al*., 2001).

Modificando a pasta de carbono, o analista pode melhorar a sensibilidade e a seletividade dos métodos eletroanalíticos (BAIG; SAJID & SALEH, 2019). Exemplos de agentes modificadores são: substâncias húmicas, sílica e matrizes contendo sílica, substratos de organismos vivos, facilitadores de troca de íons e minerais de argila. Nestes últimos, destacam-se as nanopartículas metálicas, grafeno, nanotubos de carbono e zeólitas, respectivamente (ŠVANCARA *et al*., 2001; LIU *et al*., 2019; BHARDWAJ; SUMANA & MARQUETTE, 2020; ZINOUBI *et al*., 2020; TAJIK *et al*., 2021; MANICKARAJ *et al*., 2023; JEYARAMAN *et al*., 2023; NASROLLAHPOUR *et al*., 2023; CHEN *et al*., 2023; HAN *et al*., 2023).

Vale apontar que, além dos modificadores in-/orgânicos, materiais biológicos também podem ser utilizados, originando os nomeados biossensores. Estes podem ser classificados, de acordo com o elemento biológico de reconhecimento (bioreceptores), o transdutor físico-químico, o analito e as reações que eles monitoram (TURNER, 2013). Os bioreceptores típicos para a construção de biossensores são enzimas, anticorpos, microrganismos, ácidos nucleicos e entre outros (THÉVENOT et al., 2001; ALI et al., 2017).

Para o desenvolvimento de sensores eletroquímicos modificados, os nanomateriais têm sido muito utilizados. Sendo assim, é importante a compreensão das metodologias de síntese dos mesmos, bem como as propriedades dos materiais que podem ser alteradas (TAJIK *et al*., 2021).

2.4.Nanotecnologia

Nos últimos anos, a área da nanociência e nanotecnologia tem recebido muita atenção, sofrendo um grande desenvolvimento. Isso se dá devido ao fato de que um material em nanoescala possui propriedades químicas, ópticas, mecânicas, magnéticas e elétricas bastante diferentes de um material *bulk* (AHMAD *et al.*, 2022*;* PIJEIRA *et al.*, 2022; SHAO *et al.*, 2022).

Pode-se definir nanotecnologia como uma ciência que objetiva a síntese, a caracterização e a aplicação de dispositivos, sistemas e materiais com precisão atômica, com escala nanométrica (AHMAD *et al.*, 2022*;* PIJEIRA *et al.*, 2022; SHAO *et al.*, 2022). Segundo Alinezhad e colaboradores (2020), a Fundação Nacional de Ciência dos Estados Unidos define nanotecnologia como estudos de sistemas e materiais que tenham dimensões entre 1 e 100 nm,

com síntese através de processos que demonstrem um controle sobre as propriedades físicas e químicas das estruturas moleculares e que tenham capacidade de combinar e formar estruturas maiores (ALINEZHAD *et al.*, 2020).

As áreas de aplicações da nanotecnologia são diversas, podendo estar presente em campos como biologia, medicina, eletrônica, tecnologia *bottom-up*, energia, estudos ambientais, ciência dos alimentos, tecnologia da informação (TI) e várias outras áreas (AHMAD *et al.*, 2022*;* PIJEIRA *et al.*, 2022; SHAO *et al.*, 2022).

Para a síntese de nanomateriais, existem dois procedimentos principais que podem ser realizados: *top-down* e *bottom-up*. O primeiro procedimento, que envolve técnicas como moagem, *sputtering*, litografia e dentre outras, parte do material *bulk* para produzir os materiais nanoestruturados. Já o segundo procedimento é um processo de síntese, ou seja, parte de reagentes separados para formar o nanomaterial, como na síntese química. (BAIG *et al.*, 2021).

O processo de moagem mecânica é um método econômico e eficaz para a produção de nanocompósitos, como ligas de alumínio reforçadas com óxido e carboneto, revestimentos de pulverização resistente ao desgaste e nanoligas à base de alumínio, níquel, magnésio e cobre. Nesse processo, o material *bulk* é colocado dentro de uma câmara do equipamento de moagem, onde estarão presentes esferas. Conforme a câmara de moagem for sendo rotacionada, as esferas presentes em seu interior irão adquirir uma força centrífuga e fenômenos de deformação elástica, plástica e por cisalhamento ocorrerão, ocasionando fratura, amorfização e reações químicas do material de interesse (ZHUANG *et al.*, 2016).

O *electrospinning* é um método simples utilizado para a produção de nanofibras, sendo um dos grandes avanços da técnica, o *electrospinning* coaxial. No *electrospinning* coaxial, a fieira compreende de dois capilares coaxiais, na qual dois líquidos viscosos, ou um líquido viscoso como a casca e um líquido não viscoso como o núcleo, são usados para formar fibras ultrafinas *core-shell* em larga escala (BAIG *et al.*, 2021).

A litografia é utilizada para a produção de materiais nanoestruturados utilizando um feixe de luz ou de elétrons, e pode ser dividida em litografia com ou sem máscara (PIMPIN; SRITURAVANICH, 2012). O primeiro processo inclui fotolitografia, litografia de nanoimpressão e litografia suave (SZABÓ *et al.*, 2013; KUO *et al.*, 2003; YIN; GATES; XIA,

2001). Já o segundo, litografia de sonda de varredura, litografia de feixe de íons focalizados e litografia de feixe de elétrons (XU et al., 2020; MATSUMOTO *et al.*, 2019).

O *sputtering* utiliza partículas de alta energia, como plasma ou gás, para bombardear superfícies sólidas, gerando, assim, os nanomateriais. Essa técnica é muito utilizada para a produção de filmes finos de materiais nanoestruturados (AYYUB *et al.*, 2001). No processo de bombardeio, que é realizado em uma câmara evacuada, uma alta voltagem é aplicada ao alvo do cátodo e os elétrons livres colidem com o gás para produzir íons do mesmo. Os elétrons serão, então, acelerados no campo elétrico em direção ao alvo do cátodo, no qual esses íons atingem continuamente, resultando na ejeção de átomos da superfície do alvo (MUÑOZ-GARCÍA *et al.*, 2010).

O método de descarga de arco é útil para a geração de diversos materiais nanoestruturados à base de carbono, como fulerenos, nanochifres de carbono (CNHs), nanotubos de carbono, grafeno de poucas camadas (FLG) e nanopartículas de carbono esféricas amorfas (ZHANG, D. *et al.*, 2019). Nesse método, duas hastes de grafite são ajustadas em uma câmara na qual uma certa pressão de hélio é mantida. Então, através da descarga do arco entre as extremidades das hastes de grafite, a vaporização da haste de carbono é acionada. As novas formas de nanomateriais são influenciadas pelas condições nas quais a descarga do arco ocorre (BAIG *et al.*, 2021).

Na síntese de ablação a laser, o material *bulk* é vaporizado devido à alta energia da irradiação do laser que o atinge, dando origem às nanopartículas (BAIG *et al.*, 2021). Devido a não necessidade de reagentes químicos, essa pode ser considerada uma técnica verde (AMENDOLA & MENEGHETTI, 2012). Ainda, ajustando-se variáveis como fluência e comprimento de onda, propriedades como tamanho médio e distribuição das nanopartículas podem ser controladas (BAIG *et al.*, 2021).

No método de deposição química de vapor um filme fino é formado na superfície do substrato através da reação química de precursores em fase de vapor. É necessário que um bom precursor tenha volatilidade adequada, alta pureza química, boa estabilidade durante a evaporação, baixo custo, natureza não nociva e longa vida útil (BAIG *et al.*, 2021). É importante também que após o processo de decomposição, não haja a produção de impurezas residuais

(BAIG *et al.*, 2021). No processo de decomposição, a escolha do catalisador da reação será crucial para a morfologia final e o tipo do nanomaterial obtido. Catalisadores como Ni e Co estão relacionados à produção de grafeno multicamada, por exemplo, enquanto que se o Cu for utilizado como catalisador, espera-se a formação de um grafeno monocamada (BAIG *et al.*, 2021). Esse processo de síntese é muito aplicado para nanomateriais bidimensionais (DONG *et al.*, 2020).

Nanomateriais podem, também, ser obtidos através do método hidrotérmico, através de uma reação heterogênea que ocorre em meio aquoso a alta pressão e temperatura ao redor do ponto crítico em um recipiente selado. Semelhante ao método hidrotérmico, há também o método solvotérmico, que é realizado em meio não aquoso (WU, X.; LU; WANG, L., 2011; LI & WU, 2015; CAO *et al.*, 2016). Esses métodos são bastante utilizados para produzir nanofios, nanobastões, nanofolhas e nanoesferas (JIANG *et al.*, 2018; CHAI *et al.*, 2018; DONG *et al.*, 2020).

O método sol-gel é aplicado para o desenvolvimento de nanomateriais à base de óxido metálico de alta qualidade, recebendo esse nome pois o precursor líquido, geralmente alcóxidos metálicos, é transformado em um sol, que é finalmente convertido em uma estrutura de rede que é chamada de gel (DANKS; HALL & SCHNEPP, 2016). Na primeira etapa da síntese via sol-gel, ocorre a hidrólise do óxido metálico para formar um sol, seguindo para uma etapa de condensação, formando estruturas porosas que são deixadas para envelhecer. Durante o envelhecimento, a porosidade diminui e a distância entre as partículas coloidais aumenta (BAIG *et al.*, 2021). Após o envelhecimento, realiza-se a secagem do material e, por fim, a calcinação para obter as nanopartículas (PARASHAR; SHUKLA & SINGH, 2020).

O método *soft template* tem implementação simples, condições experimentais relativamente brandas e o desenvolvimento de materiais com uma variedade de morfologias (LIU *et al.*, 2013). Os nanomateriais sintetizados por essa técnica têm como precursores copolímeros em bloco, moléculas orgânicas flexíveis e tensoativos aniônicos, catiônicos e não iônicos (LI & ZHAO, 2013). Ainda, a interação formada entre os moldes moles e os precursores podem ocorrer por ligações de hidrogênio, forças de van der Waals e forças eletrostáticas (POOLAKKANDY & MENAMPARAMBATH, 2020). Nanoesferas carbonáceas poliméricas mesoporosas, nanobastões de cristal único, aluminas porosas e grafeno N-dopado mesoporoso

podem ser produzidos através do método *soft template* (LIU, J. *et al*., 2013; LV *et al*., 2004; MARTINS *et al*., 2010; TANG *et al*., 2019). O método *hard template* utiliza materiais sólidos bem projetados como modelos, e os poros do modelo sólido são preenchidos com moléculas precursoras para obter as nanoestruturas (POOLAKKANDY & MENAMPARAMBATH, 2020). Materiais como sílica, nanotubos de carbono, partículas, cristais coloidais e conchas de madeira têm sido utilizados como moldes duros (SZCZĘŚNIAK; CHOMA & JARONIEC, 2020). Para realizar a síntese via *soft* e *hard template* o modelo original apropriado é selecionado e em seguida um precursor direcionado é preenchido nos mesoporos modelo para convertê-los em um sólido inorgânico. Por fim, o molde original é removido para obter a réplica mesoporosa (YAMAUCHI & KURODA, 2008).

No método da micela reversa, essas estruturas são formadas a partir de uma emulsão água-em-óleo, em que as cabeças hidrofílicas apontam para um núcleo que contém água (MALIK; WANI & HASHIM, 2012). O núcleo das micelas reversas atua como um nanorreator para a síntese de nanopartículas. A partir da relação água-surfactante, é possível controlar o tamanho desses nanorreatores, que influenciarão o tamanho das nanopartículas produzidas (SHIRI; HENDERSON & MUCALO, 2019).

2.5.Nanotubos de carbono

Nanotubos de carbono (NTCs) são nanoestruturas à base de carbono que apresentam propriedades elétricas, térmicas e mecânicas excepcionais (KOUR *et al*., 2020) Os NTCs possuem um grande número de grupos funcionais em sua superfície, como grupos carboxílicos, hidroxila e amino, que podem interagir com íons em solução por meio de interações eletrostáticas. Portanto, pode ser amplamente utilizado em sistemas eletroquímicos como trocadores de íons para a detecção e determinação de íons em solução (ŠVANCARA *et al*., 2001).

A estrutura dos NTCs é cilíndrica, ou seja, pode-se dizer de forma simples e geral que é uma folha de grafeno enrolada (Figura 1 a). Existem dois tipos de estruturas dos NCTs: os nanotubos de carbono de parede simples (Figura 1b), e os nanotubos de carbono de paredes múltiplas (Figura 1c) (IIJIMA & ICHIHASHI, 1993; IIJIMA, 2002). No primeiro caso, apenas uma folha de grafeno é enrolada em formato cilíndrico, enquanto que no segundo, diversas

folhas de grafeno são enrolaras e “encaixadas” uma dentro da outra (MEUNIER *et al*., 2016; KOUR *et al*., 2020). O processo de síntese dos NTCs se dá por meio de técnicas como descarga de arco elétrico, deposição de vapor químico, ablação a laser e *hard template*, como descrito no tópico anterior (JOSÉ-YACAMÁN *et al*., 1993; CHICO *et al*., 1996; THESS *et al*., 1996; ZHAO *et al*., 2019).

Figura 1: (a) Lençol de grafeno sendo enrolado em forma de cilindro. (b) Nanotubos de carbono de parede simples. (c) Nanotubos de carbono de paredes múltiplas.

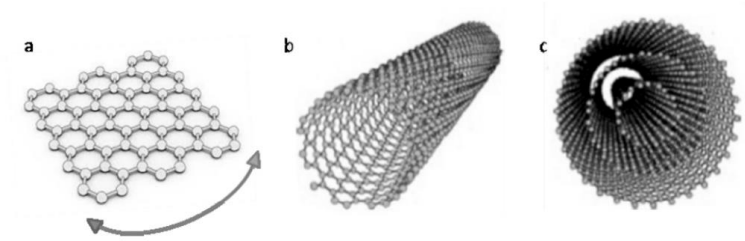

Fonte: MACHADO *et al*., 2014.

2.5.1. Tratamentos pós-síntese

De forma geral, é interessante realizar a purificação dos materiais sintetizados, a fim de retirar qualquer partícula remanescente do processo, ou alguma impureza. Sendo assim, tratamentos ácidos, de ultrassom, de filtração, tratamento térmico/oxidativo e ultracentrifugação por gradiente de densidade têm sido aplicados (TOHJI *et al*., 1997; PATOLE *et al*., 2008).

No tratamento ácido, os NTCs são colocados em uma solução de ácido sulfúrico (H_2SO_4) e ácido nítrico (HNO_3) para a remoção de partículas de catalisadores utilizados no processo de síntese, de carbono amorfo ou alguma outra impureza que pode estar presente. Após essa etapa, ocorre a lavagem dos NTCs para retirar os resíduos ácidos (PATOLE *et al*., 2008). É válido ressaltar que por meio dessa mistura ácida, pode-se ocorrer o processo de funcionalização por carboxilação da superfície dos NTCs, introduzindo grupos funcionais de ácido carboxílico à estrutura do material (BALASUBRAMANIAN & BURGHARD, 2005; SHAMSUDDIN *et al*., 2016).

Ao aplicar o ultrassom como técnica de purificação, ocorre a sonicação do material. Em um solvente, os NTCs irão receber ondas sonoras de alta frequência. Quando este processo ocorre, microbolhas são criadas dentro dos NTCs, e quando estouram, há a dispersão das impurezas que podem estar presentes na estrutura (INAMI *et al*., 2007).

O processo de filtração envolve simplesmente filtrar o material. Este método é utilizado para separar partículas maiores de NTCs. Aqui certa atenção tem que ser dada ao tamanho dos poros do filtro, pois dependendo do diâmetro de nanotubo desejado, deve-se escolher filtros de poros maiores ou menores (XU *et al*., 2011).

No tratamento térmico/oxidativo carbono amorfo e impurezas orgânicas podem ser removidos da estrutura sintetizada. Aqui, os NTCs são submetidos à altas temperaturas em uma atmosfera oxidante (ar ou oxigênio) (TOHJI *et al*., 1997; RINALDI *et al*., 2010).

Na ultracentrifugação por gradiente de densidade, os NTCs são dispersos em um meio gradiente e são submetidos à centrifugação. Neste processo, o que irá governar a separação do material será seu tamanho e sua densidade. Ou seja, é possível isolar tipos ou tamanhos específicos de NTCs, já que o material irá se separar dentro das distintas bandas de gradiente (YAYA *et al*., 2011).

2.6.Zeólitas

As zeólitas são aluminosilicatos que possuem uma estrutura cristalina tridimensional composta por unidades de tetraedros de SiO_4 e AlO_4. Elas têm microporos com dimensões regulares, além da presença de carga negativa onde se encontra o AlO_4, sendo tal carga compensada por cátions orgânicos ou inorgânicos para manter sua estrutura neutra (ČEJKA; MORRIS & NACHTIGAL, 2017).

Os tetraedros de SiO_4 e AlO_4 são as chamadas estruturas primárias das zeólitas, e são arranjadas em unidades secundárias, a rede estrutural final da zeólita, que podem ser o duplo anel de quatro membros, o duplo anel de seis membros ou a sodalita, a depender do arranjo dessas unidades, ou seja, de como elas foram conectadas. Essas estruturas ainda podem ser combinadas para formar novos arranjos cristalinos (KULPRATHIPANJA, 2010).

2.6.1. Zeólita Y

A faujasita (FAU – Figura 1) é a estrutura zeolítica responsável por formar a zeólita Y. Sua estrutura cristalina é composta por unidades de sodalita que são conectadas por anéis duplos de seis membros que são compartilhados através dos átomos de oxigênio que proporcionam essa ligação (ČEJKA; MORRIS & NACHTIGAL, 2017).

Figura 1 – Tipo de estrutura FAU.

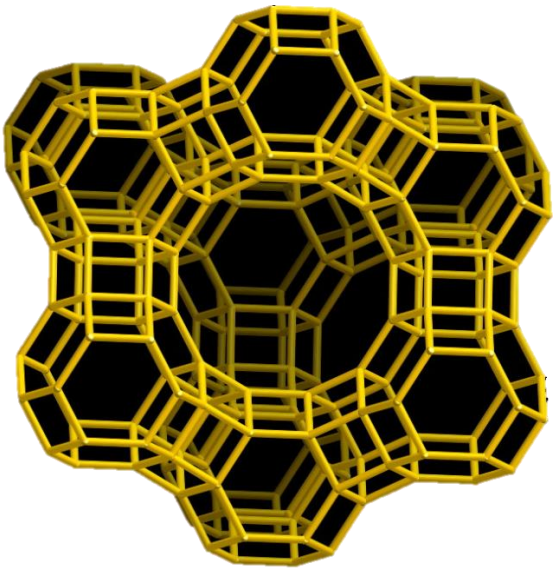

Fonte: IZA-SC (2017).

Informações quanto às características de interesse em relação à zeólita, como propriedades físico-químicas, texturais e ácidas podem ser obtidas através da aplicação de técnicas específicas. Para identificar a sua estrutura cristalina, por exemplo, pode-se utilizar a técnica de difratometria de raio-x (DRX) (RAMLI & AMIN, 2015; LÓPEZ-AGUADO *et al*., 2018). Já para observar a estrutura zeolítica numa escala micro ou até mesmo nanométrica, se torna interessante a aplicação de técnicas de microscopia, como a microscopia eletrônica de transmissão, que podem proporcionar informações quanto a defeitos estruturais da zeólita ou até mesmo sobre efeitos de tratamentos realizados pós-síntese (QIN *et al*. 2011).

2.6.2. Síntese da zeólita Y

Em termos de síntese, basicamente cinco passos são seguidos para a produção da zeólita Y: preparação do gel, envelhecimento, cristalização, lavagem e secagem e, por fim, calcinação (AL-NAYILI & RZOQY, 2022).

Na etapa da preparação do gel, mistura-se soluções aquosas de alumina, sílica e hidróxido de sódio em proporções adequadas para a zeólita a ser produzida. Após essa mistura, o gel passa pela etapa de envelhecimento, em que é deixado a uma temperatura relativamente alta (80 – 100ºC) por algumas horas ou até mesmo dias. Neste processo, acontece uma reorganização estrutural do gel, levando à formação dos precursores zeolíticos (AL-NAYILI & RZOQY, 2022).

Na terceira etapa, de cristalização, o gel envelhecido é submetido a um tratamento hidrotérmico, em que é aquecido em autoclave por várias horas. Nesta etapa os cristais da zeólita crescem e formam a estrutura Y que se deseja. Após esse tratamento, aplica-se a quarta fase, de lavagem e secagem. Aqui, o produto sólido formado é filtrado, lavado com água deionizada e em seguida é seco em temperatura moderada. Por fim, ocorre a etapa de calcinação, em que o material seco é calcinado a uma temperatura mais alta para remover qualquer impureza orgânica que possa ter permanecido e ativar a estrutura zeolítica (AL-NAYILI & RZOQY, 2022).

2.6.3. Tratamentos pós-síntese

A depender da aplicação final da zeólita, pode-se fazer necessário algum tipo de tratamento para o total aproveitamento das propriedades da mesma. Sendo assim, métodos de troca iônica, desaluminação e incorporação de cátions podem ser aplicados.

2.6.3.1.Troca iônica

Geralmente, nos métodos tradicionais de síntese da zeólita Y, o resultado é uma zeólita sódica (NaY). Contudo, como essa zeólita é comumente utilizada na sua forma ácida em processos catalíticos, faz-se necessário um tratamento de troca iônica (SATO et al., 2003).

Para tal, o método que mais se utiliza é a inserção de uma quantidade de amostra de zeólita em uma solução contendo sal de amônio (NH_4^+), de forma a ocorrer a troca iônica com o sódio. Portanto, neste momento, há uma modificação da zeólita em sua forma sódica (NaY) para a sua forma amoniacal (NH_4Y). Para, então, ocorrer a decomposição do íon amônio, basta o aquecimento para a liberação do gás amônia (NH_3), restando o íon H^+ como átomo

compensador de carga (SATO et al., 2003). Ao final do tratamento, a zeólita Y encontra-se na sua forma protônica (HY) (LUTZ, 2014).

2.6.3.2.Desaluminação

A desaluminização é um tratamento aplicado para remover Al da estrutura das zeólitas, e pode se dar tanto por tratamento com vapor d'água quanto por lixiviação ácida. Quando aplicado o tratamento com vapor d'água, utiliza-se temperaturas acima de 500 ºC (ČEJKA, CORMA & ZONES, 2010).

Para a remoção de Al, o tratamento de desaluminação age nas ligações Al – O – Si, que sofrem hidrólise e acabam por expulsar os átomos de Al da estrutura cristalina da zeólita. Com isso, acaba-se por gerar defeitos estruturais nessa estrutura e há uma amorfização parcial da rede. Com o intuito de corrigir esse defeito provocado, átomos de Si que são menos estáveis acabam por migrar para esses sítios defeituosos, preenchendo os espaços criados pela remoção de Al (ČEJKA, CORMA & ZONES, 2010).

Esse tratamento de desaluminação pode gerar uma mesoporosidade na zeólita Y, além de aumentar a razão Si/Al, melhorando a estabilidade hidrotérmica e hidrofóbica. As propriedades ácidas da zeólita também podem sofrer alterações na quantidade de sítios e na sua força (ČEJKA, CORMA & ZONES, 2010).

2.6.3.3.Incorporação de cátions

As zeólitas, em sua grande maioria, possuem a capacidade de trocar de cátions devido à substituição isomórfica de um cátion trivalente por um cátion tetravalente da rede. Assim, devido a formação de uma rede carregada negativamente, é possível realizar a incorporação de cátions nos canais que constituem a estrutura da zeólita (TATSUMI, 2009).

2.7.Hidroquinona

O uso da hidroquinona (Figura 2) em cosméticos, como cremes e géis, não provoca reações adversas quando em baixas concentrações de 2 a 4% (m/m), sendo que concentrações de 3 a 4% são as recomendadas para bons resultados para clareamento da pele. Já quando em concentrações superiores a 4% e em uso prolongado, certos efeitos colaterais podem surgir,

como coceira, dermatites e eritema, mudanças na coloração da pele e sensibilização da mesma (SAKODINSKAYA et al., 1992; COROMINAS et al., 2004).

Figura 2 – Fórmula estrutural da hidroquinona.

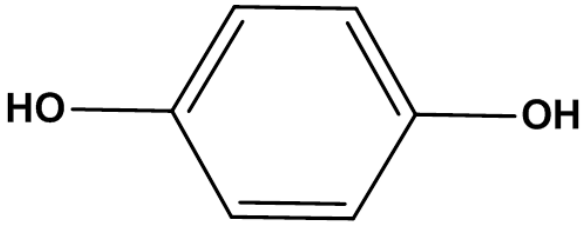

Fonte: Do autor (2023)

De acordo com a ANVISA (Agência Nacional Vigilância Sanitária), a hidroquinona era autorizada em medicamentos da categoria dos desmelanizantes numa concentração de 4%, estando na forma de creme ou gel dermatológico (ANVISA, 2016). Contudo, segundo a Resolução de Diretoria Colegiada – RDC Nº 529, de 4 de agosto de 2021, a hidroquinona está na lista de substâncias que não podem ser utilizadas em produtos de higiene pessoal, cosméticos e perfumes. Os produtos que foram fabricados de acordo com a Resolução de Diretoria Colegiada – RDC Nº 83, de 17 de junho de 2016, poderão ser comercializados até o final dos seus prazos de validade (ANVISA, 2021). Vale ressaltar que as legislações supracitadas dizem respeito a produtos de higiene pessoal, cosméticos e perfumes, como já citado. Em relação a produtos farmacêuticos, ou seja, medicamentos, recomenda-se, ainda, a concentração máxima de 4% (m/m) de HQ.

Ainda, em atualização recente, segundo a Resolução RDC Nº 642, de 24 de Março de 2022, que dispõe sobre critérios para inclusão, exclusão e alteração de concentração de substâncias utilizadas em produtos de higiene pessoal, cosméticos e perfumes na lista prevista na Resolução de Diretoria Colegiada – RDC Nº 529, de 4 de Agosto de 2021, fica firmado nos Artigos 4º e 5º as condições para pedidos de exclusão e de alteração de concentração das substâncias listadas, respectivamente, mediante estudos que comprovem a segurança do uso do produto, bem como o parecer técnico de órgãos internacionais de referência e do técnico solicitante. Assim, feito o pedido de exclusão ou alteração de concentração, a ANVISA poderá elaborar um parecer técnico que será apresentado ao Mercosul (ANVISA, 2022).

No Canadá, a hidroquinona está na lista de ingredientes proibidos para uso em cosméticos para pele desde 2008. Seu uso é completamente banido na Europa e no Japão (USA, 2009). Em 2006, nos Estados Unidos da América, a FDA (*Food and Drug Administration*) alterou a legislação de 1982, propondo que produtos contendo hidroquinona não deveriam ser disponibilizados (USA, 2006; USA, 2009). A NTP (*National Toxicology Program*), ainda realiza estudos sobre a hidroquinona e a concentração máxima permitida no país é de 2% (USA, 2009; USA, 2015).

Desta forma, visando a segurança do consumidor ao utilizar medicamentos contendo HQ, torna-se importante estabelecer métodos analíticos para a determinação de hidroquinona em diversos produtos. Além de desenvolver métodos rápidos e eficazes para serem aplicados no controle de qualidade dos produtos que contém a HQ para os estudos que devem ser realizados para pedidos de exclusão na lista da RDC Nº 529 ou alteração de concentração de HQ nos produtos de higiene pessoal, cosméticos e perfumes.

3. CONCLUSÃO

Nesta primeira parte do trabalho de dissertação, foi possível realizar uma revisão teórica sobre a temática do trabalho que foi desenvolvido, sendo possível o aprimoramento dos conhecimentos da discente para posteriores interpretações perante os resultados obtidos no decorrer da pesquisa de mestrado.

REFERÊNCIAS BIBLIOGRÁFICAS

AFKHAMI, A.; KHOSHSAFAR, H.; BAGHERI, H.; MADRAKIAN, T. Facile simultaneous electrochemical determination of codeine and acetaminophen in pharmaceutical samples and biological fluids by graphene–CoFe2O4 nancomposite modified carbon paste electrode. **Sensors and Actuators B: Chemical**, V. 203, p. 909-918, 2014.

AGLAN, R.F.; HAMED, M.M. e SALEH, H.M. Selective and sensitive determination of Cd(II) ions in various samples using a novel modified carbon paste electrode. **Journal of Analytical Science and Technology**, V. 10, n. 7, 2019.

AHMAD, W.; BHATT, S. C.; VERMA, M.; KUMAR, V.; KIM, H. A review on current trends in the green synthesis of nickel oxide nanoparticles, characterizations, and their applications. **Environmental Nanotechnology, Monitoring and Management**, V. 18, 100674, 2022.

ALEIXO, L. M. Voltametria: conceitos e técnicas. **Revista Chemkeys**, Campinas, SP, n. 3, p. 1–21, 2018.

ALI, J.; NAJEEB, J.; ALI, M. A.; ASLAM, M. F. e RAZA, A. Biosensors: Their Fundamentals, Designs, Types and Most Recent Impactful Applications: A Review. **J Biosens Bioelectron**, V. 8, p. 1–9, 2017.

ALINEZHAD, H.; PAKZAD, K.; NASROLLAHZADEH, M. Efficient Sonogashira and A3 coupling reactions catalyzed by biosynthesized magnetic Fe3O4@Ni nanoparticles from Euphorbia maculata extract. **Applied Organometallic Chemistry**, V. 34, n. 4, p. 1–16, 2020.

AL-NAYILI, A & RZOQY, M. Local silica sand as a silica source in the synthesis of Y zeolite. **Asia-Pacific Journal of Chemical Engineering**, V. 17, n. 5, p. e2824, 2022.

AMENDOLA, V. & MENEGHETTI, M. Exploring how to increase the brightness of surface-enhanced raman spectroscopy nanolabels: The effect of the raman-active molecules and of the label size. **Advanced Functional Materials**, V. 22, n. 2, p. 353–360, 2012.

ANVISA (AGÊNCIA NACIONAL DE VIGILÂNCIA SANITÁRIA). **Farmacopeia Brasileira**, 6ª edição, volume II, 2019. Disponível em: <https://www.gov.br/anvisa/pt-br/assuntos/farmacopeia/farmacopeia-brasileira/insumos-farmaceuticos-e-especialidades-com-capa.pdf>. Acesso em: maio 2023.

ANVISA (AGÊNCIA NACIONAL DE VIGILÂNCIA SANITÁRIA). **Resolução da diretoria colegiada- RDC nº 642**, de 24 de março de 2022. Disponível em: https://www.in.gov.br/en/web/dou/-/resolucao-rdc-n-642-de-24-de-marco-de-2022-389597086. Acesso em: jun. 2023.

ANVISA (AGÊNCIA NACIONAL DE VIGILÂNCIA SANITÁRIA). **Resolução da diretoria colegiada- RDC nº 83**, de 17 de junho de 2016. Disponível em:

https://bvsms.saude.gov.br/bvs/saudelegis/anvisa/2016/rdc0083_17_06_2016.pdf. Acesso em: abr. 2022.

ANVISA (AGÊNCIA NACIONAL DE VIGILÂNCIA SANITÁRIA). **Resolução da diretoria colegiada- RDC nº 529**, de 04 de agosto de 2021. Disponível em: < http://antigo.anvisa.gov.br/documents/10181/5284308/RDC_529_2021_.pdf/0ea02df4-a33d-4021-a11b-b5ca9e0af208>. Acesso em: abr. 2022.

AYYUB, P.; CHANDRA, R.; TANEJA, P.; SHARMA, A. K.; PINTO, R. Synthesis of nanocrystalline material by sputtering and laser ablation at low temperatures. **Applied Physics A: Materials Science and Processing**, V. 73, n. 1, p. 67–73, 2001.

BAIG, N.; KAMMAKAKAM, I.; FALATH, W. Nanomaterials: A review of synthesis methods, properties, recent progress, and challenges. **Materials Advances**, V. 2, n. 6, p. 1821–1871, 2021.

BAIG, N.; SAJID, M.; e SALEH, T. A. Recent trends in nanomaterial-modified electrodes for electroanalytical applications. **TrAC - Trends in Analytical Chemistry**, V. 111, p. 47-61, 2019.

BALASUBRAMANIAN, K. & BURGHARD, M. Chemically Functionalized Carbon Nanotubes. **Small**, V. 1, p. 180-192 2005.

BAZZANA, M.J.F.; ASSIS, L.C.; MARTINS, R.C.; SACZK, A.A.; FELIX, F.S.; ANGNES, L. Electrochemical Biosensors in Agricultural and Veterinary Applications. Biomaterials-Based Sensors – Springer, p. 349-385, 2023.

BEITOLLAHI, H.; IVARI, S.G.; TORKZADEH-MAHANI, M. Application of antibody-nanogold-ionic liquid-carbon paste electrode for sensitive electrochemical immunoassay of thyroid-stimulating hormone. **Biosensors and Bioelectronics**, V. 110, p. 97-102, 2018.

BHARDWAJ, H.; SUMANA, G. e MARQUETTE, C. A. A label-free ultrasensitive microfluidic surface Plasmon resonance biosensor for Aflatoxin B1 detection using nanoparticles integrated gold chip. **Food Chemistry**, V. 307, 125530. 2020.

CAO, S.; ZHAO, C.; HAN, T.; PENG, L. Hydrothermal synthesis, characterization and gas sensing properties of the WO_3 nanofibers. **Materials Letters**, V. 169, p. 17–20, 2016.

ČEJKA, J., MORRIS, R. E., NACHTIGAL, P. **Zeolites in Catalysis: Properties and Applications**. The Royal Society of Chemistry, 2017, 546 p.

ČEJKA, J.; CORMA, A.; ZONES, S. **Zeolites and Catalysis: Synthesis, Reactions and Applications**. Wiley, 2010, 918 p.

CERDÀ, V.; ESTELA, J.M.; FORTEZA, R.; CLADERA, A.; BECERRA, E.; ALTIMIRA, P.; SITJAR, P. Flow techniques in water analysis. **Talanta**, V. 50, n. 4, p. 695-705, 1999.

CHAI, B.; XU, M.; YAN, J.; REN, Z. Remarkably enhanced photocatalytic hydrogen evolution over MoS2 nanosheets loaded on uniform CdS nanospheres. **Applied Surface Science**, V. 430, p. 523–530, 2018.

CHEN, Z.; WU, C.; YUAN, Y.; XIE, Z.; LI, T.; HUANG, H.; LI, S.; DENG, J.; LIN, H.; SHI, Z.; LI, C.; HAO, Y.; TANG, Y.; YOU, Y.; AL-HARTOMY, O. A.; WAGEH, S.; AL-SEHEMI, A. G.; LU, R.; ZHANG, L.; LIN, X.; HE, Y.; ZHAO, G.; LI, D. e ZHANG, H. CRISPR-Cas13a-powered electrochemical biosensor for the detection of the L452R mutation in clinical samples of SARS-CoV-2 variants. **Journal of Nanobiotechnology**, V. 21, n. 1, p. 141, 2023.

CHICO, L.; CRESPI, V. H.; BENEDICT, L. X.; LOUIE, S. G. e COHEN, M. L. Pure Carbon Nanoscale Devices: Nanotube Heterojunctions. **PHYSICAL REVIEW LETTERS**, V. 76, p. 971, 1996.

COROMINAS, B.G.T.; ICARDO, M.C.; ZAMORA, L.L.; MATEO, J.V.G.; CALATAYUD, J. M. A tandem-flow assembly for the chemiluminometric determination of hydroquinone. **Talanta**, V. 64, p. 618-625, 2004.

COSTA, Erivaldo de Oliveira. **Desenvolvimento de sensor nanoestruturado e biossensor de dsDNA para determinação de substâncias de interesse biológico**: nitrotirosina, ácido ascórbico e ácido úrico. 2016. Tese (Doutorado em Química e Biotecnologia) - Instituto de Química e Biotecnologia, Programa de Pós-Graduação em Química e Biotecnologia, Universidade Federal de Alagoas, Maceió, 2016.

CUNHA, R. R.; TORMIN, T. F.; RICHTER, E. M.; MUNOZ, R. A. A. Determinação rápida de hidroquinona usando análise por injeção em batelada (BIA) com detecção amperométrica. **Química Nova**, V. 36, n. 5, p. 663-668, 2013.

DANKS, A. E.; HALL, S. R.; SCHNEPP, Z. The evolution of "sol-gel" chemistry as a technique for materials synthesis. **Materials Horizons**, V. 3, n. 2, p. 91–112, 2016.

DONG, Y.; DU, X.; LIANG, PEI.; MAN, X. One-pot solvothermal method to fabricate 1D-VS4 nanowires as anode materials for lithium ion batteries. **Inorganic Chemistry Communications**, V. 115, 107883, 2020.

FELIX, F. S., & ANGNES, L. Fast and Accurate Analysis of Drugs Using Amperometry Associated with Flow Injection Analysis. **Journal of Pharmaceutical Sciences**, V. 99, n. 12, p. 4784–4804, 2010.

GAUTAM, V.; SINGH, K. P. e YADAV, V.L. Polyaniline/MWCNTs/starch modified carbon paste electrode for non-enzymatic detection of cholesterol: application to real sample (cow milk). **Analytical and Bioanalytical Chemistry**, V. 410, n. 8, p. 2173-2181, 2018.

HAN, D. K.; LI, C. A.; SONG, S. H.; CHO, K.; CHOI, J. S.; SON, S. E. e SEONG, G. H. Electroanalytical biosensor based on GOx/FCA/PEG-modified SWCNT electrode for determination of glucose. **Journal of Analytical Science and Technology**, V. 14, n. 9, 2023.

HAN, L.; SHEN, H.; ZHU, J. X.; LI, Y. T. Mini review: Electrochemical electrode based on graphene and its derivatives for heavy metal ions detection. **Talanta Open**, V. 6, 100153, 2022.

IIJIMA, S. & ICHIHASHI, T. Single-shell carbon nanotubes of 1-nm diameter. **Nature**, V. 363, p. 603–605, 1993.

IIJIMA, S. Carbon nanotubes: past, present, and future. **Physica B: Condensed Matter**, V. 323, n. 1–4, p. 1-5, 2002.

INAMI, N.; MOHAMED, M. A.; SHIKOH, E.; FUJIWARA, A. Synthesis-condition dependence of carbon nanotube growth by alcohol catalytic chemical vapor deposition method. **Science and Technology of Advanced Materials**, V. 8, n. 4, p. 292-295, 2007.

IZA-SC. *Structure Commission of the International Zeolite Association - Database of Zeolite Structures* (2017). Disponível em: <https://america.iza-structure.org/IZA-SC/framework.php?STC=FAU>. Acesso em: jan. 2023.

JEYARAMAN, A.; KARUPPAIAH, B.; CHEN, S. M. e HUANG, Y. C. Development of mixed spinel metal oxide (Co-Mn-O) integrated functionalized boron nitride: Nanomolar electrochemical detection of herbicide diuron. **Colloids and Surfaces A: Physicochemical and Engineering Aspects**, V. 666, 131278, 2023.

JIANG, Y.; PENG, Z.; ZHANG, S.; LI, F.; LIU, Z.; ZHANG, J.; LIU, Y.; WANG, K. Facile in-situ Solvothermal Method to synthesize double shell $ZnIn_2S_4$ nanosheets/TiO_2 hollow nanosphere with enhanced photocatalytic activities. **Ceramics International**, V. 44, n. 6, p. 6115–6126, 2018.

JOSÉ-YACAMÁN, M.; MIKI-YOSHIDA, M.; RENDÓN, L.; SANTIESTEBAN, J. G. Catalytic growth of carbon microtubules with fullerene structure. **Applied Physics Letters**, V. 62, n. 6, p. 657–659, 1993.

KALCHER, K.; KAUFFMANN, J. M.; WANG, J.; SVANCARA, I.; VYTRAS, K.; NEUHOLD, C. e YANG, Z. Sensors Based on Carbon Paste in Electrochemical Analysis: A Review with Particular Emphasis on the Period 1990-1993. **Electroanalysis**, V. 7, n. 1, p. 5-22, 1995.

KOUR, R.; ARYA, S.; YOUNG, S. J.; GUPTA, V.; BANDHORIA P.; e KHOSLA, A. Journal of The Electrochemical Society, V. 167, p. 037555, 2020.

KULPRATHIPANJA, S. **Zeolites in Industrial Separation and Catalysis**. Wiley, 2010, 618 p.

KUO, C.-W.; SHIU, J.-Y.; CHO, Y.-H.; CHEN, P. Fabrication of large-area periodic nanopillar arrays for nanoimprint lithography using polymer colloid masks. **Advanced**

Materials, V. 15, n. 13, p. 1065–1068, 2003.

LAKHERA, P.; CHAUDHARY, V.; JHA, A.; SINGH, R.; KUSH, P.; KUMAR, P. Recent developments and fabrication of the different electrochemical biosensors based on modified screen printed and glassy carbon electrodes for the early diagnosis of diverse breast cancer biomarkers. **Materials Today Chemistry**, V. 26, 101129, 2022.

LI, J.; WU, Q.; WU, J. **Handbook of Nanoparticles**, Springer International Publishing, Cham, 2015, p. 1–28.

LI, W. & ZHAO, D. An overview of the synthesis of ordered mesoporous materials. **Chemical Communications**, V. 49, n. 10, p. 943–946, 2013.

LIANG, G.; HE, Z.; ZHEN, J.; TIAN, H.; AI, L.; PAN, L.; GONG, W. Development of the screen-printed electrodes: A mini review on the application for pesticide detection. **Environmental Technology & Innovation**, V. 28, 102922, 2022.

LIU, C.; CHEN, X.; ZONGAB, B. e MAO, S. Recent advances in sensitive and rapid mercury determination with graphene-based sensors. **Journal of Materials Chemistry A**, V. 7, p. 6616-6630, 2019.

LIU, Y.; GOEBL, J.; YIN, YADONG. Templated synthesis of nanostructured materials. **Chemical Society Reviews**, V. 42, n. 7, p. 2610–2653, 2013.

LÓPEZ-AGUADO, C., PANIAGUA, M., IGLESIAS, J., MORALES, G., GARCÍAFERRO. J. L., MELERO, J. A. Zr-USY zeolite: Efficient catalyst for the transformation of xylose into bio-products. **Catalysis Today**, V. 304, p. 80-88, 2018.

LUTZ, W. Zeolite Y: Synthesis, modification, and properties – A case revisited. **Advances in Materials Science and Engineering**. V. 2014, p. 1-20, 2014.

LV, R.; CAO, C.; ZHAI, H.; WANG, D.; LIU, S.; ZHU, H. Growth and characterization of single-crystal ZnSe nanorods via surfactant soft-template method. **Solid State Communications**, V. 130, n. 3–4, p. 241–245, 2004.

MACHADO, I. R. L.; MENDES, H. M. F.; ALVES, G. E. S.; FALEIROS, R. R. Carbon nanotubes: potential use in veterinary medicine. **Ciência Rural**, Santa Maria, V.44, n.10, p.1823-1829, 2014.

MALIK, M. A.; WANI, M. Y.; HASHIM, M. A. Microemulsion method: A novel route to synthesize organic and inorganic nanomaterials: 1st Nano Update. **Arabian Journal of Chemistry**, V. 5, n. 4, p. 397–417, 2012.

MANICKARAJ, S. S. M.; PANDIYARAJAN, S.; LIAO, A. H.; SELVAM, A. R. P.; HUANG, S. T.; VIMALA, J. R.; LEE K. Y. e CHUANG, H. C. A new class of layered Bi2O2S nanopetals by one-pot supercritical-CO2 approach: A reliable electrocatalyst for analgesic bioflavonoid detection. **Chemosphere**, V. 328, 138534, 2023.

MARTINS, L.; ROSA, M. A. A.; PULCINELLI, S. H.; SANTILLI, C. V. Preparation of hierarchically structured porous aluminas by a dual soft template method. **Microporous and Mesoporous Materials**, V. 132, n. 1–2, p. 268–275, 2010.

MATSUMOTO, R.; SADKI, E. H. S.; TANAKA, H.; YAMAMOTO, S.; ADACHI, S.; TAKEYA, H.; TAKANO, Y. Direct Patterning of Boron-doped Amorphous Carbon Using Focused Ion Beam-assisted Chemical Vapor Deposition. **Thin Solid Films**, V. 730, 138704, 2019.

MELCHERT, W. R.; REIS, B. F.; ROCHA, F. R.P. Green chemistry and the evolution of flow analysis. A review. **Analytica Chimica Acta**, V. 714, p. 8-19 2012.

MEUNIER, V.; SOUZA FILHO, A. G.; BARROS, E. B. e DRESSELHAUS, M. S. Physical properties of low-dimensional sp2-based carbon nanostructures. REVIEWS OF MODERN PHYSICS, V. 88, p. 025005, 2016.

MUÑOZ-GARCÍA, J.; GAGO, R.; VÁZQUEZ, L.; SÁNCHEZ-GARCÍA, J. A.; CUERNO, R. Observation and modeling of interrupted pattern coarsening: Surface nanostructuring by Ion Erosion. **Physical Review Letters**, V. 104, n. 2, 026101, 2010.

NASROLLAHPOUR, H.; KHALILZADEH, B.; RAHBARGHAZI, R.; ERK, N.; RASHIDI, M. R. e NASERI, A. Development of an electrochemical biosensor for the detection of

mammary gland carcinoma using molybdenum enhanced poly taurine nano-biofilms confirmed pathological findings. **Cancer Nano**, V. 14, n. 45, 2023.

OLIVEIRA, I. R. W. Z. & VIEIRA, I. C. . Construção e aplicação de biossensores usando diferentes procedimentos de imobilização da peroxidase de vegetal em matriz de quitosana. **Química Nova**, V. 29, p. 932-939, 2006.

OTEEF, M. D. Y. & IDRIS A. M. Flow Injection Techniques for Tetracycline Quantification: A Review. **Critical Reviews in Analytical Chemistry**, V. 53, n. 2, p. 396-414, 2023.

PARASHAR, M.; SHUKLA, V. K. & SINGH, R. Metal oxides nanoparticles via sol–gel method: a review on synthesis, characterization and applications. **Journal of Materials Science: Materials in Electronics**, V. 31, n. 5, p. 3729–3749, 2020.

PATOLE, S.P.; ALEGAONKAR, P.S.; LEE, H. C.; YOO, J.B. Optimization of water assisted chemical vapor deposition parameters for super growth of carbon nanotubes. **Carbon**, V. 46, n. 14, p. 1987-1993, 2008.

PIJEIRA, M. S. O.; VILTRES, H.; KOZEMPEL, J.; SAKMÁR, M.; VLK, M.; İLEM-ÖZDEMIR, D.; EKINCI, M.; SRINIVASAN, S.; RAJABZADEH, A. R.; RICCI-JUNIOR, E.; ALENCAR, L. M. R.; QAHTANI, M. A.; SANTOS-OLIVEIRA, R. Radiolabeled nanomaterials for biomedical applications: radiopharmacy in the era of nanotechnology. **EJNMMI Radiopharmacy and Chemistry**, v. 7, n. 1, 2022.

PIMPIN, A. & SRITURAVANICH, W. Reviews on micro- and nanolithography techniques and their applications. **Engineering Journal**, V. 16, n. 1, p. 37–55, 2012.

POOLAKKANDY, R. R. & MENAMPARAMBATH, M. M. Soft-template-assisted synthesis: A promising approach for the fabrication of transition metal oxides. **Nanoscale Advances**, V. 2, n. 11, p. 5015–5045, 2020.

QIN, Z., SHEN, B., GAO, X., LIN, F., WANG, B., XU, C. Mesoporous y zeolite with homogeneous aluminum distribution obtained by sequential desilication-dealumination and its performance in the catalytic cracking of cumene and 1,3,5-triisopropylbenzene. **Journal of Catalysis**, V. 278, n. 2, p.266-275, 2011.

RAMLI, N. & AMIN, N. Fe/HY zeolite as an effective catalyst for levulinic acid production from glucose: Characterization and catalytic performance. **Applied Catalysis B: Environmental**, V. 163, p.487-498, 2015.

RINALDI, A.; ZHANG, J.; FRANK, B.; SU, D.S.; ABD HAMID, S.B. e SCHLÖGL, R. Oxidative Purification of Carbon Nanotubes and Its Impact on Catalytic Performance in Oxidative Dehydrogenation Reactions. **ChemSusChem**, V. 3, p. 254-260, 2010.

SAKODINSKAYA, I.K.; DESIDERIO, C.; NARDI, A.; FANALI, S. Micellar electrokinetic chromatographic study of hydroquinone and some its ethers determination of hydroquinone in skin-toning cream. **Journal of Chromatography A**, V. 596, p. 95-100, 1992.

SATO, K., NISHIMURA, Y., MATSUBAYASHI, N., IMAMURA, M., SHIMADA, H. Structural changes of Y zeolites during ion Exchange treatment: effects of Si/Al ratio of the starting NaY. **Microporous and Mesoporous Materials**, V. 59, n. 2-3, 133-146, 2003.

SHAMSUDDIN, S. S.; DERMAN, M. N.; HASHIM, U.; KASHIF, M.; ADAM, T.; HALIM, N. H. A.; TAHIR, M. F. M. Nitric acid treated multi-walled carbon nanotubes optimized by Taguchi method. **AIP Conference Proceedings**, V. 1756, n. 1, p. 090002, 2016.

SHAO, C.; ZHAO, H.; WANG, P. Recent development in functional nanomaterials for sustainable and smart agricultural chemical technologies. **Nano Convergence**, V. 9, n. 1, 2022.

SHIRI, M. S. Z.; HENDERSON, W. & MUCALO, M. MUCALO. A Review of The Lesser-Studied Microemulsion-Based Synthesis Methodologies Used for Preparing Nanoparticle Systems of The Noble Metals, Os, Re, Ir and Rh. **Materials**, V. 12, p. 1–8, 2019.

SUN, W.; GAO, R. e JIAO K. Electrochemistry and Electrocatalysis of Hemoglobin in Nafion/nano-CaCO3 Film on a New Ionic Liquid BPPF6 Modified Carbon Paste Electrode. **The Journal of Physical Chemistry B**, V. 111, n. 17, p. 4560–4567, 2007.

ŠVANCARA, I.; VYTŘAS, K.; BAREK, J. e ZIMA, J. Carbon Paste Electrodes in Modern Electroanalysis. **Critical Reviews in Analytical Chemistry**, V. 31, n. 4, p. 311-345, 2001.

ŠVANCARA, I.; VYTŘAS, K.; KALCHER, K.; WALCARIUS, A. e WANG, J. Carbon Paste Electrodes in Facts, Numbers, and Notes: A Review on the Occasion of the 50-Years Jubilee of Carbon Paste in Electrochemistry and Electroanalysis. **Electroanalysis**, V. 21, p. 7-28, 2009.

SZABÓ, Z.; VOLK, J.; FÜLÖP, E.; DEÁK, A.; BÁRSONY, I. Regular ZnO nanopillar arrays by nanosphere photolithography. **Photonics and Nanostructures - Fundamentals and Applications**, V. 11, n. 1, p. 1–7, 2013.

SZCZĘŚNIAK, B.; CHOMA, J. & JARONIEC, M. Major advances in the development of ordered mesoporous materials. **Chemical Communications**, V. 56, n. 57, p. 7836–7848, 2020.

TAJIK, S.; BEITOLLAHI, H.; NEJAD, F. G.; DOURANDISH, Z.; KHALILZADEH, M. A.; JANG, H. W.; VENDITTI, R. A.; VARMA, R. S.; M. SHOKOUHIMEHR. Recent Developments in Polymer Nanocomposite-Based Electrochemical Sensors for Detecting Environmental Pollutants. **Industrial & Engineering Chemistry Research**, V. 60, n. 3, p. 1112–1136, 2021.

TAJIK, S.; BEITOLLAHI, H.; NEJAD, F. G.; SHEIKHSHOAIE, I.; NUGRAHA, A. S.; JANG, H. W.; YAMAUCHI, Y. e SHOKOUHIMEHR, M. Performance of metal–organic frameworks in the electrochemical sensing of environmental pollutants. **Journal of Materials Chemistry A**, V. 9, p. 8195-8220, 2021.

TANG, T.; ZHANG, T.; LI, W.; HUANG, X.; WANG, X.; QIUA, H.; HOU, Y. Mesoporous N-doped graphene prepared by a softlate method with high performance in Li-S batteries. **Nanoscale**, v. 11, n. 15, p. 7440–7446, 2019.

TATSUMI, T. Metal-Substituted Zeolites as Heterogeneous Oxidation Catalysts. **Wiley**, p. 125-155, 2009.

THESS, A.; LEE, R.; NIKOLAEV, P.; DAI, H.; PETIT, P.; ROBERT, J.; XU, C.; LEE, Y. H.; KIM, S. G.; RINZLER, A. G.; COLBERT, D. T.; SCUSERIA, G. E.; TOMÁNEK, D.; FISCHER, J. E. e SMALLEY, R. E. Crystalline Ropes of Metallic Carbon Nanotubes. **SCIENCE**, V. 273, n. 5274, p. 483-487, 1996.

THÉVENOT, D. R.; TOTH, K.; DURST, R. A. e WILSON, G. S. Electrochemical biosensors: Recommended definitions and classification. **Biosensors and Bioelectronics**, V. 16, n. 1-2, p. 121-131, 2001.

TOHJI, K.; TAKAHASHI, H.; SHINODA, Y.; SHIMIZU, N.; JEYADEVAN, B.; MATSUOKA, I.; SAITO, Y.; KASUYA, A.; ITO, S. e NISHINA, Y. Purification Procedure for Single-Walled Nanotubes. **The Journal of Physical Chemistry B**, V. 101, n. 11, p. 1974–1978, 1997.

TURNER, A. P. F. Biosensors: Sense and sensibility. **Chem Soc Rev**, V. 42, p. 3184–3196, 2013.

USA. Food & Drug Administration. **Department of health and humam services. 21 CFR Part 300**. August 29, 2006.

USA. Food & Drug Administration. **Department of health and humam services 21 CFR Part 310**. April 1, 2015.

USA. Food & Drug Administration. **Department of Health and Human Services. Hydroquinone: Nomination Profile**. 21 may 2009.

WU, Xia; LU, G. Q.; WANG, L. Shell-in-shell TiO 2 hollow spheres synthesized by one-pot hydrothermal method for dye-sensitized solar cell application. **Energy and Environmental Science**, V. 4, n. 9, p. 3565–3572, 2011.

XU, K. & CHEN, J. High-resolution scanning probe lithography technology: a review. **Applied Nanoscience**, V. 10, p. 1013-1022, 2020.

XU, Y.; DERVISHI, E.; BIRIS, A. R.; BIRIS, A. S. Chirality-enriched semiconducting carbon nanotubes synthesized on high surface area MgO-supported catalyst. **Materials Letters**, V. 65, n. 12, p. 1878-1881, 2011.

YAMAUCHI, Y. & KURODA, K. Rational design of mesoporous metals and related nanomaterials by a soft-template approach. **Chemistry - An Asian Journal**, V. 3, n. 4, p.

664–676, 2008.

YAYA, A.; EWELS, C. P.; WAGNER, Ph.; SUAREZ-MARTINEZ, I.; TEKLEY, A. G. e JENSEN, L. R. Purification of single-walled carbon nanotubes. **The European Physical Journal Applied Physics**, V. 54, n. 1, 10401, 2011.

YIN, Y.; GATES, B.; XIA, Y. A soft lithographic approach to the fabrication of single crystalline silicon nanostructures with well-defined dimensions and shapes. **Materials Research Society Symposium - Proceedings**, V. 636, n. 19, p. 1426–1430, 2001.

ZHANG, D.; YE, K.; YAO, Y.; LIANG, F.; QU, T.; MA, W.; YANG, B.; DAI, Y.; WATANABE, T. Controllable synthesis of carbon nanomaterials by direct current arc discharge from the inner wall of the chamber. **Carbon**, v. 142, p. 278–284, 2019.

ZHAO, M.; XIONG, J.; YANG, Y.; ZHAO, J. Template-Assisted Synthesis of Honeycomb-Like CoFe2O4/CNTs/rGO Composite as Anode Material for Li/Na-Ion Batteries. **ChemElectroChem**, V. 6, p. 3468, 2019.

ZHUANG, S.; LEE, E. S.; LEI, L.; NUNNA, B. B.; KUANG, L.; ZHANG, W. Synthesis of nitrogen-doped graphene catalyst by high-energy wet ball milling for electrochemical systems. International Journal of Energy Research, V. 40, n. 15, p. 2136–2149, 2016.

ZINOUBI, K.; CHROUDA, A.; SOLTANE, R.; AL-GHAMDI, Y. O.; ALMALKI, S. G.; OSMAN, G.; BARHOUMI, H. e RENAULT, N. J. Highly Sensitive Impedimetric Biosensor Based on Thermolysin Immobilized on a GCE Modified with AuNP-decorated Graphene for the Detection of Ochratoxin A. **Electroanalysis**, V. 33, n. 1, p. 136–145, 2020.

SEGUNDA PARTE

ARTIGO 1

Capítulo de livro aprovado e publicado no livro Biomaterials-Based Sensors.

Bazzana, M.J.F., Assis, L.C., Martins, R.C., Saczk, A.A., Felix, F.S., Angnes, L. (2023). Electrochemical Biosensors in Agricultural and Veterinary Applications. In: Kumar, P., Dash, S.K., Ray, S., Parween, S. (eds) Biomaterials-Based Sensors. Springer, Singapore. https://doi.org/10.1007/978-981-19-8501-0_11

Abstract

Electrochemical biosensors are sensors which utilize some biological recognition element (for example, DNA/RNA, enzymes, cells, tissues, microorganisms, and antigen/antibody) to interact with the analyte, producing a detectable electrical signal. These biosensors have been successfully employed in a variety of applications. In the agriculture and veterinary areas, for example, they are explored in the detection of mycotoxins, herbicides, and veterinary drug residues. Due to its fast fabrication, sensitive, simple, compatibility with microfabrication techniques, and affordability, electrochemical biosensors can have their analytical performance significantly enhanced by modification of their surfaces with different materials such as metal nanoparticles, graphene, carbon nanotubes, magnetic particles, and quantum dots, among others. The utilization of nanomaterials favors electronic transfer and increases the analytical signal, improving the sensitivity. Electrochemical biosensors can be voltammetric, potentiometric, conductimetric, impedimetric, or coulometric, depending on the analytical signal to be measured. Among them, the voltammetric biosensors can be highlighted, mainly those based on amperometric detection, which is possible to verify a voltage-current-time relationship in an electrochemical arrangement consisting of three electrodes (biosensor as working electrode, auxiliary, and reference electrodes). Additionally, voltammetric biosensors can be associated with injection systems (sequential injection analysis, batch injection analysis, or flow injection analysis) which provide fast analysis, elevated throughput of samples, and high reproducibility. In this chapter, a short review of electrochemical biosensors and how they are applied to agricultural and veterinary analysis is addressed.

Keywords: Agricultural waste detection. Agricultural sensors. Biosensors. Electrochemical sensors. Veterinary sensors. Veterinary product.

1 Introduction

Agriculture is one of the sectors of the economy that has significant participation in the world market when it comes to basic food to humanity and feedstock for industrialization, being considered a source of revenue and job for a large part of the populace, mainly for underdeveloped countries [1]. The advances in agricultural techniques have contributed to the increase in crop yields, by combating weeds and pests by the use of chemical herbicides, fertilizers, and pesticides. As a rule, these agrochemical products (with emphasis on

organophosphates, carbamates, and organochlorines, among others), in most cases, are applied excessively in crops, leading to environmental imbalances with acute and chronic effects on humans (such as nausea, cancer, and Parkinson's disease, among others) [2–4]. In addition, the number of people who are poisoned by agricultural chemicals grows annually. The harmful effects of these excesses are not restricted to food but extend to air, soil, and water. In all these matrices, the detection of these species needs to be monitored which is a serious challenge. These agrochemical substances are determined mainly by widely complex, laborious, time-consuming, and expensive analytical techniques, such as chromatography (GC), high-performance liquid chromatography (HPLC), capillary electrophoresis (CE), ultraviolet-visible spectroscopy (UV-Vis), nuclear magnetic resonance (NMR), and Fourier transform infrared spectroscopy (FTIR) [1, 5, 6]. More complex analysis can require hyphenated techniques such as HPLC-mass spectrometry (HPLC-MS).

In many veterinary practices such as the use of antibiotics (chloramphenicol, penicillin, and others) and chemotherapy (sulfonamides, enrofloxacin, and others) in animal husbandry has caused the appearance of veterinary drugs residues in meals produced from animals. In addition, some components (organic or inorganic) are excreted via urine or feces from infected animals as well as the inappropriate disposal of medications not administered can directly contaminate the soil, water, and even humans [7–10].

All aspects mentioned above cause economic impacts, since conventional diagnostic methods, such as NMR and HPLC or GC coupled to mass spectrometry (GC-MS), require expensive instrumentation, time-consuming sample preparation, Electrochemical Biosensors in Agricultural and Veterinary Applications 351 and skilled labor [10, 11]. Recent advances in electrochemical biosensor technologies compared to conventional methods have the potential to provide diagnostics with greater sensitivity and selectivity, rapid analyses, simplicity of automation, and thus portability and relatively inexpensive since many of the compounds (for example, pesticides, antimicrobial agents, and hormones, among others) can be easily oxidized or reduced [12].

Electrochemical biosensors are devices that use a biochemical receptor (for example, enzyme, antigen/antibody, nucleic acid, and cell, among others) in direct contact with an electrochemical transducer (conductometric, potentiometric, impedimetric, coulometric, and

voltammetric) to generate an electrical signal that is converted into analytical information on a given analyte [13–15]. The association of these sensors with Batch Injection Analysis (BIA) [16], Flow Injection Analysis (FIA) [17], or Sequential Injection Analysis (SIA) [18] will provide greater performance during chemical analysis, with increased sensitivity and reproducibility. In this context, this chapter is focused on the electrochemical biosensor applications in the field of agriculture and veterinary. Relevant examples from the literature are mentioned and fundamental information about electrochemical biosensors and their associations with injection systems (FIA, SIA, and BIA) are also addressed.

2 Electrochemical Biosensors

Biosensors are selective analytical devices capable of generating signals from biochemical interactions [19, 20]. These devices are made up of bio-receptors in touch with a signal transducer [19–22]. This transducer is the component responsible for recognizing the physical-chemical changes arising from the interaction that takes place in the bio-receptors (interaction between biological recognition element and analyte), generating a measurable analytical signal that can be related to the amount of the chemical species of interest [19, 23–26].

One of the first biosensors was designed by Clark and Lyons for the determination of glucose. This sensor was composed of the enzyme glucose oxidase in close contact with an oxygen electrode that aided in glucose monitoring (via oxygen consumption by the enzymatic reaction) [27, 28]. Biosensors can be classified according to biological component or transducer type (for example, electrochemical, acoustic, optical, or calorimetric) [22, 24], being the most reported those based on the process of recognizing electrical signals from biochemical interactions, called electrochemical biosensors [29, 30].

Electrochemical biosensors are devices that (generally) operate in conditions that do not require complicated sample pretreatment, present fast responses, ease of manufacture, and implementation in different fields such as environmental, health, and laboratory investigations [31]. They consist of (at least) three compact components, as any other biosensor, including (a) a biorecognition element, (b) an electrochemical transducer, and (c) an electronic data

management system [32– 34]. The representation of an electrochemical biosensor is shown in Fig. 1.

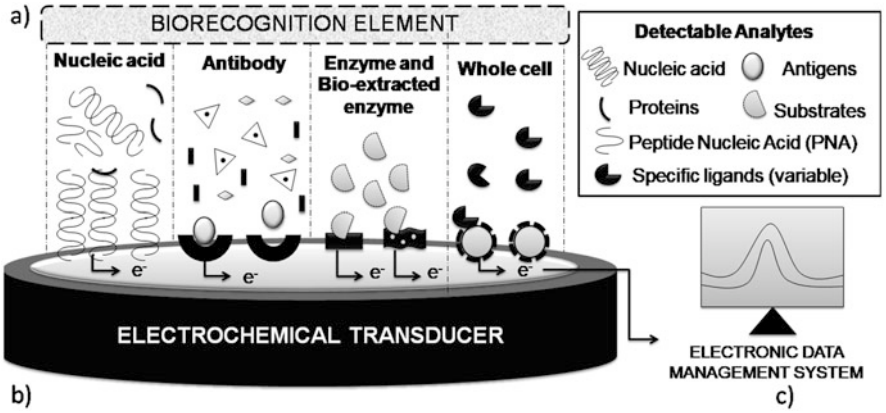

Fig. 1 Scheme of electrochemical biosensors showing (a) biorecognition element (for example, nucleic acid, antibody, enzymes, and whole cell), (b) an electrochemical signal transducer, together with (c) an electronic data management system (Figure based on [35])

The classic biorecognition elements are nucleic acids, antibodies, tissues, microorganisms, enzymes, and others [36, 37]. Such elements are important due to their roles in the recognition of the target analyte, directly affecting the sensitivity and selectivity of the electrochemical biosensor [32, 37]. Biorecognition molecules selectively bind to the target analyte to produce electrochemical responses [32]. The immobilization of biorecognition elements on the detector allows the construction of more compact and selective sensors. The responses of the voltammetric biosensors give information about the reaction rates, catalysis, or inhibition of enzymes in presence of the analyte [38].

Regarding the different types of biorecognition elements, there are many papers describing the use of one or more enzymes for the construction of biosensors, generally immobilized on different transducers and using various binding components [39]. However, many enzymes are expensive and some essential enzymatic reactions require cofactors that, if not regenerated, turn the use of enzymatic biosensors even more expensive [40].

Some researchers have explored tissues (animal, vegetable, or fungal) or crude vegetable extracts in place of purified enzymes for the manufacture of electrochemical biosensors. This choice occurs mainly due to the availability of crude tissues or extracts or even

because the biosensors have greater stability due to the enzymes being naturally immobilized in the cells of the biological material. However, the use of tissues can lead to a decrease in the selectivity of the analytical method due to a large number of interferences and contaminants [41]. In the work developed by Rahimi-Mohseni et al. (2019), a low cost, disposable amperometric biosensor built from potato tissue extract was developed to determine phenol. The potato tissue containing polyphenol oxidase was immobilized on paper using physical and chemical adsorption and it was transferred to the top of the graphite SPE. The linearity range for phenol detection was found to be 0.1–300 μmol L-1 and the detection limit Electrochemical Biosensors in Agricultural and Veterinary Applications 353 found for the developed method was 0.042 μmol L^{-1}. This method was successfully used to determine phenol in water and effluent samples [42].

Sezgintürk and collaborators (2010) developed an amperometric biosensor using zucchini tissue (Cucurbita pepo) for the quantification of ascorbic acid in drugs and plants. According to the authors, the developed biosensor presented a linear range from 5.0×10^{-6} mol L^{-1} to 1.2×10^{-3} mol L^{-1} and the correlation coefficient found for the developed method was 0.9975 [43]. In the study carried out by Sekar et al. (2015), an amperometric biosensor was developed for the determination of hydrogen peroxide using turnip plant tissue as biological material. This sensor was constructed by immobilization via physical adsorption of the enzyme peroxidase from raw turnip on a cellulose paper, ideal and biocompatible with the enzyme. Potassium hexacyanoferrate mediator was also incorporated into the paper matrix along with the crude enzyme. The developed biosensor presented a linear range from 20 to 500 μmol L^{-1} (R^2 = 0.999) and the detection limit found for the developed method was 4.1 μmol L^{-1}. According to the authors, the biosensor retained 70% of its activity after a storage time of 25 days [44].

Lata and Pudir (2013) built an amperometric biosensor for determining L-amino acid from a goat kidney immobilized on the surface of the working electrode (glassy carbon). Studies carried out with the developed biosensor indicated that the analytical response was obtained quickly (5 s) with a wide linear working range (from 0.5 μmol L^{-1} to 100 mmol L^{-1}) and sensitivity of the biosensor was 79.31 nA cm^2 μmol L^{-1}. This sensor was applied in the quantification of L-amino acids in fruit juices and alcoholic beverages, presenting a fast

response time, good durability over time, and insignificant interference during the analyzes performed [45].

In addition to animal and vegetal tissues, small molecules of oligonucleotides formed by simple strands, such as ribonucleic acids (RNA) and deoxyribonucleic (DNA), perform specific chemical bonds (high affinity) with various molecules. Such synthetic oligonucleotides are called aptamers [21, 46–48].

The high affinity and selectivity of aptamers are related to the proper selection of the oligonucleotide sequence, extracted from a set of random sequences. The process performed for the selection of the appropriate oligonucleotide sequence is carried out by the exponential enrichment (SELEX) [21, 49]. These molecules are similar to antibodies, acquiring a certain conformation, being able to join the analyte [49]. Nev Nevertheless, when the aptamers are used as elements of biorecognition in the construction of electrochemical biosensors they have not been able to completely replace traditional elements of biorecognition. This occurs due to several factors related to the characteristics of the aptamers, such as degradation, cross-reactivity, and low stability, among others [21, 46]. Villalonga et al. (2020) presented the use of an amperometric aptasensor for the quantification of carcinoembryonic antigen (CEA). This aptasensor presented a linear range concentration from 112 fmol L^{-1} to 11 μmol L^{-1} and the detection limit found for the developed method was 90 fmol L^{-1}. The analytical parameters of this sensor were evaluated in human serum samples and showed good stability, specificity, and reproducibility [50].

Electrochemical transducers are traditionally made of carbon (glassy carbon, carbon paste, and other carbon forms), metals (e.g., gold or platinum), or conductive 354 M. J. F. Bazzana et al. glass. All of them have the possibility to be chemically modified by a chemical agent composed of the selected biorecognition element [22, 36]. The analytical signals originating from the biological element and analyte interaction are received by an electronic system in which the generated data can be managed. Electrochemical sensors can be subdivided based on the way in which the physicochemical transduction is used during experiments. They can be voltammetric (special emphasis will be given to amperometric sensors in this chapter), potentiometric, impedimetric, coulometric, and conductometric. All of them present possibilities for the construction of Point of Care Testing (POCT) [23, 31, 36, 51, 52].

2.1 Voltammetric Biosensors

Among all types of existing electrochemical biosensors, voltammetric biosensors are widely used due to their analytical performance and popularity in the analysis of different matrices such as environmental, pharmaceutical, and biological samples, among others [36]. Voltammetric sensors are able to detect possible changes in analytical signals (currents) related to oxidation or reduction reaction of analytes that have the potential to oxidize or reduce (electrochemically active) [33, 53]. In many cases, the electroactive species will be identified in the voltammogram by the peak potential and the concentration of this chemical species can be determined by the peak current using an analytical curve. Different operating methods can be used in voltammetric sensors [54], which include:

- Amperometry;
- Cyclic voltammetry (CV);
- Normal pulse voltammetry (NPV);
- Differential pulse voltammetry (DPV);
- Square wave voltammetry (SWV)

In this chapter, special attention will be given to the amperometric biosensors since they are characterized by simplicity, sensitivity, portability, and reliability, as well as low consumption of samples, possibility of using microelectrodes, and performing experiments with high analytical frequency. Although amperometry has been one of the most used electroanalytical techniques during the use of biosensors, the cyclic voltammetry is a fundamental technique during initial studies to understand the redox behavior of the analyte [55–57]. Kokkinos et al. (2020) report in their review the potential and advances in the use of amperometric biosensors [58].

The amperometric biosensors are the devices most used commercially and the classic example of an amperometric biosensor produced commercially is the glucometer (Fig. 2). The amperometric glucometer generates an analytical signal based on the measured current when glucose oxidase facilitates the oxidation reaction (catalyzes) of glucose to gluconic acid thus generating the electroactive hydrogen peroxide too, or when glucose dehydrogenase catalyzes

the oxidation of glucose to gluconolactone and produces a reduced cofactor. In both cases, the products of the reaction can be related to the amount of glucose present in the blood. The resulting current is proportional to the glucose concentration and the device that will perform the analysis is calibrated to indicate the amount of glucose in the blood [59].

Fig. 2 Commercial glucometer based on an amperometric transducer.

2.2 Amperometric Biosensors

Amperometric biosensors operate under a fixed potential applied on the surface of the sensor with monitored current in the function of time [36, 54, 60–63]. The potential applied across the experiment helps in the efficiency of electron transference from the biological system (oxidase or dehydrogenase enzymes, for example). In a certain concentration range, the observed current shows a linear function with the amount of the electroactive species [19, 62, 64–66].

The electrochemical system in an amperometric cell configuration can be composed of two or more commonly three different types of electrodes (working electrode-W.E, reference electrode-R.E, and auxiliary electrode-A.E) according to the system shown in Fig. 3, which represents experiments in hydrodynamic voltammetry mode [36, 67, 68]. The second electrode to compose the amperometric cell is the reference electrode, which in the vast majority of cases is composed of Ag/AgCl. This electrode provides a fixed potential against which the working electrode's potential is controlled and measured [36, 68]. The use of amperometric biosensors

with two electrodes (working and reference electrodes) is limited since at high currents it is difficult to maintain the potential, resulting in a less linear range [36, 67]. In this sense, a third electrode is inserted into the electrochemical cell and acts as a counter electrode, another name for the auxiliary electrode. When three electrodes are utilized, the current passes through the working and the auxiliary electrodes, avoiding potential shifts of the reference electrode, preserving its stability [67, 69]. Amperometric biosensors are highly sensitive, have a quick response system, and are easy to operate [61, 66].

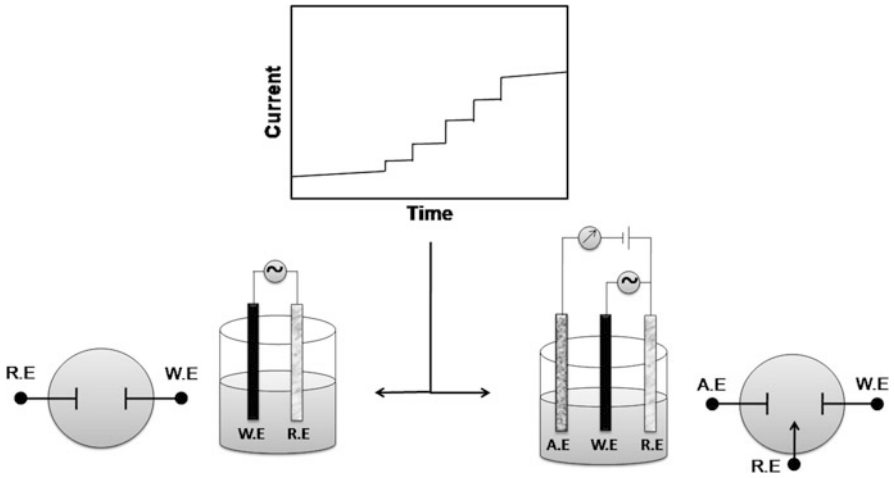

Fig. 3 Amperometric experiments with a configuration of two and three electrodes and their respective electrochemical signal (current vs time). W.E represents the working electrode, R.E represents the reference electrode, and A.E represents the auxiliary electrode (Figure based on [36])

The working electrode, detector, or transducer is composed of materials such as gold, carbon, and platinum, among others [36, 68]. These electrode materials ideally are inert and favor the transfer of electrons towards the biological system immobilized on the detector surface [19, 36]. The surface of the working electrodes, in many cases, contains conducting mediators, polymers, or nanomaterials (metallic nanoparticles, graphene, carbon nanotubes, quantum dots, among others) with the main purpose of improving electronic transference. Thus, the biological system can be covalently linked to the transducer surface covered with the functional groups or trapped in the polymeric layers [19, 70–73].

In the work developed by Zhang et al. (2019), organophosphate compounds were determined using an amperometric biosensor. For the manufacture of this biosensor, the compound 4,7-di(furan-2-yl) benzothiadiazole (FBThF) was electrochemically polymerized on the detector surface for the development of the electrochemical biosensor. Moreover, nanocomposite Ag-rGO-NH_2 and acetylcholinesterase (AChE) were modified in the membrane formed on the electrode surface [74]. This electrode explores the potential for inhibition provided by the enzymatic reaction between acetylcholinesterase and organophosphate compounds.

Recently, Ren and collaborators built an amperometric biosensor using enzymes for determining H_2O_2. The sensitivity of this sensor was 3.0×10^{-4} A/mol L^{-1} and the detection limit found for the developed method was 443 nmol L^{-1}. Moreover, the biosensor presented good reproducibility and stability too [75].

For improving the sensitivity of electrochemical sensors, nanomaterials have been incorporated into biorecognition materials [76]. These materials have the potential to build biosensors due to their thermal, optical, and electronic properties. Ideally, they have a high surface area, good electronic conductivity, and excellent chemical, magnetic, and physical properties [77, 78]. The nanomaterials most used for the development of amperometric biosensors are metal nanomaterials, carbon nanomaterials (graphene and carbon nanotube), magnetic nanoparticles, and quantum dots (Fig. 4) [77].

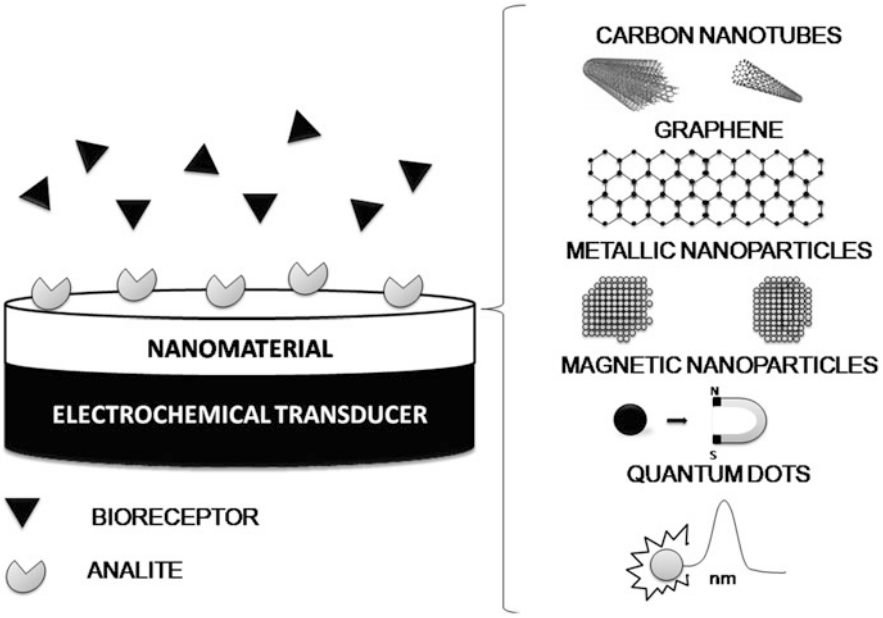

Fig. 4 Examples of nanomaterials applied in the construction of amperometric detectors (Figure based on [79]).

2.2.1 Carbon Nanotubes

Carbon nanotubes (CNTs) are found in two different ways: simple tubes-SWCNT and multiple concentric tubes-MWCNT. They are sp^2 hybridized carbon nanomaterials and are favorable for application in amperometric biosensors since they have a great surface area, in addition these materials present good chemical stability and remarkable properties—electronic and thermal [80, 81]. Also, CNTs can be functionalized with various chemical groups, favoring the connection of biomolecules or organic molecules with different biorecognition elements used in the development of biosensors [77, 82, 83].

Palomar et al. (2020) built an amperometric biosensor for the determination of two chemical substances, catechol and dopamine, with functionalized carbon nanotubes. In this work, functionalized tungsten disulfide nanotubes functionalized with carboxylic acid functions (WS_2-COOH) were used and so the tyrosinase enzyme presented better adhesion on the electrode surface and improved analyte detection. The developed method presented a good linearity in concentrations from 0.6 to 70 μmol L^{-1} and excellent selectivity with values of 10.7 ± 0.2 mA L mol^{-1} 358 M. J. F. Bazzana et al. for catechol analysis. For dopamine, the same method presented a good linearity in concentrations from 0.5 to 10 μmol L^{-1} and a good

sensitivity with a value of 6.2 ± 0.7 mA L mol^{-1}. The performance of this sensor was considered within the average when compared to other studies using carbon nanotubes [84].

In the work developed by Ramonas et al. (2019), an amperometric biosensor was used for the quantification of glycerol. This sensor was built through immobilization of alcohol dehydrogenase from Pseudomonas putida on a graphite electrode. The graphite electrode was modified with carbon nanotubes and during the experiments a redox mediator tetrathiafulvalene was used. The evaluation of the proposed biosensor showed high sensitivity to glycerol (29.2 ± 0.9 μA mmol L^{-1} cm^{-2}), low limit of detection (18 μmol L^{-1}), and linearity for concentration values varying from 0.05 to 1.0 mmol L^{-1}, with good selectivity and stability [85].

2.2.2 Graphene Graphene is an allotrope of carbon constituted by a thin sheet of atoms arranged in a 2D lattice. The carbon atoms (hybridized in sp^2) of this nanomaterial are arranged in a rigid network similar to a honeycomb [77, 86]. Graphene has good electron transfer capability, excellent thermal and electrical conductivities, mechanical resistance, large surface area, good flexibility, impermeability, and biocompatibility [77, 86, 87]. The thin thickness of the graphene sheet (theoretically) allows each carbon atom to interact directly with the analyte giving the biosensors a high sensitivity [88, 89].

A recent study reports the use of graphene in its own way of graphene oxide or incorporated into nanocomposites. In this work developed by Song and collaborators (2020), an amperometric biosensor for the quantification of ascorbic acid (AA) and dopamine (DA) was developed. It was built using nanobiocomposite derived from poly (aniline-co-thionine) (P(ANI-co-THI)) and modified with graphene oxide (GO). The analytical parameters presented a good linearity with concentration values that varied from 0.002 to 0.5 mmol L^{-1} with a limit of detection of 2 μmol L^{-1} for DA, as well as 0.5–5 mmol L^{-1} and a limit of detection of 242 μmol L^{-1} for AA. The designed electrochemical biosensor presented high selectivity, good stability, and reproducibility [90].

2.2.3 Metallic Nanomaterials

Metal nanoparticles are nanomaterials with specific physicochemical properties, which relate approximately to their size, composition, format, and structure. These materials are widely applied in the development of voltammetric biosensors because of the large surface area,

excellent electron transfer kinetics, and many absorption sites for the attachment of biorecognition materials [77, 91]. The most common metallic nanomaterials used in the building of biosensors are gold (Au), silver (Ag), and platinum (Pt).

Gold nanoparticles (AuNPs) are very popular in the construction of electrochemical biosensors due to their biocompatibility and easy protein functionality [92]. Gold presents good compatibility and has the main characteristic of making strong bonds with enzymes [93, 94]. In this sense, enzymes can be easily Electrochemical Biosensors in Agricultural and Veterinary Applications 359 immobilized on the surface of AuNPs and in many cases, their activity is increased [94, 95].

Chiang et al. (2019) developed an amperometric biosensor of high sensitivity modified with AuNP for glucose determination. The proposed amperometric biosensors demonstrated a low limit of detection of 50 μmol L^{-1} and a wide linear range of concentration when modified with AuNP electrodeposition [96].

Platinum nanoparticles (PtNPs) have the specific characteristic of being able to catalyze the decomposition of H_2O_2. In this sense, this nanomaterial is widely used in amperometric biosensors since PtNPs act as a catalyst, increasing the biosensor response when compared to traditional platinum electrodes [94, 97, 98].

Wang et al. (2019) built an amperometric microbiosensor using carbon fibers for the determination of hydrogen peroxide. During the construction step of this amperometric sensor, the electrometallization of carbon-fiber microelectrodes and electrodeposition of PtNPs were used. The hybrid structure obtained with PtNPs and carbon fiber provided a sensitivity of 7711 ± 587 μA mmol L^{-1} cm^{-2} and a limit of detection of 0.53 ± 0.16 μmol L^{-1}. Moreover, it was possible to obtain a good linearity with concentration values that varied from 0.8 μmol L^{-1} to 8.6 mmol L^{-1}, and a response time of <2 s [99].

Silver nanoparticles (AgNPs) have the same advantages presented as in other metallic nanoparticles, such as amplification of the electrochemical signal and increased sensitivity [94]. Thought about these characteristics, Hou and collaborators (2020) built an amperometric biosensor for the quantification of wild-type p53 proteins. In this work, AgNPs were deposited in situ on the gold electrode surface for amplifying the generated signal. According to the

authors, the biosensor exhibited a wide linear range of concentration and a detectable concentration as low as 0.1 pmol L^{-1} [100].

In the work published by Medyantseva et al. (2017), AgNPs and nanotubes immobilized in polyester polyols were used in the quantification of antidepressants. AgNPs and nanotubes were trapped on a carbon electrode using polyester-polyol. According to the authors, AgNPs extended the concentration range to 1.0×10^{-4} mol L^{-1} until 1.0×10^{-8} mol L^{-1} and decreased the limit of determination to 3.0×10^{-9} mol L^{-1} [101].

Metallic nanoparticles have important characteristics but are electrically unstable due to their susceptibility to salt concentrations that can cause their precipitation. In this sense, chemical and biological adjustments are necessary for the use of these nanomaterials in biological matrices with a high concentration of salt [92, 102].

2.2.4 Other Materials

Another class of nanomaterials explored for biosensing are magnetic nanoparticles (MNPs), that present specific characteristics such as large surface area, high mass transfer, specific physicochemical properties, biocompatibility with biomolecules, and easy production [77, 103, 104]. The singular and attractive aspect is that MNPs can be immobilized on the detector surface, or be dispersed in the sample for a fixed time and in sequence be attracted (through an externally generated magnetic field) on the sensor [77, 105].

The classic example of a magnetic nanomaterial is iron oxide (Fe_3O_4) nanoparticles. This material is characterized by the ability to enhance the sensitivity of biosensors constituted by oxidase enzymes [94, 106].

Magnetic nanoparticles are commonly found in amperometric biosensors modified with composites. In the work developed by Pakapongpan and Poo-arporn (2017), an amperometric glucose biosensor was built. This biosensor was modified with reduced graphene oxide (rGO) covalently conjugated to magnetic nanoparticles (Fe_3O_4NPs). The authors observed a rapid amperometric response (3s) and linearity with concentrations that varied from 0.05 mmol L^{-1} to 1 mmol L^{-1}. The limit of detection found for the developed method was 0.1 μmol L^{-1} and the

sensitivity found was 5.9 μA mmol L^{-1}. Moreover, this biosensor presented good reproducibility, high stability, and selectivity [107].

Another interesting class of nanomaterials is quantum dots (QDs). These nanomaterials are semiconductor crystals that have characteristic optical properties, such as wide absorption band, long-term photostability, with symmetric emission, among others. They can consist of carbon, graphene, or inorganic materials (CdS, ZnS, and CdT, among others) [77, 94]. In the study described by Fatina et al. (2020), quantum antimony nanodots were immobilized with catalase on the surface of the working electrode (glassy carbon). The amperometric biosensor was developed to determine hydrogen peroxide in human serum samples and showed good linearity (0.989) and the limit of detection found was 4.4 μmol L^{-1}. Amperometric measurements showed 95–103.4% recovery for H_2O_2 and electrochemical stability [108].

2.3 Potentiometric Biosensors

Potentiometric biosensors are devices that incorporate a biological element into a potentiometric transducer. The potentiometric measurement corresponds to the changes that occur between an indicator or working electrode and a reference electrode, as is schematically represented in Fig. 5. The first potentiometric biosensors were based on fixing enzymes on the surface of a glass sensor. In this case, the variations of the pH produced by the enzymatic reactions can be directly related to the amount of analyte present in the reaction medium. Many biosensors were constructed using ion-selective electrodes (ISE), mainly those based on polymeric membranes, or ion-sensitive field-effect transistors (field-effect transistors, FET). ISE are extensively used because they have the following advantages: they are more easily reproduced than FETS, are sensitive, provide quick responses, and simplicity in measurement, among others [22, 100]. They are able to record charge accumulation, in equilibrium condition created by specific chemical bonds on the electrode surface [65, 109–111]. The reference electrode provides a constant halfcell potential and the working electrode responds to the variation in the concentration of the electroactive species, indicated by a variable potential [68]. Unlike amperometric biosensors, in potentiometric biosensors, the change in potential comes from the concentration of electroactive analytes, occurring logarithmically according to the Nernst equation [68, 111].

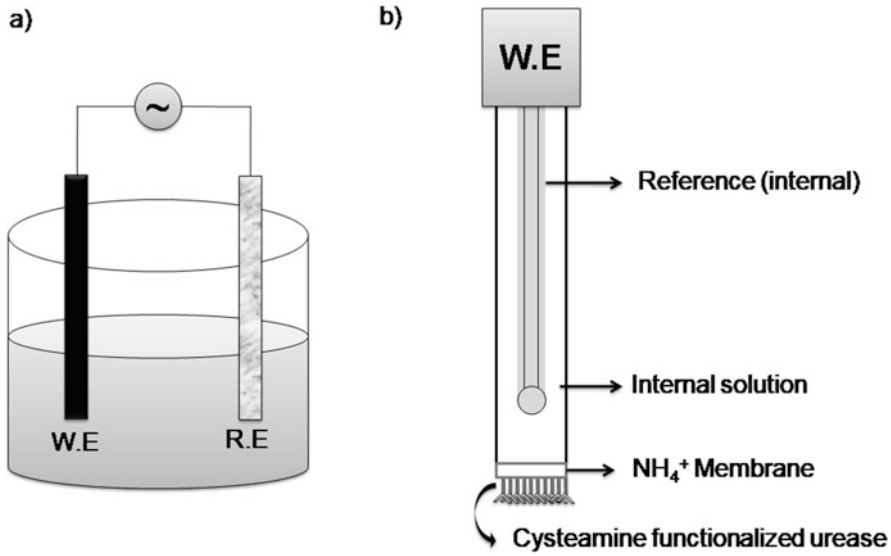

Fig. 5 Classical electrochemical cell with potentiometric sensor (a) and the representation of a potentiometric urea biosensor based on cysteamine functionalized urease immobilized on the membrane (b). W.E represents the working electrode and R.E represents the reference electrode (Figure based on [112]).

Potentiometric biosensors present some significant advantages including simplicity of use, low cost, great sensitivity, reduced size, as well as quick response acquisition [36, 113, 114]. However, low selectivity limits its use in some applications [36, 119]. This disadvantage is overcome by bio-modifications that promote specific molecular interactions and broaden the spectrum of analytes detected by potentiometric biosensors [63, 113]. In the study described by Mello et al. (2020) two potentiometric biosensors, for the quantification of glucose and urea, were proposed and their surfaces were biomodified with polyaniline films by entrapped enzymes. The produced films presented a linear dynamic range from 10- 5 mol L^{-1} until 10-1 mol L^{-1}, for both analytes [120].

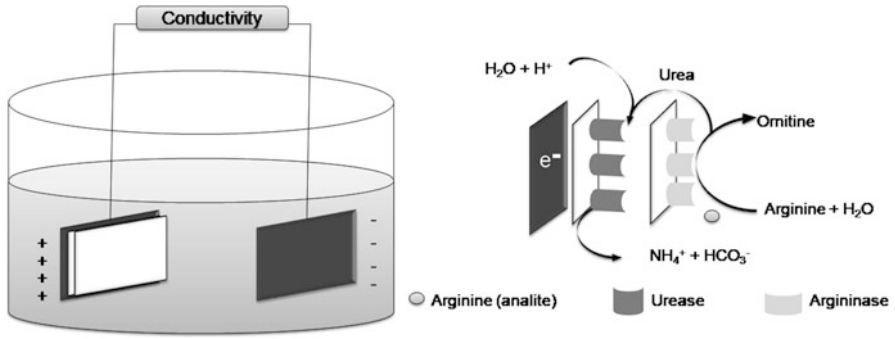

Fig. 6 Representation of a modified conductometric biosensor using two-layer membrane (Figure based on [123]).

2.4 Conductometric Biosensors

Conductometric biosensors are devices that detect changes in electrical conductivity in solution from biological recognition reactions [19, 121]. The biological recognition reactions are responsible for the production or consumption of ions, resulting in the change of conductivity in solution [111, 122].

The conductivity measurements performed by the conductometric biosensors are made relatively quickly when compared to other analytical methods, being appreciable for different applications [119]. In the work developed by Soldatkina and collaborators (2018), a conductometric biosensor was developed to determine arginine in pharmaceutical products (Fig. 6). The biosensor was built in urease and arginase enzymes (UE and AE) co-immobilized on the electrochemical transducer (Fig. 6). The function of the arginase enzyme (AE) is to cleave arginine into two other molecules: urea and ornithine, through an enzymatic reaction. The urease enzyme (UE) has the function of transforming urea into carbon dioxide and ammonia. In this sense, reactions involving enzymes produced variations in the conductivity of the supporting electrolyte and the variations were proportional to the concentration of arginine. The results indicated that the conductometric biosensor presented a limit of detection of 2.5 μmol L^{-1}. The linearity of the method developed varied from 2.5 μmol L^{-1} to 500 μmol L^{-1} and the sensitivity for arginine detection was 13.4 ± 2.4 μS/mmol L^{-1}, with a response time of 20 s [123].

Braiek et al. (2018) built a conductometric biosensor for the determination of creatinine. The detection of creatinine in a sucrose bottom solution showed a limit of detection of 2.0 μmol L^{-1} and good repeatability. According to the authors, the proposed method represented an interesting alternative for the determination of creatinine in biological samples due to the low associated cost, speed, and practicality [124].

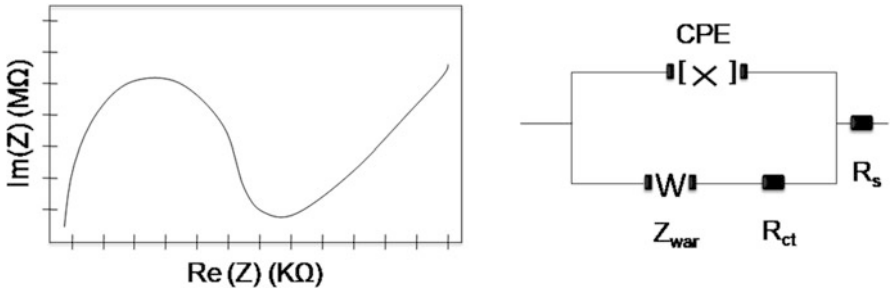

Fig. 7 Representation of impedance spectra at zero potential (a) and an equivalent circuit (b) (Figure based on [127]).

2.5 Impedimetric Biosensors

Electrochemical impedance spectroscopy is an electrochemical technique of great utility to study the mechanisms of charge accumulation that happens at the interface of the conductive electrodes. The impedimetric biosensors are able to determine electroactive species by recording changes in the impedance value from biomolecular reactions on the electrode surface [121]. The basic principle of impedimetric biosensors is the provision of small sine wave disturbances over a wide frequency range. Thus, the current that is generated can be recorded and measured, informing the biorecognition phenomena found [36, 121]. More generally, the impedance describes the dependence of the current (at different excitation frequencies) which is directly influenced by the biorecognition system placed between two electrodes [64]. The representation of impedance spectra at zero potential of an impedimetric biosensor and its equivalent electrical circuit is shown in Fig. 7. The analysis of the results with these sensors is often performed through simulation with models of equivalent electrical circuits. In the work developed by Bhat et al. (2020), the equivalent circuit analysis was essential for the rapid monitoring of small pH fluctuations in the pathophysiological range of 7.35–7.45, with high sensitivity [125].

In the circuit model shown in Fig. 7b, CPE represents the capacitance of the electrical double layer in the surface area of the electrode in solution. Rct corresponds to resistance to load transfer or faradaic impedance. The symbol W that equals Zwa corresponds to the impedance that measures the resistance to mass transport of electroactive species. And lastly, Rs corresponds to the resistance of the solution between the working and reference electrodes.

The simplest equivalent electrical circuit containing the components shown (CPE, Rct, Zwa, and Rs) is known as the Randles circuit [126].

Some authors consider that the impedimetric biosensors have low energy consumption, so they are inexpensive and can be easily miniaturized [128]. Probably the software used for data acquisition corresponds to the higher cost of common impedance equipment. Another aspect that some authors highlight as an advantage of the technique is the fact that they do not hinder most biorecognition interactions from stimulation applied. This happens because the applied sinusoidal voltage is negligible being around 5–10 mV in amplitude [36, 129].

As shown by Rocha et al. (2020) in recent studies, an impedimetric biosensor was constructed for the quantification of staphylococcal enterotoxin A, from Staphylococcus aureus found in milk samples. The biosensor was developed by modification of the working electrode (glassy carbon) with reduced graphene oxide (rGO) and Anti-Staphylococcal Enterotoxin A (anti-SEA) to prepare sandwich-type electrochemical immunosensors. This sensor detected concentrations between 0.5 mg L^{-1} and 3.5 mg $L^{-}1$ of the analyte by antigen-antibody binding. According to the authors, the proposed biosensor presented a limit of detection of 0.102 μg mL^{-1} for SEA analysis. The analyses of the milk samples showed good robustness, good specificity, and reproducibility to determine SEA [130].

2.6 Coulometric Biosensors

Coulometric biosensors are similar to voltammetric biosensors in terms of electrochemical principles, whereas in place of the maximum current generated coulometric measurements are based on the charge (= amount of electricity in Coulombs) required for the conversion of ~100% of a species by oxidation or reduction. The effectiveness in the conversion of the substance occurs since electrodes with a large active area are used during experiments. In the work presented by Tsujimura et al. (2009), a coulometric biosensor was built for the determination of D-fructose. This method was able to quantify D-fructose successfully at a concentration range from 1 mmol L^{-1} to 100 mmol L^{-1}, a much broader range than that attained by amperometry reported to date [131]. In coulometric cells, a reference electrode, a graphite counter electrode, and a mercury, gold, and carbon working electrode, among others, are used. To have good control of the potential applied in processes involving elevated currents, the

reference electrode was positioned near the coulometric transducer (working electrode) avoiding variations of the applied potential due to the IR drop. Alternatively, a Luggin capillary can be used to measure the potential close to the electrode, without significantly blocking the current flow.

In the work proposed by Cao et al. (2020), an origami-based coulometric biosensor was designed to determine multi-metabolites with a single electrode (using 0.5 μL of samples). In order to build this biosensor, a screen-printed electrode and an origami device equipped with three folding flaps were used. The linearity intervals were of 0–10 mmol L^{-1} for L-lactate, 0–5 mmol L^{-1} for cholesterol, and 0–24 mmol L^{-1} for glucose. The electrolysis efficiency found for L-lactate, cholesterol, and glucose were 99% ± 3%, 99% ± 1%, and 100% ± 2%, respectively. The limit of detections were 0.25 mmol L^{-1} for L-lactate, 0.23 mmol L^{-1} for cholesterol, and 0.03 mmol L^{-1} for glucose [132].

In the work proposed by Liu et al. (2012), a coulometric biosensor was developed for DNA determination. The biosensor was built by means of enzymatic silver deposition on gold nanoparticle (AuNP)-modified screen-printed carbon electrode (SPCE). The concentration range used was from 3.0×10^{-17} mol L^{-1} to 1.0×10^{-14} mol L^{-1}, and the limit of detection was calculated as 1.5×10^{-17} mol L^{-1} [133].

2.7 Point of Care Testing (POCT) as Biosensor

Due to its ease of use, Point of Care Testing-POCT has become widespread, since tests can be performed by the patients themselves without the need for specialization. The POCT, also known as self-test, has an advantage as minimum infrastructure requirements and excellent cost-benefit, among others [134].

The applications of POCT are beyond clinical analysis since it is currently used for environmental monitoring, food quality control, toxicological tests, and forensic sciences, aiming to minimize the time of diagnosis of diseases and contamination, among other functions [135].

He et al. (2020) designed a POCT by means of the capture of microdroplets on a tape previously sputtered with gold for rapid screening of Surface Enhanced Raman Scattering

(SERS). The device was used to determine food contaminants. This type of POCT has the potential for military applications, consumer protection, and forensics, among others, as it is easy to operate [136].

Most of the POCTs have used screen-printed electrodes (SPE) during the construction of biosensors. SPE are disposable devices, that have a chemically inert surface that enhance the advantages of POCTs due to their versatility of design (from a single printed electrode to matrices of several electrodes), fast manufacturing process, good reproducibility, fast response and portability [18, 56, 137]. The surface of the SPEs can be modified with graphene, carbon nanotube, nanoparticles, and other materials, to significantly improve electron transfer and consequent increase of the sensitivity [56].

Due to their versatility, easy access, high-quality cameras, and wireless access, they open a new perspective for diagnostic applications with POCT. Thanks to these properties, researchers have developed electrochemical sensors for the quantification of some chemical species, reducing the size of the devices, dropping the cost, and simplifying the utilization of wireless biosensors. These biosensors can be linked to smartphones in order to determine biomarkers and toxic products produced by bacteria, [48, 138, 139]. In the study developed by Zhang et al. (2015), a smartphone-based POCT system was developed to detect 2,4,6 trinitrotoluene (TNT) by electrochemical impedance. In this study, a SPE was modified with peptides to produce impedance responses to TNT. This system was able to detect TNT at concentrations below 1.0×10^{-6} mol L^{-1}. The specificity of the POCT built was efficient to differentiate TNT from other chemicals [140].

Electrochemical biosensors can be associated with injection systems in order to provide high performance in the detection of different analytes, since these systems contribute to the improvement, mainly, the sensitivity and analytical frequency.

3 Injection Systems Associated with Electrochemical Biosensors

The search for analytical methods with greater sensitivity, selectivity, reproducibility, and low-value-economic equipment, in addition to shorter analysis time constitutes a wide and constantly expanding field of research, mainly, in the area of Analytical Chemistry. For greater mechanization and increased robustness of electrochemical analysis systems, injection devices

can be implemented, such as Flow Injection Analysis Systems—FIA, Sequential Injection Analysis—SIA, and Batch Injection Analysis—BIA. These systems facilitate the transport of samples to the detector, providing several advantages during analyses, mainly low cost and high performance [141, 142]. The injection systems most commonly used in electrochemical analysis (FIA, SIA, and BIA) are briefly discussed below.

3.1 Flow Injection Analysis (FIA)

Flow Injection Analysis—FIA is a system widely explored in a large amount of analytical applications, providing simplicity of handling, low cost, use of versatile instrumentation, and greater precision, besides minimization of the waste of reagents and samples [142–144]. FIA was developed in 1975 by Ruzikca and Hansen [145] and this innovation was an important way for the automatic and accurate determination of several species in biological samples for clinical diagnosis [145, 146]. Initially, FIA was segmented, in which biological samples were transported to the spectrophotometric detector using bubbles to separate each injected sample. These bubbles were implemented in the system to decrease the dispersion of the samples and prevent contamination between successive experiments. However, these bubbles must be removed before detection and this can cause an increase in the analysis time, characterizing it as a major problem in a segmented FIA system. Over time, this segmented mode was gradually replaced by continuous flow in different applications [141, 144, 145].

Due to its efficiency and versatility, FIA has been extensively used in different detection systems in order to improve analytical performance in general [147]. This flow system can be defined as an automation process for analytical procedures. Its main function is to transport the sample within an analytical path to the detector, providing low detection limits and speed of analysis [148]. The most basic components of a FIA manifold are a propulsion system, an injection device, and a detection arrangement coupled to data analysis equipment. Its simplest mode of operation is that of a single line, as shown in Fig. 8.

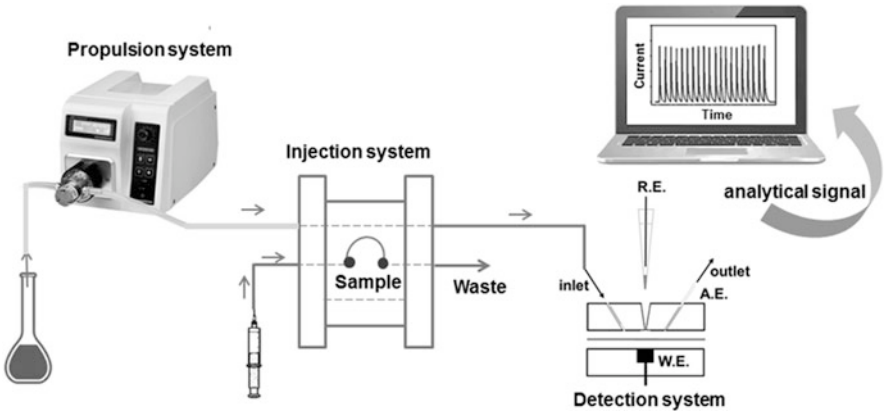

Fig. 8 Flow injection analysis manifold with amperometric detection: Propulsion system using peristaltic pump; Injection system using proportional injector; electrochemical cell constituted by W.E.—Working Electrode/A.E.—Auxiliary Electrode/R.E.—Reference Electrode.

The propulsion system has the function of boosting the fluid and promotes the continuous flow of solutions. In general, peristaltic pumps are preferred to propel the carrier fluids mainly due to the fact that they are multichannel devices. However, the peristaltic pumps produce pulsation of the flow (this process is called peristalsis) that occurs between rollers and tubes of its own pump, promoting noise and loss in sensitivity. Then, new alternatives have been developed and used to replace the peristaltic pump [141, 142, 149]. These include the use of the force of gravity [150– 153], piston or syringe pumps [154–156], pneumatic system driven by diaphragm pump [157, 158], or compressed gas [159], among others [160].

Moreira et al. (2014) developed a low-cost system with FIA and used gravity force to propel solutions and needles or metallic threads as sensors for amperometric detection. Therefore, the authors studied the behavior of $[Fe(CN)_6]^{3-}$ that has a wellestablished redox process, besides evaluating the stoichiometry of the compound formed by Cu^{2+} and EDTA and pH changes in the reaction between ascorbic acid and ferricyanide. According to the results, they developed a very satisfactory FIA system with particular emphasis on low cost and ease of handling [161].

Matos et al. (2001) used aquarium air pumps to propel solutions instead of peristaltic pumps. Aquarium pumps can withstand a pressure of 4 psi, equivalent to 0.28 bar, as well as it can be a simple and versatile way that allows continuous flow adjustment to achieve values of

up to 12.5 mL min^{-1}. According to the results, the authors observed that in tubes with an internal diameter of 0.8 mm for a very long reactor (300 cm) the flow reaches 8.0 mL min^{-1}, while tubes with a smaller internal diameter of 0.5 mm in long circuits will lead to lower flow rates. In this way, the electrochemical experiments were always carried out with the advantage of the absence of pulsation of the propelled fluid observed with peristaltic pumps. In summary, the authors have proposed an efficient and low-cost propellant system to drive and aspire to flow solutions [160].

Regarding the injection system in FIA, it serves to guarantee the insertion of a defined volume of the sample (sample loop generally situated between 10 and 200 μL) into a liquid carrier flowing through a tube with an internal diameter generally less than 1.0 mm. Moreover, this defined volume is gradually dispersed into the carrier by radial and axial diffusion and by convection [141, 161]. Initially, a hypodermic syringe (Fig. 9a) was used to insert samples into the flow system that was loaded until carried to the detector. During the evolution of methods and the sophistication of materials, the components of the FIA manifold were gradually improved, showing greater repeatability and less dependence on the operator. Among these, injectors became popular, in which the main ones are: the proportional injector (Fig. 9b) that was created by a group of researchers from CENA—USP/ Piracicaba, Brazil. Its operation is performed with the valve in the loading position, in which a defined volume is completed with the sample, and also in the discharge point, where the restricted volume in the loop is introduced in the carrier flow. Other types are the rotary valve (Fig. 9c), in which this valve is changed and the sample or carrier flow is directed to the detection system and the solenoid valves (Fig. 9d) that enable reproducible solution delivering in small volumes (for example, 10 μL) into the manifold [162, 163].

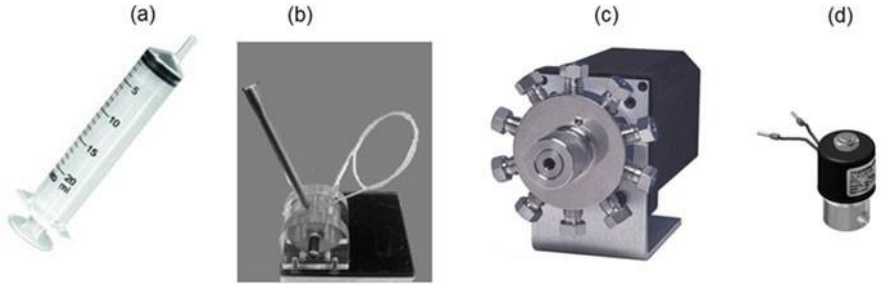

Fig. 9 Different ways for solution injection in FIA: Hypodermic syringe (a), Proportional injector (b), Rotary valve used in high-performance liquid chromatography (HPLC) (c), and Solenoid valve (d).

Aguiar et al. (2006) built a flow injection system with low operating cost and easy automation, aiming at the amperometric determination of iodide ions in commercial expectorant syrups. The method was carried out in an acid medium using the reaction of the iodide with nitrite ions. The propulsion system of this FIA system was performed by gravitational pressure at a flow rate of 4 mL min^{-1}. The aliquots of the samples and standard solutions were injected using a hypodermic syringe. As a result, the proposed method was fast (100 injections h^{-1}) and precise (RSD = 1.9%), with the detection of limit (LOD) calculated as 8.0×10^{-7} mol L^{-1} [164].

Dilgin et al. (2018) built a biosensor using electroanalytical techniques for glucose analysis, and the detection was performed by amperometry. For the construction of this sensor, a graphite electrode was modified by electropolymerization of polymethylene blue on its surface. To perform the FIA experiments, a singlechannel peristaltic pump and a sample injection rotary valve were used for the injection system. Polyethylene tubes (0.75 mm) were used to connect all parts of the arrangement. Thus, they obtained a glucose biosensor with a detection of limit (LOD) of 4.0 μmol L^{-1} [165].

FIA is a very versatile system and allows association with different detectors [166–169]. As already mentioned earlier in this chapter, electrochemical detection, when compared to other detection systems, can offer many advantages such as the simplicity of application and reduction of sample preparation steps, in addition to low instrumentation cost with high precision and sensitivity [142, 170, 171].

Tvorynska et al. (2019) performed amperometric experiments in association with flow injection system—FIA for the quantification of choline (Ch). In this study, enzymes were immobilized covalently with glutaraldehyde in mesoporous silica powder previously covered by NH_2 groups. The detection of Ch occurred through amperometric monitoring of the oxygen consumed during the enzymatic reaction, which had a direct proportion to the concentration of

Ch. The biosensor showed a linear range of concentration of 80–700 μmol L^{-1}, repeatability of 3.9%, in addition to high reproducibility for the detection of Ch [172].

Nikolaos et al. (2012) carried out studies involving the association between flow injection and potentiometric detection. They proposed a biosensor for the determination of uric acid manufactured by immobilizing uricase in stabilized lipid films, using as a transducer zinc oxide (ZnO) nanowires. Thus, they obtained a detection limit of 0.4 × 10-3 mol L^{-1} and good reproducibility (RSD lower than 5%) [173].

Chiriaco et al. (2019) proposed an impedimetric biosensor associated with FIA for the quantification of cholera toxin (CT). This system used two reaction chambers with eight detection areas for biorecognition among antibodies immobilized on the surface of gold electrodes. Standard tests for CT detection include the GM1 technique and the immobilization of antibodies on standard ELISA screening plates. A detection limit of less than 10 pmol L^{-1} was reached, thousands of times less than the lethal dose. The proposed biosensors presented a low price and fast response, besides allowing screening in crops, with clinical and medicinal applications [174].

Despite the FIA success described in the literature, there is a restriction regarding the use of these systems in industrial processes, due to the need for frequent maintenance of fluid transmission lines. Therefore, the need for a system designed to monitor different processes favored the emergence of sequential injection analysis (SIA) [175].

3.2 Sequencial Injection Analysis (SIA)

Sequential Injection Analysis—SIA was developed by Ruzicka and Marshall in 1990 [175], and presents the same important analytical characteristics as the FIA system, such as improvements in reproducibility, low consumption of samples and reagents, and minimal human interference. SIA presents advantages compared with FIA, between them the low need for maintenance of the SIA system, the lower consumption of reagents and samples, as well as greater robustness and stability, makes this system quite attractive [175, 176]. The main disadvantage is the price of its components. Figure 10 illustrates a typical SIA system, composed of a propulsion device (usually a syringe pump) and a precise injection valve (a

rotating selection valve), responsible for the controlled dispersion and control of the reaction times with high repeatability, so as for the transport to the detection system [177].

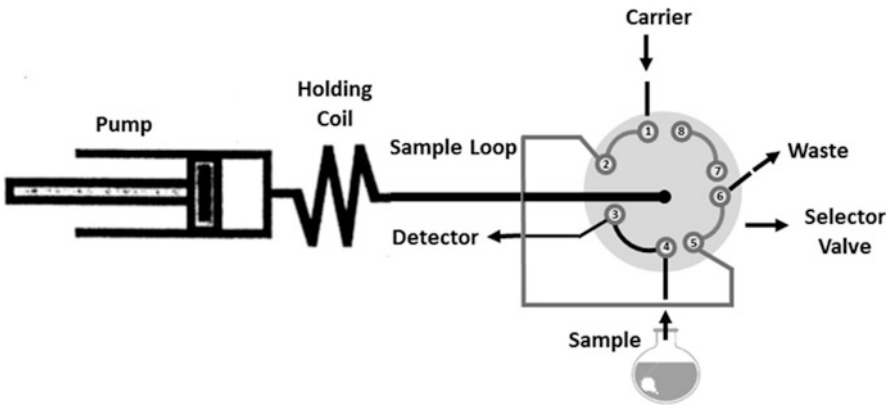

Fig. 10 Basic scheme of a SIA manifold with rotating selector valve consisting of eight ports.

In a typical SIA manifold (Fig. 10), samples and reagents are aspirated sequentially using a piston pump or a syringe pump, or even a peristaltic pump. Piston and syringe pumps provide greater precision in the aspirated or injected volumes. A rotary selector valve, which has many input channels, is used to select different solutions. The entire operation is controlled by a computer that monitors the synchronization between the pump and the valve. For carrying out an analysis, defined volumes of carrier and sample solutions are aspirated into the collector. After the position of the multichannel valve is changed and the flow direction is reversed, passing the solution to be pumped to the detector [176–178]. SIA has a low analytical frequency when compared to the FIA due to its operational characteristics. Additionally, some computer programming knowledge is required, making it a little more difficult to use for some electroanalysis users [176]. Figure 11 shows the popularity of FIA rather than SIA in association with electrochemical biosensors over the years.

Since its development, SIA has been used in the analysis of several types of samples, from food and pesticides to beverages, such as milk, juices, and wines. Applications involving the use of biosensors were also explored, although in smaller numbers than those involving FIA [141, 178]. Over the past 14 years, the number of papers involving the association between SIA and electrochemical biosensors was approximately 10. This small number of papers probably is proportional to the small number of SIA users.

In 2006, Staden et al. explored a SIA system to develop a carbon paste-based biosensor with amperometric detection for the simultaneous quantification of creatinine and creatine. According to the results, the proposed system can be used reliably for online detection of these chemical species in pharmaceutical products, with an analytical frequency of 34 samples per hour and RSD values better than 0.16% [178].

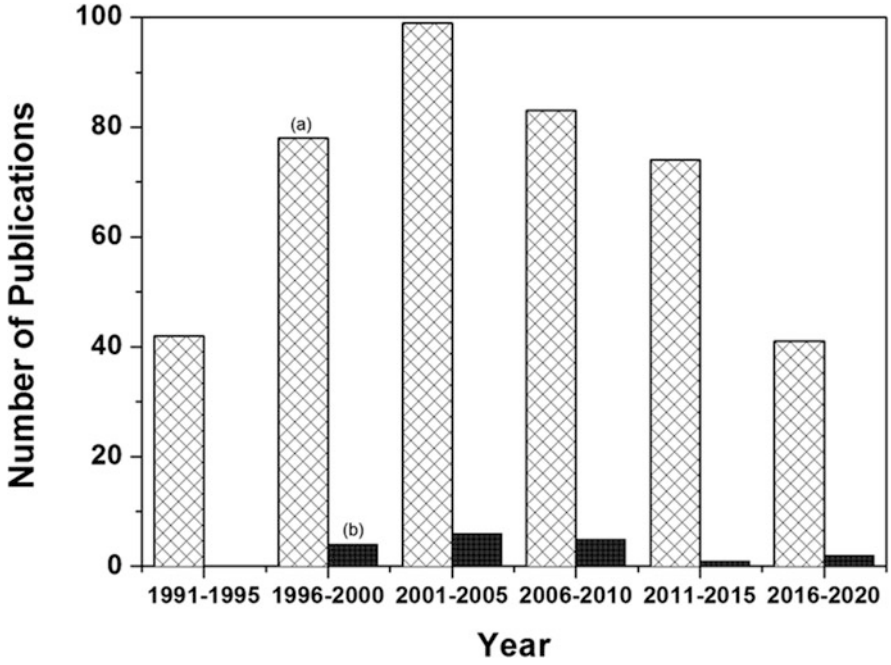

Fig. 11 Publications from the association between (a) Biosensors and FIA and (b) biosensors and SIA (Web of Sciense® database).

3.3 Batch Injection Analysis (BIA)

Batch Injection Analysis—BIA was developed by Wang and Taha in 1990, it is a tool which has been explored by some research groups as an option to perform, in a very simple way, quick analyzes. In BIA, an aliquot of the analyte solution is injected, using an automatic micropipette, in the central part of the working electrode, localized in the center of the bottom of the electrochemical cell, which was specially designed for this purpose (wall-jet cell) (Fig. 12a). In this experimental arrangement, the injection of the analyte produces a transient signal. The height or area of the peak is directly related to the concentration of the analyte (Fig. 12b) [141, 177].

Before the injection of the analyte, the cell is filled with electrolyte and the detection potential is applied. When the chosen potential is applied, initially the current is elevated (due to the charging of the electrical double-layer process). This current decreases exponentially and after a certain time, the signal tends to be very low (low microamperes or even nanoamperes) corresponding to the baseline. When the analyte is injected, an increase in current occurs due to the redox process. During the injection, the current generated increases rapidly and remains constant and maximum for a short time, and when the injection ends, the current drops very rapidly. The signal decreases to almost the same minimal signal that the one that was recorded before the injection. Even having now, the analyte dispersed in the electrolyte, its contribution is very small compared with the signal generated by the injection of the analyte. This aspect was not clear at the beginning of the studies using BIA. In the first studies, cells with volumes of about 1 L were used. Over time, it was learned that the major difference in transport was represented by the injection of the sample (centimeters or even meters per second) and diffusion (somewhere around 10-6 cm^{-2}). As equilibrium is reached, the current stabilizes again until another sample or standard aliquot is injected on the electrode surface, leaving only a residual current in the system [141, 177, 179]. Thus, the transient signal is obtained during experiments (Fig. 12b).

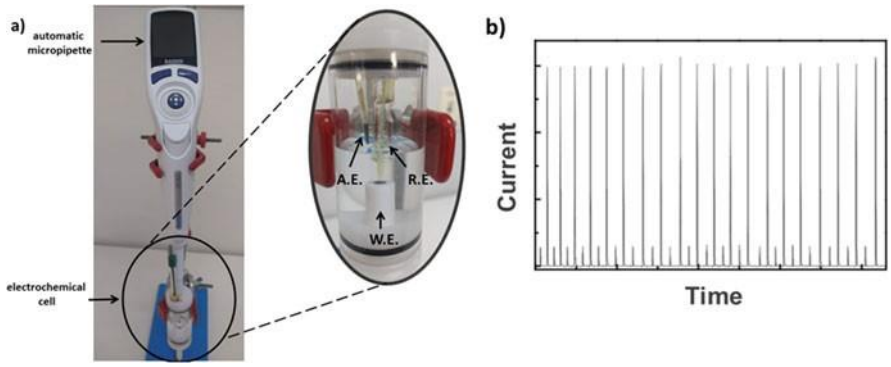

Fig. 12 (a) Representation of a BIA system with amperometric detection and in the detail the electrochemical cell constituted by: W.E.—Working Electrode/A.E.—Auxiliary Electrode/R.E.— Reference Electrode. (b) Analytical signals from alternate injections of 1.0×10^{-6} mol L^{-1} (smaller peaks) and 1.0×10^{-5} mol L^{-1} (larger peaks) ferricyanide standard solution during experiments of BIA with amperometric detection.

The BIA system presents several advantages, such as the elimination of typical problems related to valves and pumps in the FIA or SIA systems, high sensitivity, greater analytical frequency, low consumption of electrolytic solution, and portability [180].

Despite the advantages of BIA, so far in the literature, there is no research on the development of biosensors in agricultural and veterinary applications that has yet adopted this system. However, there are some studies on electrochemical biosensors in association with BIA for the determination of glucose in saliva and urine [181] and hydroquinone in pharmaceutical samples [182], among others.

Baronas et al. in 2004 explored the association of an electrochemical biosensor within batch and flow injection modes. Chemometric models of the proposed biosensor were built to simulate amperometric responses for mixtures of compounds. For this, the authors used principal component analysis—PCA to optimize the calibration data, as well as used artificial neural networks to differentiate molecules or mixtures and predict the concentration of each molecule. The amperometric biosensor in association with both flow injection and batch analysis showed a 99% prediction of each component [183].

The biosensor is an important device to diagnose, and, therefore, assist in the inspection of contaminants in soils, water, and food, in the monitoring of epidemics that are a serious cause of death of animals, among other applications. The next section will cover biosensor applications in association with electroanalytical techniques exploring agriculture and veterinary medicine samples.

4 Electrochemical Biosensors Applied in Agricultural and Veterinary Matrices

Toxic agrochemicals are used in crops to prevent or control the development of weeds, insect infestation pests, and diseases that can cause harm from the birth, growth, and production of the plant, or during storage, processing, or transport of food. However, pesticides can contaminate the environment with toxic effects on humans. Seeking to determine toxic agrochemicals, such as triazine and urea, Buonasera et al. (2010) proposed changes in the surface of carbon electrodes with photosynthetic organisms (S. oleracea thylakoid) for the manufacture of sensitive and low-cost biosensors. The developed device was applied in the quantification of different triazinic and ureic herbicides using amperometry and fluorescence

spectroscopy as detection systems. During amperometric experiments in dynamic mode (FIA), a working potential of +0.20 V (vs. Ag/AgCl) was used and the current signal decreased with increasing concentration (from 1.0×10^{-8} mol L^{-1} to 1.0×10^{-10} mol L^{-1}) of herbicides, for example, atrazine, diuron, linuron, or terbuthylazine [184].

Gramberg et al. (2012) reported an approach using a membrane containing antibodies for the determination of cherry leaf roll/CLRV virus and tobacco mosaic virus/TMV. The detection principle of the bacteria biosensors was based on the measurement of changes in the membrane potentials as a result of bindings between virus and antibody. With this sensor, the limit of detection—LOD of 1 pg mL-1 was calculated for both TMV and CLRV [185].

Yang et al. (2014) proposed a sensitive biosensor of Magnaporthe oryzae in rice plants, using amperometric detection M. oryzae is an extremely effective plant pathogen because it can reproduce sexually or asexually, and it is very destructive to rice fields. The authors used a biochemical marker from M. oryzae's chitinases (Mgchi) and as a recognition probe a rice cDNA from Oryza sativa that encodes lectin related to mannose jacalinization (Os-mbl). Moreover, for the construction of the electrochemical biosensor, they modified a gold electrode with nanoparticles of palladium magnetic spheres in order to increase the sensitivity. The amperometric studies were performed using a working potential of +0.2 V (vs. Ag/AgCl). The proposed sensor allowed reaching the detection of 6.1×10^{-12} mol L^{-1} for Mgchi [186].

Tarasov et al. (2015) explored the capabilities of a biosensor with potentiometric detection for rapid analysis of the main viral pathogen in bovine respiratory diseases, bovine virus-1 (BHV-1). During the construction of this sensor for application in bovine serum samples, the viral protein gE of the bovine herpes virus-1 (BHV-1) was immobilized on the gold surface to capture the BHV-1 antibody. In comparison to ELISA, it provided results much faster (~10 min vs 19 h) with high sensitivity and selectivity [187].

Cesarino et al. (2012) built an amperometric biosensor for the detection of carbamates in fruits and vegetables. The authors modified a glassy carbon electrode with a core-shell structure of carbon nanotubes and polyaniline for subsequent immobilization of acetylcholinesterase. During the experiments, values of LOD of 1.40 and 0.95 μmol L^{-1} were calculated for the carbaryl and methomyl toxins, respectively [188].

Crew et al. (2011) reported the use of electrochemical sensors for the determination of various organophosphates (such as chlorpyrifos-oxon, dichlorvos, naloxone, among others) in environmental and food samples. For this, six acetylcholinesterase enzymes were immobilized in gold arrays. These sensors were produced based on screen-printing technology for large-scale manufacturing and low cost, as well as they incorporated a neural network program. These organophosphates were determined by amperometry and a working potential of 0.0 V (vs. Ag/AgCl), with measurements within 10 s, was used. In this system, it was possible to obtain a wide linear range from 1.0×10^{-5} mol L^{-1} to 1.0×10^{-9} mol L^{-1} in phosphate buffer 0.05 mol L^{-1} (pH 8.0) [189].

Gong et al. (2013) developed a biosensor with amperometric detection associated with Flow Injection Analysis to detect organophosphate pesticides in environmental and food samples. During experiments, glassy carbon electrode was modified with inorganic layered double hydroxides and acetylcholinesterase. Next, it was dipped into saturated glutaraldehyde to enhance the stability of the sensor. The pesticide Methyl parathion-MP was used as a model and biosensor inhibition. The response of this sensor was linear in two distinct ranges from 0.002 μg mL^{-1} to 0.3 μg mL^{-1} and 0.3 μg mL^{-1} to 4.0 μg mL^{-1}, with correlation coefficients of 0.999, for both two ranges. Recovery analyzes were made from different concentrations of MP in cabbage, apple, and garlic samples and recoveries ranged from 97.2 to 104.6% [190].

Luo et al. (2010) functionalized the surface of nitrocellulose nanofibers with silver to construct a working electrode that was modified with appropriate antibody (with formation of sandwich complex) for bovine pathogenic detection. During conductometric experiments with this biosensor, it was possible to obtain detection limits of 61 CFU/mL and 103 CCID/mL for Escherichia coli bacterium and bovine viral diarrhea virus, respectively [191].

Ma et al. (2008) built an electrochemical biosensor from a gold disk electrode modified with self-assembled monolayers of p-aminothiophenol and nano-SiO_2 for immobilization and hybridization of DNA. This biosensor was constructed for detecting phosphinothricin acetyltransferase gene (PAT), which is an important indicator of transgenic plants. The impedance results indicated a high sensitivity of the DNA biosensor for the wide concentration range of the PAT, varying from 1.0×10^{-11} mol L^{-1} to 1.0×10^{-6} mol L^{-1} [192].

Song et al. (2011) developed a voltammetric sensor to determine carbaryl, an extremely toxic pesticide. For the construction of this sensor, a glassy carbon electrode (GCE) modified with chitosan and Prussian blue film was used, followed by the immobilization of acetylcholinesterase-AChE. The voltammetric results indicated that the changes in the concentration of the carbaryl were proportional to the inhibition of the pesticide on the action of AChE, with a correlation coefficient of 0.999 and a limit of detection—LOD calculated as 3.0 nmol L^{-1} [193].

Muhammad-Tahir et al. (2005) developed a conductometric biosensor for the detection of bovine viral diarrhea virus (BVDV) and other agents related to agricultural bioterrorism, using culture media and blood serum samples. The developed biosensor showed good sensitivity to a concentration of 103 CCID/mL of BVDV antigens. The authors indicated that it is necessary to make modifications in the proposed biosensor to obtain a rapid device that identifies outbreaks of infectious diseases in the livestock population in an agricultural terrorism event [194].

Wei et al. (2015) proposed an acetylcholinesterase-AChE biosensor for the determination of the dichlorvos pesticide in lettuce leaves. This biosensor was manufactured using a boron-doped diamond electrode. Next, this electrode was modified with gold nanoparticles grown in porous carbon material and ionic liquids to improve the dispersion and subsequently immobilization of AChE. During experiments using the differential pulse voltammetry technique, it was possible to observe linear responses in the interval of 10^{-6} g L^{-1} –10^{-10} g L^{-1} and a limit of detection—LOD of 6.61×10^{-11} g L^{-1} (2.99×10^{-13} mol L^{-1}) [195].

Durrieu et al. (2011) developed optical and conductometric biosensors based on the measurement of the metabolic activities of marine algae for quantification of pesticides (for example, diuron and glyphosate) capable of contaminating southern France. Algal suspension was immobilized on two identical pairs of interdigitated gold electrodes using the self-assembled monolayers during the construction of a conductometric sensor. The activity of the D. tertiolecta esterase algae varied in presence of diuron, leading to a change in the conductivity signal due to a decrease of ionic species in solution. One of the diuron pesticide inhibition results showed a residual activity of esterase algae of about 30% [196].

5 Concluding Remarks

In this chapter, a general view about electrochemical biosensors and the different forms of their utilization associated with different techniques, under quiescent and under flowing processes, was presented. The different electrochemical techniques covered in this chapter allow the analyst to choose the most suitable technique to be used. The association of voltammetric techniques with injection analysis techniques (FIA, SIA, and BIA) allows faster analyzes, with greater precision and more importantly, with enhanced sensitivity, thanks to the significant increase in the transport of the electroactive species to the surface of the working electrode. Besides the electrochemical methods and the flowing systems, many of the electrochemical biosensors are modified to improve sensitivity and selectivity according to the analyte and type of sample, among others. Increasingly, the technology developed based on electrochemical biosensors is present in the life of the population directly or indirectly. Proof of this is the growing advances in the development of POCT that allows the rapid diagnosis of diseases and contaminants via smartphones. Significant advances are also noted in the monitoring, through electrochemical biosensors, of environmental contaminants from activities that affect the soil, water, and food, among others. Veterinary applications with electrochemical biosensors are also found in this chapter, presenting potential for the residual analysis of veterinary drugs, pathogens, and other compounds in complex matrices (blood, urine, feces, and so on). In this perspective, the potentiality of the electrochemical biosensors for applications in agricultural and veterinary areas is just starting. It can be expected that more and more studies will be carried out, seeking to quickly and effectively meet agricultural and veterinary needs with selective and sensitive electrochemical devices.

Acknowledgments

The authors gratefully thank the financial support from Brazilian Research Founding Agencies FAPESP (projects 2017/13137-5 and 2014/50867-3), FAPEMIG, CNPq (project 311847-2018-8), CAPES (finance code 001), and EMBRAPA-CAFÉ (20/2018-code 145).

References

1. Kundu M, Krishnan P, Kotnala RK, Sumana G. Recent developments in biosensors to combat agricultural challenges and their future prospects. Trends Food Sci Technol. 2019;88:157–78.

2. Noori JS, Mortensen J, Geto A. Recent development on the electrochemical detection of selected pesticides: a focused review. Sensors (Switzerland). 2020;20(8):2221. https://doi.org/10.3390/s20082221.

3. Chiarello M, Graeff RN, Minetto L, et al. Determinação de agrotóxicos na água e sedimentos por HPLC-HRMS e sua relação com o uso e ocupação do solo. Quim Nova. 2017;40:158–65.

4. Meira APG. Vista do Técnicas de análise de resíduos de agrotóxicos em alimentos de origem vegetal_ uma revisão.pdf. Segur Aliment Nutr. 2015;22:766–77.

5. Chauhan N, Narang J, Jain U. Amperometric acetylcholinesterase biosensor for pesticides monitoring utilising iron oxide nanoparticles and poly(indole-5-carboxylic acid). J Exp Nanosci. 2016;11:111–22.

6. Fang Y, Ramasamy RP. Current and prospective methods for plant disease detection. Biosensors. 2015;5:537–61.

7. Du X, Zhou J. Application of biosensors to detection of epidemic diseases in animals. Res Vet Sci. 2018;118:444–8.

8. Schmidt V, de Itapema Cardoso MR. Sobrevivência e perfil de resistência a antimicrobianos de Salmonella sp. isoladas em um sistema de tratamento de dejetos de suínos. Ciênc Rural. 2003;33:881–8.

9. Gaudin V. Advances in biosensor development for the screening of antibiotic residues in food products of animal origin—a comprehensive review. Biosens Bioelectron. 2017;90:363–77.

10. Pinto GMF, da Silva KR, de Pereira RFAB. Study of residential expired medicines disposal in Paulínia (SP) area, Brazil. Eng Sanit Ambient. 2014;19:219–24.

11. Velasco-Garcia MN, Mottram T. Biosensor technology addressing agricultural problems. Biosyst Eng. 2003;84:1–12.

12. Griesche C, Baeumner AJ. Biosensors to support sustainable agriculture and food safety. TrAC Trends Anal Chem. 2020;128:115906. https://doi.org/10.1016/j.trac.2020.115906.

13. Rezaei B, Irannejad N. Chapter 2: Electrochemical detection techniques in biosensor applications. In: Ensafi AABT-EB, editor. Elsevier; 2019. p. 11–43.

14. Ensafi AA. Chapter 1: An introduction to sensors and biosensors. In: Ensafi AABT-EB, editor. Elsevier; 2019. p. 1–10.

15. Verma N, Bhardwaj A. Biosensor technology for pesticides—a review. Appl Biochem Biotechnol. 2015;175:3093–119.

16. Tormin T, Cunha R, Silva R, et al. Combination of screen-printed electrodes and batch injection analysis: a simple, robust, high-throughput, and portable electrochemical system. Sensors Actuators B Chem. 2014;202:93–8.

17. Titoiu AM, Necula-Petrareanu G, Visinescu D, et al. Flow injection enzymatic biosensor for aldehydes based on a Meldola Blue-Ni complex electrochemical mediator. Microchim Acta. 2020;187:550. https://doi.org/10.1007/s00604-020-04477-3.

18. Taleat Z, Khoshroo A, Mazloum-Ardakani M. Screen-printed electrodes for biosensing: a review (2008-2013). Microchim Acta. 2014;181:865–91.

19. Antony N, Unnikrishnan L, Mohanty S, Nayak SK. The imperative role of polymers in enzymatic cholesterol biosensors—an overview. Polym Technol Mater. 2019;58:1713–41.

20. Parlak O, Richter-Dahlfors A. A bacterial sensing and biofilm monitoring for infection diagnostics. Macromol Biosci. 2020;20:2000129. https://doi.org/10.1002/mabi.202000129.

21. Cesewski E, Johnson BN. Electrochemical biosensors for pathogen detection. Biosens Bioelectron. 2020;159:112214. https://doi.org/10.1016/j.bios.2020.112214.

22. Thevenot DR, Toth K, Durst RA, Wilson GS. Electrochemical biosensors: recommended definitions and classification. Biosens Bioelectron. 2001;16:121–31.

23. Yoo E-H, Lee S-Y. Glucose biosensors: an overview of use in clinical practice. Sensors. 2010;10:4558–76.

24. Mandpe P, Prabhakar B, Gupta H, Shende P. Glucose oxidase-based biosensor for glucose detection from biological fluids. Sens Rev. 2020;40:497–511.

25. Shende P, Sahu P, Gaud R. A technology roadmap of smart biosensors from conventional glucose monitoring systems. Ther Deliv. 2017;8:411–23.

26. Takke A, Shende P. Non-invasive biodiversified sensors: a modernized screening technology for cancer. Curr Pharm Des. 2019;25:4108–20.

27. Ferri S, Sode K. Biomolecular engineering of biosensing molecules—the challenges in creating sensing molecules for glycated protein biosensing. Electrochemistry. 2012;80:293–8.

28. Clark LC, Lyons C. Electrode systems for continuous monitoring in cardiovascular surgery. Ann N Y Acad Sci. 1962;102:29–45.

29. Mustafa F, Andreescu S. Nanotechnology-based approaches for food sensing and packaging applications. RSC Adv. 2020;10:19309–36.

30. Lv L, Wang X. Recent advances in ochratoxin a electrochemical biosensors: recognition elements, sensitization technologies, and their applications. J Agric Food Chem. 2020;68: 4769–87.

31. Sanati A, Jalali M, Raeissi K, et al. A review on recent advancements in electrochemical biosensing using carbonaceous nanomaterials. Microchim Acta. 2019;186:773. https://doi.org/10.1007/s00604-019-3854-2.

32. Khanmohammadi A, Jalili Ghazizadeh A, Hashemi P, et al. An overview to electrochemical biosensors and sensors for the detection of environmental contaminants. J Iran Chem Soc. 2020;17:2429–47.

33. Zhang R, Belwal T, Li L, et al. Nanomaterial-based biosensors for sensing key foodborne pathogens: advances from recent decades. Compr Rev Food Sci Food Saf. 2020;19:1465–87.

34. Bandodkar AJ, Wang J. Non-invasive wearable electrochemical sensors: a review. Trends Biotechnol. 2014;32:363–71.

35. Kaisti M. Detection principles of biological and chemical FET sensors. Biosens Bioelectron. 2017;98:437–48.

36. Yang X, Cheng H. Recent developments of flexible and stretchable electrochemical biosensors. Micromachines. 2020;11:243. https://doi.org/10.3390/mi11030243.

37. Justino CIL, Freitas AC, Pereira R, et al. Recent developments in recognition elements for chemical sensors and biosensors. TrAC Trends Anal Chem. 2015;68:2–17.

38. Armstrong FA. Recent developments in dynamic electrochemical studies of adsorbed enzymes and their active sites. Curr Opin Chem Biol. 2005;9:110–7.

39. Alvarez-Malmagro J, García-Molina G, De Lacey AL. Electrochemical biosensors based on membrane-bound enzymes in biomimetic configurations. Sensors (Switzerland). 2020;20:1– 17.

40. Kucherenko IS, Soldatkin OO, Dzyadevych SV, Soldatkin AP. Electrochemical biosensors based on multienzyme systems: main groups, advantages and limitations—a review. Anal Chim Acta. 2020;1111:114–31.

41. Fatibello-Filho O, Lupetti KO, Vieira IC. Chronoamperometric determination of paracetamol using an avocado tissue (Persea americana) biosensor. Talanta. 2001;55:685–92.

42. Rahimi-Mohseni M, Raoof JB, Aghajanzadeh TA, Ojani R. Rapid determination of phenolic compounds in water samples: development of a paper-based nanobiosensor modified with functionalized silica nanoparticles and potato tissue. Electroanalysis. 2019;31:2311–8.

43. Sezgintrk MK, Koca HB, Özben YS, Dinçkaya E. A biosensor based on zucchini (Cucurbita Pepo L.) homogenate as a biorecognition layer for ascorbic acid determination. Artif Cells Blood Substit Immobil Biotechnol. 2010;38:215–21.

44. Sekar NC, Ge L, Mousavi Shaegh SA, et al. A mediated turnip tissue paper-based amperometric hydrogen peroxide biosensor. Sensors Actuators B Chem. 2015;210:336–42.

45. Lata S, Pundir CS. L-amino acid biosensor based on L-amino acid oxidase immobilized onto NiHCNFe/c-MWCNT/PPy/GC electrode. Int J Biol Macromol. 2013;54:250–7.

46. Lakhin AV, Tarantul VZ, Gening LV. Aptamers: problems, solutions and prospects. Acta Nat. 2013;5:34–43.

47. Reverdatto S, Burz DS, Shekhtman A. Peptide aptamers: development and applications. Curr Top Med Chem. 2015;15:1082–101.

48. Kaur N, Prabhakar N. Current scenario in organophosphates detection using electrochemical biosensors. TrAC Trends Anal Chem. 2017;92:62–85.

49. Stoltenburg R, Reinemann C, Strehlitz B. SELEX-A (r)evolutionary method to generate highaffinity nucleic acid ligands. Biomol Eng. 2007;24:381–403.

50. Villalonga A, Vegas B, Paniagua G, et al. Amperometric aptasensor for carcinoembryonic antigen based on a reduced graphene oxide/gold nanoparticles modified electrode. J Electroanal Chem. 2020;877:114511. https://doi.org/10.1016/j.jelechem.2020.114511.

51. Habermuller L, Mosbach M, Schuhmann W. Electron-transfer mechanisms in amperometric biosensors. Fresenius J Anal Chem. 2000;366:560–8.

52. Pearson JE, Gill A, Vadgama P. Analytical aspects of biosensors. Ann Clin Biochem. 2000;37: 119–45.

53. Chillawar RR, Tadi KK, Motghare RV. Voltammetric techniques at chemically modified electrodes. J Anal Chem. 2015;70:399–418.

54. Ghorbani F, Abbaszadeh H, Mehdizadeh A, et al. Biosensors and nanobiosensors for rapid detection of autoimmune diseases: a review. Microchim Acta. 2019;186:838. https://doi.org/ 10.1007/s00604-019-3844-4.

55. Felix FS, Yamashita M, Angnes L. Epinephrine quantification in pharmaceutical formulations utilizing plant tissue biosensors. Biosens Bioelectron. 2006;21:2283–9.

56. Felix FS, Baccaro ALB, Angnes L. Disposable voltammetric immunosensors integrated with microfluidic platforms for biomedical, agricultural and food analyses: a review. Sensors (Basel). 2018;18:4124. https://doi.org/10.3390/s18124124.

57. Felix FS, Angnes L. Electrochemical immunosensors—a powerful tool for analytical applications. Biosens Bioelectron. 2018;102:470–8.

58. Kokkinos C, Economou A. Recent advances in voltammetric, amperometric and ion-selective (bio)sensors fabricated by microengineering manufacturing approaches. Curr Opin Electrochem. 2020;23:21–5.

59. Ginsberg BH. Factors affecting blood glucose monitoring: sources of errors in measurement. J Diabetes Sci Technol. 2009;3:903–13.

60. Perumal V, Hashim U. Advances in biosensors: principle, architecture and applications. J Appl Biomed. 2014;12:1–15.

61. Anusha JR, Kim BC, Yu K-H, Raj CJ. Electrochemical biosensing of mosquito-borne viral disease, dengue: a review. Biosens Bioelectron. 2019;142:111511. https://doi.org/10.1016/j. bios.2019.111511.

62. Prajapati DG, Kandasubramanian B. Progress in the development of intrinsically conducting polymer composites as biosensors. Macromol Chem Phys. 2019;220:1800561. https://doi.org/ 10.1002/macp.201800561.

63. Rogers KR. Principles of affinity-based biosensors. Mol Biotechnol. 2000;14:109–29.

64. Marco MP, Barcelo D. Environmental applications of analytical biosensors. Meas Sci Technol. 1996;7:1547–62.

65. Sabu C, Henna TK, Raphey VR, et al. Advanced biosensors for glucose and insulin. Biosens Bioelectron. 2019;141:111201. https://doi.org/10.1016/j.bios.2019.03.034.

66. Pundir CS, Malik M, Chaudhary R. Quantification of pyruvate with special emphasis on biosensors: a review. Microchem J. 2019;146:1102–12.

67. Neelam, Chhillar AK, Rana JS. Enzyme nanoparticles and their biosensing applications: a review. Anal Biochem. 2019;581:113345. https://doi.org/10.1016/j.ab.2019.113345.

68. D'Orazio P. Biosensors in clinical chemistry. Clin Chim Acta. 2003;334:41–69.

69. Sadeghi SJ. Amperometric biosensors. In: Encyclopedia of biophysics. 2013. https://doi.org/ 10.1007/978-3-642-16712-6.

70. Gerard M, Chaubey A, Malhotra BD. Application of conducting polymers to biosensors. Biosens Bioelectron. 2002;17:345–59.

71. Bartlett PN, Whitaker RG. Electrochemical immobilization of enzymes. 2. Glucose-oxidase immobilized in poly-n-methylpyrrole. J Electroanal Chem. 1987;224:37–48.

72. Umana M, Waller J. Protein-modified electrodes—the glucose-oxidase polypyrrole system. Anal Chem. 1986;58:2979–83.

73. Hammerle M, Schuhmann W, Schmidt HL. Amperometric polypyrrole enzyme electrodes— effect of permeability and enzyme location. Sensors Actuators B Chem. 1992;6:106–12.

74. Zhang P, Sun T, Rong S, et al. A sensitive amperometric AChE-biosensor for organophosphate pesticides detection based on conjugated polymer and Ag-rGO-NH2 nanocomposite. Bioelectrochemistry. 2019;127:163–70.

75. Ren Q-Q, Yang F, Ren W, et al. Amperometric biosensor based on coimmobilization of multiwalled carbon nanotubes and horseradish peroxidase-gold nanocluster bioconjugates for detecting H2O2. J Nanomater. 2020;2020:1. https://doi.org/10.1155/2020/9627697.

76. Christopher FC, Kumar PS, Christopher FJ, et al. Recent advancements in rapid analysis of pesticides using nano biosensors: a present and future perspective. J Clean Prod. 2020;269: 122356. https://doi.org/10.1016/j.jclepro.2020.122356.

77. Lan L, Yao Y, Ping J, Ying Y. Recent advances in nanomaterial-based biosensors for antibiotics detection. Biosens Bioelectron. 2017;91:504–14.

78. Wang G, Wang Y, Chen L, Choo J. Nanomaterial-assisted aptamers for optical sensing. Biosens Bioelectron. 2010;25:1859–68.

79. Wang Y, Qu K, Tang L, et al. Nanomaterials in carbohydrate biosensors. TrAC Trends Anal Chem. 2014;58:54–70.

80. Sehit E, Altintas Z. Significance of nanomaterials in electrochemical glucose sensors: an updated review (2016-2020). Biosens Bioelectron. 2020;159:112165. https://doi.org/10.1016/j.bios.2020.112165.

81. Pirzada M, Altintas Z. Nanomaterials for healthcare biosensing applications. Sensors (Switzerland). 2019;19:5311. https://doi.org/10.3390/s19235311.

82. Katz E, Willner I. Biomolecule-functionalized carbon nanotubes: applications in nanobioelectronics. ChemPhysChem. 2004;5:1084–104.

83. Torrinha Á, Oliveira TMBF, Ribeiro FWP, et al. Application of nanostructured carbon-based electrochemical (Bio)sensors for screening of emerging pharmaceutical pollutants in waters and aquatic species: a review. Nanomaterials. 2020;10:1–29.

84. Palomar Q, Gondran C, Lellouche J-P, et al. Functionalized tungsten disulfide nanotubes for dopamine and catechol detection in a tyrosinase-based amperometric biosensor design. J Mater Chem B. 2020;8:3566–73.

85. Ramonas E, Ratautas D, Dagys M, et al. Highly sensitive amperometric biosensor based on alcohol dehydrogenase for determination of glycerol in human urine. Talanta. 2019;200:333– 9.

86. Ehtesabi H. Carbon nanomaterials for salivary-based biosensors: a review. Mater Today Chem. 2020;17:100342. https://doi.org/10.1016/j.mtchem.2020.100342.

87. Mannoor MS, Tao H, Clayton JD, et al. Graphene-based wireless bacteria detection on tooth enamel. Nat Commun. 2012;3:763. https://doi.org/10.1038/ncomms1767.

88. Jiang Z, Feng B, Xu J, et al. Graphene biosensors for bacterial and viral pathogens. Biosens Bioelectron. 2020;166:112471. https://doi.org/10.1016/j.bios.2020.112471.

89. Justino CIL, Gomes AR, Freitas AC, et al. Graphene based sensors and biosensors. TrAC Trends Anal Chem. 2017;91:53–66.

90. Song N-N, Wang Y-Z, Yang X-Y, et al. A novel electrochemical biosensor for the determination of dopamine and ascorbic acid based on graphene oxide/poly(aniline-co-thionine) nanocomposite. J Electroanal Chem. 2020;873:114352. https://doi.org/10.1016/j.jelechem. 2020.114352.

91. Sozer N, Kokini JL. Nanotechnology and its applications in the food sector. Trends Biotechnol. 2009;27:82–9.

92. Cho I-H, Kim DH, Park S. Electrochemical biosensors: perspective on functional nanomaterials for on-site analysis. Biomater Res. 2020;24:6. https://doi.org/10.1186/s40824-019-0181-y.

93. Kerman K, Saito M, Tamiya E, et al. Nanomaterial-based electrochemical biosensors for medical applications. TrAC Trends Anal Chem. 2008;27:585–92.

94. Kucherenko IS, Soldatkin OO, Kucherenko DY, et al. Advances in nanomaterial application in enzyme-based electrochemical biosensors: a review. Nanoscale Adv. 2019;1:4560–77.

95. Hondred JA, Breger JC, Garland NT, et al. Enhanced enzymatic activity from phosphotriesterase trimer gold nanoparticle bioconjugates for pesticide detection. Analyst. 2017;142:3261–71.

96. Chiang H-C, Wang Y, Zhang Q, Levon K. Optimization of the electrodeposition of gold nanoparticles for the application of highly sensitive, label-free biosensor. Biosensors. 2019;9: 50. https://doi.org/10.3390/bios9020050.

97. Li Y, Sella C, Lemaître F, et al. Highly sensitive platinum-black coated platinum electrodes for electrochemical detection of hydrogen peroxide and nitrite in microchannel. Electroanalysis. 2013;25:895–902.

98. Rismetov B, Ivandini TA, Saepudin E, Einaga Y. Electrochemical detection of hydrogen peroxide at platinum-modified diamond electrodes for an application in melamine strip tests. Diam Relat Mater. 2014;48:88–95.

99. Wang B, Wen X, Chiou P-Y, Maidment NT. Pt nanoparticle-modified carbon fiber microelectrode for selective electrochemical sensing of hydrogen peroxide. Electroanalysis. 2019;31: 1641–5.

100. Hou L, Huang Y, Hou W, et al. Modification-free amperometric biosensor for the detection of wild-type p53 protein based on the in situ formation of silver nanoparticle networks for signal amplification. Int J Biol Macromol. 2020;158:580–6.

101. Medyantseva EP, Brusnitsyn DV, Varlamova RM, et al. Hyperbranched polyesterpolyols as components of amperometric monoamine oxidase biosensors based on electrodes modified with nanomaterials for determination of antidepressants. Russ J Appl Chem. 2017;90:97–105.

102. Cho I-H, Lee J, Kim J, et al. Current technologies of electrochemical immunosensors: perspective on signal amplification. Sensors (Switzerland). 2018;18:207. https://doi.org/10. 3390/s18010207.

103. Akbarzadeh A, Samiei M, Davaran S. Magnetic nanoparticles: preparation, physical properties, and applications in biomedicine. Nanoscale Res Lett. 2012;7:144. https://doi.org/ 10.1186/1556-276X-7-144.

104. Reddy LH, Arias JL, Nicolas J, Couvreur P. Magnetic nanoparticles: design and characterization, toxicity and biocompatibility, pharmaceutical and biomedical applications. Chem Rev. 2012;112:5818–78.

105. Rocha-Santos TAP. Sensors and biosensors based on magnetic nanoparticles. TrAC Trends Anal Chem. 2014;62:28–36.

106. Gao L, Fan K, Yan X. Iron oxide nanozyme: a multifunctional enzyme mimetic for biomedical applications. Theranostics. 2017;7:3207–27.

107. Pakapongpan S, Poo-arporn RP. Self-assembly of glucose oxidase on reduced graphene oxidemagnetic nanoparticles nanocomposite-based direct electrochemistry for reagentless glucose biosensor. Mater Sci Eng C. 2017;76:398–405.

108. Fatima B, Hussain D, Bashir S, et al. Catalase immobilized antimonene quantum dots used as an electrochemical biosensor for quantitative determination of H2O2 from CA-125 diagnosed ovarian cancer samples. Mater Sci Eng C. 2020;117:111296. https://doi.org/10.1016/j.msec. 2020.111296.

109. Shah J, Wilkins E. Electrochemical biosensors for detection of biological warfare agents. Electroanalysis. 2003;15:157–67.

110. Jaffari SA, Turner APF. Recent advances in amperometric glucose biosensors for in-vivo monitoring. Physiol Meas. 1995;16:1–15.

111. Luppa PB, Sokoll LJ, Chan DW. Immunosensors—principles and applications to clinical chemistry. Clin Chim Acta. 2001;314:1–26.

112. Jakhar S, Pundir CS. Preparation, characterization and application of urease nanoparticles for construction of an improved potentiometric urea biosensor. Biosens Bioelectron. 2018;100: 242–50.

113. Koncki R. Recent developments in potentiometric biosensors for biomedical analysis. Anal Chim Acta. 2007;599:7–15.

114. Ding J, Qin W. Recent advances in potentiometric biosensors. TrAC Trends Anal Chem. 2020;124:115803. https://doi.org/10.1016/j.trac.2019.115803.

115. Buhlmann P, Pretsch E, Bakker E. Carrier-based ion-selective electrodes and bulk optodes. 2. Ionophores for potentiometric and optical sensors. Chem Rev. 1998;98:1593–687.

116. Bakker E, Buhlmann P, Pretsch E. Carrier-based ion-selective electrodes and bulk optodes. 1. General characteristics. Chem Rev. 1997;97:3083–132.

117. Lindner E, Pendley BD. A tutorial on the application of ion-selective electrode potentiometry: an analytical method with unique qualities, unexplored opportunities and potential pitfalls; Tutorial. Anal Chim Acta. 2013;762:1–13.

118. Sakata T, Hagio M, Saito A, et al. Biocompatible and flexible paper-based metal electrode for potentiometric wearable wireless biosensing. Sci Technol Adv Mater. 2020;21:379–87.

119. Karyakin AA, Bobrova OA, Luckachova LV, Karyakina EE. Potentiometric biosensors based on polyaniline semiconductor films. Sensors Actuators B Chem. 1996;33:34–8.

120. Pedroza Dias Mello HJN, Mulato M. Enzymatically functionalized polyaniline thin films produced with one-step electrochemical immobilization and its application in glucose and urea potentiometric biosensors. Biomed Microdevices. 2020;22:22. https://doi.org/10.1007/s10544-020-00478-4.

121. Chen Y, Wang Z, Liu Y, et al. Recent advances in rapid pathogen detection method based on biosensors. Eur J Clin Microbiol Infect Dis. 2018;37:1021–37.

122. Su L, Jia W, Hou C, Lei Y. Microbial biosensors: a review. Biosens Bioelectron. 2011;26: 1788–99.

123. Soldatkina OV, Soldatkin OO, Velychko TP, et al. Conductometric biosensor for arginine determination in pharmaceutics. Bioelectrochemistry. 2018;124:40–6.

124. Braiek M, Djebbi MA, Chateaux J-F, et al. A conductometric creatinine biosensor prepared through contact printing of polyvinyl alcohol/polyethyleneimine based enzymatic membrane. Microelectron Eng. 2018;187:43–9.

125. Bhat A, Amanor-Boadu JM, Guiseppi-Elie A. Toward impedimetric measurement of acidosis with a pH-responsive hydrogel sensor. ACS Sensors. 2020;5:500–9.

126. De Carvalho LA, De Andrade AR, Bueno PR. Electrochemical impedance spectroscopy applied in the study of heterogeneous reactions at dimensionally stable anodes. Quim Nova. 2006;29:796–804.

127. He H, Chang DC, Lee Y-K. Nonlinear current response of micro electroporation and resealing dynamics for human cancer cells. Bioelectrochemistry. 2008;72:161–8.

128. Hassanpour S, Baradaran B, de la Guardia M, et al. Diagnosis of hepatitis via nanomaterialbased electrochemical, optical or piezoelectrical biosensors: a review on recent advancements. Microchim Acta. 2018;185:568. https://doi.org/10.1007/s00604-018-3088-8.

129. Lin Z, Li X, Kraatz H-B. Impedimetric immobilized DNA-based sensor for simultaneous detection of Pb2+, Ag+ , and Hg2+. Anal Chem. 2011;83:6896–901.

130. Rocha GS, Silva MKL, Cesarino I. Reduced graphene oxide-based impedimetric immunosensor for detection of enterotoxin a in milk samples. Materials (Basel). 2020;13: 1751. https://doi.org/10.3390/ma13071751.

131. Tsujimura S, Nishina A, Kamitaka Y, Kano K. Coulometric D-fructose biosensor based on direct electron transfer using D-fructose dehydrogenase. Anal Chem. 2009;81:9383–7.

132. Cao Q, Liang B, Yu C, et al. High accuracy determination of multi metabolite by an origamibased coulometric electrochemical biosensor. J Electroanal Chem. 2020;873:114358. https:// doi.org/10.1016/j.jelechem.2020.114358.

133. Liu J, Yuan X, Gao Q, et al. Ultrasensitive DNA detection based on coulometric measurement of enzymatic silver deposition on gold nanoparticle-modified screen-printed carbon electrode. Sensors Actuators B Chem. 2012;162:384–90.

134. Godino N, Gorkin R, Bourke K, Ducrée J. Fabricating electrodes for amperometric detection in hybrid paper/polymer lab-on-a-chip devices. Lab Chip. 2012;12:3281–4.

135. van Dongen JE, Berendsen JTW, Steenbergen RDM, et al. Point-of-care CRISPR/Cas nucleic acid detection: recent advances, challenges and opportunities. Biosens Bioelectron. 2020;166: 112445. https://doi.org/10.1016/j.bios.2020.112445.

136. He X, Yang S, Xu T, et al. Microdroplet-captured tapes for rapid sampling and SERS detection of food contaminants. Biosens Bioelectron. 2020;152:112013. https://doi.org/10.1016/j.bios. 2020.112013.

137. Couto RAS, Lima JLFC, Quinaz MB. Recent developments, characteristics and potential applications of screen-printed electrodes in pharmaceutical and biological analysis. Talanta. 2016;146:801–14.

138. Bueno D, Muñoz R, Marty JL. Fluorescence analyzer based on smartphone camera and wireless for detection of Ochratoxin A. Sensors Actuators B Chem. 2016;232:462–8.

139. Gopinath SCB, Tang T-H, Chen Y, et al. Bacterial detection: from microscope to smartphone. Biosens Bioelectron. 2014;60:332–42.

140. Zhang D, Jiang J, Chen J, et al. Smartphone-based portable biosensing system using impedance measurement with printed electrodes for 2,4,6-trinitrotoluene (TNT) detection. Biosens Bioelectron. 2015;70:81–8.

141. De Resende MAC, Da Silva DN, Pereira AC. Sistemas de injeção em fluxo e em batelada com detecção eletroquímica aplicados na determinação de fármacos. Rev Virtual Quím. 2016;12: 1186. https://doi.org/10.21577/1984-6835.20200095.

142. Dos Santos WTP, Gimenes DT, Richter EM, Angnes L. Análise por injeção em fluxo com detecção amperométrica de múltiplos pulsos: Potencialidades e aplicações. Quim Nova. 2011;34:1753–61.

143. Miranda CES, Carrilho E, Gervasio AP, Giné MF. Sistemas interfaceados de análise por injeção em fluxo e eletroforese capilar (FIA - CE): desafios, aplicações e perspectivas. Quim Nova. 2002;25:412–9.

144. Bezerra MA, Lemos VA, de Oliveira DM, et al. Automation of continuous flow analysis systems—a review. Microchem J. 2020;155:104731. https://doi.org/10.1016/j.microc.2020.104731.

145. Ṙuz ic ka J, Hansen EH. Flow injection analyses: part I. A new concept of fast continuous flow analysis. Anal Chim Acta. 1975;78:145–57.

146. Reis BF. Análise Química por Injeção em Fluxo: Vinte Anos de Desenvolvimento. Quim Nova. 1996;19:51–8.

147. van Staden JF, van Staden RIS. Flow-injection analysis systems with different detection devices and other related techniques for the in vitro and in vivo determination of dopamine as neurotransmitter. A review. Talanta. 2012;102:34–43.

148. Prieto-Simón B, Campàs M, Andreescu S, Marty JL. Trends in flow-based biosensing systems for pesticide assessment. Sensors. 2006;6:1161–86.

149. Skoog DA, Hanlan J, West DM. Principles of instrumental analysis. 7th ed. 2016. p. 854–5.

150. Augelli M, Nascimento V, Pedrotti J, et al. Flow-through cell based on an array of gold microelectrodes obtained from modified integrated circuit chips. Analyst. 1997;122:843–7.

151. Matos RC, Augelli MA, Pedrotti JJ, et al. Amperometric differential determination of ascorbic acid in beverages and vitamin C tablets using a flow cell containing an array of gold microelectrodes modified with palladium. Electroanalysis. 1998;10:887–90.

152. Richter EM, Kume GH, Augelli MA, Angnes L. Mercury as a global pollutant. 5th Intern. Rio de Janeiro; 1999.

153. Richter EM, Augelli MA, Kume GH, et al. Gold electrodes from recordable CDs for mercury quantification by flow injection analysis. Fresenius J Anal Chem. 2000;366:444–8.

154. Christian GD. Novel flow injection analysis systems for drug analysis. J Pharm Biomed Anal. 1992;10:769–73.

155. Chaniotakis NA, Tsagatakis JK, Moschou EA, et al. Magnesium ion-selective electrode: optimization and flow injection analysis application. Anal Chim Acta. 1997;356:105–11.

156. Albertús F, Horstkotte B, Cladera A, Cerdá V. A robust multisyringe system for process flow analysis. Part I. On-line dilution and single point titration of protolytes. Analyst. 1999;124: 1373–81.

157. Grudpan K, Taylor C, Sitter H, Keller C. Flow injection analysis using an aquarium air pump. Fresenius J Anal Chem. 1993;346:882–4.

158. Weeks DA, Johnson KS. Solenoid pumps for flow injection analysis. Anal Chem. 1996;68: 2717–9.

159. Wang RY, Jarratt JA, Keay PJ, et al. Development of an automated on-line analysis system using flow injection, ultrasound filtration and CCD detection. Talanta. 2000;52:129–39.

160. Matos RC, Gutz IGR, Angnes L, et al. Propulsor pneumático versátil e isento de pulsação para sistemas de análise em fluxo. Quim Nova. 2001;24:795–8.

161. Moreira BCS, Takeuchi RM, Richter EM, Santos AL. Desenvolvimento de um sistema de análise por injeção em fluxo utilizando materiais alternativos de baixo custo para fins didáticos. Quim Nova. 2014;37:1566–72.

162. Fabiano S, Palgrossi JJP, Gutz IGR. Injetor multicanal com válvulas de estrangulamento para análise em fluxo. Quim Nova. 2001;24:689–92.

163. Felix FS, Brett CMA, Angnes L. Flow injection analysis using carbon film resistor electrodes for amperometric determination of ambroxol. Talanta. 2008;76:128–33.

164. Aguiar MAS, Berbigão PN, Mori V. Amperometric determination of iodide in expectorant oral solution by flow injection analysis using iodide/nitrite reaction. Eclet Quim. 2006;31:63–8.

165. Dilgin DG, Ertek B, Dilgin Y. A low-cost, fast, disposable and sensitive biosensor study: flow injection analysis of glucose at poly-methylene blue-modified pencil graphite electrode. J Iran Chem Soc. 2018;15:1355–63.

166. Islam MA, Mahbub P, Nesterenko PN, et al. Prospects of pulsed amperometric detection in flow-based analytical systems—a review. Anal Chim Acta. 2019;1052:10–26.

167. Eletxigerra U, Martínez-Perdiguero J, Juarros A, et al. Real-time label-free impedimetric protein detection using interdigitated gold microelectrodes and flow injection analysis. Proc Eng. 2012;47:1390–3.

168. Koncki R, Rudnicka K, Tymecki Ł. Flow injection system for potentiometric determination of alkaline phosphatase inhibitors. Anal Chim Acta. 2006;577:134–9.

169. Frenzel W, Liu C-Y. Potentiometric and conductometric determination of ammonium by gas-diffusion flow injection analysis. Fresenius J Anal Chem. 1992;342:276–80.

170. Yashin YI, Yashin AY. Analysis of food products and beverages using high-performance liquid chromatography and ion chromatography with electrochemical detectors. J Anal Chem. 2004;59:1121–7.

171. Galli A, De Souza D, Garbellini GS, et al. Utilização de técnicas eletroanalíticas na determinação de pesticidas em alimentos. Quím Nova. 2006;29:105–12.

172. Tvorynska S, Barek J, Josypčuk B. Amperometric biosensor based on enzymatic reactor for choline determination in flow systems. Electroanalysis. 2019;31:1901–12.

173. Tzamtzis N, Psychoyios VN, Nikoleli G-P, Nikolelis DP, Psaroudakis N, Willander M, Qadir Israr M. Flow potentiometric injection analysis of uric acid using lipid stabilized films with incorporated uricase on ZnO nanowires. Electroanalysis. 2012;24:1719–25.

174. Chiriacò MS, Primiceri E, D'Amone E, et al. EIS microfluidic chips for flow immunoassay and ultrasensitive cholera toxin detection. Lab Chip. 2011;11:658–63.

175. Ruzicka J, Marshall GD. Sequential injection: a new concept for chemical sensors, process analysis and laboratory assays. Anal Chim Acta. 1990;237:329–43.

176. Dos Santos ACV, Masini JC. A análise por injeção sequencial (SIA): Vinte anos em uma perspectiva brasileira. Quim Nova. 2010;33:1949–56.

177. Felix FS, Angnes L. Flow-injection analysis with electrochemical detection, first. Wiley; 2015. https://doi.org/10.1002/9781118684030.ch3.

178. Stefan-Van Staden RI, Bokretsion RG, Van Staden JF, Aboul-Enein HY. Simultaneous detection of creatine and creatinine using a sequential injection analysis/biosensor system. Prep Biochem Biotechnol. 2006;36:287–96.

179. Quintino MSM, Angnes L. Batch injection analysis: an almost unexplored powerful tool. Electroanalysis. 2004;16:513–23.

180. Pereira PF, da Silva WP, Munoz RAA, Richter EM. Determinação rápida e simultânea de sulfametoxazol e trimetoprima utilizando análise por injeção em batelada com detecção amperométrica e eletrodo de diamante dopado com boro. Quim Nova. 2015;38:663–8.

181. Cardoso RM, Silva PRL, Lima AP, et al. 3D-Printed graphene/polylactic acid electrode for bioanalysis: biosensing of glucose and simultaneous determination of uric acid and nitrite in biological fluids. Sensors Actuators B Chem. 2020;307:127621. https://doi.org/10.1016/j.snb. 2019.127621.

182. Montes RHO, Marra MC, Rodrigues MM, et al. Fast determination of ciprofloxacin by batch injection analysis with amperometric detection and capillary electrophoresis with capacitively coupled contactless conductivity detection. Electroanalysis. 2014;26:432–8.

183. Baronas R, Ivanauskas F, Maslovskis R, Vaitkus P. An analysis of mixtures using amperometric biosensors and artificial neural networks. J Math Chem. 2004;36:281–97.

184. Buonasera K, Pezzotti G, Scognamiglio V, et al. New platform of biosensors for prescreening of pesticide residues to support laboratory analyses. J Agric Food Chem. 2010;58:5982–90.

185. Gramberg B, Kintzios S, Schmidt U, et al. A basic approach towards the development of bioelectric bacterial biosensors for the detection of plant viruses. J Phytopathol. 2012;160: 106–11.

186. Yang W, Zhang H, Li M, et al. Early diagnosis of blast fungus, Magnaporthe oryzae, in rice plant by using an ultra-sensitive electrically magnetic-controllable electrochemical biosensor. Anal Chim Acta. 2014;850:85–91.

187. Tarasov A, Gray DW, Tsai M-Y, et al. A potentiometric biosensor for rapid on-site disease diagnostics. Biosens Bioelectron. 2016;79:669–78.

188. Cesarino I, Moraes FC, Lanza MRV, Machado SAS. Electrochemical detection of carbamate pesticides in fruit and vegetables with a biosensor based on acetylcholinesterase immobilised on a composite of polyaniline–carbon nanotubes. Food Chem. 2012;135:873–9.

189. Crew A, Lonsdale D, Byrd N, et al. A screen-printed, amperometric biosensor array incorporated into a novel automated system for the simultaneous determination of organophosphate pesticides. Biosens Bioelectron. 2011;26:2847–51.

190. Gong J, Guan Z, Song D. Biosensor based on acetylcholinesterase immobilized onto layered double hydroxides for flow injection/amperometric detection of organophosphate pesticides. Biosens Bioelectron. 2013;39:320–3.

191. Luo Y, Nartker S, Miller H, et al. Surface functionalization of electrospun nanofibers for detecting E. coli O157:H7 and BVDV cells in a direct-charge transfer biosensor. Biosens Bioelectron. 2010;26:1612–7.

192. Ma Y, Jiao K, Yang T, Sun D. Sensitive PAT gene sequence detection by nano-SiO2/paminothiophenol self-assembled films DNA electrochemical biosensor based on impedance measurement. Sensors Actuators B Chem. 2008;131:565–71.

193. Song Y, Zhang M, Wang L, et al. A novel biosensor based on acetylecholinesterase/prussian blue–chitosan modified electrode for detection of carbaryl pesticides. Electrochim Acta. 2011;56:7267–71.

194. Muhammad-Tahir Z, Alocilja EC, Grooms DL. Rapid detection of bovine viral diarrhea virus as surrogate of bioterrorism agents. IEEE Sensors J. 2005;5:757–62.

195. Wei M, Wang J. A novel acetylcholinesterase biosensor based on ionic liquids-AuNPs-porous carbon composite matrix for detection of organophosphate pesticides. Sensors Actuators B Chem. 2015;211:290–6.

196. Durrieu C, Guedri H, Fremion F, Volatier L. Unicellular algae used as biosensors for chemical detection in Mediterranean lagoon and coastal waters. Res Microbiol. 2011;162:908–14.

ARTIGO 2

Artigo submetido na revista Environmental Research.

Recent advances of electrochemical nano-immunosensors for determination of mycotoxins in food

Roberta Castro Martins, Ana Carolina de Faria Alves, Camila A. Proenca, Tayane A. Freitas, Thaisa A. Baldo, Alexandre L. B. Baccaro, Laíse Nayra dos Santos Pereira and Fabiana S. Felix.

Abstract

Mycotoxins are low molecular weight compounds produced by fungi genera as secondary metabolites during pre- and post-harvest storage of crops and foodstuff. Among the most studied mycotoxins are deoxynivalenol (DON), ochratoxin A (OTA), zearalenone (ZEN), and aflatoxins (AFs). Recent reports show highly concerning issues ascribed to their carcinogenic, genotoxic, immunosuppressive, and teratogenic properties. Several instrumental methods are available for the determination of mycotoxins: liquid chromatography, capillary electrophoresis, Raman spectroscopy, and enzyme-linked immunosorbent assay (ELISA). Despite of their favorable analytical performances, most of them are expensive and time-consuming. In this regard, electrochemical nano-immunosensors are emerging biosensors that combine the fast, cheap, sensitive and selective immunological electrochemical analysis with nanostructured materials, to further enhance the sensitivity of mycotoxin determination methodologies. This review shows recent applications of electrochemical nano-immunosensors for the determination of mycotoxins in foodstuff analysis. Emphasis is given to their fundamentals, sensors assembly, and respective applications.

Keywords: mycotoxins, nano-immunosensors, nanomaterials, electrochemical biosensors, food analysis.

1. Introduction

The class of the mycotoxins is a group of low molecular weight compounds produced by molds in food. They are secreted as secondary metabolites of several fungi species, like Aspergillus, Fusarium, Penicillium, and Alternaria, during pre- and post-harvest storage of crops and foodstuff. Among commonly studied mycotoxins are the aflatoxins (Afs), ochratoxins (OTA), and patulin (PAT) (Anfossi, Giovannoli, and Baggiani 2016).

Aflatoxins are the most investigated group, including the aflatoxins B1, B2, G1 and G2, produced by Aspergillus flavus. They have drawn a lot of attention due to their high cytotoxicity and carcinogenicity (Evtugyn and Hianik 2019).

Aspergillus and Penicillium genus produce the ochratoxins mycotoxins, which include ochratoxin A, ascribed to toxic pathologies on human renal system. Some Penicillium strains genus can additionally produce some tremorgenic mycotoxins. Other mycotoxins include the trichothecene group generated by the Fusarium genus, which can cause oral lesions such as dermatitis, irritation and bleeding (Pohanka, Jun, and Kuca 2007).

It is important to emphasize the terrible economic risks these toxic agents pose over the market due to the contamination of commodities (e.g. food and feeds commerce), sick leaves and early sick-retirements caused by non-curable diseases such as cancer, nephrotoxic, teratogenic and immunotoxic diseases. That's why mycotoxins are contaminants that need to be continuously monitored in food and foodstuff products to preserve the quality of human life. Critical stages of food chain must be strictly monitored and controlled by inspecting raw materials, food supply and processing, final products, and also the storage (Tothill 2011).

Many traditional analytical methods are available to accurately and sensitively detect mycotoxins in foods: thin-layer chromatography (Matysik and Giryn 1996), capillary electrophoresis (Kecskemeti et al. 2020), liquid chromatography coupled with mass spectrometry (Pallares et al. 2021), Raman spectroscopy (R.P. Chen et al. 2021), and gas chromatography coupled with UV-detector (Anfossi, Giovannoli, and Baggiani 2016) are some examples.

Analytical chemistry has changed a lot in the last decades, much driven by automation, miniaturization, and system integration with high throughput for multiple tasks (Hasanzadeh et al. 2013). Field measurements became a reality, at least for screening analysis, which can accelerate measurements, response, decisions and improve business profit in the agriculture niche.

One should mind the importance of performing fast measurements in the sample collection site, giving a fast overview of the situation regarding the mycotoxins. Even if samples

still have to be forwarded to traditional costly and lengthy analysis, the reduction in the number of samples to be representatively collected, processed, prepared and analyzed represents a great cost and time savings. Nevertheless, this reality can still be highly improved by the full substitution of the lab-bench techniques by in situ specific techniques with improved accuracy, precision and sensitivity. One way to perform that is by the development of miniaturized electrochemical nano-immunosensors.

Immunosensors are a class of highly-specific biosensors that use antibodies as bioreceptors. Their functioning mechanism is based on the interaction between antibody and its respective antigen, forming the immunocomplexes that blocks the surface of electrodes, hindering, e.g., the conductivity, voltammetric or other transducer signal (Bahadir and Sezginturk 2016).

Among immunological bioreceptors, aptamers are attracting much attention recently, mainly, due to their low cost, reasonable stability and good applicability in pH and temperature wide ranges, with label-free detection (Xu et al. 2021). Changes in their conformation or hybridization caused by the analyte bonding trigger the formation of the electrochemical signal (Irfan Azizan et al. 2023).

Many transducing mechanisms are possible, with special regard to electrochemical methods that are considerably simple and sensitive enough for most of studied applications (interesting typical detection limits – LODs) (Heydari-Bafrooei and Ensafi 2023; A. Khan et al. 2023). They can be classified as voltammetric, impedimetric, conductometric or potentiometric transducers.

Voltammetric determinations are based on the measurement of faradaic (anodic or cathodic) currents developed during the application of controlled potential programs. Impedimetric sensors measure by Electrochemical Impedance Spectroscopy (EIS) the changes in charge conductance and capacitance at the sensor surface, as the selective binding of the target occurs. Conductometric measurements are based on conductivity transients generated by the bioreceptor interaction, while potentiometric determinations monitor the zero-current potential changes during this same step.

In this entire context, nanotechnology can be regarded to accomplish different roles in a way to improve, e.g., methodologies sensitivity. Since the replacement of traditional markers and signal amplifiers (Tothill 2011; Campanile et al. 2020), biomolecules surface functionalization (H.A. Chen et al. 2023) and fixation (Huan Wang et al. 2016b), until fluorescence signal generators (S.Y. Zhou et al. 2020), nanomaterials are implemented in very different ways, conferring versatility to the sensor assembling process.

In this review, fundamentals of the electrochemical biosensing are herein introduced converging to the immunosensing technology. Then, fundamentals of nanomaterials are covered: basic physical, chemical and physical-chemical properties, their synthesis, analytical characterization and up-to-date most common applications. Finally, a selected variation of distinctive nano-immunosensors applications for the mycotoxin detection in food and foodstuff samples are herein reported, highlighting their respective analytical performances. Perspectives are shown as well, pointing out possible trends in such multidisciplinary field, with very promising strategies to detect and measure this worrying class of toxins.

2. Electrochemical biosensors

In the decades, sensor platforms have been widely used as attractive, promising and efficient analytical methods. They have several advantages, such as high sensitivity, portability, low cost, ease of automation and miniaturization. Furthermore, in order to improve the selectiveness and sensitiveness of sensors, the so-called biosensors have been developed (Noh et al. 2021). Biosensors are analytical devices used to specifically detect analytes, composed by two main stages: the bioreception and the transducing (Heydari-Bafrooei and Ensafi 2023).

A bioreceptor (or biorecognition element) is a biochemical compound that selectively interacts with the analyte. Usually they are enzymes, antibodies, nucleic acids or aptamers (Fig. 1) (Dali et al. 2018; Xiang 2011; L. Cui, Wu, and Ju 2015; X.J. Chen et al. 2014). When immobilized on the surface of a transducer, it becomes possible to convert the biological response into a physical signal, which enables the analyte detection at samples (A. Khan et al. 2023).

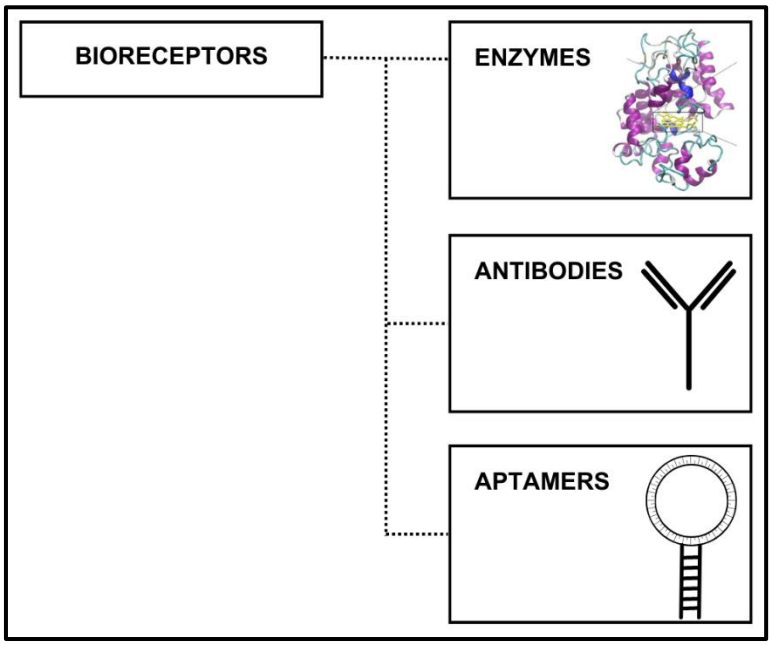

Fig. 1. Schematic diagram representing the commonly used bioreceptors at biosensors.

Enzymes are the most known bioreceptors for electrochemical biosensors (Naresh and Lee 2021). They are easily synthesized, with well-established reaction mechanisms and kinetics, providing high sensitivity and selectivity to their methodologies. (Liu et al. 2019) Enzymatic action usually occurs by three ways during analysis (Justino et al. 2015):

1. Measurement of the analyte enzymatic metabolization rate;
2. Measurement of the enzymatic activation/inhibition rate;
3. Measurement of the enzymatic changes rate caused by the analyte.

Despite of the mentioned advantages, enzymatic bioreceptors show considerable disadvantages, mainly ascribed to their structure sensitivity. They can be expensive, easily denatured, with instabilities at varying pH and temperatures, and low specificity, all of that under labeled-type detection (Irfan Azizan et al. 2023).

Antibodies can also be applied as bioreceptors, in the so-called immunosensors. Like enzymes, they have high sensitivity and known mechanisms, but in addition, they possess higher specificities and detections can be labeled, or even, unlabeled (Irfan Azizan et al. 2023).

Their means of action happens by the interaction between antibody and antigen (Fig. 2), which react each other to form the immunocomplex, generating a blocking layer on the electrode surface. That usually leads to an impediment in the electrode surface, decreasing the monitored electrochemical response (Bahadir and Sezginturk 2016).

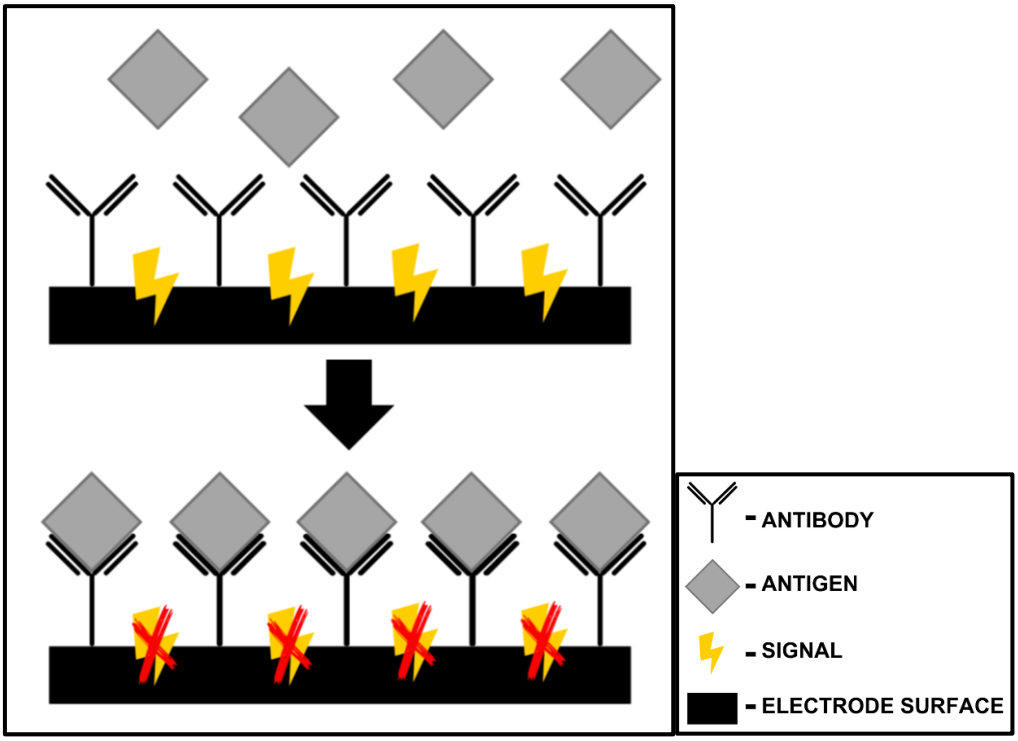

Fig. 2. Schematic diagram showing the usual formation of the blocking layer on the immunosensor surface.

Some disadvantages of using antibodies as bioreceptors are: the high costs involved; their considerable synthesis complexity and; the denaturation possibility under their direct adsorption on the electrode surface (Phopin and Tantimongcolwat 2020; Bahadir and Sezginturk 2016). As viable bioreceptors, aptamers have attracted a lot of attention due to their advantages over other biomolecule, such as: their comparative lower costs and simpler synthesis, better stability, good applicability in a wide pH and temperature ranges, longer shelf lives, reversible denaturation, high specificity and label-free detection (Xu et al. 2021).

Aptamers are synthesized by the Systematic Evolution of Ligands by Exponential Enrichment (SELEX) (Naresh and Lee 2021). Their mechanism in electrochemical aptasensors

work based on conformational or hybridization changes that can be triggered by the analyte, generating the electrochemical signal (Irfan Azizan et al. 2023). Application of aptamers as bioreceptors is considered something very recent. One of the few important disadvantages that can be listed is their destabilization when in contact with the nuclease enzyme in the human body (Irfan Azizan et al. 2023).

Regarding the transducing stage, it can happen by electrochemical, optical, calorimetric, gravimetric or impedimetric measurements. Electrochemical methods are widely used due to their simple structure and acceptable detection limit (LOD) values (Heydari-Bafrooei and Ensafi 2023; A. Khan et al. 2023). Depending on the detection principle, the electrochemical transducer can be classified as voltammetric, amperometric, impedimetric, conductometric or even potentiometric one (Lakhera et al. 2022).

Usual voltammetric techniques used include the cyclic voltammetry (CV), differential pulse voltammetry (DPV), square wave voltammetry (SWV) and amperometry. These techniques provide good sensitivity to the biosensor, recording current values by applying specific potential programs (current-potential plots) or a constant potential (current-time plots) (Lakhera et al. 2022; Tajik et al. 2021; Noh et al. 2021).

Electrochemical impedance spectroscopy (EIS) is an effective technique to measure the electrode surface impedance value during the frequency shift process. This technique can also be applied in order to perform a characterization of the electrode surface, in addition to evaluating the electrode/analyte binding kinetics and the electrode/electrolyte interface (Lakhera et al. 2022).

In amperometry, the current is measured in function of an elapsed-time during the application of a controlled constant potential (Lakhera et al. 2022). Conductometry evaluates the conductance-recognition event relationship while, potentiometry will measure the zero-current potential against a reference electrode (e.g. Ag/AgCl).

Biosensors have been applied in many fields of analytical chemistry, comprising several kinds of determinations and samples, such as Enzyme-linked voltammetric detection of MicroRNAs (Erdem, Congur, and Eksin 2013), paraquat pesticide determination in

DNA/AuNP composite electrode (Ribeiro et al. 2010), anti-doping testosterone control by biotin-nanobody/GCE impedimetric immunosensor (G. Li et al. 2016), anti-doping Erythropoietin determination in human serum by AuNPs/ amino-terminated polyamidoamine (PAMAM)/ fullerene (C_{60}) nanoprobe (J. Han et al. 2015), and so on.

Specifically to mycotoxins detection, Zinoubi et al. 2020, developed an enzymatic biosensor to determine (OTA) in coffee plantations. Cross-linked calcium cellulose (CCLC) was used to improve the sensitivity and reproducibility of the new biosensor, as well as acting as a stabilizing agent for the electrochemical formation of AuNP in graphene nanosheets. The proposed biosensor was developed by immobilizing the thermolysin enzyme (TLN) in a Polyvinyl alcohol/polyethyleneimine matrix, covering the graphene decorated with CCLC/AuNP. As a result, a sensitive, reversible and stable biosensor was obtained for the detection of ochratoxin A, with a detection limit of 0.2 nmol L^{-1} (Zinoubi et al. 2021).

Many other applications like that one will be herein covered. However, discussions will be oriented accordingly to the specific type of nanomaterial used, after the proper introduction of their respective fundamentals.

3. Nanotechnology and electrochemical biosensors

Sensors are devices capable of measuring analytes in samples, responding continuously and in a reversible trend, avoiding sample destruction when necessary. Nanosensors implement at least one nanostructure to detect, e.g., gases, chemicals, biomolecules, electric fields, light, and heat, to increase the sensitivity of the analytical methodology (Xiaoping Huang, Zhu, and Kianfar 2021).

As discussed above, biosensors use a biological element to specifically recognize the analyte in the bioreception stage, comprising applications with DNA strand, antibodies, enzymes, and even the whole cell. Electrochemical nano- biosensors are those that use bioreceptors, the transducer electrode, and nanostructures to fill the gap between the converter and the bioreceptor, enhancing the sensitivity of electrochemical techniques (Xiaoping Huang, Zhu, and Kianfar 2021).

Different types of nanomaterials can be considered for biosensing applications: metallic nanoparticles (MeNP), nanotubes (NTs), nanowires (NW), nanorods (NR), carbon allotropes (e.g., CNTs, fullerene, graphene-compounds), and quantum dots (QD). The choice of nanomaterials over larger structures is driven by several factors, including a high area-to-volume ratio, increased atom exposure to the surrounding environment, and notable quantum effects (Rosado et al. 2023; Fiorio et al. 2022). However, exploring nanoengineering methods at the sub-nano or atomic levels proves highly attractive since they offer opportunities to comprehend the intricate interplay between parameters such as shape, size, composition, structure, electronic properties, and support interaction (Rangel de Melo Rodrigues et al. 2022). These investigations provide valuable insights into the relationships between structure and performance. Among several available morphologies beyond the classical sphere-like shaped NPs, nanowires, nanorods, and nanocubes are interesting, to name just a few. However, other structures may be interesting for sensing applications aiming for an increased surface area. Figure 3 showcases a series of microscopy images highlighting the NiO nanoflowers at varying magnifications, which the authors used for highly selective and sensitive electrocatalytic detection of hydrazine. One can notice that the authors showed transmission, scanning, and high-resolution electron microscopy images and elemental mapping, discussing further the material and its importance in the sensing process (R.M. Ferreira et al. 2023).

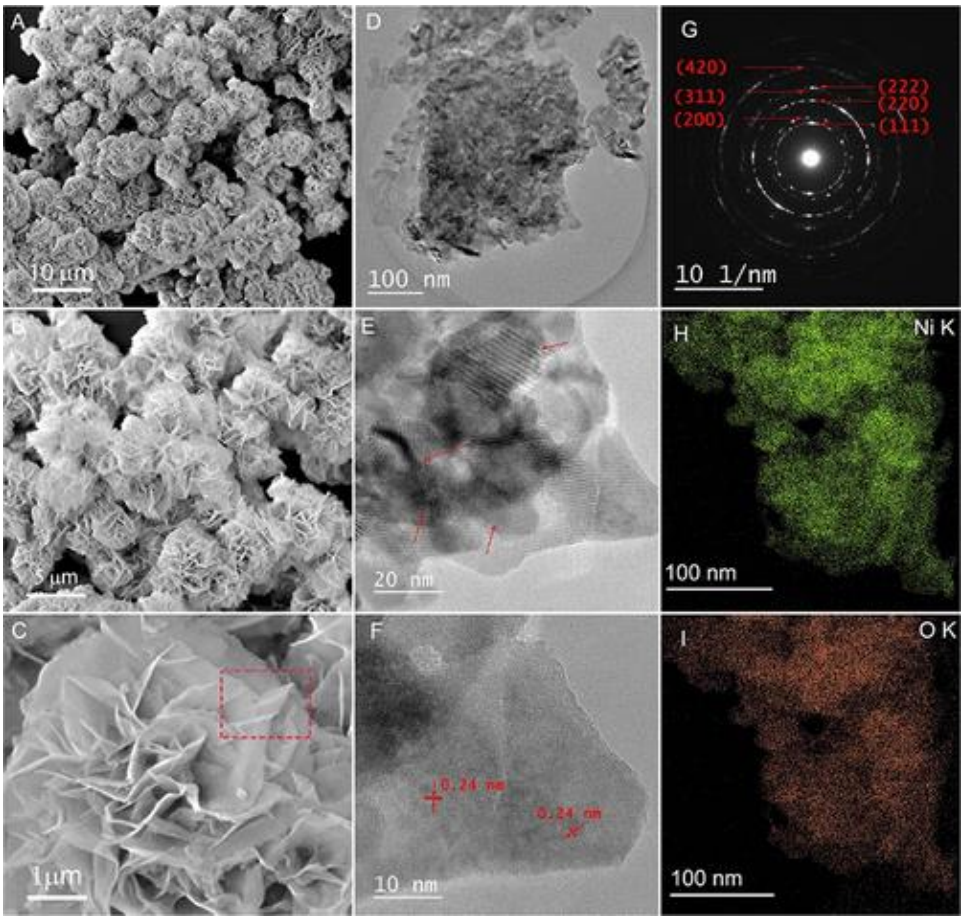

Fig. 3. Scanning electron microscopy images with different magnification of the nanoflowers (A–C). Additionally, a low-magnification transmission electron microscopy image (D) is included. A high-resolution transmission electron microscopy image exhibits Moiré fringes, which are indicated by arrows (E). Atomic plane spacing of the material (F). The selected area diffraction pattern of image (D) is displayed, and the structures are indexed (G). Elemental mapping displays the distribution of Ni (H) and O (I). Copyright 2023, with permission from ACS publications/ACS Omega (R.M. Ferreira et al. 2023).

Many medical and biological applications include not just one nanomaterial but nanostructured composites with different purposes that, in the end, aim for the sensors to improve performance and efficiency.

4. Metallic Nanoparticles

Metallic nanoparticles have been used for centuries, from ancient times in Indian medicine to Rome aesthetics and Muslim culture. However, the first scientific application of metallic NPs was reported by Michael Faraday in 1857. After that, in 1959, Richard P. Feynman showed great support for nanotechnology in a lecture to the American Physical Society (APS). Since then, the attention to NPs has grown, mainly with improving characterization techniques, such as electronic microscopies (Asgari, Nikkam, and Saniee 2022).

To synthesize these nanoscale products, there are two main approaches: the “top-down” and the “bottom-up” pathways (Fig. 4). The first one is based on physical processes to produce nanomaterials from bulk materials, and that includes ball milling, sputtering, electron beam evaporation, laser ablation, and electrospraying. The second one uses cheaper chemical pathways, like sol-gel synthesis, hydrothermal synthesis, co-precipitation method, microemulsion technique, and chemical vapor deposition (Ahmad et al. 2022; Ekrami et al. 2022).

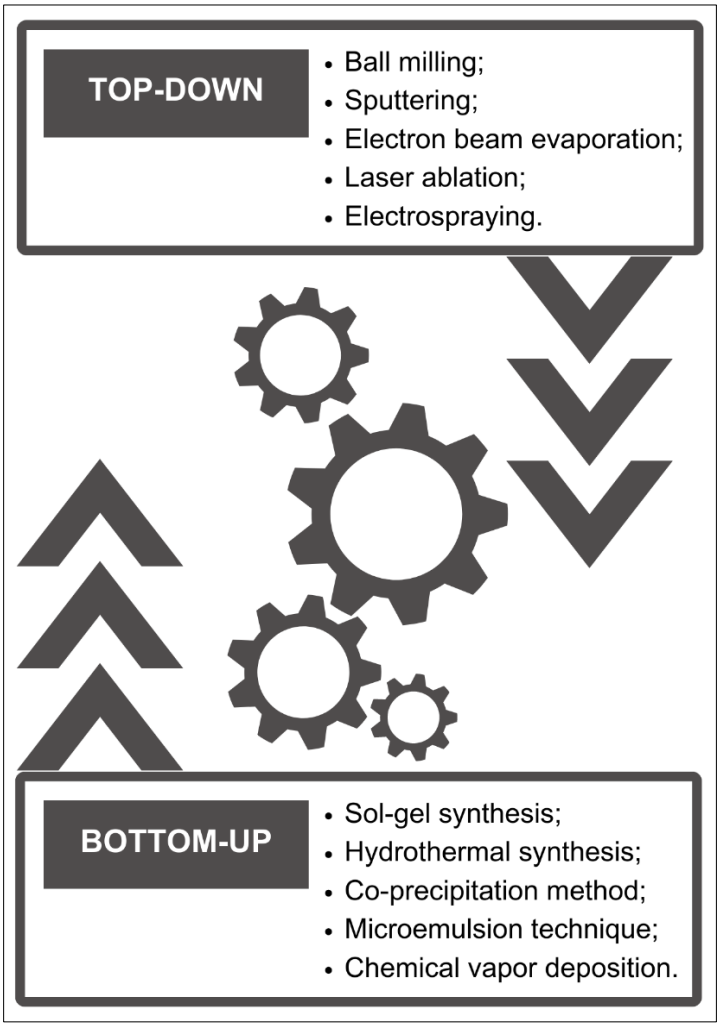

Fig. 4. "Top-down" and the "bottom-up" pathways used to synthesize the nanoscale structures.

It is essential to mention that some biological or green synthesis methods are also feasible. NPs can be produced by mixing precursors with plant extracts, bacteria and fungi, without adding traditional chemicals (Asgari, Nikkam, and Saniee 2022).

4.1. Synthesis processes

4.1.1. Ball milling

The ball milling process is an effective low-cost method for producing nanocomposites such as oxide and carbide aluminum alloys, resistant spray coatings and Al-, Ni-, Mg-, Cu-based nanoalloys. During the process, the bulk material is placed inside a grinding chamber

with milling spheres, which will acquire mechanical energy with the chamber rotation. The material undergoes deformation and is fractured, causing amorphization and some local chemical reactions (Zhuang et al. 2016).

4.1.2. Sputtering

High-energy particles, such as plasma or gas, are used to bombard solid surfaces to produce thin films of nanostructured materials (Ayyub et al. 2001). The process is carried out in an evacuated chamber, usually filled with Argon (Ar) or another sputtering gas. A high voltage is applied to a magnetron cathode against a grounded anode target, generating high-density plasma, positive ionized Argon (Ar^+), and free electrons that collide with Argon to produce even more ions. The Ar^+ is accelerated in the electric field toward the cathode target, colliding and ejecting atoms from its surface, which in turn, will deposit on the anode substrate to form the thin nanostructured film (Muñoz-García et al. 2010).

4.1.3. Laser ablation

The bulk material is vaporized due to the high energy of the incident laser irradiation, producing the nanoparticles (Baig, Kammakakam, and Falath 2021). Laser ablation is considered a green technique, since no chemicals are applied (Amendola and Meneghetti 2012). Furthermore, by adjusting variables such as the laser fluence, wavelength and by adding salts, properties regarding to the nanoparticles size distribution can be readily controlled (Baig, Kammakakam, and Falath 2021).

4.1.4. Sol-gel synthesis

The sol-gel method is usually applied to synthesize metal-oxide nanomaterials. The metal oxide undergoes hydrolysis to form a sol, followed by the condensation step, forming porous structures that are left to age to decrease its porosity, and to separate the colloidal particles (Baig, Kammakakam, and Falath 2021). After aging, the material is calcined to obtain the dried nanoparticles (Parashar, Shukla, and Singh 2020).

4.1.5. Hydrothermal synthesis

The hydrothermal method promotes an aqueous heterogeneous reaction in a sealed container, under high pressures, and controlled temperatures around the critical point. For non-aqueous medium, the method is then so-called solvothermal method (X. Wu, Lu, and Wang 2011; S. Cao et al. 2016). They are widely used to produce nanowires, nanorods, nanosheets and nanospheres (Y. Dong et al. 2020; Jiang et al. 2018; Chai et al. 2018).

4.1.6. Chemical vapor deposition

A thin film is formed on the substrate surface through the chemical reaction of precursors in the vapor phase. A good precursor shows adequate volatility, high chemical purity, good stability during evaporation, low-cost, non-hazardous nature, and long shelf-life (Baig, Kammakakam, and Falath 2021). During the decomposition process, the choice of reaction catalyst will be crucial for the final morphology and the type of nanomaterial obtained, e.g. Ni and Co are related to the production of multilayer graphene, while Cu leads to the formation of a monolayer graphene (Baig, Kammakakam, and Falath 2021). This synthesis process is widely applied to synthesize two-dimensional nanomaterials (Y. Dong et al. 2020), and it is also important to be aware about residual impurities after the decomposition process (Baig, Kammakakam, and Falath 2021).

5. Nanoparticles (NPs)

Nanoparticles exhibit unique properties and behaviors due to their small size and higher surface to volume ratio compared to larger particles. Nanoparticles can be composed of many materials, including metals, metal oxides, dentrimers, mesoporous silica, micelle, liposome, magnetic materials, polymers, carbon-based materials, and nanoparticles that employ biological materials used in green synthesis, such as extracts derived from plants in the production of metallic nanomaterials and metallic oxides (Fig. 5) (Horky et al. 2018; Xie et al. 2015).

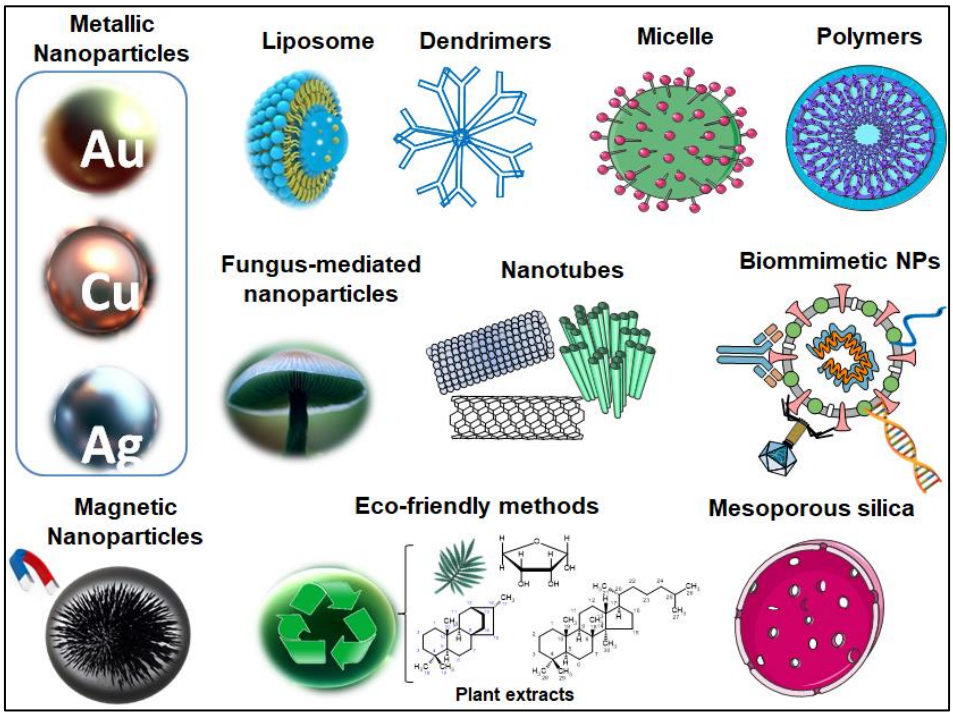

Fig. 5. Different nanoparticles for mycotoxin detection.

5.1. Superparamagnetic iron oxide NPs (SPIONs)

Nanoparticles formed from iron oxide crystallites are known as SPIONs. The most popular ones are magnetite (Fe_3O_4), maghemite (γ-Fe_2O_3) and hematite (α- Fe_2O_3). Magnetite is widely used due to its strong magnetic properties, and the presence of both Fe(II) and Fe(III) ions, approximately in a 1:2 ratio (Teja and Koh 2009), which triggers the Fenton reaction, generating reactive oxygen species (ROS) for advanced oxidation processes (Asgari, Nikkam, and Saniee 2022).

To synthesize SPIONs, a number of factors should be considered, such as the envisioned application, shape and size. Different chemical, physical and even biological methods can be used. Chemical methods are highly suggested, since they provide a better control of the material morphology (Gupta and Gupta 2005). Many synthetic strategies have been previously reported, like the thermal decomposition, co-precipitation, microemulsion systems, sol-gel, hydrothermal, sonochemical decomposition and electrochemical deposition (Asgari, Nikkam, and Saniee 2022).

Regarding to their applications, these NPs have been used for nanotheranostics for personalized medicine, hyperthermia, biomedical imaging as Magnetic Resonance Imaging (MRI) and Magnetic Particle Imaging (MPI), catalysis, tissue repair, biomolecules separation, sensing, and even data storage (Hedayatnasab, Abnisa, and Daud 2017; de Sousa Cunha et al. 2019; Jin et al. 2014; Ferguson et al. 2015; Siddiqi et al.).

5.2. Silver NPs (AgNPs)

Silver NPs have gained great attention due to their disinfectant properties. Once compared to routine biocides and antibiotics, AgNPs have a shorter time of action with a wide effectiveness spectrum against bacteria, fungi, and viruses (Gopinath et al. 2017). So, AgNPs have been used to coat medical devices, dressings, and textile fabrics (Furno et al. 2004; Haixia X Fau - de Barros et al. ; Yeo and Jeong 2003).

Synthesis methods include the same physical or chemical strategies. However, the use of traditional synthesis approaches can show serious consequences related to their toxicity to human cells, and impact on the environment due to highly toxic chemicals involved (Roy et al. 2013). Some of the effects caused by the toxicity of these nanoparticles are: potential DNA damage (cancer precursor), delay, malformation or death of embryos, oxidative stress and activation of inflammatory responses (Roy et al. 2013). That’s why ecofriendly synthesis methods have been better developed. This approach ensures safety, effectiveness and also cheaper non-toxic nanoparticles (Borase et al. 2013).

5.3. Gold NPs (AuNPs)

Biocompatibility and non-toxicity are some of the most interesting characteristics of gold for nanotechnology: the great range of nanosizes (1-150 nm), the possibility of surface functionalization, colloidal stability, photostability, and high surface to volume ratio make these NPs effective in active and passive cell targeting (Connor et al. 2005; Daniel and Astruc 2004; Gao et al. 2004; Almeida, Figueroa, and Drezek 2014).

The synthesis of AuNPs involves the reduction of gold salts (usually Au(III)) to nucleate Au(0) into the AuNPs form. Other synthesis methods include the physical reduction,

microwave irradiation, solvent evaporation techniques and eco-friendly methods (Sun, Mayers, and Xia 2003; Kundu, Peng, and Liang 2008; Pyrpassopoulos et al. 2007). Still, AuNPs have size-dependent biological applications: e.g. enhancement of transfection efficiency of DNA/RNA (6 nm), photothermal therapy (30 nm), delivery of functional proteins to the living cells (2.5 nm) and drug delivery (31 nm) (McIntosh et al. ; Xiaohua Huang et al. 2007; Ghosh et al. 2010; Brown et al. 2010; Hwu et al. 2009).

5.4. Copper NPs (CuNPs)

CuNPs are ductile, cost-effective, economically promising and show antimicrobial properties (Nagar and Devra 2018). Copper NPs are highly reactive due to their high surface to volume ratio (I. Khan, Saeed, and Khan 2019). They can be used for catalysis, optics, electronics, lubricants production, conductive films and medicine applications (Ojha et al. 2017).

Bottom-up or top-down approaches are both used to produce CuNPs (Umer et al. 2012), with the chemical microemulsion technique being the most popular one. Physical methods such as laser ablation and radiolysis can also be used. As a green alternative synthesis, plant extracts have been used as well (Thakkar, Mhatre, and Parikh 2010).

6. Eco-friendly methods: a green alternative

With the growing discussions about sustainability and green chemistry, alternative sources to toxic chemicals used in the nanoparticle synthesis process have been studied. Thus, green synthesis emerges as an economical and ecologically correct approach (Kombaiah et al. 2018).

Green synthesis uses biological sources such as plants, microorganisms, fruits and seaweed to synthesize nanoparticles (Nasrollahzadeh, Sajadi, et al. 2019; Nasrollahzadeh, Atarod, et al. 2019). Certain advantages such as better energy efficiency, process economy and nanoparticles biocompatibility arise once compared to physical-chemical traditional synthesis, which require a large amount of energy and toxic chemicals. Thus, the main advantage of green

synthesis is the lower toxicity of the produced nanoparticles (J.A. Kumar et al. 2021; Molina et al. 2019).

Among the biological materials used at the green synthesis, plant-derived extracts stand out in the production of metal and metal oxide nanomaterials. The procedure is simple and it is even possible to synthesize nanomaterials on a better production scale (Ahmad et al. 2021).

The phytochemical compounds of plant extracts are the key point in the green synthesis, since they are responsible for the bioreduction and stabilization processes, necessary in the synthesis of nanoparticles. Such compounds are phenolics, flavonoids, phenolic acids, terpenoids, vitamins, glycosides, polysaccharides, organic acids and proteins. An important point to be emphasized is that, depending on which part of the plant the extract was obtained from (leaves, stem, flowers, fruits or seeds); their constituents will vary (Ahmad et al. 2021).

Among the phytochemical compounds, phenolics are the largest category. These compounds are secondary metabolites of plants, and protect them against insects, fungi, bacteria and viruses. In the subgroup of phenolics, flavonoids have interesting factors, such as their antioxidant potential and their free hydrogen, which are both involved at the MNP synthesis. Thus, the flavonoid presence in plant extracts is good indicator of the potential feasibility to synthesize metallic nanoparticles (Nasrollahzadeh, Sajadi, et al. 2019; Nasrollahzadeh, Atarod, et al. 2019).

7. Applicatins of metallic NPs

Currently, metal nanoparticles have been applied specifically to replace enzymes as markers and signal amplifiers in biosensing (Tothill 2011; Campanile et al. 2020).

Zhang *et al.*, 2016 used a gold electrode modified with a biocompatible film of carbon nanotubes / poly (dialyldimethylammonium chloride) / Pd-Au nanoparticles (CNTs / PDDA / Pd-Au) in the development of an immunosensor for detection of aflatoxin B1. PDDA was herein used to improve the dispersion of CNTs in aqueous solutions, and promote the adsorption of Pd and Au nanoparticles on them. CNTs are used for a rapid electron transfer, while Pd and Au nanoparticles are substrates for the antibodies immobilization. The analytical performance

of the immunosensor was tested under optimal experimental conditions in differential pulse voltammetry. The developed immunosensor demonstrated high sensitivity in a linear range between 0.05 and 25 ng mL^{-1}, with LOD of 0.03 ng mL^{-1}. The intraassay reproducibility showed CV of 7.2%, while for interassay, CV was 6.6% (n = 5). Regarding stability, approximately 93% of the initial response was maintained after 1 week and 87% of the initial response was maintained after 4 weeks (S. Zhang et al. 2016).

Wang *et al.,* 2016 proposed a new disposable electrochemical immunosensor based on voltammetric stripping analysis, using copper ions as a signal marker for the detection of aflatoxin B1 (AFB1). To assemble the immunosensor, the AFB1 antibody (Ab) was fixed on the carbon electrode printed on a modified screen of gold nanoparticles (AuNPs) (SPCE). The low-cost immunosensor developed high sensitivity, fast analysis and showed a linear concentration range from 1.0 pg mL^{-1} to 100 ng mL^{-1} with a detection limit of 0.2 pg mL^{-1}. The reproducibility test showed RSD of 3.8% (n = 5). For stability test, RSD was 1.2 %. The immunosensor was applied for the analysis of milk and peanut oil samples. Recoveries were in the range of 95.5–110% and 90–102%, respectively (H. Wang et al. 2016a).

To increase its surface area and the sensitivity of the analytical response, Adány *et al*., 2018, immobilized gold nanoparticles on the optical waveguide lightmode spectroscopy (OWLS) sensor, used to detect aflatoxin B1 in paprika. A competitive immunoassay was performed and, as a result, authors were able to perform real-time determinations in a dynamic range from 0.01 to 10 ng mL^{-1}, with an EC50 of 0.044 ± 0.005 ng mL^{-1}. The OWLS immunosensor technique can be applied both to the analysis of food and environmental samples (Adányi et al. 2018).

Wu *et al*., 2018 used platinum-coated gold nanorods (AuNR@Pt) and upconverting nanoparticles (UCNPs), to perform an aptamer-based fluorometric assay for the detection of staphylococcal enterotoxin B (SEB) in milk samples. Authors realized that in SEB concentrations between 2.0 and 400 pg mL^{-1}, the fluorescence signal increased linearly. A LOD of 0.9 pg mL^{-1} was calculated and, after application in milk samples, average recoveries between 91.2% and 104.6% were observed (Z. Wu, He, and Cui 2018).

Bhardwaj et al., 2019, performed a comparative study to verify the influence of modifying the gold detection chip of self-assembled monolayers (SAM) with gold nanoparticles (AuNPs) for the detection of aflatoxin B1 (AFB1). Results were promising, with linear range of AFB1 from 0.01 to 50 nmol L^{-1}, and LOD of 0.003 nmol L^{-1}. For the unmodified gold chip, the linear detection ranged from 1.0 to 50 nmol L^{-1} and the LOD was 0.19 nmol L^{-1}. The developed sensor was applied to quantify AFB1 in enriched wheat samples, and average recovery values were found between 90.1% and 93% (H. Bhardwaj, Sumana, and Marquette 2020).

Di Nardo *et al*., 2019, used blue and red gold nanoparticles to develop a multiplex lateral flow immunoassay to determine aflatoxin B1 (AFB1) and fumonisins type B (FMs), simultaneously, in cereals and cereal-based food products. Depending on the analyte nature and concentration, tests resulted on different detection colors. It is important to note that no false positive or negative results were obtained, and contaminants were correctly identified in all positive tests, according to the color coding. Concentrations used were 1.0 ng mL^{-1} for AFB1, and 50 ng mL^{-1} for FMs (visual cut-off level). For further studies, authors estimated a semi-quantitative analytical response by RGB data analysis from samples images. Data correlations of $r^2 = 0.9937$ for AFB1, and $r^2 = 0.9966$ for FMs were obtained, with RSD values between 1.5 % and 5.9 %. (Di Nardo et al. 2019)

Zinoubi *et al*., 2020 developed a thermolysin-based biosensor for the impedimetric detection of ochratoxin A (OTA) in food matrices. A film of cross-linked calcium cellulose (CCLC) was used as stabilizer for the electrochemical formation of gold nanoparticles in graphene nanosheets deposited on glassy-carbon electrodes. A matrix of polyvinyl alcohol (PVA) / polyethylenimine (PEI) was used to immobilize the thermolysin enzyme (TLN). The developed biosensor demonstrated a wide linear range from 0.2 nmol L^{-1} to 100 nmol L^{-1}, with LOD of 0.2 nmol L^{-1} (Zinoubi et al. 2021).

8. Quantum Dots

8.1. Quantum Confinement, Band Gap and QD Morphologies

When it comes to very small sizes, nanoparticles might be inferred as (*i*) clusters (giant molecules), with thousands of atoms and atomic orbitals (build up approach) or, (*ii*) as very small crystals torn apart from the bulk (top-down approach) (Iqbal, Preece, and Mendes 2012).

Nanoparticles with a few nm sizes (< 6 nm) are called Quantum Dots (QD) (Mittelstädt, Schliwa, and Klenovský 2022). They usually are semiconducting nanocrystals with high density of levels in the middle of their band, and discrete levels on the borders, something ascribed to the so-called Quantum Confinement Effect (de Mello Donegá 2014; Thambidurai et al. 2010).

The quantum confinement effect disrupts the Quasi-continuity of energy levels of the band theory, with a measurable increase in the Band Gap energy (Eg) by the reduction of particle sizes due to the difference of HOMO and LUMO energy levels (Fig. 6). That allows absorption and emission light properties to be tuned by the size, shape and composition of the QD (Zhu et al. 2017).

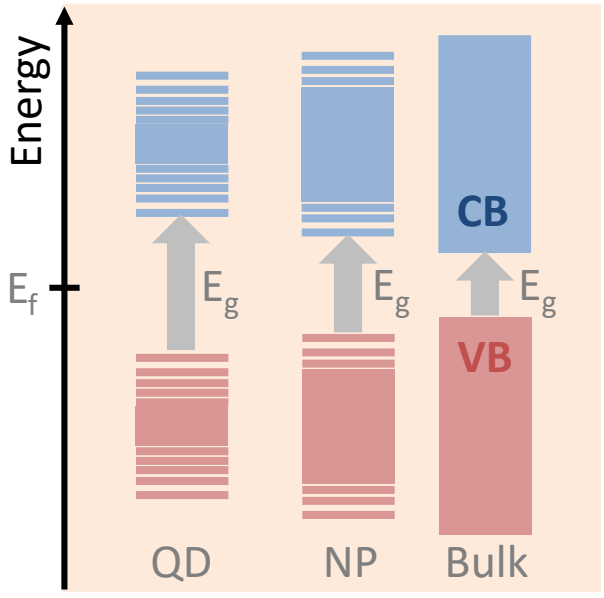

Fig. 6. Energy levels distribution for Quantum Dots (QD), Nanoparticles (NP), and the bulk of a hypothetical semiconductor. Observe that the band gap (Eg) diminishes with increasing sizes. Fermi-level (Ef) remains approximately in the middle of the band gap for intrinsic semiconducting materials.

The dimensional thresholds for the confinement regime are dictated by the exciton Bohr radius (r_B) (Koole et al. 2014).

$$r_B = \frac{h^2 \varepsilon_0 \varepsilon}{e^2 \pi m_{ef}}$$

The r_B is the exciton Bohr radius, h is the normalized Planck constant, ε_0 is the vacuum permittivity, ε is the particle dielectric constant, "e" is elementary charge value and m_{ef} is effective mass of carriers. The exciton Bohr radius (r_B) is interpreted as the most probable distance between electron and holes (charge-carriers). Particle sizes close or smaller than r_B designate a strong confinement effect, which both carriers show enough kinetics energy to overcame the coulombic interaction, and be treated as energetically independent quasi-entities. The arithmetic addition of their energies is the so-called confinement energy that shall be summed to the bulk band gap to determine the QD band gap. That's why higher QD band gaps are observed than the original bulk ones, even for the same material and composition (Koole et al. 2014). When particle size overcomes twice or three times r_B, a weak confinement effect is observed, with much attenuated optical effects.

A quite interesting relation is observed for r_B with corresponding band gaps (E_g): the higher E_g, the lower r_B is. That means that different materials show different sizes thresholds to be under a reasonable confinement effect (Table 1). The quantum explanation for that is that effective masses (m_{ef}) increases with the E_g, and so the exciton localization, which demands smaller particle sizes to propitiate the confinement conditions (Koole et al. 2014).

Table 1. Band Gaps (Eg) and Exciton Bohr Radius (rB) for PbSe and ZnS semiconductors.

Material	Band Gap (Eg)	Exciton Bohr radius (r_B)
PbSe	0.26 eV (4769 nm)	46 nm
ZnS	3.7 eV (335 nm)	1.5 nm

Data from: (Moreels et al. 2007; Y. Li et al. 1999)

The exciton confinement is observed at several nanoarchitectures, which might provide a three-dimensional confinement with no degrees of spatial freedom, the so-called zero-dimensional confinement (0-D). That happens due to the lower potential energy of carriers inside the QD than in the surroundings, forming a potential well (Groeneveld and de Mello Donegá 2014). Examples of these architectures are the (*i*) colloidal semiconductors nanocrystals (Donegá 2011), prepared by wet chemical synthesis; the (*ii*) self-assembled QDs that are synthesized by vapor phase epitaxy (Bhattacharya, Ghosh, and Stiff-Roberts 2004)and; (*iii*) epitaxial laterally gated QDs (Elzerman et al. 2004), formed in a semiconductor crystal by the field effect of a gate electrode over a 2-dimensional electron gas (2DEG) (Elzerman et al. 2004).

Those are typical cases of 0-D spherical QDs, with spherical potential well. Apart from them, many other shapes can be obtained during the colloidal synthesis of nanocrystals, *e.g.* cubes, stars, pyramids and several other polyhedra. There is still the 1-D (*e.g.* nanorods) and the 2-D (*e.g.* disks) shapes, and even more complex morphologies (*e.g.* nanorings) (Donegá 2011).

Molecular-beam epitaxy usually leads to non-spherical 0-D, like pyramids or thin films. Nanowires might be grown by several other strategies, reported elsewhere (Hocevar et al. 2012). Non-spherical QDs are possible once all dimensions are small enough compared to exciton Bohr radius, leading to discrete energy levels. The confinement might vary along different directions as well (Alivisatos 1996). Quantum Wires or Quantum Rods are examples of 2-D confinements (their differentiation depends on aspect ratio). Quantum Wells are observed for 1-D exciton confinements in the thickness direction.

It is important to mention that properties of metallic nanoparticles (*e.g.* gold) (Link and El-Sayed 1999) can also be size-dependent. However, they do not create excitons, but plasmon resonances (oscillations of free electrons) observed at sizes smaller than 50 nm. The highest energy band of metals is partially filled, and the Fermi level lies close to the middle of it. As a result, the density of states near the center of the band is only affected when sizes approach the cluster regime, which is comparable or smaller than the Fermi wavelength of the metal (< 2

nm). No quantum confinement is observed for sizes above that, only the spatial confinement of plasmon resonances of metals, which explains changes in colors of their colloidal suspensions.

8.2. Optical Transitions in QD

The absorption spectra of QD (Fig. 7) comprise a series of peaks ascribed to parity-allowed optical transitions between QD discrete energy levels. An electron is excited from a ground state orbital to an excited state orbital by the absorption of a resonant photon, forming the exciton. Electron and hole occupies discrete levels available in the conduction and valence bands, respectively. A hot exciton is characterized by both carriers occupying excited states (i.e. above/under the first level of bottom/top of bands). They decay to ground states by the intraband non-radiative relaxation, in a mechanism characterized by the translational entropy gain and heat dissipation (Koole et al. 2014; H.-Z. Song 2020; Kambhampati 2011).

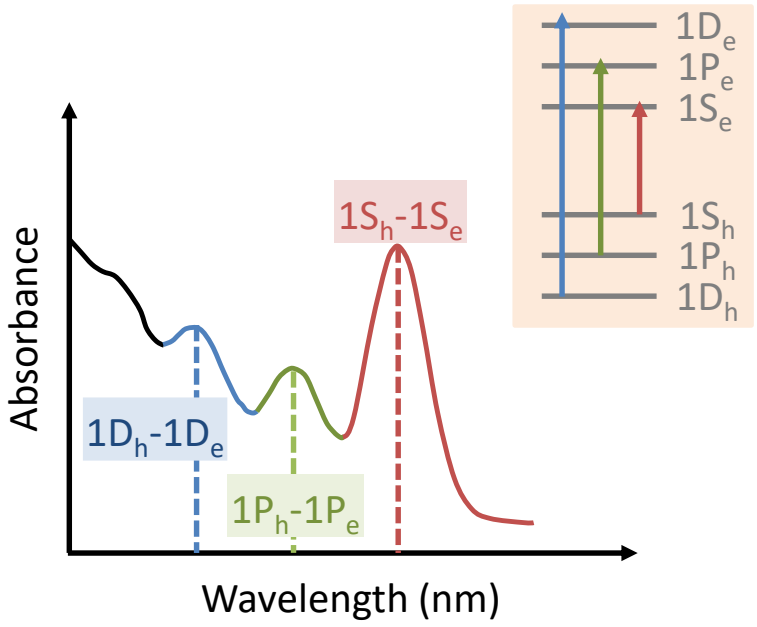

Fig. 7. Hypothetical representation of absorption spectrum of a colloidal quantum dot with transitions assignment. Inset: schematics of three lowest electron (e) and hole (h) energy levels in a semiconducting QD, with corresponding parity allowed transitions represented by arrows.

Once in ground state, further relaxation only can happen by the electron-hole recombination, i.e., excited electrons return to valence band and the exciton energy is released radiatively (by photon emission) or non-radiatively (Bockelmann 1993). The result is a well-defined peak with very close energy to the lowest energy absorption transition, that is, usually, the band gap.

The QD size is herein important to determine the absorption transitions, as well as its size and shape distributions are responsible for the peak width, under an inhomogeneous line broadening mechanism. The fluorescence of QD commonly happens by a spontaneous non-stimulated emission, which is dependent of the vacuum fluctuations. So it depends on the magnitude of the dipole moment of the transition, and the density of optical modes in vacuum that might assist the transition by the coupling (Zijlstra, Orrit, and Femius Koenderink 2014).

Competing with radiative recombination is the recombination mediated by defects or impurities in the QD semiconductor matrix. The trapping of excited electrons or holes is a very fast process that localizes the carriers, decreasing their wave-function overlap, and quenching the exciton emission. In traps, carriers can undergo relaxation by coupling with phonons in a non-radiative phenomenon, or they can emit a broad emission band at lower energies than the band gap, in a process with low quantum yields (< 5 %) (Donegá 2011).

The surface is the most abundant source of traps in nanocrystals, since interfacial atoms do not experience the interior neighboring effects, and possess unsatisfied coordination field, with dangling bounds (Alivisatos 1996; Donegá 2011). The unshared orbitals constitute energy levels inside the semiconductor band gap, which are surface states that act like carrier traps. Surface defects supplies energy states as well that can trap carriers even more effectively than interfacial dangling bounds. Therefore, the surface of semiconducting QD must be passivated to eliminate these dangling bounds, even by overgrowing a more insulating semiconductor shell around them, or by their coating with some proper organic ligands (Donegá 2011).

Another non-radiative pathway for exciton recombination is the inter-QD energy transfer called resonant exciton energy transfer (ET) (Fig. 8). Neighboring QDs transfer the exciton one to another through a dipole-dipole interaction (Rogach et al. 2009), instead of a

radiative ET by QD reabsorption of light. To happen, some conditions must be attended: (i) the distance between both QDs must be very small; (ii) the transitions of the acceptor QD must be resonant with the transition of the donor QD (spectral overlap) and; (iii) the transfer rate is dictated by the orientation of both dipoles (Rogach et al. 2009).

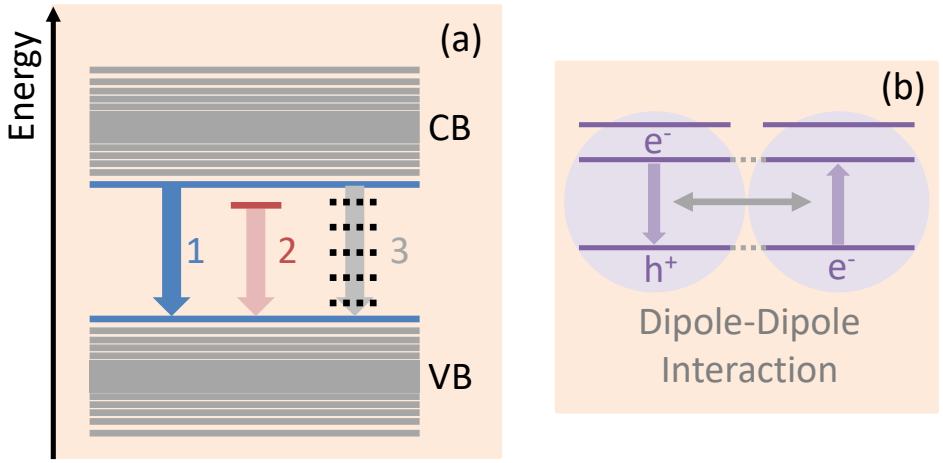

Fig. 8. (a) Schematic hypothetical representation of the exciton recombination in QDs: (1) radiative, (2) defect-assisted radiative recombination, and (3) non-radiative recombination. (b) Representation of exciton energy transfer from a QD donor to a QD acceptor mediated by a dipole-dipole interaction.

To control the spectroscopic relations in QDs, it is important to measure their exciton lifetime, which is possible using the photoluminescence (PL) decay times (τ), described by:

$$\tau = \frac{1}{W_{tot}} = \frac{1}{Q_{rad}} + \frac{1}{W_{NRad}} + \frac{1}{W_{ET}}$$

The Wtot is the total decay rate, Wrad is the radiative decay rate, WNRad is the non-radiative decay rate and WET is the energy transfer rate (negligible for diluted QD suspensions). For merely radiative decays, PL follows a single exponential behavior:

$$N(t) = N_0 e^{-t/\tau}$$

Considering t the elapsed times starting from the excitation, τ the exciton radiative life time, and N0 the population of emitting state for null time, determining initial PL. When the other components are observed (NRad and ET), PL decays might be fit by a multiexponential

function with different contributions for the rates. The ratio between radiative and non-radiative decay rates reflects the PL quantum yield (QY), the direct relation between the emitted and absorbed photons. The QY is a very important parameter of QDs system, minding the sensitivity of analytical procedures based on the PL optical detection (Zijlstra, Orrit, and Femius Koenderink 2014). A myriad of other applications might be envisioned, like Lasers (Y.-S. Park et al. 2021), Optical amplifiers (Sugawara et al. 2004), Single-photon sources (Senellart, Solomon, and White 2017), LEDs (Wood and Bulović 2010), biomedical imaging (Wagner et al. 2019), photovoltaic applications (Duan et al. 2021), and photocatalysis (R. Wang et al. 2017).

8.3. Heteronanostructures of Semiconducting QDs

Heteronanostrucutured QDs (HNC) are semiconducting heteronanocrystals with two or more different materials joined in the same particle by one or more heterointerfaces (Donegá 2011). Their syntheses contemplate novel optoelectronic characteristics to extend QDs applicability, by the nanotailoring of charge carrier localization regimes by the alignment of energy levels of materials in the heterojunction. Three major types might be identified: type-I, type-I1/2 (or quasi-type II) and type-II (Donegá 2011).

Type-I comprises a regime which the band gap of one semiconductor lays entirely within the band gap of the other, confining carriers in the narrower gap material and, thus, resulting in a direct exciton (e.g. CdSe/ZnS). They are the most investigated colloidal semiconducting QDs (Reiss, Protière, and Li 2009) for the fact that the exciton remains confined in the core, protected against photodegradation and trapping by both surface dangling orbitals and defects. Their QY are usually very high (QY > 50 %) (Reiss, Protière, and Li 2009). The excitation process is mainly ruled by the lower core Eg, despite the exciton leakage, which the exciton wave function is partially spread to the shell semiconductor, and a red shift is observed for emission and absorption peaks.

Type-II describes a regime with the alignment of semiconductors levels, spatially separating photoexcited electrons from holes, and forming an indirect exciton (e.g. CdTe-CdSe). That leads to longer radioactive lifetimes (Ivanov et al. 2007; de Mello Donegá 2010),

increased exciton polarizability (Ivanov et al. 2007), and emission at lower energies than the band gap of both semiconductors (Donegá 2011). This red-shift is usually large, ascribing type-II HNC to promising near-IR emitters.

Thick shells are still demanded to achieve the type-II regime, since thin shells normally sustains the type-I1/2 HNCs. Some drawbacks regarding to type-II regime are the loss of the lower energy absorption band with increased bandwidths (de Mello Donegá 2010; Donegá 2011), the reasonable reduction of absorption cross sections at emission energies, and the longer exciton radiative lifetimes with 1–2 magnitude orders longer than direct excitons of the exact same semiconductor (de Mello Donegá 2010; Donegá 2011).

Type-I1/2 regime is characterized by the confinement of a single carrier in one of the semiconducting components; while the other is delocalized over the whole HNC (e.g. CdSe/CdS core/shell QD with holes confined in CdSe core and electron delocalized over the entire HNC (A. Pandey and Guyot-Sionnest 2007). Redshift is much larger than that observed for type-I HNCs, since there is considerable loss on the confinement energy due to the delocalization of one of the carriers in the whole HNC (de Mello Donegá 2010). Stokes shift is small and comparable to the type-I HNC, with distinct and well-defined peaks (de Mello Donegá 2010), and even higher PL QYs (~ 80 %) (A. Pandey and Guyot-Sionnest 2007; de Mello Donegá 2010)

8.4. Synthesis and Characterization of QDs

The synthesis of nanomaterials in general follows, mainly, the Top-down or Bottom-up approaches (Brydson and Hammond 2005b; Thanh, Maclean, and Mahiddine 2014). In Top-down process, the nanostructure is removed apart from a bulk material by lithography, electron or ion beam or even X-rays. Bottom-up processes use atoms and molecules as building blocks to progressively produce larger structures until the nanoscale. We will focus our attention on these last methods, since they are most common ones to produce QDs. (Fig. 4)

Vapor phase deposition might be divided in physical vapor deposition (PVD) or chemical vapor deposition (CVD). Both are used to fabricate thin films multilayers, nanotubes or even freestanding/embedded nanoparticles (Brydson and Hammond 2005a). CVD is

performed by the reaction/thermal decomposition of a gas precursor at temperatures between 500 and 1000 ºC, followed by deposition on a substrate. The Molecular Beam Epitaxy (MBE) is a variation of CVD, and the precursors are deposited directly on the substrate, allowing the growth of layers with atomic precision.

This technique can also be termed as Chemical Beam Epitaxy (CBE), Metallorganic MBE (MOMBE) or Metallorganic CVD (MOCVD), depending on the type of precursor. MOCVD is important to assemble compound semiconductors thin-films, like AlGaAs. The composition of subsequent layers is changed to fabricate complex multicomponent nanostructured thin-films. A smaller band gap material is usually sandwiched between wider band gap semiconductors in a 2D-condined quantum well. 0D-confined quantum dots can be produced as well, embedded in a wider band gap semiconductor matrix (H.-Z. Song 2020).

The Vapor-Liquid-Solid (VLS) method deposits a metal nanoparticle on a substrate, and heats it above the eutectic temperature of the system, under a vapor-phase source of semiconductor, resulting in a droplet of the metal-semiconductor alloy. Proceeding with the semiconductor feeding into the droplet supersaturates the eutectic, nucleating and growing the solid semiconductor in the nanowire form at the solid-liquid interface (McIntyre and Fontcuberta i Morral 2020).

Liquid-phase methods perform a precipitation reaction in solution, and are divided in colloidal (Burda et al. 2005), sol-gel (Lee et al. 2016) and templated growth (Alvarez-Paneque et al. 2013) methods. Templated growth is observed in liquid-phase under templating and confining structures. In sol-gel methods (Lee et al. 2016), the metal precursors undergo hydrolysis and condensation reactions, resulting in colloidal sols that aggregate into a gel porous network. The gel undergoes the syneresis densification, with pores contraction and solvent expel. It can still be dried to achieve a nanoporous structure, and thermally treated to become a glass monolith. It is commonly used to synthesize nanopowders, thin films (50 to 500 nm), fibers and nanocomposites.

Colloidal methods rely on nucleation and nanoparticles growth under chemical reactions within a solvent, forming a colloidal sol (Donegá 2011; Burda et al. 2005). These methods are

inexpensive, facile and scalable, with high versatility into the production of nanoparticles with variable compositions: since single compounds, alloys and doped materials, until any combination of two or more materials, joined by one or more interfaces. Sizes herein achieved are small compared to MBE or MOCVD synthesized materials (with relative large lateral dimensions of more than 10 nm, and usual weak quantum confinement regime). Colloidal nanoparticles can still be subjected to post-synthesis procedures, as size selection, surface functionalization, and processing with polymers to form nanocomposites. Films of such nanoparticulate materials are prone to be applied in optoelectronic devices as LEDs, solar cells, photodiodes, photoconductors and field-effect transistors (Shirasaki et al. 2013).

The properties of synthesized nanomaterials must be thoroughly examined for their characterization and alignment with envisioned applications. It is a broad subject, with deep particularities; so, our role here is to merely point a brief overview of the essential.

As clearly discussed, size shape and the crystal structure is fundamental to understand many properties of the material, such as its optical transitions. Transmission Electron Microscopy (TEM) and High-Resolution TEM (HRTEM) are tools to observe size and shape, while HRTEM can also provide information about the crystal structure and chemical composition of nanomaterials associated with the electron diffraction analysis, and energy-dispersive X-ray spectroscopy (EDS). X-ray diffraction (XRD) is used to study the crystal structure of nanomaterials and can provide information of the nanoparticles size by peak broadening in XRD patterns (Donegá 2011).

Surface characterizations can be performed by combined small-angle X-ray scattering (SAXS) and high-energy wide-angle X-ray scattering (WAXS), observing the degree of interior strain and disorder, but also by extended X-ray absorption fine structure (EXAFS). Nuclear Magnetic Resonance Spectroscopy (NMR) has been applied to investigate the in situ composition of surfactant layers in colloidal nanoparticles (Donegá 2011).

To investigate the optical transitions and electronic structure of nanomaterials in general, a myriad of spectroscopic techniques is required (Rogach et al. 2009; Gaponenko 2010). Absorption spectroscopy, photoluminescence (PL) and PL excitation (PLE) provide

information about the energy level structure, and can identify radiative recombination at dopants and/or defects. Time-resolved PL spectroscopy (TRPL) is used to study the photoexcitation dynamics in colloidal nanoparticles, supplying information of radiative and non-radiative recombination. For intraband relaxation, multiexciton generation/decay and charge injection (fast processes in nature), the combination of ultrafast TR techniques is applied, such as transient absorption and THz rime-domain spectroscopy. Scanning Tunneling Spectroscopy (STS) is used to unravel the electronic energy levels of individual metallic and semiconducting nanoparticles. Finally, the Electron Paramagnetic Resonance (EPR) spectroscopy is important to determine paramagnetic ions in nanoparticles to differentiate surface from inner dopants (Donegá 2011), besides the study of donor/acceptor interactions with exciton carriers.

8.5. Application of Quantum Dots for Mycotoxins Analysis

Considering the mycotoxins maximum levels allowed in cereals and related cereal products by, e.g., the European Commission Regulation (1881/2006), there is a substantial challenge for detecting such low concentrations at ppb magnitude order in complex food products (e.g. TAF (4 ng/g), DON (200–500 ng/g), ZEN (20–50 ng g^{-1}), and OTA (0.5 ng g^{-1}).

Still, the identification of emerging mycotoxins and their synergistic effects (Freire and Sant'Ana 2018) usually requires the use of multi-target procedures, demanding advanced instrumental methods such as the liquid chromatography-electrospray ionization-tandem mass spectrometry (LC-ESI/MS) (D.B. Kim et al. 2019), with long sample processing times and high instrument costs that impair the screening of a large number of samples (S.Y. Zhou et al. 2020). That’s why mycotoxin immunoassay development has approached and nearly surpassed chromatographic methods (S.Y. Zhou et al. 2020).

Hundreds of immunoassay methods have been developed addressing the fast mycotoxins detection, using ELISA, flow injection immunoassay (FIIA), chemiluminescence (CL) immunoassay, lateral flow immunoassay (LFIA), and flow immunoassay (J. Singh and Mehta 2020; Matabaro et al. 2017; Sarter and Zakhia 2004; S.Y. Zhou et al. 2020). Among other immunological methods, ELISA, and LFIAS stand out for their simplicity, agility and

long-term stability under different climatic conditions, ascribing them to suitable on-site mycotoxin detection (S.Y. Zhou et al. 2020).

Nanomaterials play an important role on all the immunoassay development due to their good biocompatibility, high stability, versatility, ease of synthesis, and surface modification. Gold nanoparticles (GNPs) combined with enzymes, antibodies or DNA are very well established in immunoassay (S.Y. Zhou et al. 2020), with the crucial function of amplifying the signal to improve the method sensitivity with long-term stability. In this context, quantum dots (QDs), as nanoparticles subclass, exhibit unique characteristics that make them hold great promise as well. QDs can be also used in construction of aptamers with good performance.

One should only be aware of some QDs cytotoxicity (e.g. CdTe), which can be reduced by QD wrapping in a core-shell nanostructure. CdTe cytotoxicity comes from both Cd(II) QD corrosion release and the intracellular distribution of nanoparticles associated with the nanoscale effect (X. Han et al. 2019), which should be carefully considered when using QDs as labels.

Electrochemical sensors (EC) have been gradually applied to monitor mycotoxins on account of their high sensitivity, easy operation, cost-effectiveness, and rapid detection. (S. Dong et al. 2022) EC biosensors use antibodies, nucleic acids or aptamers to react with the target in a recognition mechanism, and then apply the sensitivity of EC transducers to convert the concentration change of target analyte into an electrical signal. QDs might be involved in a myriad of EC sensors, playing different roles according to their applications.

Amperometric biosensors use the current generated by electroactive substances under surface redox reactions as the analytical signal. Usually, pulsed voltammetric techniques are herein used for the signal acquisition due to their improved current-to-noise ratios.

Photoelectrochemical (PEC) biosensors quantify the mycotoxin target by measuring the photocurrent or photopotential developed based on the photovoltaic principle(Xing et al. 2020). During operation, materials are excited by incident light forming the exciton and the corresponding charge-carriers. For the so-called “Signal-on” PEC biosensors, photocurrents directly increases with the mycotoxin content, being of competitive or non-competitive kind.

Competitive sensors refer to limited specifically binding sites of biomolecules, filled with the target analyte and/or labeled analyte (the tracer). As mycotoxin increases, few labeled compounds will attach to the biomolecule sites, changing the signal recording. Using these concepts, Youxiu et al. (Lin et al. 2016) devised a signal-on PEC immunosensor platform for quantitative monitoring of aflatoxin B (AFB, as a model) in foodstuff based on the ion exchange reaction of silver nanolabels with CdTe QDs.

First, a competitive immunoreaction was accomplished on a high-binding microplate with silver nanoparticles labeled with AFB1-bovine serum albumin (AFB1-BSA), the so-called tags. Then, these tags were dissolved by acid to release the Ag(I), which performed an ion-exchange with the CdTe QDs immobilized on the electrode, forming a surface exciton trap that decreases the photocurrent of the modified electrode. However, the photocurrent increases with the augment of target AFB, with a dynamic range from 10 ng L^{-1} to 15 µg L^{-1}, and LOD of 3.0 ng L^{-1}. Besides, the method have shown high enough specificity, reproducibility, and accuracy to detect the naturally contaminated and spiked blank peanut samples, being even validated with reference ELISA method (Lin et al. 2016).

For another PEC competitive-type immunoassay approach of Knopp's group (Lin et al. 2017), the immunoreaction was accomplished on anti-AFB1 antibody-modified magnetic beads using glucose oxidase (GOx)-labeled AFB1-bovine serum albumin (AFB1–BSA) as the tags. Visual and PEC evaluations were performed with carbon QDs (CQDs)-functionalized MnO_2 nanosheets. By the immunocomplexes formation, the GOx generates the oxidizing hydrogen peroxide from the glucose substrate, which reduces the MnO2 nanosheets into Mn(II) ions and dissociates the CQDs from the electrode surface. Detection could be evidenced by both the visual inspection of the MnO_2-CQDs-coated electrode and the photocurrent decrease. And again, the photocurrent directly increased with the augment of the target AFB1, with a dynamic range of 0.01 to 20 µg L^{-1}, LOD of 2.1 ng L^{-1}. Good reproducibility and reasonable accuracy were found from investigations, with well-matched results with AFB1 ELISA. Other PEC methodologies with similar detecting principles can be found elsewhere (Tang et al. 2019) (Su, Song, et al. 2019).

The so-called “signal off” PEC sensing describes methods which, photocurrents (or photopotentials) from the sensing substance interaction with captured biomolecules decay with increasing concentrations of mycotoxin, still addressing competitive or non-competitive types.

As a competitive “signal off” PEC biosensor, Zhang et al. (Su, Tong, et al. 2019) reported an immunoassay with amorphous TiO2 and perovskite CsPbBr3 QDs (CsPbBr3/a-TiO2) for the sensitive detection of AFB1 in foodstuff. The a-TiO2 layer was used both as a charge-transfer layer and to stabilize CsPbBr3 nanocrystals, improving the photocurrent response. The competitive enzyme immunoreaction was performed on a microplate with analyte interaction with alkaline phosphatase (ALP)-labeled AFB1-bovine serum albumin (AFB1-BSA) conjugate. The carried ALP generates the enzymatic hydrolysis to produce the ascorbic acid electron donor, a photocurrent enhancer of CsPbBr3/a-TiO2-modified electrode. Coupled with the competitive enzyme immunoassay, the modified electrode photocurrent decreased with the augment of target AFB1 concentration, forming a 0.01 μg L^{-1} to 15 μg L^{-1} working range with LOD of 2.8 ng L^{-1}. Real samples of peanut and corn were analyzed, supplying acceptable accuracy once compared with the referenced AFB1 enzyme-linked immunosorbent assay (ELISA) method.

QDs properties render them an interesting role in the development of highly sensitive Lateral Flow Immunoassays (LFI), endowing them with great application prospect. However, original QDs were synthesized with toxic Pb, Cd, and Si, which represents great environmental harm. Carbon QDs (CQDs) are an interesting alternative, showing stable optical properties, low toxicity, low price of production, and simple synthesis routes. Still, QDs show low chemical stability in biological environment, leading to inaccurate quantitative analysis. Several groups have recently proposed the doping or encapsulating of QDs to improve their stability and detectability by increasing the amount of immobilized QDs in each device (Xing et al. 2020).

Allying the inherent properties of PEC with the specific affinity of bio-recognition elements, highly selective and sensitive methodologies can be developed, something that is even more pronounced with new arising nanomaterials and detection formats based on novel principles. QDs are very interesting materials for that, since their quantum confinement effect spread the charge-carrier wavelength through the whole nanocrystal, reducing charge

recombination with the improved inner particle charge transport (Baccaro and Gutz 2018). However, the electrode/electrolyte interface deserves great attention since it plays crucial role on charge-transfer kinetics and outer particle recombination.

Nevertheless, traditional PEC biosensors usually are not able to simultaneously detect groups of analytes due to the confinement of the sensing interface on the electrode, which limits practical applications. Split-type and integrating PEC biosensors with arrays, microfluidics and chips might contribute to high-throughput and automation. Finally, the PEC biosensors portability is crucial for the point-of-care or in situ field detection on crops and foodstuff, consolidating hand-held instruments and miniaturized signaling devices, such as the user's smartphone(Q. Zhou and Tang 2020) .

9. Carbon-based Materials

Carbon-based materials refer to a wide range of substances that are primarily composed of carbon atoms. Carbon is a versatile element that can form various structures, resulting in diverse materials with different properties and applications. Some common examples of carbon-based materials include graphene, diamond, graphite, carbon nanotubes, fullerenes, carbon fibers, and carbon black (Fig. 9)(Speranza 2021).

Carbon atoms can form long chains of atoms. They can display distinct physical structures with different properties despite of the same chemical composition depending on electronic structure and atomic size. Carbon atoms can hybridize with sp, sp^2, sp^3 and a narrow band gap between their 2s and 2p electron shells. Sp^3 hybridized diamond and sp^2 hybridized graphite are two commonly known allotropic forms of carbon. The basic criterion for their classification is the geometric structure of nanomaterial particles. The particles may be in the shape of tubes, horns, spheres or ellipsoids. The tube-shaped or corner-shaped particles are called carbon nanotubes (CNTs) or carbon nanorods (CNHs), respectively; 0D nanodiamonds, 1D nanotubes, 2D graphene nano-sheets can act as a prototype nanocomposite (Kour et al. 2020). Advances in nanomaterial synthesis have resulted in sensing systems that display improved analytical performance. The use of nanomaterials within sensors provides new routes for the detection of target molecules (Speranza 2021).

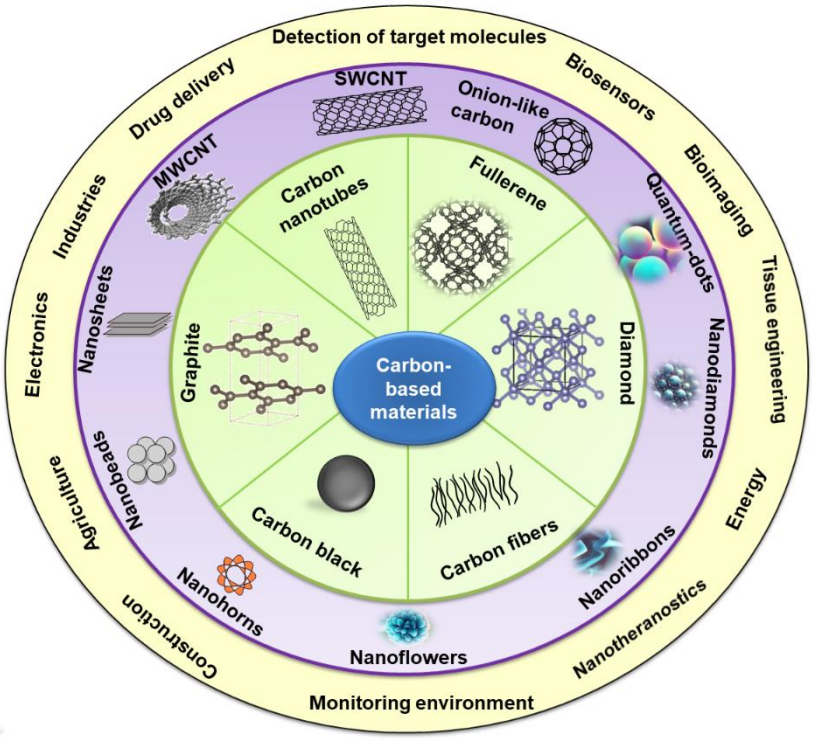

Fig. 9. Carbon-based materials and their applications.

Furthermore, carbon-based sensors have demonstrated biocompatibility, good sensitivity and selectivity, and lower limits of detection for a wide range of molecules. Due to their characteristics, which include a high specific surface area, high electrical conductivity, and flexibility that support their usage in sensing applications, carbon nanomaterials are among the most investigated materials (Speranza 2021). Thus, carbon's ability to form diverse structures allows for a wide range of properties and applications in different fields, including electronics, construction, agriculture, energy, monitoring environment, nanotheranostics, and detecting toxins in food applications. (Luo et al.),(Isakovski et al. 2021; Liang et al. 2021; S. Pandey et al. 2023)

9.1. Graphene

Honeycomb two-dimensional graphene gained considerable attention since its discovery in 2004 (Fang et al. 2011). Among carbon-based materials, graphene stands out due to its unique characteristics, which make it promising in applications such as polymer-

composite materials, hydrogen storage and energy systems (Hou et al. 2011), electronics, biomedical applications such as drug delivery, tissue engineering, biosensors and bioimaging (Shen et al. 2012), water and sewage treatment, removal of heavy metals and desalination. (Liang et al. 2021)

Graphene has also been employed in many biosensors approach, especially for electrochemistry-based sensing platforms. Graphene shows the same intrinsic physical and chemical properties as graphite, including a high surface area and numerous active sites. Its superiority comes from the higher electron transfer rate, increased thermal conductivity, mechanical flexibility, and biocompatibility (Y. Wang et al. 2011).

In general graphene is considered chemically inert, and its surface in the pristine form normally interacts with other molecules via physical adsorption (π-π interactions). To improve reactivity, surface defects or functional surface groups are usually introduced: e.g., the chemical doping with B or N atoms and the introduction of carboxyl, carbonyl, and amine groups can adjust the surface and electronic properties of graphene. The electrical conductivity (up to 2.104 S/cm) and the high electron mobility (2.105 cm^2/Vs, more than 100 times higher than silicon) in graphene monolayers result from a small effective mass. Once the structure electronics of a graphene monolayer overlaps two conical points in the Brillouin zone, the charge carriers can be understood as “massless” electrons or Dirac fermions (D. Chen, Tang, and Li 2010).

The electrons in a single layer of graphene behave like massless particles, moving at a speed of approximately 106 m/s. (Novoselov 2011; Wei and Kivioja 2013). Moreover, its thermal conductivity at room temperatures can reach 5000 W/m K (e.g., copper is 400 W/m K), which suggests potential uses for thermal management applications. It has a very high surface area (2600 m^2/g), much greater than graphite surface areas (10 m^2/g), and carbon nanotubes (1300 m^2/g). Regarding the optical properties, graphene might be considered almost transparent, absorbing a fraction of 2.3% of the sunlight, which is related to its electronic properties, as well as the low-energy electronic structure (conic bands meeting at the Dirac point). Graphene system still allows the ultrafast tuning of its optical properties. (Wei and Kivioja 2013)

9.1.2. Synthesis of Graphene

Methods for graphene preparation can be divided into different groups: mechanical exfoliation of layers from highly oriented pyrolytic graphite (Y. Wang et al. 2011), chemical vapor deposition (CVD) with hydrocarbon decomposition on metals (Sutter, Flege, and Sutter 2008; K.S. Kim et al. 2009; Y.S. Dedkov et al. 2008; Reina et al. 2009; Coraux et al. 2008), deposition of thin films (< 75 μm) on Ni, Cu and Co, epitaxial growth on Silicon Carbide (SiC) for template growing graphene, and SiC decomposition to produce no-defects thin films (>50 μm) (Ohta et al. 2006; Y. Dedkov and Voloshina 2020), are some examples.

Electrical arc discharge method can provide nanosheets up to10 μm with high crystallinity, low cost and allows large-scale production (Eda, Fanchini, and Chhowalla 2008; L. Huang et al. 2013) However, non-uniform sheets and low purity materials are produced. Graphene nanoflakes can be obtained by chemical method using graphite dispersions (Stankovich et al. 2006).

Most scalable, cost-effective and productive method is the graphite exfoliation on graphene-type materials, like graphite oxides (GO) (S. Park and Ruoff 2009). GO is obtained as a highly oxidized form of graphene, produced by its surface reaction with strong oxidizing agents. GO shows excellent surface functionability, amphiphilicity, fluorescence quenching ability and surface-enhanced Raman's scattering property (Chung et al. 2013). These exceptional characteristics are due to small sp^2 carbon domains that are enclosed by sp^3 domains, and the oxygen-containing hydrophilic functional groups (Loh et al. 2010).

Hummer's method is widely used to synthesize GO. It includes the oxidation of graphite by potassium permanganate and sulfuric acid (Ponnamma et al. 2015). This exfoliation step followed by sonication result in graphite functionalized salts, which act as GO precursors (Fig. 10). Thermal and chemical reduction processes convert GO into a graphene analog. GO is usually produced by such strategies. Graphite is oxidized to enlarge its interlayer spacing and base planes, so GO monolayer can be peeled off (Allen, Tung, and Kaner 2010).

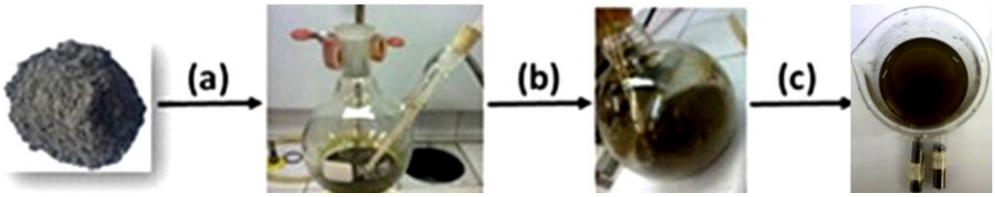

Fig. 10. Schematic representation of graphite oxidation to obtain GO using Hummer's method: system containing graphite powder, sodium nitrate, sulfuric acid and potassium permanganate (a), addition of hydrogen peroxide and deionized water (b), after centrifugation and drying of the material (c).

After the peel off, GO must be reduced to achieve the desired electrochemical properties. Many reaction pathways can be used: thermal annealing and chemical reduction by reducing agents (such as hydrazine or sodium borohydride) are examples. (Allen, Tung, and Kaner 2010). To fully access graphene's outstanding capabilities, it is still important to functionalize it. Surface functionalization can turn pristine graphene or GO into chemically sensitive and dispersible materials, making them suitable for sensing applications.

9.1.3. Functionalization of Graphene

Covalent functionalization is one of the most common surface modification methods for graphene. The structural change may take place both on the basal surface and at the margins/corners. Graphene can be covalently functionalized through reactions with its unsaturated bonds, heteroatoms doping, and rehybridization of sp^2 carbon into sp^3 (Basta et al. 2021).

The covalent functionalization can be achieved by nucleophilic substitution, electrophilic expansion, buildup, and expansion. As a result, a significant layer of sp^3 hybridized carbons is formed in the network, disrupting the delocalized π-cloud. Amino, hydroxyl, sulfonate, or alkyl groups are introduced onto graphene through covalent bonding (Basta et al. 2021; Ramanathan et al. 2008). These groups can also act as anchoring sites to embed proteins, amino acids, and polymers on the surface of graphene (Ramanathan et al. 2008; Farouq 2022).

The formation of covalent carbon-carbon bonds involving the basal plane of carbon atoms offers key advantages, such as greater stability of the hybrid material, controllability over the functionalization degree and reproducibility. As a disadvantage, although covalent strategies can effectively, stably, and specifically install functionalities, they unavoidably cause a loss of the free π electrons (Allen, Tung, and Kaner 2010).

The non-covalent graphene surface functionalization basically includes hydrophobic and hydrophilic interactions: Van der Waals, π-π stacking and electrostatic interactions, and require the adsorption of appropriate atoms on the graphene surface. This non-covalent functionalization does not influence the conductivity of the material (W. Yang et al. 2013). Small aromatic molecules such as quinones, have been used to functionalize carbonaceous materials. Polymer wrapping, the adsorption of surfactants or small aromatic molecules, and interactions with porphyrins or biomolecules, as the deoxyribonucleic acid (DNA), are all methods of non-covalent functionalization (Speranza 2021). This method allows for reversible functionalization, while preserving the original structure of graphene. However, physical adsorption is nonspecific and there is little control over the degree of functionalization. Thus, non-covalent functionalization may be less stable, reproducible and susceptible to environmental conditions of application (Xiao et al. 2023).

There are also other forms of graphene functionalization: doping and plasma treatment. Doping refers to the intentional introduction of impurities into graphene by creating defects and gaps to alter its electrical or optical properties (Loh et al. 2010) Doping can significantly modify graphene band structure, allowing applications in electronics, sensors, and energy storage. Plasma functionalization involves exposing graphene surface to a reactive ionized gas, which can introduce several types of functional groups (Senthilnathan et al. 2014).

9.2. Fullerene

Fullerenes are hollow carbon molecules with a spherical, tubular, or cage-like structure. Fullerenes are composed of isomers, such as C_{60}, C_{70}; C_{240}, C_{540}, and C_{720}, that are commonly used in analytical separations, and chemical species detection (Paukov et al. 2023). The most well-known fullerene is buckminsterfullerene (C_{60}). Fullerenes contain alternating single and

double carbon-carbon bonds, resulting in delocalized π electrons(Yao et al. 2020). This gives them unique electronic properties, such as high electron affinity, and the ability to accept or donate electrons. Molecules are stable with carbon atoms linked themselves by strong covalent bonds.

9.2.1. Synthesis of Fullerene

The process of synthesis of fullerenes, particularly C_{60}, can be performed by several methods (Yao et al. 2020). Most used ones are herein barely described.

9.2.1.1. Arc Discharge Method

Arc discharge method involves vaporizing carbon rods in a high-temperature electric arc. The process normally takes place in an atmosphere of an inert gas, such as helium (Yao et al. 2020). Carbon rods are placed in a chamber, and a high voltage electrical discharge is applied between them. The high temperature generated by the electric arc causes the carbon rods to evaporate and form a cloud of carbon vapor. As the vapor cools, fullerenes begin to form. The resulting soot contains a mixture of fullerenes, which can be extracted and purified using various techniques, such as solvent extraction and chromatography.

9.2.1.2. Laser Pyrolysis of Hydrocarbons

Pyrolysis hydrocarbons in the gas, vapor or aerosol phase are heated and decomposed by absorbing infrared photons emitted by a high power CO_2 continuous laser. Three ways are used to introduce hydrocarbon precursors. The first consists of introducing the gas phase mixture of ethylene and acetylene. The second form uses benzene in the vapor phase, carried out in the laser beam by a mixture of argon and SF_6. And the third way uses liquid hydrocarbon aerosols (benzene or benzene/cyclopentadiene mixture). Then, the carbonaceous powders are collected in a glass chamber containing a metallic filter. (Stevenson et al. 1997)

9.2.1.3. Laser Vaporization Method

High-power laser is used to vaporize a solid source of carbon, such as graphite. (Yao et al. 2020) The laser vaporization process takes place in a chamber filled with an inert gas, such

as helium or argon. The vaporized carbon atoms are rapidly cooled, and then condensed to form clumps, which undergo further reactions to form fullerenes. The resulting mixture is similar to those obtained by the arc discharge method and requires purification.

9.2.1.4. Graphite Heating Resistive Arc Synthesis

This method involves the application of high electrical currents through two graphite electrodes, creating an electric arc between them. (Kyesmen, Onoja, and Amah 2016) As the electric arc heats up, it causes the surrounding carbon material, such as graphite, to undergo thermal decomposition. The high temperatures break down the carbon bonds, leading to the synthesis of new carbon-based compounds.

9.2.1.5. Laser irradiation of poly aromatic hydrocarbon

The synthesis is based on the laser irradiation of polycyclic aromatic hydrocarbons (PAHs) to induce structural changes. The high-energy photons from the laser break carbon-carbon bonds to cause the rearrangements of atoms, leading to the formation of the fullerene structure (Amsharov and Jansen 2008).

9.2.2. Functionalization of Fullerene

The functionalization of fullerenes allows obtaining excellent properties, such as the high electronic affinity, fast charge transfer capabilities, and adjustable structural and textural properties. (Yao et al. 2020) It involves attaching different chemical groups or molecules to the carbon framework of fullerene molecules (Shrestha et al. 2013). There are several types of functionalization techniques that can be used to modify fullerenes, including those below.

9.2.2.1. Addition Reactions

Addition reactions involve attaching functional groups by breaking one or more carbon-carbon bonds in the fullerene structure. Common addition reactions include:

1. *Prato Reaction:* it involves the addition of nucleophiles, such as amines or alcohols, to the fullerene cage through a cycloaddition reaction (Biglova 2021).

2. Bingel Reaction: it involves the addition of nucleophiles, such as malonates or thiols, to the fullerene cage via a cyclopropanation reaction. (Thong et al. 2016)

3. Diels-Alder Reaction: it is employed to attach dienophiles to fullerenes, resulting in the formation of cycloadducts. This reaction can occur at various sites on the fullerene cage (Yadav et al. 2022).

9.2.2.2. Radical Reactions

Radical reactions involve the attachment of functional groups to fullerenes through the generation and subsequent reaction of carbon-centered radicals. Photochemical reactions that involve fullerenes can generate radical species that subsequently react with suitable reagents, enabling its functionalization (Paukov et al. 2023).

9.2.2.3. Electrochemical Functionalization

The electrochemical functionalization of fullerenes takes place on the surface of electrodes, involving redox reactions, where electrons are transferred between the electrode and the fullerene molecules. Depending on the desired functionalization, suitable precursors or reagents are introduced into the electrolyte (Paukov et al. 2023). These reagents can undergo specific reactions with the fullerene, such as addition or substitution. The functionalization process can be controlled by adjusting various parameters, such as the applied potential, current, reaction time and temperature cell. These parameters influence the kinetics and selectivity of the reaction, allowing a fine tuning of the functionalization process. The resulting product is typically characterized using spectroscopic (e.g. UV-Vis, FT-IR, NMR) and mass spectrometry analytical techniques. Purification methods, such as chromatography or recrystallization, are employed to isolate the functionalized fullerenes from the reaction media (García-Simón et al. 2014).

9.2.3. Purification of Fullerene

After the synthesis process, extracted fullerenes often contain impurities, residual solvents, by-products and unwanted substances. Several purification methods are employed, such as high-performance liquid chromatography (HPLC), column chromatography,

sublimation and recrystallization (García-Simón et al. 2014). These methods allow the separation and isolation of specific fullerenes from the mixture. In HPLC and column chromatography, fullerenes are purified based on their size, shape, and polarity. Silica gel, alumina or other stationary phases are often used in combination with different mobile phases (Y. Cui et al. 1992). In sublimation, impurities and volatile components are removed by heating the crude fullerene sample. The mixture is heated under vacuum and the more volatile impurities sublimate, leaving behind the purified fullerenes. Sublimation can be performed in various devices, such as tube ovens or sublimation chambers. The recrystallization involves dissolving the crude fullerene mixture in a suitable heated solvent, and then cooling the solution to allow the crystallization (J. Kim et al. 2016).

Other important method is the solvent extraction, which involves dissolving the crude fullerene mixture in a suitable solvent (e.g. toluene, o-xylene, or carbon disulfide), followed by selective precipitation or filtration. The choice of solvent depends on the fullerenes and impurities solubility. Soxhlet extraction is extensively used to purify fullerenes (D.B. Zhou et al. 2018).

9.3. Carbon Nanotubes

Carbon nanotubes (CNTs) are cylindrical structures made of carbon atoms arranged in a hexagonal lattice. CNTs can be divided in two types: single-walled carbon nanotubes (SWCNTs) and multi-walled carbon nanotubes (MWCNTs) (Andrews et al. 2002; Dai 2002; Zamolo, Vazquez, and Prato 2014). SWCNTs consist of a single graphene sheet rolled into a seamless cylinder. They have diameters on the nanometer size, ranging from 0.4 to 3 nm (Bystrzejewski et al. 2008). MWCNTs consist of multiple concentric layers of graphene sheets. (Kour et al., 2020) MWCNTs have a larger outer diameter compared to SWCNTs, typically ranging from 2 to 100 nanometers (Andrews et al. 2002). The presence of multiple layers contributes to their enhanced mechanical performance compared to SWCNTs. MWCNTs exhibit high thermal conductivity due to the sp^2 carbon structure, and efficient heat transfer along graphene layers.

CNTs exhibit remarkable electrical, mechanical, and chemical properties (Dai 2002; Zamolo, Vazquez, and Prato 2014), with applications in several fields such as materials science, nanotechnology, nanoelectronics, and nanomedicine. Researchers are exploring the use of CNTs in various biomedical applications, including drug delivery (Ruhunage et al. 2023), tissue engineering (Akiyama et al. 2023), and biosensors (Xiang 2011). CNTs are used in the development of supercapacitors and batteries (Rajavel et al. 2012). They can be used into polymer composites to enhance their mechanical, electrical, (Dai 2002) and thermal conductivity properties, beside conferring photo-luminescence. CNTs have a great potential as adsorbent for mycotoxins in antimicrobial food packaging (Dubey et al. 2021), as well as microbicide toward some pathogens (S. Pandey et al. 2023).

CNTs limitations include their low dispersibility (Katouzian and Jafari 2019) in most solvents, which restrict their use (Murphy et al., 2019) and require surface functionalization (Zamolo, Vazquez, and Prato 2014). (Police Patil et al. 2023). The good charge transfer characteristics of CNTs allow their application in the assembling of many immunosensors and electrochemical sensing platforms.

9.3.1. Synthesis of CNTs

Some of the most common methods used for the synthesis of carbon nanotubes are electric arc discharge (Dai 2002), chemical vapor deposition (CVD) (G. Yang et al. 2023), laser ablation (Bystrzejewski et al. 2008), Chemical Vapor Infiltration (CVI) (Manocha et al. 2009), and template-assisted synthesis (Zuo et al. 2023). (Fig. 11). An overview of each method is presented below.

9.3.1.1. Electric arc discharge

In the electric arc discharge, a high-current electric arc is generated between two graphite electrodes in an inert gas atmosphere, such as helium. The high temperature and electric field cause the vaporization of carbon, leading to the formation of carbon nanotubes as a byproduct. This method is relatively simple, but yields a mixture of carbon nanotubes and other carbonaceous materials. It uses high temperatures (above 1700°C) for CNT synthesis, which causes the expansion of CNTs with less structural defects compared to other methods

(Guo et al. 2021). Electric arc discharge provides a high yield and better control over the size of synthesized nanotubes. (Eatemadi et al. 2014)

9.3.1.2. Laser ablation

This method involves the vaporization of a carbon target, typically graphite, using a laser beam in the presence of a catalyst. The high-energy laser vaporizes the carbon, and the vapor condenses and forms carbon nanotubes on the catalyst surface. Laser ablation can yield high-quality carbon nanotubes, but it is a complex and expensive method. The operation of the technique consists of vaporizing the graphite inside the quartz chamber, using laser irradiation with metal particles as catalysts to graphite targets. It should be noted that this method requires a high consumption of energy and carbonaceous material. It has potential to produce SWNTs with high purity, yield, and quality. On the other hand, it may show resulting larger CNT diameters (Ayyub et al. 2001; Dai 2002) Laser properties and other factors such as gas, chamber pressure and temperature, structural, and chemical composition can influence the final characteristics of CNTs. (Bystrzejewski et al. 2008)

9.3.1.3. Chemical vapor deposition (CVD)

CVD is widely used for the controlled synthesis of carbon nanotubes. It involves the decomposition of hydrocarbon precursors at approximately 700°C, in the presence of a metallic catalyst (Reina et al. 2009) (usually iron, cobalt, nickel or other combinations such as MgO and Al_2O_3 (Eatemadi et al. 2014)). Nanoparticles size of the catalysts influence the diameter size of the synthesized nanotubes (0.5–5 nm for SWCNTs; 8 to 10 nm or MWCNTs) (Andrews et al. 2002). Hydrocarbon gas, such as methane or ethylene, is introduced into a reactor at high temperatures, and carbon nanotubes grow on the surface of the catalyst. CVD allows the growth of vertically aligned and well-aligned carbon nanotubes. In addition to the traditional CVD method, there are also modifications that can be optimized, such as catalytic chemical vapor deposition (CCVD) - thermal CVD (Vernardou et al. 2020), or plasma enhanced (PE) oxygen-assisted CVD, and water-assisted CVD (Bystrzejewski et al. 2008). Compared with laser ablation, CVD is practical, economic, and easily controlled, producing high quality CNTs.

9.3.1.4. Chemical Vapor Infiltration (CVI)

CVI is a method used for the synthesis of carbon nanotubes on a template or substrate (Manocha et al. 2009). A carbon-containing precursor gas, such as acetylene or methane, is introduced onto the substrate, which is pre-coated with a catalyst (Manocha et al. 2009). The carbon atoms from the precursor gas are deposited onto the catalyst surface, leading to the growth of carbon nanotubes. CVI allows for the synthesis of aligned carbon nanotubes on specific substrates.

9.3.1.5. Template-assisted synthesis

This method involves the use of templates, such as alumina or porous silica, with nanoscale pores or channels. The template is coated with a catalyst, and carbon is deposited onto the catalyst via techniques like CVD or CVI. (Zuo et al. 2023) The template is then removed, leaving behind carbon nanotubes with the same dimensions of the template's pores. Template-assisted synthesis allows precise control over the resulting dimensions of CNTs (Zuo et al. 2023; Dai 2002). Figure 11 shows a comparative view of the different synthesis methods of CNTs.

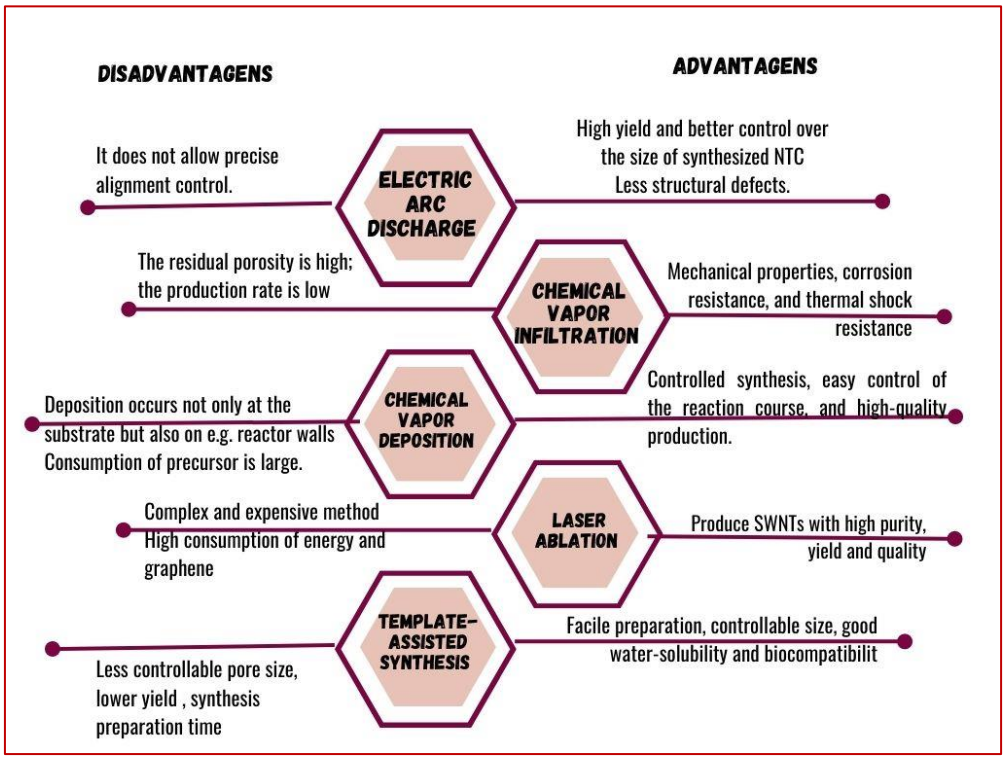

Fig. 11. Comparison of different synthesis processes of carbon nanotubes (CNTs).

9.3.2. Purification of CNTs

Due to significant differences of CNTs synthesis methodologies, resulting materials should be purified to proceed to chromatography processes for size separation (Rajavel et al. 2012) (Eatemadi et al. 2014): e.g., removal of large graphite particles and aggregates by filtration, and elimination of catalyst and fullerenes by dissolution. Purification techniques aim to isolate and enhance the quality of the CNTs for posterior applications. Common purification techniques used for CNTs are described below.

9.3.2.1. Acid treatment

Acid treatment involves immerging the CNTs in strong acids, such as nitric acid or its mixture with sulfuric acid (Yun et al. 2006). The acid treatment helps to remove metal catalyst particles, amorphous carbon, and other present impurities. Acid treatment is normally followed by thorough rinsing and filtration of CNTs. Boiling SWNTs in nitric acid or hydrofluoric acid solutions has shown interesting results to remove amorphous carbon and metallic particles of synthesized CNTs, as well (Yun et al. 2006; Eatemadi et al. 2014).

9.3.2.2. Ultrasonication

Ultrasonication involves cavitation of CNTs in a solvent using high frequency sound waves. The cavitation creates microbubbles that implode near the surface of the nanotubes, dislodging and dispersing impurities. It is often combined with other purification methods, such as acid treatment or solvent washing, to enhance impurity removal. Some researchers prefer to use nanotube sonication and subsequent thermal oxidation of the SWNT material, as well as treatments with hydrochloric acid (C. Li et al. 2022).

9.3.2.3. Filtration

Filtration is a commonly used technique to separate CNTs from larger particles and aggregates. Filters with pore sizes greater (but close) to the desired nanotube diameters are used to trap and retain larger impurities, allowing CNTs to pass through it (Eatemadi et al. 2014).

9.3.2.4. Chromatographic techniques

Different chromatography techniques can be used for purification and separation of CNTs, such as size exclusion chromatography (SEC), or high performance liquid chromatography (HPLC) (Eatemadi et al. 2014). These methods rely on the differential adsorption or elution of nanotubes in a chromatographic column. (Eatemadi et al. 2014) Huang and coworkers described a way to separate semiconductor and metallic SWNTs, using a combination of DNA-dispersed carbon nanotube size exclusion chromatography technique, with ion exchange chromatography for purification of chiral compounds (X. Huang, Mclean, and Zheng 2005).

9.3.2.5. Thermal/Oxidative Treatment

Thermal or oxidative treatment involves subjecting CNTs to high temperatures in an oxidizing atmosphere, such as air or oxygen (Guo et al. 2021). This process can remove amorphous carbon and some types of organic impurities. CNTs are heated to temperatures typically above 400°C, but below their thermal breakdown point. The oxidizing environment helps burn off impurities, leaving CNTs intact (S. Cao et al. 2016).

9.3.2.6. Density Gradient Ultracentrifugation

Density Gradient Ultracentrifugation (DGU) is a method used to separate carbon nanotubes based on their size and density. CNTs are dispersed in density gradient medium and subjected to ultracentrifugation. Due to their different densities, the nanotubes separate into distinct bands within the gradient. This technique allows the isolation of specific types or sizes of nanotubes. Density gradient ultracentrifugation has been used for separation of SWNT based on diameter(Jang et al. 2016).

9.3.3. Chemical Functionalization of CNTs

Carbon nanotubes (CNTs) exhibit remarkable physical and chemical properties, making them a subject of great interest in various fields of science. However, its low dispersibility in aqueous and organic solvents has hindered its use and application (Dubey et al. 2021). An alternative to this problem consists in the functionalization of this material. It involves

modifying their surface, attaching functional groups or molecules to improve their physicochemical properties, increase their ease of dispersion, manipulation, processability, and opening new paths in nanotechnology (Speranza 2021). Among the various ways to functionalize CNTs, the main ones are based in substitution reactions, such as the replacement of carbon atoms in the tube wall by boron or nitrogen. The functionalization of NTCs can confer several properties, and allow applications in areas such as electronics, energy storage, detection, and biomedical fields. (Fig. 12) The choice of functionalization method depends on the desired properties, stability, and intended applications. CNTs are functionalized by irreversibly binding polymers to their wall, or at defect points located at edges, called grafts (Dubey et al. 2021). Functionalization can be achieved through covalent or non-covalent methods (Figure 12). Here follows some common approaches.

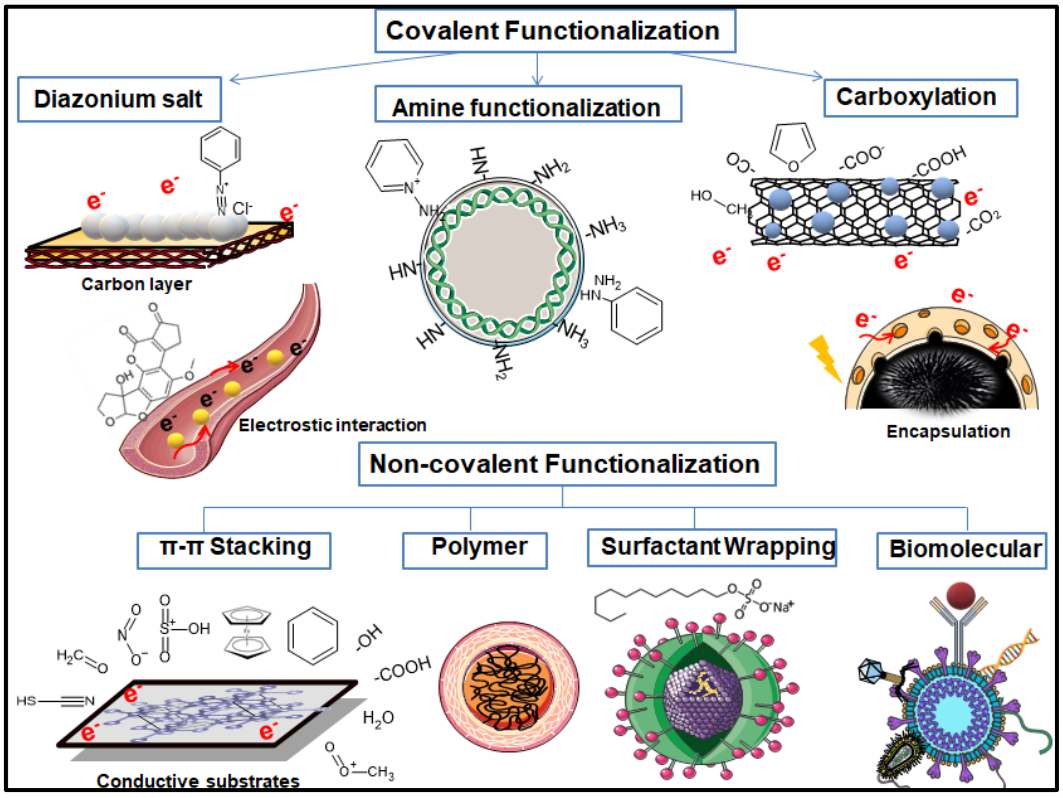

Fig. 12. Different functionalization of CNTs.

9.3.3.1. Covalent Functionalization

Covalent functionalization involves chemically bonding functional groups directly onto the sidewalls or ends of carbon nanotubes. Common methods for covalent functionalization include:

1. Diazonium Salt Functionalization: diazonium salts are used to graft various functional groups onto the surface of CNTs. The process involves the formation of a diazonium intermediate that reacts with the surface of the nanotube, creating covalent bonds(D. Li, Luo, et al. 2021).

2. Carboxylation: carboxylation involves the introduction of carboxylic acid functional groups (-COOH) onto the surface of CNTs (Balasubramanian and Burghard 2005). This can be achieved through oxidation using strong acids or oxidizing agents, such as nitric acid or its mixture with sulfuric acid. The oxidation of CNTs may originate ketone, carboxyl, hydroxyl, carbonyl, and epoxy groups on the CNTs surface that improve their interaction with polymers (Tajik et al. 2021).

3. Amine functionalization: amines can be introduced into CNTs via reaction with amine-containing compounds, such as primary or secondary amines.

4. Other Functionalization Reactions: various other chemical reactions, such as hydrogenation (J. Zhang et al. 2008), halogenation (Norizan et al. 2020), nitration, fluorination (Hayashi et al. 2008), addition reactions, Diels-Alder reaction, and addition of carbene and nitrene (A. Bhardwaj et al. 2017), can be employed to introduce different functional groups into CNTs.

9.3.3.2. Non-Covalent Functionalization

Non-covalent functionalization involves binding molecules or polymers to CNTs through weak interactions, such as Van der Waals forces, π-π stacking, or hydrophobic interactions (Abousalman-Rezvani et al. 2020). It is very attractive due to the possibility of adsorbing several groups of ordered architectures on the surface of CNTs, without disturbing the prolonged conjugation of the nanotubes (Norizan et al. 2020). The main methods of this functionalization include:

1. Surfactant Wrapping: Surfactants or polymers with hydrophobic regions can wrap around the CNTs, creating a stable dispersion. This method increases the dispersibility of CNTs in solvents or matrices, using surfactants such as sodium dodecyl sulfate, sodium dodecyl benzene sulfonate, sodium bromide of cetyltrimethylammonium (Fujigaya and Nakashima 2015).

2. π-π Stacking: Aromatic molecules or polymers with π-electron systems can interact with the π-conjugated structure of CNTs through π-π stacking interactions. This method can enhance the stability and provide additional functionality to the CNTs (Abousalman-Rezvani et al. 2020).

3. Polymer Functionalization: Polymers with functional groups, such as polyethylene glycol (PEG), can be adsorbed onto the CNTs' surface, providing steric stabilization and enabling the attachment of other molecules or biomolecules (Dubey et al. 2021).

4. Biomolecular Functionalization: Biomolecules, such as DNA, proteins, or antibodies, can be attached to CNTs through non-covalent interactions. This allows for specific targeting or sensing applications (Xiang 2011), such as drug delivery, DNA and genes, and biosensing (Xiang 2011; Pohanka, Jun, and Kuca 2007).

9.4. Carbon Fibers

Carbon fibers (CNFs) are cylindrical wire shaped nanostructures with graphene sheets piled in different arrangements, such as ribbon-like, platelet or herringbone (G. Kim et al. 2022). CNFs are carbon threads materials that have high chemical, heat and tensile strength resistance, and are lightweight. (Z. Ali, Gao, et al. 2021) They are manufactured through carbonization, which involves converting carbon-rich precursors, usually polyacrylonitrile (PAN) fibers or pitch fibers, into carbon fibers through thermal treatments (J. Cao, Zhao, and Gao 2018).

CNFs go through several manufacturing steps; the first step consists of selecting the appropriate precursor material, such as PAN fibers or rosin fibers. (J. Cao, Zhao, and Gao 2018). Next, the precursor fibers are subjected to a stabilization or pre-oxidation process.

During this step, fibers are heated in an oxygen-rich environment to chemically alter their molecular structure, and prevent them from melting during subsequent pyrolysis. The stabilized fibers undergo a carbonization process which they are heated at high temperatures to eliminate non-carbon elements. The temperature and duration of carbonization influence the mechanical properties and crystallinity of the resulting carbon fibers. After carbonization, carbon fibers can undergo surface treatment, such as oxidation or bonding, to improve their adhesion properties or compatibility with specific applications (Frank et al. 2014).

Surface treatments may involve oxidation, plasma treatment, or the application of coatings to modify the surface chemistry and structure of CNF. In the final step, the CNFs are treated with a sizing agent, which is a protective coating applied to improve their handling, compatibility, and performance during subsequent composite manufacturing (Frank et al. 2014). The sizing agent can provide lubrication, improve adhesion with matrix materials, and protect the fibers from environmental factors.

CNFs have good electrical conductivity along the fiber axis, enabling their use in various sensor applications. CNFs can be easily functionalized to suit a particular detection mechanism (Frank et al. 2014). It's important to emphasize that the synthesis of carbon fibers is a complex and specialized process that requires precise control of various parameters, including: temperature, atmosphere and processing conditions.

9.4.1. Functionalization of CNFs

The functionalization of carbon fibers involves modifying its surface by attaching functional groups, or introducing specific chemical functionalities to improve their properties, or even allow new applications. (Norizan et al. 2020) Functionalization can be chemically achieved by reagents to introduce functional groups onto the fiber surface. Common functionalization techniques include: surface oxidation, diazonium chemistry, and silane coupling agents. Carbon fibers can be oxidized using strong oxidizing agents, such as nitric acid or potassium permanganate, to introduce oxygen-containing functional groups, like carboxyl (-COOH) or hydroxyl (-OH) groups (Z. Ali, Gao, et al. 2021). These functional groups can enhance fiber-matrix adhesion and improve compatibility with other materials. Diazonium

salts can be used to graft organic functional groups onto the carbon fiber surface. The diazonium reagents react with the carbon fiber surface, forming covalent bonds and introducing specific functional groups. In addition, silane coupling agents containing reactive groups can be used to modify carbon fiber surfaces. (G. Kim et al. 2022).

Some other alternatives for the CNFs functionalization are the electrochemical method, that allow precise control over the type and density of the functional groups introduced on the surface of the fiber (Q. Cao et al. 2021), and the polymer coating by dip coating, spin coating or chemical vapor deposition. The polymer layer can provide specific functionalities and modify the surface properties of the carbon fibers (J. Song et al. 2020).

9.4.2. Purification of CNFs

Purification is essential to enhance mechanical properties, purity, and performance of the carbon fibers. Thermal treatment is a common purification method for CNFs. Fibers are heated to high temperatures under controlled conditions, typically in an inert atmosphere or under a vacuum (Zoppas et al. 2020). This process helps to remove volatile impurities, such as residual solvents and organic compounds, by promoting their decomposition and evaporation. In addition to this method, chemical treatments also can be used to remove non-carbon impurities from CNFs. One common method is the acid treatment, which fibers are immersed in strong acids, such as sulfuric or nitric acids, to dissolve or oxidize impurities (Tran et al. 2017). Alkali treatment with strong bases, such as sodium hydroxide, can also be employed to remove organic impurities. These chemical treatments can improve carbon fibers' purity and surface cleanliness.

9.5. Carbon Black

Carbon black (CB) is a fine powder consisting of small carbon particles. It is produced by the incomplete combustion or thermal decomposition of hydrocarbons, such as natural gas or petroleum oil. CB particles are formed through a process called pyrolysis, in which hydrocarbon molecules break down into smaller carbon clumps in a high temperature environment. CB particles have a highly complex structure, with a high surface area, providing ample surface for interactions with other materials (S. Pandey et al. 2023; Arduini et al. 2020).

Due to its graphitic structure and high carbon content, CB exhibits good tensile strength, electrical conductivity, and excellent resistance to ultraviolet (UV) radiation, providing stability and protection against UV-induced degradation. They can be used for the detection of analytes for biosensing applications. (Arduini et al. 2020) The use of carbon black provides several advantages, such as its high surface area, electrical conductivity, and compatibility with biomolecule immobilization. These properties enable efficient binding of the recognition elements and sensitive detection of, e.g., mycotoxin B1.

CB NPs can be prepared by employing pyrolysis of polymer and hydrocarbon, plasma synthesis, and hydrolysis of natural resources (Picheau et al. 2023). The preparation process is cheap and straightforward. The properties of carbon black can be easily tailored by introducing other materials such as polymers or metallic nanoparticles for better electrochemical sensing applications (Speranza 2021).

9.5.1. Functionalization of CB

Functionalization of CB involves modifying its surface to introduce specific functional groups or chemical functionalities. For example, coating CB with polymers can improve its dispersibility in solvents or increase its compatibility with polymer matrices. (Morales-Lara et al. 2016) The surface coating is an alternative of CB functionalization. The coating material can be a polymer, metal, oxide or other compounds. Polymer grafting can be used in functionalization, and involves attaching polymer chains to the CB surface (L.M.C. Ferreira et al. 2022). This can be achieved through in situ polymerization or coupling reactions (J. Huang et al. 2008).

Plasma treatment involves exposing CB to low pressure plasma containing reactive gases (oxygen or nitrogen). (Leistenschneider et al. 2018) Plasma treatment can introduce functional groups onto the CB surface through chemical reactions, resulting in greater dispersibility and better compatibility with different matrices.

A purification option is the chemical modification, which involves treating CB with reactive chemicals to introduce functional groups onto its surface (Tran et al. 2017). Common methods include:

1. CB can be treated with diazonium salts to graft organic functional groups onto its surface. Diazonium reagents react with the CB surface, forming covalent bonds and introducing specific functional groups (J. Huang et al. 2008);

2. CB can be oxidized using strong oxidizing agents, such as nitric acid or potassium permanganate, to introduce oxygen-containing functional groups, such as carboxyl or hydroxyl groups;

3. Silane coupling agents containing reactive groups, such as amino or epoxy, can be used to modify CB surfaces (Leistenschneider et al. 2018).

All these modifications increase compatibility with other materials and improve dispersion in matrices, allowing new interactions.

9.5.2. Purification of CB

Carbon black purification aims to remove impurities such as residual organic compounds, metals and other contaminants that can affect its quality and performance. (Arduini et al. 2020) The main methods used in the purification of carbon black are thermal treatment, which consists of submitting carbon black to high temperatures in an inert atmosphere, or under vacuum. Heat promotes the decomposition and vaporization of these impurities, leaving behind the purified CB. Acid digestion treatments are implemented with strong acids, such as nitric or sulfuric acids, to remove metallic impurities. Alkaline treatments using strong alkaline solutions, such as sodium hydroxide or potassium hydroxide, are used to remove acidic impurities and residual organic compounds. (Costa et al. 2022) Washing and filtration are also employed to remove soluble impurities and contaminants. Purification processes are normally followed by drying and packaging to ensure the stability and quality of the purified carbon black (Antonelli et al. 2019).

9.6. Application of Carbon-based Materials for Mycotoxins Analysis

Electrochemical biosensors based on carbon materials arouse much interest for the detection of food toxins. Some important studies are herein reported (Table 2).

Gaozhi Ou et al. developed a label-free electrochemical immunosensor for the determination of aflatoxin B1 (AFB1), based on Au nanoparticles decorated with urchin-like Bi_2S_3 (Au/Bi_2S_3), anchored on electrochemically reduced graphene oxide (ERGO) modified carbon fiber (CNFs) microelectrodes (Au/Bi_2S_3/ERGO/CF). Under the optimum conditions, the label-free electrochemical immunosensor detected AFB1 within the linear range of 10 pg mL^{-1} to 20 ng mL^{-1}, with a detection limit of 8 pg mL^{-1}, and sensitivity of 0.48 μA ng mL^{-1}. The immunosensor was applied to detect AFB1 in cornflour samples, offering excellent reliability and accuracy compared with typical detection methods (Ou et al. 2023).

Glassy carbon electrode modified with nickel/nickel hydroxide NPs-decorated reduced graphene oxide ($Ni/Ni(OH)_2$-rGO) was used for non-enzymatic detection of xanthomegnin. $Ni/Ni(OH)_2$-rGO composites were synthesized through a simple microwave-assisted technique with a less harmful reducing agent. The sensor exhibited a limit of detection of 0.12 μmol L^{-1}. The selectivity, stability, and analytical recovery studies proved the potential use of the sensor for the detection of xanthomegnin in real samples (Swetha et al. 2023).

Molecularly imprinted electrochemical sensor was exploited to detect zearalenone (ZEA) by the synergistic effect of reduced graphene nanoribbons (rGNRs) and gold nanoparticles (AuNPs). The oxidized GNRs are firstly produced by an improved Hummers' oxidation method, and then reduced and modified with AuNPs onto a glassy carbon electrode, by electrodeposition technique. It was found that the constructed sensor shows a wide linear range of 1–500 ng mL^{-1} for ZEA, with a detection limit as low as 0.34 ng mL^{-1} (B. Zhou et al. 2023).

Saurabh Srivastava proposed a label-free immunosensor for electrochemical detection of AFB1, using nickel NPs-decorated reduced graphene oxide (rGO–Ni NPs) sheets. The rGO–Ni NPs have been electrophoretically deposited onto an indium tin oxide (ITO) coated glass electrode. It exhibits a limit of detection of 0.16 ng mL^{-1} for AFB1. The rGO-Ni NPs sheets showed excellent electrocatalytic properties of Ni NPs, besides the good sensitivity.(Srivastava et al. 2016)

Dhiman et al. fabricated an electrochemical microfluidic biosensing platform to detect FU-B1 with Ag-CeO_2 nanocomposite using maskless lithography. The resulting nanobiochip showed an excellent linear response to antigen-FU-B1, with limit of detection and limit of quantification of 1.5 pg mL^{-1} and 3.9 pg mL^{-1}, respectively. These results indicate that an electrochemical microfluidic nanobiochip can be used for rapid, label-free, and highly sensitive detection of antigen FU-B1 (Dhiman et al. 2021).

OU et al. (Ou et al. 2023) developed an immunosensor for the determination of AFB1 based on Au NPs-decorated urchin-like Bi_2S_3 (Au/Bi_2S_3) anchored on electrochemically reduced graphene oxide (ERGO) modified carbon fiber (CNFs) microelectrode (Au/Bi_2S_3/ERGO/CNFs). The electrochemical immunosensor detected a linear range from 10 pg mL^{-1} to 20 ng mL^{-1}, with a low detection limit of 8.0 pg mL^{-1}, and high sensitivity (0.48 μA/ng mL). The immunosensor was applied to wheat flour samples, and showed good reproducibility and acceptable stability.

Studies using nanodiamonds (NDs) were also found in the literature. The use of NDs seems effective to adsorb mycotoxins (Puzyr' et al., 2007). Gibson et al. reported that AFB1 adsorption on NDs is directly related to aggregate size, while OTA adsorption is primarily centered on electrostatic interactions that depend on the type of the surface functional groups. The results showed that modified NDs with small aggregation sizes (~40 nm) have greater adsorption capacities for AFB1 than yeast cell walls and untreated NDs from various vendors, but comparable to activated charcoal. Furthermore, the adsorption capabilities of ND can be preserved over a wide pH range (Gibson et al. 2011).

Kovac et al. (Kovač et al. 2018) studied the antiaflatoxigenic effect of C_{60} fullerene nanoparticles at 4 different concentrations (0, 10, 50 and 100 ng mL^{-1}), on Aspergillus flavus growth, and aflatoxin production in culture media. Such results clearly demonstrate the volatility of the nC_{60} effect on the mycotoxigenic potential of A. flavus.

Single-walled carbon nanotubes (SWCNT) was used as nanomaterial to modify a screen-printed carbon working electrode, during the development of an electrochemical immunosensor for aflatoxin M1 in milk. The developed immunosensor method achieved a limit

of detection of 39 ng L^{-1}, with a linear dynamic detection range up to 1000 ng L^{-1} (Nugen et al. 2009).

Singh et al. prepared composite c-MWCNTs/ITO electrodes by one-step electrophoretic deposition of c-MWCNTs on ITO glass. BSA/anti-AFB1/MWCNTs/ITO immune electrode was prepared by covalently coupling aflatoxin monoclonal antibody. The results showed that the method had high sensitivity in the linear range of 0.25–1.375 ng mL^{-1}, (LOD = 0.08 ng/mL) (C. Singh et al. 2013).

Zhang et al. assessed carbon nanotubes/poly(diallyldimethylammonium chloride/gold-palladium nanoparticles for AFB1 detection. The results showed good electron transfer capability, which ensured high sensitivity to detect AFB1 in a range of 0.05-25 ng mL^{-1}, with a detection limit of 0.03 ng mL^{-1} (S. Zhang et al. 2016).

Wang et al. (Z. Wang et al. 2014) developed a molecularly imprinted electrochemical method using a stepwise approach for the detection of AFB1 in gutter oil. Au/Pt bimetallic nanoparticles were electrodeposited on glassy carbon electrode modified with MWNTs. The performance of the imprinted sensor showed a linear range of 1.0 x 10^{-10} – 1.0 x 10^{-5} mol L^{-1}, with a detection limit of 0.03 nmol L^{-1}.

Forintos et al. showed a study with carbon fibers as sensors, investigating how temperature and relative humidity affect the electrical resistance of carbon fibers reinforced by polymeric composites. As a result, carbon fibers can be used in different applications (e.g., for monitoring the curing process). On the other hand, effects must be offset when carbon fiber strength is measured in a health monitoring application (Forintos and Czigany 2020).

Huang et al. proposed an amperometric immunosensor of carbon nanofibers (CNFs) coated with gold nanoparticles for the detection of aflatoxin B1 in wheat samples. In comparison to common CNTs, the CNFs network derived from bacterial cellulose biomass possesses a unique hierarchically porous structure for fast electrolyte diffusion and a larger electrochemical active area, which increases the peak current of differential pulse voltammetry curves for an immunosensor. The limit of detection was 0.027 ng mL^{-1}, the reproducibility,

storage stability and selectivity of the immunosensor were proved to be satisfactory (Y. Huang et al. 2021).

Smartphone-based magnetoimmunosensor development on screen-printed electrodes modified with carbon black was employed for detection of aflatoxin B1 in cereals. (Jafari et al. 2022) The electrode was modified with nanometric carbon black. For buffered analyte solutions and a corn extract sample, the assay demonstrated a low detection limit of 13 and 24 pg mL^{-1}, respectively. The study was the first smartphone-based electrochemical system for screening aflatoxin B1 in samples searching for possible contaminations.

Zhang et al. (H. Zhang et al. 2019) developed an electrochemical immunosensor for detection of aflatoxin B1 in agricultural products by modifying multi-walled carbon nanotubes (MWNTs) with ferrocene (FC), fixed on the surface of a screen-printed carbon electrode (SPCE) via MWNTs and chitosan (CS). The increase in the specific surface area of SPCE modified by Fc/MWNT/CS facilitated the binding of AFB1-Bovine serum albumin, while the excellent electrical conductivity of FC/MWNT/CS promoted good electron transfer rate. These advantages not only amplify the immunosensor signal, but also improve immunosensor sensitivity, selectivity and stability.

Table 2. Comparison of different carbon-based materials sensors used for mycotoxin detection.

Analyte	Sensor	Linear range	Matrix	Method	LOD	Ref.
AFB1	Au/Bi_2S_3/ERGO/CF	10 pg mL^{-1} –20 ng mL^{-1}	Corn flour	DPV	8 pg mL^{-1}	(Ou et al. 2023)
AFB1	MWCNT/CS	0.0001 a 10 ng mL^{-1}	Palm kernel cake	DPV	0.1 pg mL^{-1}	(Azri, Selamat, and Sukor 2017)
FB1	NanoMIPs	1 fM–10 Pm	Maize	DPV	0.03 Fm	(Munawar et al. 2020)

ZEN	MIP/AuNPs/rGNRs/GCE	1–500 ng mL^{-1}	Maize flour	DPV	0.34 ng mL^{-1}	(B. Zhou et al. 2023)
AFB1	AuE/MoS_2-rGO	1–100 ng mL^{-1}	Corn oil, Peanut oil	DPV	0.0003 ng mL^{-1}	(Yu et al. 2022)
ZEN	AuE/MoS_2-rGO	1 pg mL^{-1} –100 ng mL^{-1}	Corn oil, Peanut oil	DPV	0.0003 ng mL^{-1}	(Yu et al. 2022)
AFB1	rGO–Ni NPs	1-8 ng mL^{-1}	-	DPV	0.16 ng mL^{-1}	(Srivastava et al. 2016)
AFB1	GO/AuNW/SPCE	5.0–750.0 pM	Pistachio	DPV	1.4 pM	(Mousavi Noudoushan et al. 2019)
AFM1	SPE/GO-CS/CeO_2-C	0.01–1 µg L^{-1}	Milk	DPV	0.009 µg L^{-1}	(An et al. 2020)
AFB1	GQD-AuNPs	0.1– 3.0 ng mL^{-1}	Corn	CV	0.008 ng mL^{-1}	(H. Bhardwaj et al. 2019)
AFM1	Quantum-Dot Au-NPs composite	100 pM–2 nM	Milk	DPV	0.3 nM	(Ramalingam, Elsayed, and Singh 2023)
AFB1	Carbon-Dots-Fe_2O_3-Fe_3O_4 nanocomposite	0.001–100.0 nM	Beer, rice, peanuts	DPV	0.5 pM	(Q. Huang et al. 2022)

ZEN	SPCE/CS-CNT-Pd	0.25–16 ng mL^{-1}	Corn	CV	0.25 ng mL^{-1}	(V.S. Kumar et al. 2023)
ZEN	3D CF-L Tb^{3+}/Co_3O_4 NC	0.001–500.0 μM	Milk	VPD	0.34 nM	(Zaman et al. 2023)
DON	P-Arg-MIP-$COOH^-$ MWCNTs	0.1–70 μM	Wheat flour	CV	0.07 μM	(W. Li, Diao, et al. 2021)
AFB1	AU/PtNPs-MCNTs–GCE	$l\times10^{-10}$–$1x10^{-5}$ mol L^{-1}	Gutter oil	DPV	0.03 nmol L^{-1}	(Z. Wang et al. 2014)
AFB1	c-MWCNTs/ITO	0.25–1.375 ng mL^{-1}	-	CV	0,08 ng mL^{-1}	(C. Singh et al. 2013)
FB1	ITO-AuNPs Immunosensor	0.3–140 ng mL^{-1}	Corn	DPV	97 pg mL^{-1}	(Lu and Gunasekaran 2019)
DON	ITO-AuNPs Immunosensor	0.2–60 ng mL^{-1}	Corn	DPV	35 pg mL^{-1}	(Lu and Gunasekaran 2019)
AFB1	Fc/MWCNT/CS	10^{-3} ~2×10^4 ng mL^{-1}	Corn flour, peanut, rice flour	DPV	0.159 pg mL^{-1}	(H. Zhang et al. 2019)

AFT: Aflatoxin; AFB1: Aflatoxin B1; AFM1: Aflatoxin M1; $Au/Bi_2S_3/ERGO/CF$: Au nanoparticles decorated urchin-like Bi_2S_3 anchored on electrochemically reduced graphene oxide modified carbon fiber;; AuE/MoS_2-rGO: Gold electrode/molybdenum disulfide-reduced graphene oxide; Au NW: Gold nanowires; AuNPs: Gold nanoparticles; BDD: Boron-doped diamond; CB: Carbon black; c-MWCNTs: carboxylated multiwalled carbon nanotubes; CS:

Chitosan; CV: Voltammetry Cyclic; CeO_2-CS: Cerium oxide-chitosan; DON: Deoxynivalenol; DPV: Differential Pulse Voltammetry; FBI: Fumonisin B1; Fc: Ferrocene; GO/AuNW/SPCE: Graphene oxide/gold nanowires/screen-printed carbon electrode; GQD-AuNPs: graphene quantum dots and gold nanoparticles; GQD: Graphene quantum-dot; ITO: Indium tin oxide; nanoMIPs: Molecularly imprinted polymer nanoparticles; MWCNTs: multiwalled carbon nanotubes; rGO–Ni NPs: Nickel nanoparticle decorated reduced graphene oxide sheets; SPCE: Screen-printed gold electrode; SPCE/CS-CNT-Pd: Palladium nanoparticle embedded functionalized carbon nanotube-chitosan-screen-printed gold electrodes; ZEN: Zearalenone; 3DCF-LTb^{3+}/Co_3O_4 NC: Three dimensional carnation flower-like Tb$^{3+/}$$Co_3O_4$ nanocomposite.

10. Magnetic Beads

The use of magnetic particles in immunoassays has increased significantly in the last decade. Achieving low limits of detection and improving device performance are advantages achieved by integrating this material. Commonly, magnetic particles (MPs) consist of iron oxides (magnetite-Fe_3O_4 and maghemite-γ-Fe_2O_3) and can be functionalized with a variety of materials (carboxyl, hydroxyl, tosyl, amine, or epoxy groups). (Yáñez-Sedeño, Campuzano, and Pingarrón 2016) MPs have sizes ranging from micrometers to nanometers. In addition, these MPs can have irregular shapes (shapes of tubes, cubes, wires, and others), but the spherical shape (magnetic beads- MBs) is the most common due to its hydrodynamic properties. (Yáñez-Sedeño, Campuzano, and Pingarrón 2016) Many magnetic beads are commercially available in a variety of functional groups and sizes.

10.1. Synthesis of MBs

MBs can be synthesized through coprecipitation, hydrothermal, thermal decomposition, and other methods (Schladt et al. 2011),(W. Wu et al. 2015) . The main chemical methods for the synthesis of magnetic particles are briefly described below.

10.1.1. Coprecipitation Method

The coprecipitation method is widely used in the synthesis of magnetic particles as it provides greater control over the size of the MPs; easy adaptation for large-scale production;

good stability and dispersion, in addition to requiring low temperatures in its synthesis process (A. Ali, Shah, et al. 2021). In this method, metal ions are precipitated into a solution containing a reducing and a stabilizing agent (A. Ali, Shah, et al. 2021). In general, Fe^{2+} and Fe^{3+} ions are used to obtain Fe_3O_4 MPs, which can be functionalized with different groups e.g., amines (X. Wang, Niessner, and Knopp 2014), carboxyls, and polymerics. Particle size can be controlled by reagent concentration and reaction conditions.

Another advantage associated with this synthesis method is the flexibility in particle composition (A. Ali, Shah, et al. 2021). This makes it possible to use different metal ions, allowing the magnetic and chemical properties of the particles to be changed to fit the demands of each application (A. Ali, Shah, et al. 2021). In this sense, Proença et al. synthesized particles with Co, Zn, and Fe ($Co_{0.25}Zn_{0.75}Fe_2O_4$) to obtain MPs with superparamagnetic properties and greater biocompatibility(Proença et al. 2019). Similarly, Pereira et al.(Pereira et al. 2012) synthesized spinel-type superparamagnetic ferrite nanoparticles (MFe_2O_4), where M is Fe, Co, or Mn metal.

10.1.2. Hydrothermal Method

The hydrothermal approach to obtain magnetic particles includes controlled chemical reactions at high temperatures and pressures (J. Li, Wu, and Wu 2016). In this procedure, the reagents are put in a sealed container and heated hydrothermally with a solvent (water). The formation of particles occurs due to interactions between reagents and conditions of high pressure and temperature, which favor nucleation and controlled growth of particles (A. Ali, Shah, et al. 2021), (García-Nicolás, Arroyo-Manzanares, and Viñas 2023). On the other hand, the formation of these particles is also conditioned by the solubility of metallic salts in an aqueous medium.(A. Ali, Shah, et al. 2021) The hydrothermal method offers a wide range of materials that can be synthesized, including iron oxide (Fe_3O_4) (Cai et al. 2013), and cobalt oxide ($CoFe_2O_4$)(Meng et al. 2009) . Cai et al.,(Cai et al. 2013) used the hydrothermal approach to obtain polyethyleneimine (PEI)-coated iron oxide nanoparticles (Fe_3O_4–PEI NPs). In this work, the authors obtained particles of different sizes by varying the mass ratio of the reagents. Already Mohamed et al., (Mohamed et al. 2020) synthesized a spinel nanostructure $CoFe_2O_4$ via the hydrothermal method and applied it for the trace determination of Cu(II).

10.1.3. Thermal Decomposition Method

This synthesis route involves the thermal decomposition of metallic precursors in the presence of a high boiling solvent and a reducing/stabilizing agent under controlled conditions (A. Ali, Shah, et al. 2021; Odularu 2018). Thus, this method allows obtaining magnetic particles with controlled properties such as size, shape, specific composition, and high purity(A. Ali, Shah, et al. 2021). The most commonly used precursors are organometallic compounds and metal complexes, e.g., iron (III) acetylacetonate ($Fe(acac)_3$). In general, these precursors should have good thermal stability and solubility in the synthesis solvent (Varanda et al. 2019). Regarding the stabilizing agent, it plays an important role in this synthesis route as it can delay the nucleation of the particles (Varanda et al. 2019). Thus, they control particle growth, producing materials less than 30 nm and spherical in shape. For this function of stabilizing agent, fatty acids, natural polymers, and artificial polymers are generally used (Varanda et al. 2019).

Different metal ions can also be used to obtain spinel-type magnetic ferrites such as Co, Ni, Zn, Cu, and Mn. Thus, high chemical stability and good magnetic properties are achieved. Dippong et al. investigated the structural, morphological, and magnetic characteristics of the ferrites of these metals (Dippong, Levei, and Cadar 2022). Toyos-Rodriguez et al.,(Toyos-Rodríguez et al. 2022) also used the thermal decomposition method to obtain beads with high magnetism. In this case, in addition to the Zn2+ ions doped in magnetite, they also use encapsulation with a polymeric material. The use of these materials facilitates the application of magnetic beads for immunoassays(Toyos-Rodríguez et al. 2022).

10.2. Application of Magnetic Beads for Mycotoxins Analysis

Generally, the application of these magnetic materials in the detection or control of mycotoxins has been explored for extraction and purification steps samples(Du, Fang, and den Toonder 2016). This strategy uses biorecognition elements (such as antibodies, aptamers, DNA, or molecules with affinity for mycotoxins) immobilized on the surface of the MBs. Thus, the capture and pre-concentration of the analyte are simplified because magnetic fields can be applied externally through magnets, providing an efficient and fast separation in the incubation

and washing steps.(Pastucha et al. 2019; Dixit et al. 2016; Kuramitz 2009) Furthermore, the magnetic beads improve the performance of the immunological reaction due to an increase in the surface area. Thus, the number of these immobilized elements is significantly higher than those immobilized on flat surfaces of typical systems, which gives greater sensitivity to immunoassays and also reduces the volume of reagents(Pastucha et al. 2019). Various analysis systems can be integrated into this type of strategy, which includes chromatographic (Zhihong Xuan et al. 2019), ELISA(Urusov et al. 2014), lateral flow(R. Li et al. 2019) , and electrochemical(J. Wang, Liang, and Qin 2020). In particular, most of the electrochemical immunoassays and immunosensor involving magnetic beads use the competitive-type configuration for mycotoxins(Paniel, Radoi, and Marty 2010).

Competitive-type configuration for mycotoxins is the most common because it is a low molecular weight compound. Thus, the first electrochemical immunoassays consisted of a simple approach, with MBs as support for immobilizing antibodies for the affinity reaction, while electrodes were used for the transduction step (Fig. 13 A) (Jodra, López, and Escarpa 2015). Hervás et al.,(M. Hervás, López, and Escarpa 2010) developed a disposable immunosensing for the zearalenone determination in different food matrices. Based on a competition scheme, mycotoxin Zea (standard or sample solutions) and Zea-HRP competed for the binding sites of the specific antibody. These Zea-specific monoclonal antibodies were covalently immobilized on the surface of the MBs containing Protein G. Finally, the immunoaffinity reaction was evaluated by the addition of the enzymatic substrate and electrochemical mediator whose reduction on the electrode surface corresponds to the activity of HRP-Zea. Under the optimized conditions, this immunosensing exhibited a low LOD of 7.0 ng L^{-1} for Zea and excellent accuracy with a recovery rate of 101–111% for the analysis of zearalenone in baby food samples. Jodra et al.,(Jodra, López, and Escarpa 2015) developed an immunosensing for the fumonisins (FB1, FB2, and FB3) detection, also based on the competition between mycotoxin FB and its HRP enzyme-labeled derivative for their binding to antibodies immobilized on MBs (Fig. 13 A). This immunoconjugate was transferred and retained onto the transducer surface (screen-printed carbon electrodes) by external magnets, and the electrochemical detection of the HRP enzyme used as the label was performed. The limit of detection attained was 0.33 μg L^{-1}.

Beyond the competitive immunosensors already mentioned, others have also been developed for the detection of aflatoxin M1 (Paniel, Radoi, and Marty 2010), ochratoxin A (Vidal et al. 2012), and zearalenone (M. Hervás, López, and Escarpa 2010). All these works sought to increase the practicality and portability of their systems using screen-printed electrodes (SPEs) as a transducer. SPEs have numerous advantages associated with their use, such as stability, accuracy, disposability, low cost, and can be used in the on-site analysis(Dixit et al. 2016). In addition, these SPEs can be designed for the development of analyzes of multiple samples simultaneously or multiple targets. An example is the multi-channel electrochemical immunoassay for fumonisin B1 detection developed by Ezquerra et al., (Ezquerra et al. 2015) (Fig. 13 B). In this direct competitive electrochemical immunoassay, the immunocomplex formation steps were carried out on a 96-well plate with a magnetic separator for the removal of supernatants from samples bound to MBs, and the amperometric transduction of HQ and H_2O_2 occurred in the SPE array. The authors report a significant decrease in analysis times and improvement in reproducibility using this 8-electrode array. This method presented a LOD of 0.58 μg L^{-1} and was validated with certified reference material (Ezquerra et al. 2015). Until now, works using multiplexed electrochemical detection with discrimination of different mycotoxins and magnetic beads have not been found.

On the other hand, miniaturization and easy automation, associated with lower consumption of reagents and samples, can also be achieved with microfluidic systems. Hervás et al., (M. Hervás, López, and Escarpa 2010) integrated electrokinetic magnetic beads and microfluidic chips into the electrochemical immunoassay for ZEA determination (Fig. 13 C). The strategy implied the use of an electromigration microchip, containing the simple channel layout of the double-T microfluidic chip, to sequentially carry out the immunointeraction and the enzymatic reaction(M. Hervás, López, and Escarpa 2010) . In this case, the electromigration to conduct the fluids in the different chambers occurred with the electric field application, favoring the simplicity system due to the elimination of valves and pumps. Similar to other competitive immunoassays, here MBs were also used for immobilization of anti-ZEA, which acted in the ZEA and ZEA-HRP capture in the immunological reaction chamber (IRC). This immunoconjugate was then transported to the enzyme reaction chamber, where ZEA-HRP, the enzyme-substrate, and the redox mediator reacted, providing a LOD of 0.4 μg L^{-1}. Panini et al.,

(Panini et al. 2011) developed another microfluidic systems approach for ZEA detection. Unlike the previous system, in this work, the microfluidic chip was coupled to a flow injection system that used syringe pumps to assist in the steps of sample introduction, flow interruption, and the washing procedure. The system configuration was also based on the competition between ZEA and an enzyme-labeled derivative by antibodies supported on MBs, using a gold electrode for electrochemical detection of the 4-tert-butyl catechol catalytic reaction. The limit of detection obtained for this immunoassay was 0.41 μg kg^{-1}. In another immunoassay using magnetic beads and a microfluidic device, a LOD of 0.05 μg kg^{-1} was obtained for the detection of ochratoxin A(Fernández-Baldo et al. 2011).

In contrast to other techniques outlined thus far, there are systems where magnetic particles are employed solely for the purpose of sample clean-up. Thus, the MBs do not participate in the final structure of the electrode, being used only for capture, separation, and pre-concentration of the target analyte in the sample, with subsequent release of this analyte by elution, magnetic separation, and detection of the solution (Fernández-Baldo et al. 2011). Recently, this assay configuration has been discussed for electrochemical analysis. In their work, Xuan et al.(Z. Xuan et al. 2020) developed an electrochemical immunoassay using quantum dots with magnetically controlled pretreatment to automatically detect aflatoxin B1 (AFB1) (Fig. 11 D). The method described in the article utilizes immunoaffinity magnetic beads (IMBs) to pre-treat the sample, remove interferents, and enhance the assay's sensitivity. In this context, IMBs specifically capture the mycotoxin AFB1. Following the capture, undesired species that have adsorbed onto the IMB-AFB1 conjugate are easily removed through simple washing steps. Subsequently, the sample is incubated with a solution containing specific antibodies for Aflatoxin B1 and quantum dots labeled with these antibodies. Finally, the IMB-captured quantum dots are treated with an acidic solution to release the corresponding metal ions, which are then evaluated electrochemically. This developed immunoassay has demonstrated high sensitivity and selectivity, enabling the detection of concentrations as low as 0.05 μg kg^{-1}. Moreover, the magnetic pretreatment system has facilitated automated and simplified sample analysis, reducing the need for manual manipulation and making the method more user-friendly in field applications.

Still, regarding immunoassays and magnetic beads for mycotoxins detection, only two works were developed using a system configuration that was non-competitive. The first was a label-free immunosensor for the detection of ochratoxin A developed by Zamfir et al. (Zhihong Xuan et al. 2019) In this configuration, antibody–OTA covalently immobilized on the surface of magnetic nanoparticles (MNPs) interacted with the mycotoxin and were attached to the gold electrode using a magnetic field. The label-free detection was possible because of the increased charge transfer resistance of the redox couple $[Fe(CN)_6]_4^{3-}$ in solution in the presence of OTA/anti-OTA antibody conjugation on the electrode. This immunoassay presented a LOD of 0.01 ng mL^{-1}. The other was a sandwich-type system developed by Chauhan et al., (Chauhan and Basu 2015) but based on competition between conjugate aflatoxin B1 and free aflatoxin B1. In this immunosensor, a concentrated AFB1 solution selectively interacted with capture antibodies immobilized on the surface of a quartz crystal electrode. Subsequently, this AFB1-conjugate and free AFB1 were placed to interact with secondary antibody (immobilized on gold-coated iron oxide core-shell (Au-Fe_3O_4) and detected by electrochemical quartz crystal microbalance. The sandwich-competitive method provided a wide linear range and a LOD of 0.07 ng mL^{-1}, with the possibility of immunosensor regeneration. This strategy of regenerating the immunoelectrode using an external magnet brings an interesting approach in the application of MBs and the advantage of reusing this immunosensor about 15 times.

Table 3 provides a detailed description of the electrochemical immunoassays and immunosensor involving magnetic beads for mycotoxins analysis.

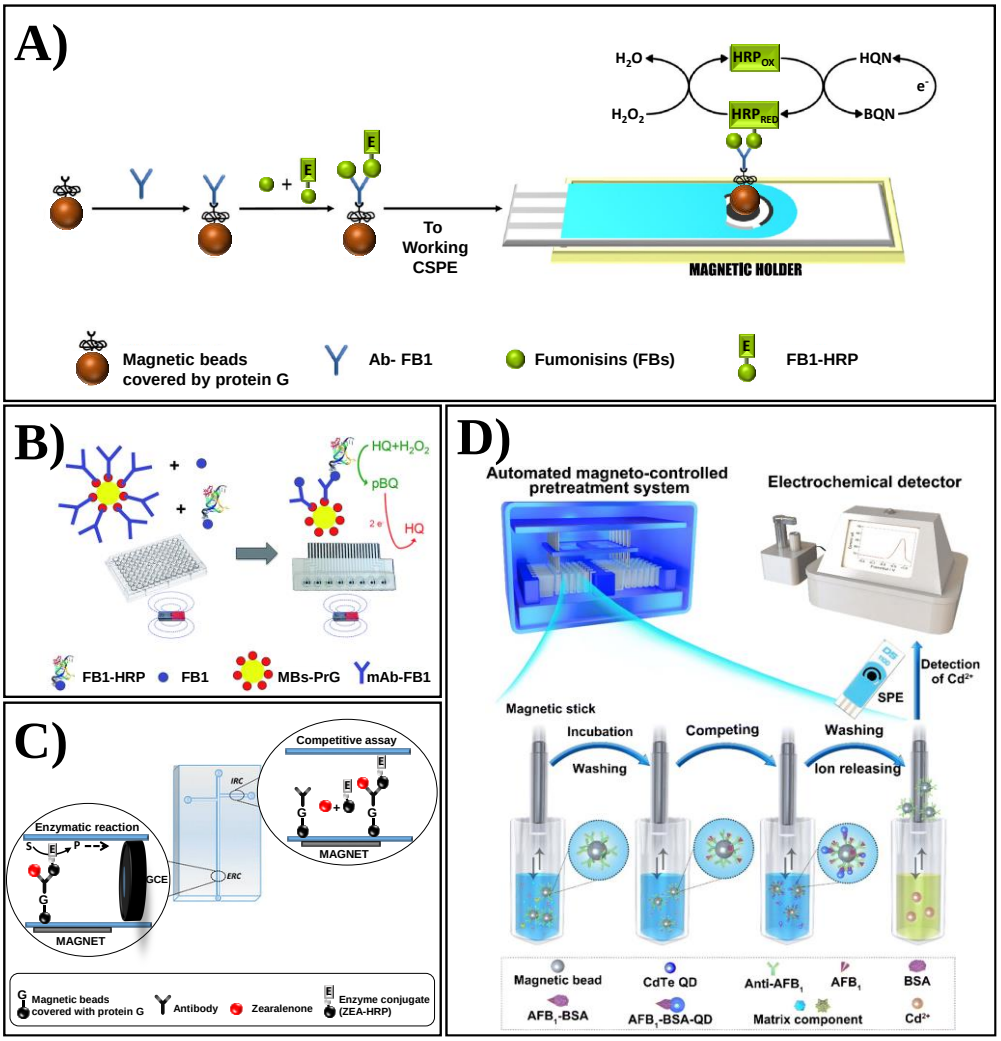

Fig. 13. A) Schematic representation of the competitive electrochemical immunoassay for the detection of total fumonisins (FB1, FB2, and FB3) using the horseradish peroxidase (HRP) as enzyme label (Reprinted with permission from Elsevier Ref.(Jodra, López, and Escarpa 2015). B) Schematic illustration of the multi-channel electrochemical immunoassay using HRP as the label for fumonisin B1 determination (Reprinted with permission from Royal Society of Chemistry Ref.(Ezquerra et al. 2015). C) Schematic illustration of a magnetic bead-based electrochemical immunoassay on microfluidic chips for zearalenone detection (Reprinted with permission from Royal Society of Chemistry Ref.(M. Hervás, López, and Escarpa 2010). D) Schematic diagram of the quantum dot-based electrochemical immunosensor for aflatoxin B1 with automated magneto-controlled pretreatment system (Reprinted with permission from PMC Copyright Springer Nature Ref. (Zhihong Xuan et al. 2019))

Table 3. Electrochemical immunosensing based on magnetic beads for mycotoxins detection.

Analyte	Modification of magnetic beads	Biosensor type	Electrode type	Detection techinique	LOD	Applicability	Ref.
ZEA	MBs covered by Protein G	Competitive	SPCE	Amperometry	0.011 μg L^{-1}	Maize certified reference material; Baby food cereal	Miriam Hervás, López, and Escarpa 2009a)
ZEA	MBs covered by Protein G	Competitive	SPCE	DPV	0.007 μg L^{-1}	Baby foods	M. Hervás, López, and Escarpa 2010)
FB	MBs covered by Protein G	Competitive	SPCE	Amperometry	0.33 μg L^{-1}	Beer	Jodra, López, and Escarpa 2015)
AFM1	MBs covered by Protein G	Competitive	SPCE	Amperometry	0.01 μg L^{-1}	Milk	Paniel, Radoi, and

							Marty 2010)
OTA	MBs covered by Streptavidin	Competitive	SPCE	DPV	0.11 ng L^{-1}	Wine	Vidal et al. 2012)
OTA	MBs covered by Protein G	Competitive	SPCE	Amperometry	0.32 μg L^{-1}	Coffee	Jodra et al. 2015)
OTA	MNPs with carboxylic acid group	Competitive	SPCE	DPV	0.007 ng mL^{-1}	Corn, wheat and feedstuff	X. Zhang et al. 2018)
FB1	MBs covered by Protein G	Competitive	SPCE array	Amperometry	0.58 μg L^{-1}	Maize	Vidal et al. 2012)
ZEA	MBs covered by Protein G	Competitive	GCE	Amperometry	1.00 μg L^{-1}	Baby foods	Miriam Hervás, López, and Escarpa 2009b)
ZEA	MBs covered by Protein G	Competitive	GCE	Amperometry	0.4 μg L^{-1}	Baby food	Miria

							n Hervás, López, and Escarpa 2011)
ZEA	PMB amino-functionalized	Competitive	Layer gold	Amperometry	0.41 μg kg^{-1}	Feedstuffs samples	Panini et al. 2011)
OTA	MNPs amino-functionalized	Competitive	Layer gold	Amperometry	0.05 μg kg^{-1}	Apples	Fernández-Baldo et al. 2011)
AFB1	MBs	Competitive	SPCE	ASV	0.05 μg kg^{-1}	Maize, husky rice, and peanut oil	Z. Xuan et al. 2020)
OTA	MNPs carboxyl-functionalized	Label-free	Gold	EIS	0.01 ng mL^{-1}	White wine	Zamfir et al. 2011)
AFB1	Au-Fe_3O_4 nanosuspension	Sandwich	Au-QC	CV	0.07 ng mL^{-1}	Cereal	Chauhan and Basu

							2015)
OTA	MBs covered by Protein G	Competitive	SPCE	SWV	0.008 μg L^{-1}	Red wine	Perrotta et al. 2012)
DON	MBs tosyl-activated	Competitive	GEC	ASV	342.4 μg kg^{-1}	Wheat	Valera et al. 2019)
OTA	MBs covered by Protein G	Competitive	SPCE and SPGE	Amperometry	150 pM	Beer	Höfs et al. 2021)

MBs: Magnetic Beads; MNPs Magnetic Nanoparticles; PMB: Paramagnetic beads; SPCE: Screen-Printed Carbon Electrode; GCE: Glassy Carbon Electrode; GEC: Graphite−Epoxy Composite; SPGE: Screen-Printed Gold Electrode; Au-QC: Gold coated Quartz Crystal DPV: Differential Pulse Voltammetry; SWV: Square Wave Voltammetry; ASV: Anode Stripping Voltammetry; CV: Cyclic Voltammetric.

5. Conclusions and future perspectives

A wide variety of strategies have been developed in the field of electrochemical nano-immunosensors to improve their performance toward food control, clinical diagnosis, and environmental analyses. Immunosensors are electrochemical specific transducers that have much to gain in terms of sensitivity by coupling with the nanomaterial science. In addition to their specificity, these nanodevices provide fast, versatile and reliable analyses, while requiring low sample volumes, and relatively simple instrumentation, favoring the point-of-care testing approach. However, to face a real commercial uptake, electrochemical immunosensors must be further improved in terms of the simultaneous quantification of multiple biomarkers, the use of

microfluidic tools, and the association of artificial intelligence with nanotechnology in their fabrication.

Author Contributions: Investigation, Ana Carolina de Faria Alves.; Resources, Camila A. Proenca, Tayane A. Freitas; Writing—original draft preparation, Alexandre L. B. Baccaro, Tayane A. Freitas; Writing—review and editing, Roberta Castro Martins, Laíse Nayra dos Santos Pereira; Conceptualization and Supervision, Fabiana S. Felix. All authors have read and agreed to the published version of the manuscript.

Funding: This research received no external funding.

Acknowledgments: To FAPEMIG, CNPq, CAPES (Finance code 001), EMBRAPA-CAFÉ (Notice 20/2018 and code 145).

Conflicts of Interest: The authors declare no conflict of interest.

References

Abousalman-Rezvani, Z., P. Eskandari, H. Roghani-Mamaqani, and M. Salami-Kalajahi. 2020. "Functionalization of carbon nanotubes by combination of controlled radical polymerization and "grafting to" method." *Adv Colloid Interface Sci* 278: 102126. https://doi.org/10.1016/j.cis.2020.102126. https://www.ncbi.nlm.nih.gov/pubmed/32114292.

Adányi, Nóra, Ádám György Nagy, Bettina Takács, István Szendrő, George Szakacs, Rózsa Szűcs, Eszter Tóth-Szeles, István Lagzi, Diána Weiser, Viktória Bódai, Péter Sátorhelyi, and Balázs Erdélyi. 2018. "Sensitivity enhancement for mycotoxin determination by optical waveguide lightmode spectroscopy using gold nanoparticles of different size and origin." *Food Chemistry* 267: 10-14. https://doi.org/https://doi.org/10.1016/j.foodchem.2018.04.089. https://www.sciencedirect.com/science/article/pii/S0308814618307295.

Ahmad, Waseem, Sumit Chandra Bhatt, Monu Verma, Vinod Kumar, and Hyunook Kim. 2022. "A review on current trends in the green synthesis of nickel oxide nanoparticles, characterizations, and their applications." *Environmental Nanotechnology, Monitoring &*

Management 18: 100674. https://doi.org/https://doi.org/10.1016/j.enmm.2022.100674. https://www.sciencedirect.com/science/article/pii/S2215153222000344.

Ahmad, Waseem, Agrima Pandey, Vishal Rajput, Vinod Kumar, Monu Verma, and Hyunook Kim. 2021. "Plant extract mediated cost-effective tin oxide nanoparticles: A review on synthesis, properties, and potential applications." *Current Research in Green and Sustainable Chemistry* 4: 100211. https://doi.org/https://doi.org/10.1016/j.crgsc.2021.100211. https://www.sciencedirect.com/science/article/pii/S2666086521001582.

Akiyama, N., K. D. Patel, E. J. Jang, M. R. Shannon, R. Patel, M. Patel, and A. W. Perriman. 2023. "Tubular nanomaterials for bone tissue engineering." *J Mater Chem B*. https://doi.org/10.1039/d3tb00905j. https://www.ncbi.nlm.nih.gov/pubmed/37309580.

Ali, Arbab, Tufail Shah, Rehmat Ullah, Pingfan Zhou, Manlin Guo, Muhammad Ovais, Zhiqiang Tan, and YuKui Rui. 2021. "Review on Recent Progress in Magnetic Nanoparticles: Synthesis, Characterization, and Diverse Applications." *Frontiers in chemistry* 9: 629054-629054. https://doi.org/10.3389/fchem.2021.629054.

Ali, Z., Y. Gao, B. Tang, X. Wu, Y. Wang, M. Li, X. Hou, L. Li, N. Jiang, and J. Yu. 2021. "Preparation, Properties and Mechanisms of Carbon Fiber/Polymer Composites for Thermal Management Applications." *Polymers (Basel)* 13 (1). https://doi.org/10.3390/polym13010169. https://www.ncbi.nlm.nih.gov/pubmed/33466509.

Alivisatos, A. P. 1996. "Perspectives on the Physical Chemistry of Semiconductor Nanocrystals." *The Journal of Physical Chemistry* 100 (31): 13226-13239. https://doi.org/10.1021/jp9535506. https://doi.org/10.1021/jp9535506.

Allen, M. J., V. C. Tung, and R. B. Kaner. 2010. "Honeycomb carbon: a review of graphene." *Chem Rev* 110 (1): 132-45. https://doi.org/10.1021/cr900070d. https://www.ncbi.nlm.nih.gov/pubmed/19610631.

Almeida, Joao Paulo Mattos, Elizabeth Raquel Figueroa, and Rebekah Anna Drezek. 2014. "Gold nanoparticle mediated cancer immunotherapy." *Nanomedicine: Nanotechnology, Biology and Medicine* 10 (3): 503-514.

https://doi.org/https://doi.org/10.1016/j.nano.2013.09.011. https://www.sciencedirect.com/science/article/pii/S1549963413005455.

Alvarez-Paneque, Alejandro F., Benito Rodríguez-González, Isabel Pastoriza-Santos, and Luis M. Liz-Marzán. 2013. "Shape-Templated Growth of Au@Cu Nanoparticles." *The Journal of Physical Chemistry C* 117 (6): 2474-2479. https://doi.org/10.1021/jp3062724. https://doi.org/10.1021/jp3062724.

Amendola, Vincenzo, and Moreno Meneghetti. 2012. "Exploring How to Increase the Brightness of Surface-Enhanced Raman Spectroscopy Nanolabels: The Effect of the Raman-Active Molecules and of the Label Size." *Advanced Functional Materials* 22 (2): 353-360. https://doi.org/https://doi.org/10.1002/adfm.201101539. https://doi.org/10.1002/adfm.201101539.

Amsharov, K. Y., and M. Jansen. 2008. "A C78 fullerene precursor: toward the direct synthesis of higher fullerenes." *J Org Chem* 73 (7): 2931-4. https://doi.org/10.1021/jo7027008. https://www.ncbi.nlm.nih.gov/pubmed/18321126.

An, Xingshuang, Xiaojie Shi, Hui Zhang, Yao Yao, Guangxian Wang, Qingqing Yang, Lianming Xia, and Xia Sun. 2020. "An electrochemical immunosensor based on a combined amplification strategy with the GO–CS/CeO2–CS nanocomposite for the detection of aflatoxin M1." *New Journal of Chemistry* 44 (4): 1362-1370. https://doi.org/10.1039/C9NJ04804A. http://dx.doi.org/10.1039/C9NJ04804A.

Andrews, R., D. Jacques, D. Qian, and T. Rantell. 2002. "Multiwall carbon nanotubes: synthesis and application." *Acc Chem Res* 35 (12): 1008-17. https://doi.org/10.1021/ar010151m. https://www.ncbi.nlm.nih.gov/pubmed/12484788.

Anfossi, L., C. Giovannoli, and C. Baggiani. 2016. "Mycotoxin detection." *Current Opinion in Biotechnology* 37: 120-126. https://doi.org/10.1016/j.copbio.2015.11.005. <Go to ISI>://WOS:000370458800016.

Antonelli, M., B. Benedetti, C. Cavaliere, A. Cerrato, G. La Barbera, C. M. Montone, S. Piovesana, and A. Laganà. 2019. "Enrichment procedure based on graphitized carbon black and

liquid chromatography-high resolution mass spectrometry for elucidating sulfolipids composition of microalgae." *Talanta* 205: 120162. https://doi.org/10.1016/j.talanta.2019.120162. https://www.ncbi.nlm.nih.gov/pubmed/31450465.

Arduini, F., S. Cinti, V. Mazzaracchio, V. Scognamiglio, A. Amine, and D. Moscone. 2020. "Carbon black as an outstanding and affordable nanomaterial for electrochemical (bio)sensor design." *Biosens Bioelectron* 156: 112033. https://doi.org/10.1016/j.bios.2020.112033. https://www.ncbi.nlm.nih.gov/pubmed/32174547.

Asgari, Shahrzad, Nader Nikkam, and Parastoo Saniee. 2022. "Metallic Nanoparticles as promising tools to eradicate H. pylori: A comprehensive review on recent advancements." *Talanta Open* 6: 100129. https://doi.org/https://doi.org/10.1016/j.talo.2022.100129. https://www.sciencedirect.com/science/article/pii/S2666831922000467.

Ayyub, P., R. Chandra, P. Taneja, A. K. Sharma, and R. Pinto. 2001. "Synthesis of nanocrystalline material by sputtering and laser ablation at low temperatures." *Applied Physics A* 73 (1): 67-73. https://doi.org/10.1007/s003390100833. https://doi.org/10.1007/s003390100833.

Azri, Farah Asilah, Jinap Selamat, and Rashidah Sukor. 2017. "Electrochemical Immunosensor for the Detection of Aflatoxin B1 in Palm Kernel Cake and Feed Samples." *Sensors* 17 (12): 2776. https://www.mdpi.com/1424-8220/17/12/2776.

Baccaro, Alexandre L. B., and Ivano G. R. Gutz. 2018. "FOTOELETROCATÁLISE EM SEMICONDUTORES: DOS PRINCÍPIOS BÁSICOS ATÉ SUA CONFORMAÇÃO À NANOESCALA." *Química Nova* 41 (3): 326-339. https://doi.org/10.21577/0100-4042.20170174.

Bahadir, E. B., and M. K. Sezginturk. 2016. "A review on impedimetric biosensors." *Artificial Cells Nanomedicine and Biotechnology* 44 (1): 248-262. https://doi.org/10.3109/21691401.2014.942456. <Go to ISI>://WOS:000368022400033.

Baig, Nadeem, Irshad Kammakakam, and Wail Falath. 2021. "Nanomaterials: a review of synthesis methods, properties, recent progress, and challenges." *Materials Advances* 2 (6): 1821-1871. https://doi.org/10.1039/D0MA00807A. http://dx.doi.org/10.1039/D0MA00807A.

Balasubramanian, K., and M. Burghard. 2005. "Chemically functionalized carbon nanotubes." *Small* 1 (2): 180-92. https://doi.org/10.1002/smll.200400118. https://www.ncbi.nlm.nih.gov/pubmed/17193428.

Basta, L., A. Moscardini, F. Fabbri, L. Bellucci, V. Tozzini, S. Rubini, A. Griesi, M. Gemmi, S. Heun, and S. Veronesi. 2021. "Correction: Covalent organic functionalization of graphene nanosheets and reduced graphene oxide." *Nanoscale Adv* 3 (21): 6242. https://doi.org/10.1039/d1na90092g. https://www.ncbi.nlm.nih.gov/pubmed/36136413.

Bhardwaj, A., J. Kaur, M. Wuest, and F. Wuest. 2017. "In situ click chemistry generation of cyclooxygenase-2 inhibitors." *Nat Commun* 8 (1): 1. https://doi.org/10.1038/s41467-016-0009-6. https://www.ncbi.nlm.nih.gov/pubmed/28232747.

Bhardwaj, Hema, Manoj Kumar Pandey, Rajesh, and Gajjala Sumana. 2019. "Electrochemical Aflatoxin B1 immunosensor based on the use of graphene quantum dots and gold nanoparticles." *Microchimica Acta* 186 (8): 592. https://doi.org/10.1007/s00604-019-3701-5. https://doi.org/10.1007/s00604-019-3701-5.

Bhardwaj, Hema, Gajjala Sumana, and Christophe A. Marquette. 2020. "A label-free ultrasensitive microfluidic surface Plasmon resonance biosensor for Aflatoxin B1 detection using nanoparticles integrated gold chip." *Food Chemistry* 307: 125530. https://doi.org/https://doi.org/10.1016/j.foodchem.2019.125530. https://www.sciencedirect.com/science/article/pii/S0308814619316498.

Bhattacharya, P., S. Ghosh, and A. D. Stiff-Roberts. 2004. "QUANTUM DOT OPTO-ELECTRONIC DEVICES." *Annual Review of Materials Research* 34 (1): 1-40. https://doi.org/10.1146/annurev.matsci.34.040203.111535. https://doi.org/10.1146/annurev.matsci.34.040203.111535.

Biglova, Y. N. 2021. "[2 + 1] Cycloaddition reactions of fullerene C." *Beilstein J Org Chem* 17: 630-670. https://doi.org/10.3762/bjoc.17.55. https://www.ncbi.nlm.nih.gov/pubmed/33747235.

Bockelmann, U. 1993. "Exciton relaxation and radiative recombination in semiconductor quantum dots." *Physical Review B* 48 (23): 17637-17640. https://doi.org/10.1103/PhysRevB.48.17637. https://link.aps.org/doi/10.1103/PhysRevB.48.17637.

Borase, Hemant P., Chandrashekhar D. Patil, Ismael P. Sauter, Marilise B. Rott, and Satish V. Patil. 2013. "Amoebicidal activity of phytosynthesized silver nanoparticles and their in vitro cytotoxicity to human cells." *FEMS Microbiology Letters* 345 (2): 127-131. https://doi.org/10.1111/1574-6968.12195. https://doi.org/10.1111/1574-6968.12195.

Brown, Sarah D., Paola Nativo, Jo-Ann Smith, David Stirling, Paul R. Edwards, Balaji Venugopal, David J. Flint, Jane A. Plumb, Duncan Graham, and Nial J. Wheate. 2010. "Gold Nanoparticles for the Improved Anticancer Drug Delivery of the Active Component of Oxaliplatin." *Journal of the American Chemical Society* 132 (13): 4678-4684. https://doi.org/10.1021/ja908117a. https://doi.org/10.1021/ja908117a.

Brydson, Rik M., and Chris Hammond. 2005a. "Generic Methodologies for Nanotechnology: Characterization." In *Nanoscale Science and Technology*, 56-129.

---. 2005b. "Generic Methodologies for Nanotechnology: Classification and Fabrication." In *Nanoscale Science and Technology*, 1-55.

Burda, Clemens, Xiaobo Chen, Radha Narayanan, and Mostafa A. El-Sayed. 2005. "Chemistry and Properties of Nanocrystals of Different Shapes." *Chemical Reviews* 105 (4): 1025-1102. https://doi.org/10.1021/cr030063a. https://doi.org/10.1021/cr030063a.

Bystrzejewski, M., M. H. Rümmeli, H. Lange, A. Huczko, P. Baranowski, T. Gemming, and T. Pichler. 2008. "Single-walled carbon nanotubes synthesis: a direct comparison of laser ablation and carbon arc routes." *J Nanosci Nanotechnol* 8 (11): 6178-86. https://doi.org/10.1166/jnn.2008.sw05. https://www.ncbi.nlm.nih.gov/pubmed/19198361.

Cai, H., X. An, J. Cui, J. Li, S. Wen, K. Li, M. Shen, L. Zheng, G. Zhang, and X. Shi. 2013. "Facile hydrothermal synthesis and surface functionalization of polyethyleneimine-coated iron oxide nanoparticles for biomedical applications." *ACS Appl Mater Interfaces* 5 (5): 1722-31. https://doi.org/10.1021/am302883m. https://www.ncbi.nlm.nih.gov/pubmed/23388099.

Campanile, R., E. Scardapane, A. Forente, C. Granata, R. Germano, R. Di Girolamo, A. Minopoli, R. Velotta, B. Della Ventura, and V. Iannotti. 2020. "Core-Shell Magnetic Nanoparticles for Highly Sensitive Magnetoelastic Immunosensor." *Nanomaterials* 10 (8). https://doi.org/10.3390/nano10081526. <Go to ISI>://WOS:000564613600001.

Cao, J., W. Zhao, and S. Gao. 2018. "Properties and Structure of In Situ Transformed PAN-Based Carbon Fibers." *Materials (Basel)* 11 (6). https://doi.org/10.3390/ma11061017. https://www.ncbi.nlm.nih.gov/pubmed/29914047.

Cao, Q., J. Lucktong, Z. Shao, Y. Chang, and B. J. Venton. 2021. "Electrochemical treatment in KOH renews and activates carbon fiber microelectrode surfaces." *Anal Bioanal Chem* 413 (27): 6737-6746. https://doi.org/10.1007/s00216-021-03539-6. https://www.ncbi.nlm.nih.gov/pubmed/34302181.

Cao, Shixiu, Cong Zhao, Tao Han, and Lingling Peng. 2016. "Hydrothermal synthesis, characterization and gas sensing properties of the WO3 nanofibers." *Materials Letters* 169: 17-20. https://doi.org/https://doi.org/10.1016/j.matlet.2016.01.053. https://www.sciencedirect.com/science/article/pii/S0167577X16300520.

Chai, Bo, Mengqiu Xu, Juntao Yan, and Zhandong Ren. 2018. "Remarkably enhanced photocatalytic hydrogen evolution over MoS2 nanosheets loaded on uniform CdS nanospheres." *Applied Surface Science* 430: 523-530. https://doi.org/https://doi.org/10.1016/j.apsusc.2017.07.292. https://www.sciencedirect.com/science/article/pii/S0169433217322924.

Chauhan, Ruchika, and T. Basu. 2015. "Functionalised Au coated iron oxide nanocomposites based reusable immunosensor for AFB1 detection." *J. Nanomaterials* 2015: Article 4. https://doi.org/10.1155/2015/607268. https://doi.org/10.1155/2015/607268.

Chen, D., L. Tang, and J. Li. 2010. "Graphene-based materials in electrochemistry." *Chem Soc Rev* 39 (8): 3157-80. https://doi.org/10.1039/b923596e. https://www.ncbi.nlm.nih.gov/pubmed/20589275.

Chen, H. A., Y. Y. Li, Y. C. Song, F. J. Liu, D. M. Deng, X. L. Zhu, H. B. He, X. X. Yan, and L. Q. Luo. 2023. "A sandwich-type electrochemical immunosensor based on spherical nucleic acids-templated Ag nanoclusters for ultrasensitive detection of tumor biomarker." *Biosensors & Bioelectronics* 223. https://doi.org/10.1016/j.bios.2022.115029. <Go to ISI>://WOS:000914114900001.

Chen, R. P., S. Li, Y. F. Sun, B. Y. Huo, Y. T. Xia, Y. K. Qin, S. N. Li, B. D. Shi, D. F. He, J. Liang, and Z. X. Gao. 2021. "Surface-enhanced Raman spectroscopy aptasensor for simultaneous determination of ochratoxin A and zearalenone using Au@Ag core-shell nanoparticles and gold nanorods." *Microchimica Acta* 188 (8). https://doi.org/10.1007/s00604-021-04919-6. <Go to ISI>://WOS:000691561000001.

Chen, X. J., R. Tian, Q. Zhang, and C. Yao. 2014. "Target-induced electronic switch for ultrasensitive detection of Pb2+ based on three dimensionally ordered macroporous Au-Pd bimetallic electrode." *Biosensors & Bioelectronics* 53: 90-98. https://doi.org/10.1016/j.bios.2013.09.028. <Go to ISI>://WOS:000329881100015.

Chung, C., Y. K. Kim, D. Shin, S. R. Ryoo, B. H. Hong, and D. H. Min. 2013. "Biomedical applications of graphene and graphene oxide." *Acc Chem Res* 46 (10): 2211-24. https://doi.org/10.1021/ar300159f. https://www.ncbi.nlm.nih.gov/pubmed/23480658.

Connor, Ellen E, Judith Mwamuka, Anand Gole, Catherine J Murphy, and Michael D Wyatt. 2005. "Gold Nanoparticles Are Taken Up by Human Cells but Do Not Cause Acute Cytotoxicity." *Small* 1 (3): 325-327. https://doi.org/https://doi.org/10.1002/smll.200400093. https://doi.org/10.1002/smll.200400093.

Coraux, J., A. T. N'Diaye, C. Busse, and T. Michely. 2008. "Structural coherency of graphene on Ir(111)." *Nano Lett* 8 (2): 565-70. https://doi.org/10.1021/nl0728874. https://www.ncbi.nlm.nih.gov/pubmed/18189442.

Costa, S. M. R., D. Fowler, G. A. Carreira, I. Portugal, and C. M. Silva. 2022. "Production and Upgrading of Recovered Carbon Black from the Pyrolysis of End-of-Life Tires." *Materials (Basel)* 15 (6). https://doi.org/10.3390/ma15062030. https://www.ncbi.nlm.nih.gov/pubmed/35329479.

Cui, L., J. Wu, and H. X. Ju. 2015. "Electrochemical sensing of heavy metal ions with inorganic, organic and bio-materials." *Biosensors & Bioelectronics* 63: 276-286. https://doi.org/10.1016/j.bios.2014.07.052. <Go to ISI>://WOS:000343337000039.

Cui, Y., S. T. Lee, S. V. Olesik, W. Flory, and M. Mearini. 1992. "Retention of C60 and C70 fullerenes on reversed-phase high-performance liquid chromatographic stationary phases." *J Chromatogr* 625 (2): 131-40. https://doi.org/10.1016/0021-9673(92)85194-x. https://www.ncbi.nlm.nih.gov/pubmed/1474120.

Dai, H. 2002. "Carbon nanotubes: synthesis, integration, and properties." *Acc Chem Res* 35 (12): 1035-44. https://doi.org/10.1021/ar0101640. https://www.ncbi.nlm.nih.gov/pubmed/12484791.

Dali, M., K. Zinoubi, A. Chrouda, S. Abderrahmane, S. Cherrad, and N. Jaffrezic-Renault. 2018. "A biosensor based on fungal soil biomass for electrochemical detection of lead (II) and cadmium (II) by differential pulse anodic stripping voltammetry." *Journal of Electroanalytical Chemistry* 813: 9-19. https://doi.org/10.1016/j.jelechem.2018.02.009. <Go to ISI>://WOS:000428488300002.

Daniel, Marie-Christine, and Didier Astruc. 2004. "Gold Nanoparticles: Assembly, Supramolecular Chemistry, Quantum-Size-Related Properties, and Applications toward Biology, Catalysis, and Nanotechnology." *Chemical Reviews* 104 (1): 293-346. https://doi.org/10.1021/cr030698+. https://doi.org/10.1021/cr030698+.

de Mello Donegá, Celso. 2010. "Formation of nanoscale spatially indirect excitons: Evolution of the type-II optical character of CdTe/CdSe heteronanocrystals." *Physical Review B* 81 (16): 165303. https://doi.org/10.1103/PhysRevB.81.165303. https://link.aps.org/doi/10.1103/PhysRevB.81.165303.

---. 2014. "The Nanoscience Paradigm: “Size Matters!”." In *Nanoparticles: Workhorses of Nanoscience*, edited by Celso de Mello Donegá, 1-12. Berlin, Heidelberg: Springer Berlin Heidelberg.

de Sousa Cunha, Fabiana, Laise Nayra dos Santos Pereira, Thâmara Pryscilla de Costa e Silva, Roberto Alves de Sousa Luz, and Anderson Nogueira Mendes. 2019. "Development of nanoparticulate systems with action in breast and ovarian cancer: nanotheragnostics." *Journal of Drug Targeting* 27 (7): 732-741. https://doi.org/10.1080/1061186X.2018.1523418. https://doi.org/10.1080/1061186X.2018.1523418.

Dedkov, Y. S., M. Fonin, U. Rüdiger, and C. Laubschat. 2008. "Rashba effect in the graphene/ni(111) system." *Phys Rev Lett* 100 (10): 107602. https://doi.org/10.1103/PhysRevLett.100.107602. https://www.ncbi.nlm.nih.gov/pubmed/18352231.

Dedkov, Y., and E. Voloshina. 2020. "Epitaxial graphene/Ge interfaces: a minireview." *Nanoscale* 12 (21): 11416-11426. https://doi.org/10.1039/d0nr00185f. https://www.ncbi.nlm.nih.gov/pubmed/32458957.

Dhiman, Tarun Kumar, G. B. V. S. Lakshmi, Kashyap Dave, Appan Roychoudhury, Nishu Dalal, Sandeep K. Jha, Anil Kumar, Ki-Ho Han, and Pratima R. Solanki. 2021. "Rapid and Label-Free Electrochemical Detection of Fumonisin-B1 Using Microfluidic Biosensing Platform Based on Ag-CeO2 Nanocomposite." *Journal of the Electrochemical Society* 168 (7). https://doi.org/10.1149/1945-7111/ac13cf.

Di Nardo, Fabio, Eugenio Alladio, Claudio Baggiani, Simone Cavalera, Cristina Giovannoli, Giulia Spano, and Laura Anfossi. 2019. "Colour-encoded lateral flow immunoassay for the simultaneous detection of aflatoxin B1 and type-B fumonisins in a single Test line." *Talanta* 192: 288-294. https://doi.org/https://doi.org/10.1016/j.talanta.2018.09.037. https://www.sciencedirect.com/science/article/pii/S0039914018309512.

Dippong, Thomas, Erika Andrea Levei, and Oana Cadar. 2022. "Investigation of Structural, Morphological and Magnetic Properties of MFe2O4 (M = Co, Ni, Zn, Cu, Mn) Obtained by

Thermal Decomposition." *International journal of molecular sciences* 23 (15): 8483. https://doi.org/10.3390/ijms23158483.

Dixit, C. K., K. Kadimisetty, B. A. Otieno, C. Tang, S. Malla, C. E. Krause, and J. F. Rusling. 2016. "Electrochemistry-based approaches to low cost, high sensitivity, automated, multiplexed protein immunoassays for cancer diagnostics." *Analyst* 141 (2): 536-47. https://doi.org/10.1039/c5an01829c. https://www.ncbi.nlm.nih.gov/pubmed/26525998.

Donegá, Celso de Mello. 2011. "Synthesis and properties of colloidal heteronanocrystals." *Chemical Society Reviews* 40 (3): 1512-1546. https://doi.org/10.1039/C0CS00055H. http://dx.doi.org/10.1039/C0CS00055H.

Dong, Shaoqing, Jixian Yan, Shuang Zhou, and Qing Zhou. 2022. "Mycotoxins Detection Based on Electrochemical Approaches." *Electroanalysis (New York, N.Y.)* 34 (2): 132-147. https://doi.org/10.1002/elan.202100349.

Dong, Yingfeng, Xiao-qing Du, Pei Liang, and Xiao-lei Man. 2020. "One-pot solvothermal method to fabricate 1D-VS4 nanowires as anode materials for lithium ion batteries." *Inorganic Chemistry Communications* 115: 107883. https://doi.org/https://doi.org/10.1016/j.inoche.2020.107883. https://www.sciencedirect.com/science/article/pii/S1387700320301891.

Du, G., Q. Fang, and J. M. den Toonder. 2016. "Microfluidics for cell-based high throughput screening platforms - A review." *Anal Chim Acta* 903: 36-50. https://doi.org/10.1016/j.aca.2015.11.023. https://www.ncbi.nlm.nih.gov/pubmed/26709297.

Duan, Leiping, Long Hu, Xinwei Guan, Chun-Ho Lin, Dewei Chu, Shujuan Huang, Xiaogang Liu, Jianyu Yuan, and Tom Wu. 2021. "Quantum Dots for Photovoltaics: A Tale of Two Materials." *Advanced Energy Materials* 11 (20): 2100354. https://doi.org/https://doi.org/10.1002/aenm.202100354. https://doi.org/10.1002/aenm.202100354.

Dubey, R., D. Dutta, A. Sarkar, and P. Chattopadhyay. 2021. "Functionalized carbon nanotubes: synthesis, properties and applications in water purification, drug delivery, and

material and biomedical sciences." *Nanoscale Adv* 3 (20): 5722-5744. https://doi.org/10.1039/d1na00293g. https://www.ncbi.nlm.nih.gov/pubmed/36132675.

Eatemadi, A., H. Daraee, H. Karimkhanloo, M. Kouhi, N. Zarghami, A. Akbarzadeh, M. Abasi, Y. Hanifehpour, and S. W. Joo. 2014. "Carbon nanotubes: properties, synthesis, purification, and medical applications." *Nanoscale Res Lett* 9 (1): 393. https://doi.org/10.1186/1556-276X-9-393. https://www.ncbi.nlm.nih.gov/pubmed/25170330.

Eda, G., G. Fanchini, and M. Chhowalla. 2008. "Large-area ultrathin films of reduced graphene oxide as a transparent and flexible electronic material." *Nat Nanotechnol* 3 (5): 270-4. https://doi.org/10.1038/nnano.2008.83. https://www.ncbi.nlm.nih.gov/pubmed/18654522.

Ekrami, Elena, Mahdi Pouresmaieli, Elham sadat Hashemiyoon, Negin Noorbakhsh, and Matin Mahmoudifard. 2022. "Nanotechnology: A sustainable solution for heavy metals remediation." *Environmental Nanotechnology, Monitoring & Management* 18: 100718. https://doi.org/https://doi.org/10.1016/j.enmm.2022.100718. https://www.sciencedirect.com/science/article/pii/S2215153222000782.

Elzerman, J. M., R. Hanson, L. H. Willems van Beveren, B. Witkamp, L. M. K. Vandersypen, and L. P. Kouwenhoven. 2004. "Single-shot read-out of an individual electron spin in a quantum dot." *Nature* 430 (6998): 431-435. https://doi.org/10.1038/nature02693. https://doi.org/10.1038/nature02693.

Erdem, Arzum, Gulsah Congur, and Ece Eksin. 2013. "Multi channel screen printed array of electrodes for enzyme-linked voltammetric detection of MicroRNAs." *Sensors and Actuators B: Chemical* 188: 1089-1095. https://doi.org/https://doi.org/10.1016/j.snb.2013.07.114. https://www.sciencedirect.com/science/article/pii/S0925400513009209.

Evtugyn, G., and T. Hianik. 2019. "Electrochemical Immuno- and Aptasensors for Mycotoxin Determination." *Chemosensors* 7 (1). https://doi.org/10.3390/chemosensors7010010. <Go to ISI>://WOS:000464080600001.

Ezquerra, Alba, Juan C. Vidal, Laura Bonel, and Juan R. Castillo. 2015. "A validated multi-channel electrochemical immunoassay for rapid fumonisin B1 determination in cereal

samples." *Analytical Methods* 7 (9): 3742-3749. https://doi.org/10.1039/C4AY02897J. http://dx.doi.org/10.1039/C4AY02897J.

Fang, T. H., T. H. Wang, J. C. Yang, and Y. J. Hsiao. 2011. "Mechanical characterization of nanoindented graphene via molecular dynamics simulations." *Nanoscale Res Lett* 6 (1): 481. https://doi.org/10.1186/1556-276X-6-481. https://www.ncbi.nlm.nih.gov/pubmed/21813011.

Farouq, R. 2022. "Functionalized graphene/polystyrene composite, green synthesis and characterization." *Sci Rep* 12 (1): 21757. https://doi.org/10.1038/s41598-022-26270-3. https://www.ncbi.nlm.nih.gov/pubmed/36526669.

Ferguson, R. M., A. P. Khandhar, S. J. Kemp, H. Arami, E. U. Saritas, L. R. Croft, J. Konkle, P. W. Goodwill, A. Halkola, J. Rahmer, J. Borgert, S. M. Conolly, and K. M. Krishnan. 2015. "Magnetic Particle Imaging With Tailored Iron Oxide Nanoparticle Tracers." *Ieee Transactions on Medical Imaging* 34 (5): 1077-1084. https://doi.org/10.1109/tmi.2014.2375065. <Go to ISI>://WOS:000353899600006.

Fernández-Baldo, Martín A., Franco A. Bertolino, Gastón Fernández, Germán A. Messina, María I. Sanz, and Julio Raba. 2011. "Determination of Ochratoxin A in apples contaminated with Aspergillus ochraceus by using a microfluidic competitive immunosensor with magnetic nanoparticles." *Analyst* 136 (13): 2756-2762. https://doi.org/10.1039/C1AN15148G. http://dx.doi.org/10.1039/C1AN15148G.

Ferreira, L. M. C., P. S. Silva, K. K. L. Augusto, P. C. Gomes-Júnior, S. O. D. Farra, T. A. Silva, O. Fatibello-Filho, and F. C. Vicentini. 2022. "Using nanostructured carbon black-based electrochemical (bio)sensors for pharmaceutical and biomedical analyses: A comprehensive review." *J Pharm Biomed Anal* 221: 115032. https://doi.org/10.1016/j.jpba.2022.115032. https://www.ncbi.nlm.nih.gov/pubmed/36152488.

Ferreira, Rayse M., Franciele M. Morawski, Emanuel C. Pessanha, Scarllett L. S. de Lima, Diana S. da Costa, Geyse A. C. Ribeiro, João Vaz, Rodolpho Mouta, Auro A. Tanaka, Liying Liu, Maria I. P. da Silva, Aryane Tofanello, Hector A. Vitorino, Anderson G. M. da Silva, and Marco A. S. Garcia. 2023. "Facile Gram-Scale Synthesis of NiO Nanoflowers for Highly

Selective and Sensitive Electrocatalytic Detection of Hydrazine." *ACS Omega* 8 (13): 11978-11986. https://doi.org/10.1021/acsomega.2c07638. https://doi.org/10.1021/acsomega.2c07638.

Fiorio, Jhonatan L., Maitê L. Gothe, Emerson C. Kohlrausch, Maria L. Zardo, Auro A. Tanaka, Roberto B. de Lima, Anderson G. da Silva, Marco A. Garcia, Pedro Vidinha, and Giovanna Machado. 2022. Nanoengineering of Catalysts for Enhanced Hydrogen Production. *Hydrogen* 3 (2): 218-254. https://doi.org/10.3390/hydrogen3020014.

Forintos, N., and T. Czigany. 2020. "Reinforcing carbon fibers as sensors: The effect of temperature and humidity." *Composites. Part A, Applied science and manufacturing* 131: 105819. https://doi.org/10.1016/j.compositesa.2020.105819.

Frank, E., L. M. Steudle, D. Ingildeev, J. M. Spörl, and M. R. Buchmeiser. 2014. "Carbon fibers: precursor systems, processing, structure, and properties." *Angew Chem Int Ed Engl* 53 (21): 5262-98. https://doi.org/10.1002/anie.201306129. https://www.ncbi.nlm.nih.gov/pubmed/24668878.

Freire, L., and A. S. Sant'Ana. 2018. "Modified mycotoxins: An updated review on their formation, detection, occurrence, and toxic effects." *Food Chem Toxicol* 111: 189-205. https://doi.org/10.1016/j.fct.2017.11.021. https://www.ncbi.nlm.nih.gov/pubmed/29158197.

Fujigaya, T., and N. Nakashima. 2015. "Non-covalent polymer wrapping of carbon nanotubes and the role of wrapped polymers as functional dispersants." *Sci Technol Adv Mater* 16 (2): 024802. https://doi.org/10.1088/1468-6996/16/2/024802. https://www.ncbi.nlm.nih.gov/pubmed/27877763.

Furno, Franck, Kelly S. Morley, Ben Wong, Barry L. Sharp, Polly L. Arnold, Steven M. Howdle, Roger Bayston, Paul D. Brown, Peter D. Winship, and Helen J. Reid. 2004. "Silver nanoparticles and polymeric medical devices: a new approach to prevention of infection?" *Journal of Antimicrobial Chemotherapy* 54 (6): 1019-1024. https://doi.org/10.1093/jac/dkh478. https://doi.org/10.1093/jac/dkh478.

Gao, Xiaohu, Yuanyuan Cui, Richard M. Levenson, Leland W. K. Chung, and Shuming Nie. 2004. "In vivo cancer targeting and imaging with semiconductor quantum dots." *Nature Biotechnology* 22 (8): 969-976. https://doi.org/10.1038/nbt994. https://doi.org/10.1038/nbt994.

Gaponenko, Sergey V. 2010. *Introduction to Nanophotonics*. Cambridge: Cambridge University Press.

García-Nicolás, María, Natalia Arroyo-Manzanares, and Pilar Viñas. 2023. "Dispersive Magnetic Solid-Phase Extraction as a Novelty Sample Treatment for the Determination of the Main Aflatoxins in Paprika." *Toxins* 15 (2): 160. https://www.mdpi.com/2072-6651/15/2/160.

García-Simón, C., M. Garcia-Borràs, L. Gómez, T. Parella, S. Osuna, J. Juanhuix, I. Imaz, D. Maspoch, M. Costas, and X. Ribas. 2014. "Sponge-like molecular cage for purification of fullerenes." *Nat Commun* 5: 5557. https://doi.org/10.1038/ncomms6557. https://www.ncbi.nlm.nih.gov/pubmed/25424201.

Ghosh, Partha, Xiaochao Yang, Rochelle Arvizo, Zheng-Jiang Zhu, Sarit S. Agasti, Zhihong Mo, and Vincent M. Rotello. 2010. "Intracellular Delivery of a Membrane-Impermeable Enzyme in Active Form Using Functionalized Gold Nanoparticles." *Journal of the American Chemical Society* 132 (8): 2642-2645. https://doi.org/10.1021/ja907887z. https://doi.org/10.1021/ja907887z.

Gibson, N. M., T. J. M. Luo, D. W. Brenner, and O. Shenderova. 2011. "Immobilization of mycotoxins on modified nanodiamond substrates." *Biointerphases* 6 (4): 210-217. https://doi.org/10.1116/1.3672489.

Gopinath, V., S. Priyadarshini, Mun Fai Loke, J. Arunkumar, Enrico Marsili, D. MubarakAli, P. Velusamy, and Jamuna Vadivelu. 2017. "Biogenic synthesis, characterization of antibacterial silver nanoparticles and its cell cytotoxicity." *Arabian Journal of Chemistry* 10 (8): 1107-1117. https://doi.org/https://doi.org/10.1016/j.arabjc.2015.11.011. https://www.sciencedirect.com/science/article/pii/S1878535215003238.

Groeneveld, Esther, and Celso de Mello Donegá. 2014. "The Challenge of Colloidal Nanoparticle Synthesis." In *Nanoparticles: Workhorses of Nanoscience*, edited by Celso de Mello Donegá, 145-189. Berlin, Heidelberg: Springer Berlin Heidelberg.

Guo, J., H. Jiang, Y. Teng, Y. Xiong, Z. Chen, L. You, and D. Xiao. 2021. "Recent advances in magnetic carbon nanotubes: synthesis, challenges and highlighted applications." *J Mater Chem B* 9 (44): 9076-9099. https://doi.org/10.1039/d1tb01242h. https://www.ncbi.nlm.nih.gov/pubmed/34668920.

Gupta, Ajay Kumar, and Mona Gupta. 2005. "Synthesis and surface engineering of iron oxide nanoparticles for biomedical applications." *Biomaterials* 26 (18): 3995-4021. https://doi.org/https://doi.org/10.1016/j.biomaterials.2004.10.012. https://www.sciencedirect.com/science/article/pii/S0142961204009317.

Haixia X Fau - de Barros, Aline Oliveira da Silva, Francisco do Vale Chaves de Barros Aods Fau - E Mello, Fan E Mello Fdvc Fau - Sozzi-Guo, Cristina Sozzi-Guo F Fau - Müller, Sara Müller C Fau - Gemini-Piperni, Luciana Magalhães Rebelo Gemini-Piperni S Fau - Alencar, Francisco Franciné Alencar Lmr Fau - Maia, Valder Nogueira Maia Ff Fau - Freire, Frederico Duarte Freire Vn Fau - de Menezes, Veronica de Menezes Fd Fau - Aran, Sylvie Aran V Fau - Devalle, Vivaldo Devalle S Fau - Moura-Neto, Eduardo Moura-Neto V Fau - Ricci-Junior, Eliete Ricci-Junior E Fau - Bouskela, Konstantin Bouskela E Fau - Pikula, Kirill Pikula K Fau - Golokhvast, Ralph Golokhvast K Fau - Santos-Oliveira, and R. Santos-Oliveira. "Graphene: Insights on Biological, Radiochemical and Ecotoxicological Aspects." (1550-7033 (Print)).

Han, Jing, Ying Zhuo, Ya-Qin Chai, Yun Xiang, and Ruo Yuan. 2015. "New Type of Redox Nanoprobe: C60-Based Nanomaterial and Its Application in Electrochemical Immunoassay for Doping Detection." *Analytical Chemistry* 87 (3): 1669-1675. https://doi.org/10.1021/ac503406p. https://doi.org/10.1021/ac503406p.

Han, X., J. Lei, K. Chen, Q. Li, H. Hao, T. Zhou, F. L. Jiang, M. Li, and Y. Liu. 2019. "Cytotoxicity of CdTe quantum dots with different surface coatings against yeast Saccharomyces cerevisiae." *Ecotoxicol Environ Saf* 174: 467-474.

https://doi.org/10.1016/j.ecoenv.2019.03.013.
https://www.ncbi.nlm.nih.gov/pubmed/30852312.

Hasanzadeh, M., N. Shadjou, M. Eskandani, M. de la Guardia, and E. Omidinia. 2013. "Electrochemical nano-immunosensing of effective cardiac biomarkers for acute myocardial infarction." *Trac-Trends in Analytical Chemistry* 49: 20-30. https://doi.org/10.1016/j.trac.2013.04.009. <Go to ISI>://WOS:000323399100002.

Hayashi, T., D. Shimamoto, Y. A. Kim, H. Muramatsu, F. Okino, H. Touhara, T. Shimada, Y. Miyauchi, S. Maruyama, M. Terrones, M. S. Dresselhaus, and M. Endo. 2008. "Selective optical property modification of double-walled carbon nanotubes by fluorination." *ACS Nano* 2 (3): 485-8. https://doi.org/10.1021/nn700391w. https://www.ncbi.nlm.nih.gov/pubmed/19206574.

Hedayatnasab, Ziba, Faisal Abnisa, and Wan Mohd Ashri Wan Daud. 2017. "Review on magnetic nanoparticles for magnetic nanofluid hyperthermia application." *Materials & Design* 123: 174-196. https://doi.org/https://doi.org/10.1016/j.matdes.2017.03.036. https://www.sciencedirect.com/science/article/pii/S0264127517302757.

Hervás, M., M. A. López, and A. Escarpa. 2010. "Simplified calibration and analysis on screen-printed disposable platforms for electrochemical magnetic bead-based immunosensing of zearalenone in baby food samples." *Biosens Bioelectron* 25 (7): 1755-60. https://doi.org/10.1016/j.bios.2009.12.031. https://www.ncbi.nlm.nih.gov/pubmed/20097055.

Hervás, Miriam, Miguel Ángel López, and Alberto Escarpa. 2009a. "Electrochemical immunoassay using magnetic beads for the determination of zearalenone in baby food: An anticipated analytical tool for food safety." *Analytica chimica acta* 653 (2): 167-172. https://doi.org/10.1016/j.aca.2009.09.024.

---. 2009b. "Electrochemical microfluidic chips coupled to magnetic bead-based ELISA to control allowable levels of zearalenone in baby foods using simplified calibration." *Analyst* 134 (12): 2405-2411. https://doi.org/10.1039/B911839J. http://dx.doi.org/10.1039/B911839J.

Hervás, Mirian, Miguel A. López, and Alberto Escarpa. 2011. "Integrated electrokinetic magnetic bead-based electrochemical immunoassay on microfluidic chips for reliable control of permitted levels of zearalenone in infant foods." *Analyst* 136 (10): 2131-2138. https://doi.org/10.1039/C1AN15081B. http://dx.doi.org/10.1039/C1AN15081B.

Heydari-Bafrooei, Esmaeil, and Ali A. Ensafi. 2023. "Nanomaterials-based biosensing strategies for biomarkers diagnosis, a review." *Biosensors and Bioelectronics: X* 13: 100245. https://doi.org/https://doi.org/10.1016/j.biosx.2022.100245. https://www.sciencedirect.com/science/article/pii/S2590137022001388.

Hocevar, Moïra, George Immink, Marcel Verheijen, Nika Akopian, Val Zwiller, Leo Kouwenhoven, and Erik Bakkers. 2012. "Growth and optical properties of axial hybrid III–V/silicon nanowires." *Nature Communications* 3 (1): 1266. https://doi.org/10.1038/ncomms2277. https://doi.org/10.1038/ncomms2277.

Horky, P., S. Skalickova, D. Baholet, and J. Skladanka. 2018. "Nanoparticles as a Solution for Eliminating the Risk of Mycotoxins." *Nanomaterials* 8 (9). https://doi.org/10.3390/nano8090727. <Go to ISI>://WOS:000448659200095.

Hou, J., Y. Shao, M. W. Ellis, R. B. Moore, and B. Yi. 2011. "Graphene-based electrochemical energy conversion and storage: fuel cells, supercapacitors and lithium ion batteries." *Phys Chem Chem Phys* 13 (34): 15384-402. https://doi.org/10.1039/c1cp21915d. https://www.ncbi.nlm.nih.gov/pubmed/21799983.

Huang, J., F. Shen, X. Li, X. Zhou, B. Li, R. Xu, and C. Wu. 2008. "Chemical modification of carbon black by a simple non-liquid-phase approach." *J Colloid Interface Sci* 328 (1): 92-7. https://doi.org/10.1016/j.jcis.2008.08.044. https://www.ncbi.nlm.nih.gov/pubmed/18829042.

Huang, L., B. Wu, J. Chen, Y. Xue, D. Geng, Y. Guo, G. Yu, and Y. Liu. 2013. "Gram-scale synthesis of graphene sheets by a catalytic arc-discharge method." *Small* 9 (8): 1330-5. https://doi.org/10.1002/smll.201202802. https://www.ncbi.nlm.nih.gov/pubmed/23463696.

Huang, Qitong, Xiaofeng Lin, Dejian Chen, and Qing-Xiao Tong. 2022. "Carbon Dots/α-Fe2O3-Fe3O4 nanocomposite: Efficient synthesis and application as a novel electrochemical

aptasensor for the ultrasensitive determination of aflatoxin B1." *Food chemistry* 373: 131415-131415. https://doi.org/10.1016/j.foodchem.2021.131415.

Huang, X., R. S. Mclean, and M. Zheng. 2005. "High-resolution length sorting and purification of DNA-wrapped carbon nanotubes by size-exclusion chromatography." *Anal Chem* 77 (19): 6225-8. https://doi.org/10.1021/ac0508954. https://www.ncbi.nlm.nih.gov/pubmed/16194082.

Huang, Xiaohua, Wei Qian, Ivan H. El-Sayed, and Mostafa A. El-Sayed. 2007. "The potential use of the enhanced nonlinear properties of gold nanospheres in photothermal cancer therapy." *Lasers in Surgery and Medicine* 39 (9): 747-753. https://doi.org/https://doi.org/10.1002/lsm.20577. https://doi.org/10.1002/lsm.20577.

Huang, Xiaoping, Yufang Zhu, and Ehsan Kianfar. 2021. "Nano Biosensors: Properties, applications and electrochemical techniques." *Journal of Materials Research and Technology* 12: 1649-1672. https://doi.org/https://doi.org/10.1016/j.jmrt.2021.03.048. https://www.sciencedirect.com/science/article/pii/S2238785421002751.

Huang, Yunhong, Fei Zhu, Jinhua Guan, Wei Wei, and Long Zou. 2021. "Label-Free Amperometric Immunosensor Based on Versatile Carbon Nanofibers Network Coupled with Au Nanoparticles for Aflatoxin B1 Detection." *Biosensors* 11 (1): 5. https://www.mdpi.com/2079-6374/11/1/5.

Hwu, Jih Ru, Yu Sern Lin, Thainashmuthu Josephrajan, Ming-Hua Hsu, Fong-Yu Cheng, Chen-Sheng Yeh, Wu-Chou Su, and Dar-Bin Shieh. 2009. "Targeted Paclitaxel by Conjugation to Iron Oxide and Gold Nanoparticles." *Journal of the American Chemical Society* 131 (1): 66-68. https://doi.org/10.1021/ja804947u. https://doi.org/10.1021/ja804947u.

Höfs, Soraya, Deniz Hülagü, Francesca Bennet, Peter Carl, Sabine Flemig, Thomas Schmid, Jörg A. Schenk, Vasile-Dan Hodoroaba, and Rudolf J. Schneider. 2021. "Electrochemical Immunomagnetic Ochratoxin A Sensing: Steps Forward in the Application of 3,3',5,5'-Tetramethylbenzidine in Amperometric Assays." *ChemElectroChem* 8 (13): 2597-2606. https://doi.org/10.1002/celc.202100446.

Iqbal, Parvez, Jon A. Preece, and Paula M. Mendes. 2012. "Nanotechnology: The “Top-Down” and “Bottom-Up” Approaches." In *Supramolecular Chemistry*.

Irfan Azizan, Muhammad Amir, Safura Taufik, Mohd Nurazzi Norizan, and Jahwarhar Izuan Abdul Rashid. 2023. "A review on surface modification in the development of electrochemical biosensor for malathion." *Biosensors and Bioelectronics: X* 13: 100291. https://doi.org/https://doi.org/10.1016/j.biosx.2022.100291. https://www.sciencedirect.com/science/article/pii/S2590137022001844.

Isakovski, M. K., J. Beljin, J. Tričković, S. Rončević, and S. Maletić. 2021. "Current State and Future Perspectives of Carbon-Based Materials in the Environment: Fate and Application." *Recent Pat Nanotechnol* 15 (3): 183-196. https://doi.org/10.2174/1872210514666201217150323. https://www.ncbi.nlm.nih.gov/pubmed/33334300.

Ivanov, Sergei A., Andrei Piryatinski, Jagjit Nanda, Sergei Tretiak, Kevin R. Zavadil, William O. Wallace, Don Werder, and Victor I. Klimov. 2007. "Type-II Core/Shell CdS/ZnSe Nanocrystals: Synthesis, Electronic Structures, and Spectroscopic Properties." *Journal of the American Chemical Society* 129 (38): 11708-11719. https://doi.org/10.1021/ja068351m. https://doi.org/10.1021/ja068351m.

Jafari, Safiye, Loïc Burr, Davide Migliorelli, Roger Galve, M. Pilar Marco, Katrina Campbell, Chris Elliott, Michele Suman, Shana J. Sturla, and Silvia Generelli. 2022. "Smartphone-based magneto-immunosensor on carbon black modified screen-printed electrodes for point-of-need detection of aflatoxin B1 in cereals." *Analytica chimica acta* 1221: 340118-340118. https://doi.org/10.1016/j.aca.2022.340118.

Jang, M., S. Kim, H. Jeong, and S. Y. Ju. 2016. "Affinity-mediated sorting order reversal of single-walled carbon nanotubes in density gradient ultracentrifugation." *Nanotechnology* 27 (41): 41LT01. https://doi.org/10.1088/0957-4484/27/41/41LT01. https://www.ncbi.nlm.nih.gov/pubmed/27595315.

Jiang, Yinhua, ZhiYuan Peng, Shuaibin Zhang, Fan Li, Zhanchao Liu, Jianming Zhang, Yan Liu, and Kun Wang. 2018. "Facile in-situ Solvothermal Method to synthesize double shell ZnIn2S4 nanosheets/TiO2 hollow nanosphere with enhanced photocatalytic activities." *Ceramics International* 44 (6): 6115-6126. https://doi.org/https://doi.org/10.1016/j.ceramint.2017.12.244. https://www.sciencedirect.com/science/article/pii/S0272884217329528.

Jin, Rongrong, Bingbing Lin, Danyang Li, and Hua Ai. 2014. "Superparamagnetic iron oxide nanoparticles for MR imaging and therapy: design considerations and clinical applications." *Current Opinion in Pharmacology* 18: 18-27. https://doi.org/https://doi.org/10.1016/j.coph.2014.08.002. https://www.sciencedirect.com/science/article/pii/S1471489214000940.

Jodra, Adrián, Mirian Hervás, Miguel Ángel López, and Alberto Escarpa. 2015. "Disposable electrochemical magneto immunosensor for simultaneous simplified calibration and determination of Ochratoxin A in coffee samples." *Sensors and actuators. B, Chemical* 221: 777-783. https://doi.org/10.1016/j.snb.2015.07.007.

Jodra, Adrián, Miguel Ángel López, and Alberto Escarpa. 2015. "Disposable and reliable electrochemical magnetoimmunosensor for Fumonisins simplified determination in maize-based foodstuffs." *Biosensors & bioelectronics* 64: 633-638. https://doi.org/10.1016/j.bios.2014.09.054.

Justino, Celine I. L., Ana C. Freitas, Ruth Pereira, Armando C. Duarte, and Teresa A. P. Rocha Santos. 2015. "Recent developments in recognition elements for chemical sensors and biosensors." *TrAC Trends in Analytical Chemistry* 68: 2-17. https://doi.org/https://doi.org/10.1016/j.trac.2015.03.006. https://www.sciencedirect.com/science/article/pii/S016599361500062X.

Kambhampati, Patanjali. 2011. "Hot Exciton Relaxation Dynamics in Semiconductor Quantum Dots: Radiationless Transitions on the Nanoscale." *The Journal of Physical Chemistry C* 115 (45): 22089-22109. https://doi.org/10.1021/jp2058673. https://doi.org/10.1021/jp2058673.

Katouzian, I., and S. M. Jafari. 2019. "Protein nanotubes as state-of-the-art nanocarriers: Synthesis methods, simulation and applications." *J Control Release* 303: 302-318. https://doi.org/10.1016/j.jconrel.2019.04.026. https://www.ncbi.nlm.nih.gov/pubmed/31009647.

Kecskemeti, A., C. Nagy, P. Biro, Z. Szabo, I. Pocsi, T. Bartok, and A. Gaspar. 2020. "Analysis of fumonisin mycotoxins with capillary electrophoresis - mass spectrometry." *Food Additives and Contaminants Part a-Chemistry Analysis Control Exposure & Risk Assessment* 37 (9): 1553-1563. https://doi.org/10.1080/19440049.2020.1778797. <Go to ISI>://WOS:000550710500001.

Khan, A., M. N. Haque, D. C. Kabiraz, Yeasin Al, H. Al Rashid, A. C. Sarker, and G. Hossain. 2023. "A review on advanced nanocomposites materials based smart textile biosensor for healthcare monitoring from human sweat." *Sensors and Actuators a-Physical* 350. https://doi.org/10.1016/j.sna.2022.114093. <Go to ISI>://WOS:000974578600001.

Khan, Ibrahim, Khalid Saeed, and Idrees Khan. 2019. "Nanoparticles: Properties, applications and toxicities." *Arabian Journal of Chemistry* 12 (7): 908-931. https://doi.org/https://doi.org/10.1016/j.arabjc.2017.05.011. https://www.sciencedirect.com/science/article/pii/S1878535217300990.

Kim, D. B., N. E. Song, T. G. Nam, S. Lee, D. Seo, and M. Yoo. 2019. "Occurrence of emerging mycotoxins in cereals and cereal-based products from the Korean market using LC-MS/MS." *Food Addit Contam Part A Chem Anal Control Expo Risk Assess* 36 (2): 289-295. https://doi.org/10.1080/19440049.2018.1562233. https://www.ncbi.nlm.nih.gov/pubmed/30676884.

Kim, G., H. Lee, K. Kim, and D. U. Kim. 2022. "Effects of Heat Treatment Atmosphere and Temperature on the Properties of Carbon Fibers." *Polymers (Basel)* 14 (12). https://doi.org/10.3390/polym14122412. https://www.ncbi.nlm.nih.gov/pubmed/35745989.

Kim, J., C. Park, I. Song, M. Lee, H. Kim, and H. C. Choi. 2016. "Unique Crystallization of Fullerenes: Fullerene Flowers." *Sci Rep* 6: 32205. https://doi.org/10.1038/srep32205. https://www.ncbi.nlm.nih.gov/pubmed/27561446.

Kim, K. S., Y. Zhao, H. Jang, S. Y. Lee, J. M. Kim, J. H. Ahn, P. Kim, J. Y. Choi, and B. H. Hong. 2009. "Large-scale pattern growth of graphene films for stretchable transparent electrodes." *Nature* 457 (7230): 706-10. https://doi.org/10.1038/nature07719. https://www.ncbi.nlm.nih.gov/pubmed/19145232.

Kombaiah, K., J. Judith Vijaya, L. John Kennedy, M. Bououdina, and Basma Al-Najar. 2018. "Conventional and microwave combustion synthesis of optomagnetic CuFe2O4 nanoparticles for hyperthermia studies." *Journal of Physics and Chemistry of Solids* 115: 162-171. https://doi.org/https://doi.org/10.1016/j.jpcs.2017.12.024. https://www.sciencedirect.com/science/article/pii/S0022369717320000.

Koole, Rolf, Esther Groeneveld, Daniel Vanmaekelbergh, Andries Meijerink, and Celso de Mello Donegá. 2014. "Size Effects on Semiconductor Nanoparticles." In *Nanoparticles: Workhorses of Nanoscience*, edited by Celso de Mello Donegá, 13-51. Berlin, Heidelberg: Springer Berlin Heidelberg.

Kour, Ravinder, Sandeep Arya, Sheng-Joue Young, Vinay Gupta, Pankaj Bandhoria, and Ajit Khosla. 2020. "Review-Recent Advances in Carbon Nanomaterials as Electrochemical Biosensors." *Journal of the Electrochemical Society* 167 (3): 37555. https://doi.org/10.1149/1945-7111/ab6bc4.

Kovač, Tihomir, Bojan Šarkanj, Tomislav Klapec, Ivana Borišev, Marija Kovač, Ante Nevistić, and Ivica Strelec. 2018. "Antiaflatoxigenic effect of fullerene C60 nanoparticles at environmentally plausible concentrations." *AMB Express* 8 (1): 14. https://doi.org/10.1186/s13568-018-0544-0. https://doi.org/10.1186/s13568-018-0544-0.

Kumar, J. Aravind, T. Krithiga, S. Manigandan, S. Sathish, A. Annam Renita, P. Prakash, B. S. Naveen Prasad, T. R. Praveen Kumar, M. Rajasimman, A. Hosseini-Bandegharaei, D. Prabu, and S. Crispin. 2021. "A focus to green synthesis of metal/metal based oxide nanoparticles:

Various mechanisms and applications towards ecological approach." *Journal of Cleaner Production* 324: 129198. https://doi.org/https://doi.org/10.1016/j.jclepro.2021.129198. https://www.sciencedirect.com/science/article/pii/S0959652621033849.

Kumar, V. Sunil, Shekher Kummari, Gaëlle Catanante, K. Vengatajalabathy Gobi, Jean Louis Marty, and K. Yugender Goud. 2023. "A label-free impedimetric immunosensor for zearalenone based on CS-CNT-Pd nanocomposite modified screen-printed disposable electrodes." *Sensors and actuators. B, Chemical* 377: 133077. https://doi.org/10.1016/j.snb.2022.133077.

Kundu, Subrata, Luohan Peng, and Hong Liang. 2008. "A New Route to Obtain High-Yield Multiple-Shaped Gold Nanoparticles in Aqueous Solution using Microwave Irradiation." *Inorganic Chemistry* 47 (14): 6344-6352. https://doi.org/10.1021/ic8004135. https://doi.org/10.1021/ic8004135.

Kuramitz, Hideki. 2009. "Magnetic microbead-based electrochemical immunoassays." *Analytical and bioanalytical chemistry* 394 (1): 61-69. https://doi.org/10.1007/s00216-009-2650-y.

Kyesmen, P. I., A. Onoja, and A. N. Amah. 2016. "Fullerenes synthesis by combined resistive heating and arc discharge techniques." *Springerplus* 5 (1): 1323. https://doi.org/10.1186/s40064-016-2994-7. https://www.ncbi.nlm.nih.gov/pubmed/27563518.

Lakhera, P., V. Chaudhary, A. Jha, R. Singh, P. Kush, and P. Kumar. 2022. "Recent developments and fabrication of the different electrochemical biosensors based on modified screen printed and glassy carbon electrodes for the early diagnosis of diverse breast cancer biomarkers." *Materials Today Chemistry* 26: 101129. https://doi.org/https://doi.org/10.1016/j.mtchem.2022.101129. https://www.sciencedirect.com/science/article/pii/S2468519422003585.

Lee, Jisoo, Jiwoong Yang, Soon Gu Kwon, and Taeghwan Hyeon. 2016. "Nonclassical nucleation and growth of inorganic nanoparticles." *Nature Reviews Materials* 1 (8): 16034. https://doi.org/10.1038/natrevmats.2016.34. https://doi.org/10.1038/natrevmats.2016.34.

Leistenschneider, Desirée, Katharina Zürbes, Christina Schneidermann, Sven Grätz, Steffen Oswald, Karl Wegner, Benjamin Klemmed, Lars Giebeler, Alexander Eychmüller, and Lars Borchardt. 2018. "Mechanochemical Functionalization of Carbon Black at Room Temperature." *C* 4 (1): 14. https://www.mdpi.com/2311-5629/4/1/14.

Li, C., Z. Yang, X. Zhang, Y. Ru, D. Gao, D. Wu, and J. Sun. 2022. "Ultrasonic-Assisted Method for the Preparation of Carbon Nanotube-Graphene/Polydimethylsiloxane Composites with Integrated Thermal Conductivity, Electromagnetic Interference Shielding, and Mechanical Performances." *Int J Mol Sci* 23 (23). https://doi.org/10.3390/ijms232315007. https://www.ncbi.nlm.nih.gov/pubmed/36499333.

Li, D., Y. Luo, D. Onidas, L. He, M. Jin, F. Gazeau, J. Pinson, and C. Mangeney. 2021. "Surface functionalization of nanomaterials by aryl diazonium salts for biomedical sciences." *Adv Colloid Interface Sci* 294: 102479. https://doi.org/10.1016/j.cis.2021.102479. https://www.ncbi.nlm.nih.gov/pubmed/34237631.

Li, Guanghui, Min Zhu, Lu Ma, Junrong Yan, Xiaoling Lu, Yanfei Shen, and Yakun Wan. 2016. "Generation of Small Single Domain Nanobody Binders for Sensitive Detection of Testosterone by Electrochemical Impedance Spectroscopy." *ACS Applied Materials & Interfaces* 8 (22): 13830-13839. https://doi.org/10.1021/acsami.6b04658. https://doi.org/10.1021/acsami.6b04658.

Li, Jianlin, Qingliu Wu, and Ji Wu. 2016. "Synthesis of Nanoparticles via Solvothermal and Hydrothermal Methods." In *Handbook of Nanoparticles*, edited by Mahmood Aliofkhazraei, 295-328. Cham: Springer International Publishing.

Li, R., C. Meng, Y. Wen, W. Fu, and P. He. 2019. "Fluorometric lateral flow immunoassay for simultaneous determination of three mycotoxins (aflatoxin B." *Mikrochim Acta* 186 (12): 748.

https://doi.org/10.1007/s00604-019-3879-6.
https://www.ncbi.nlm.nih.gov/pubmed/31696359.

Li, Weiqiang, Kaisheng Diao, Daoyang Qiu, Yifang Zeng, Kaijie Tang, Yifu Zhu, Yingying Sheng, Yangping Wen, and Mingfang Li. 2021. "A highly-sensitive and selective antibody-like sensor based on molecularly imprinted poly(L-arginine) on COOH-MWCNTs for electrochemical recognition and detection of deoxynivalenol." *Food chemistry* 350: 129229. https://doi.org/10.1016/j.foodchem.2021.129229.

Li, Yadong, Yi Ding, Yue Zhang, and Yitai Qian. 1999. "Photophysical properties of ZnS quantum dots." *Journal of Physics and Chemistry of Solids* 60 (1): 13-15. https://doi.org/https://doi.org/10.1016/S0022-3697(98)00247-9.
https://www.sciencedirect.com/science/article/pii/S0022369798002479.

Liang, S., L. Zhu, S. Wang, L. Chen, and H. Fang. 2021. "Fast Reduced Graphene-Based Membranes with High Desalination Performance." *Membranes (Basel)* 11 (11). https://doi.org/10.3390/membranes11110846.
https://www.ncbi.nlm.nih.gov/pubmed/34832075.

Lin, Y., Q. Zhou, D. Tang, R. Niessner, and D. Knopp. 2017. "Signal-On Photoelectrochemical Immunoassay for Aflatoxin B(1) Based on Enzymatic Product-Etching MnO(2) Nanosheets for Dissociation of Carbon Dots." *Anal Chem* 89 (10): 5637-5645. https://doi.org/10.1021/acs.analchem.7b00942.
https://www.ncbi.nlm.nih.gov/pubmed/28409636.

Lin, Y., Q. Zhou, D. Tang, R. Niessner, H. Yang, and D. Knopp. 2016. "Silver Nanolabels-Assisted Ion-Exchange Reaction with CdTe Quantum Dots Mediated Exciton Trapping for Signal-On Photoelectrochemical Immunoassay of Mycotoxins." *Anal Chem* 88 (15): 7858-66. https://doi.org/10.1021/acs.analchem.6b02124.
https://www.ncbi.nlm.nih.gov/pubmed/27348353.

Link, Stephan, and Mostafa A. El-Sayed. 1999. "Size and Temperature Dependence of the Plasmon Absorption of Colloidal Gold Nanoparticles." *The Journal of Physical Chemistry B* 103 (21): 4212-4217. https://doi.org/10.1021/jp984796o. https://doi.org/10.1021/jp984796o.

Liu, Haoran, Jun Ge, Eugene Ma, and Lei Yang. 2019. "10 - Advanced biomaterials for biosensor and theranostics." In *Biomaterials in Translational Medicine*, edited by Lei Yang, Sarit B. Bhaduri and Thomas J. Webster, 213-255. Academic Press.

Loh, K. P., Q. Bao, G. Eda, and M. Chhowalla. 2010. "Graphene oxide as a chemically tunable platform for optical applications." *Nat Chem* 2 (12): 1015-24. https://doi.org/10.1038/nchem.907. https://www.ncbi.nlm.nih.gov/pubmed/21107364.

Lu, Lin, and Sundaram Gunasekaran. 2019. "Dual-channel ITO-microfluidic electrochemical immunosensor for simultaneous detection of two mycotoxins." *Talanta (Oxford)* 194: 709-716. https://doi.org/10.1016/j.talanta.2018.10.091.

Luo, L., X. Liu, S. Ma, L. Li, and T. You. 2020. "Quantification of zearalenone in mildewing cereal crops using an innovative photoelectrochemical aptamer sensing strategy based on ZnO-NGQDs composites." *Food Chem* 322: 126778. https://doi.org/10.1016/j.foodchem.2020.126778. https://www.ncbi.nlm.nih.gov/pubmed/32305007.

Manocha, L. M., H. Patel, S. Manocha, A. K. Roy, and J. P. Singh. 2009. "Development of carbon/carbon composites with carbon nanotubes as reinforcement and chemical vapor infiltration carbon as matrix." *J Nanosci Nanotechnol* 9 (5): 3119-24. https://doi.org/10.1166/jnn.2009.034. https://www.ncbi.nlm.nih.gov/pubmed/19452978.

Matabaro, E., N. Ishimwe, E. Uwimbabazi, and B. H. Lee. 2017. "Current Immunoassay Methods for the Rapid Detection of Aflatoxin in Milk and Dairy Products." *Compr Rev Food Sci Food Saf* 16 (5): 808-820. https://doi.org/10.1111/1541-4337.12287. https://www.ncbi.nlm.nih.gov/pubmed/33371606.

Matysik, G., and H. Giryn. 1996. "Gradient thin-layer chromatography and densitometry determination of Alternaria mycotoxins." *Chromatographia* 42 (9-10): 555-558. https://doi.org/10.1007/bf02290291. <Go to ISI>://WOS:A1996UT61000011.

McIntosh, C. M., A. K. Esposito Ea 3rd Fau - Boal, J. M. Boal Ak Fau - Simard, C. T. Simard Jm Fau - Martin, V. M. Martin Ct Fau - Rotello, and V. M. Rotello. "Inhibition of DNA transcription using cationic mixed monolayer protected gold clusters." (0002-7863 (Print)).

McIntyre, P. C., and A. Fontcuberta i Morral. 2020. "Semiconductor nanowires: to grow or not to grow?" *Materials Today Nano* 9: 100058. https://doi.org/https://doi.org/10.1016/j.mtnano.2019.100058. https://www.sciencedirect.com/science/article/pii/S2588842019301270.

Meng, L., J. Jin, G. Yang, T. Lu, H. Zhang, and C. Cai. 2009. "Nonenzymatic electrochemical detection of glucose based on palladium-single-walled carbon nanotube hybrid nanostructures." *Anal Chem* 81 (17): 7271-80. https://doi.org/10.1021/ac901005p. https://www.ncbi.nlm.nih.gov/pubmed/19715358.

Mittelstädt, Alexander, Andrei Schliwa, and Petr Klenovský. 2022. "Modeling electronic and optical properties of III–V quantum dots—selected recent developments." *Light: Science & Applications* 11 (1): 17. https://doi.org/10.1038/s41377-021-00700-9. https://doi.org/10.1038/s41377-021-00700-9.

Mohamed, Mona A., Nahla N. Salama, Maha A. Sultan, Hadeer F. Manie, and Maha M. Abou El-Alamin. 2020. "Cobalt ferrite magnetic nanoparticles as a highly efficient electrochemical platform for simultaneous determination of dexlansoprazole and granisetron hydrochloride." *Microchemical journal* 159: 105424. https://doi.org/10.1016/j.microc.2020.105424.

Molina, Gustavo A., Rodrigo Esparza, J. Luis López-Miranda, Angel R. Hernández-Martínez, Beatriz L. España-Sánchez, Eduardo A. Elizalde-Peña, and Miriam Estevez. 2019. "Green synthesis of Ag nanoflowers using Kalanchoe Daigremontiana extract for enhanced photocatalytic and antibacterial activities." *Colloids and Surfaces B: Biointerfaces* 180: 141-

149. https://doi.org/https://doi.org/10.1016/j.colsurfb.2019.04.044. https://www.sciencedirect.com/science/article/pii/S0927776519302759.

Morales-Lara, F., M. Domingo-García, R. López-Garzón, M. Luz Godino-Salido, A. Peñas-Sanjuán, F. J. López-Garzón, M. Pérez-Mendoza, and M. Melguizo. 2016. "Grafting the surface of carbon nanotubes and carbon black with the chemical properties of hyperbranched polyamines." *Sci Technol Adv Mater* 17 (1): 541-553. https://doi.org/10.1080/14686996.2016.1221728. https://www.ncbi.nlm.nih.gov/pubmed/27877902.

Moreels, Iwan, Karel Lambert, David De Muynck, Frank Vanhaecke, Dirk Poelman, José C. Martins, Guy Allan, and Zeger Hens. 2007. "Composition and Size-Dependent Extinction Coefficient of Colloidal PbSe Quantum Dots." *Chemistry of Materials* 19 (25): 6101-6106. https://doi.org/10.1021/cm071410q. https://doi.org/10.1021/cm071410q.

Mousavi Nodoushan, Somayeh, Navid Nasirizadeh, Reza Kachuei, and Abbas Ali Imani Fooladi. 2019. "Electrochemical detection of aflatoxin B1: an aptasensor prepared using graphene oxide and gold nanowires." *Analytical methods* 11 (47): 633-642. https://doi.org/10.1039/c9ay01673b.

Munawar, Hasim, Alvaro Garcia-Cruz, Marta Majewska, Kal Karim, Wlodzimierz Kutner, and Sergey A. Piletsky. 2020. "Electrochemical determination of fumonisin B1 using a chemosensor with a recognition unit comprising molecularly imprinted polymer nanoparticles." *Sensors and actuators. B, Chemical* 321: 128552. https://doi.org/10.1016/j.snb.2020.128552.

Muñoz-García, Javier, Raúl Gago, Luis Vázquez, José Angel Sánchez-García, and Rodolfo Cuerno. 2010. "Observation and Modeling of Interrupted Pattern Coarsening: Surface Nanostructuring by Ion Erosion." *Physical Review Letters* 104 (2): 026101. https://doi.org/10.1103/PhysRevLett.104.026101. https://link.aps.org/doi/10.1103/PhysRevLett.104.026101.

Murphy, M., K. Theyagarajan, Prabusankar Ganesan, Sellappan Senthilkumar, Kathavarayan Thenmozhi. 2019. "Electrochemical biosensor for the detection of hydrogen peroxide using

cytochrome c covalently immobilized on carboxyl functionalized ionic liquid/multiwalled carbon nanotube hybrid". *Applied Surface Science* 492: 718-725. https://doi.org/10.1016/j.apsusc.2019.06.283.

Nagar, Niharika, and Vijay Devra. 2018. "Green synthesis and characterization of copper nanoparticles using Azadirachta indica leaves." *Materials Chemistry and Physics* 213: 44-51. https://doi.org/https://doi.org/10.1016/j.matchemphys.2018.04.007. https://www.sciencedirect.com/science/article/pii/S0254058418302694.

Naresh, V., and N. Lee. 2021. "A Review on Biosensors and Recent Development of Nanostructured Materials-Enabled Biosensors." *Sensors* 21 (4). https://doi.org/10.3390/s21041109. <Go to ISI>://WOS:000624705200001.

Nasrollahzadeh, Mahmoud, Monireh Atarod, Mohaddeseh Sajjadi, S. Mohammad Sajadi, and Zahra Issaabadi. 2019. "Chapter 6 - Plant-Mediated Green Synthesis of Nanostructures: Mechanisms, Characterization, and Applications." In *Interface Science and Technology*, edited by Mahmoud Nasrollahzadeh, S. Mohammad Sajadi, Mohaddeseh Sajjadi, Zahra Issaabadi and Monireh Atarod, 199-322. Elsevier.

Nasrollahzadeh, Mahmoud, S. Mohammad Sajadi, Zahra Issaabadi, and Mohaddeseh Sajjadi. 2019. "Chapter 3 - Biological Sources Used in Green Nanotechnology." In *Interface Science and Technology*, edited by Mahmoud Nasrollahzadeh, S. Mohammad Sajadi, Mohaddeseh Sajjadi, Zahra Issaabadi and Monireh Atarod, 81-111. Elsevier.

Noh, S., J. Kim, G. Kim, C. Park, H. Jang, M. Lee, and T. Lee. 2021. "Recent Advances in CRP Biosensor Based on Electrical, Electrochemical and Optical Methods." *Sensors* 21 (9). https://doi.org/10.3390/s21093024. <Go to ISI>://WOS:000650794000001.

Norizan, M. N., M. H. Moklis, S. Z. Ngah Demon, N. A. Halim, A. Samsuri, I. S. Mohamad, V. F. Knight, and N. Abdullah. 2020. "Carbon nanotubes: functionalisation and their application in chemical sensors." *RSC Adv* 10 (71): 43704-43732. https://doi.org/10.1039/d0ra09438b. https://www.ncbi.nlm.nih.gov/pubmed/35519676.

Novoselov, K. S. 2011. "Graphene: materials in the Flatland (Nobel lecture)." *Angew Chem Int Ed Engl* 50 (31): 6986-7002. https://doi.org/10.1002/anie.201101502. https://www.ncbi.nlm.nih.gov/pubmed/21732505.

Nugen, S. R., P. J. Asiello, J. T. Connelly, and A. J. Baeumner. 2009. "PMMA biosensor for nucleic acids with integrated mixer and electrochemical detection." *Biosens Bioelectron* 24 (8): 2428-33. https://doi.org/10.1016/j.bios.2008.12.025. https://www.ncbi.nlm.nih.gov/pubmed/19168346.

Odularu, Ayodele Temidayo. 2018. "Metal Nanoparticles: Thermal Decomposition, Biomedicinal Applications to Cancer Treatment, and Future Perspectives." *Bioinorganic Chemistry and Applications* 2018: 9354708. https://doi.org/10.1155/2018/9354708. https://doi.org/10.1155/2018/9354708.

Ohta, T., A. Bostwick, T. Seyller, K. Horn, and E. Rotenberg. 2006. "Controlling the electronic structure of bilayer graphene." *Science* 313 (5789): 951-4. https://doi.org/10.1126/science.1130681. https://www.ncbi.nlm.nih.gov/pubmed/16917057.

Ojha, Nisha Kant, Grigory V. Zyryanov, Adinath Majee, Valery N. Charushin, Oleg N. Chupakhin, and Sougata Santra. 2017. "Copper nanoparticles as inexpensive and efficient catalyst: A valuable contribution in organic synthesis." *Coordination Chemistry Reviews* 353: 1-57. https://doi.org/https://doi.org/10.1016/j.ccr.2017.10.004. https://www.sciencedirect.com/science/article/pii/S0010854517303296.

Ou, Gaozhi, Anshun Zhao, Hui Liao, Zhaowei Zhang, and Fei Xiao. 2023. "Au nanopartics decorated urchin-like Bi.sub.2S.sub.3 on graphene wrapped carbon fiber microelectrode: Towards electrochemical immunosensor for sensitive determination of aflatoxin B1." *Journal of electroanalytical chemistry (Lausanne, Switzerland)* 929. https://doi.org/10.1016/j.jelechem.2022.117124.

Pallares, N., A. Sebastia, V. Martinez-Lucas, M. Gonzalez-Angulo, F. J. Barba, H. Berrada, and E. Ferrer. 2021. "High Pressure Processing Impact on Alternariol and Aflatoxins of Grape

Juice and Fruit Juice-Milk Based Beverages." *Molecules* 26 (12). https://doi.org/10.3390/molecules26123769. <Go to ISI>://WOS:000666715300001.

Pandey, Anshu, and Philippe Guyot-Sionnest. 2007. "Intraband spectroscopy and band offsets of colloidal II-VI core/shell structures." *The Journal of Chemical Physics* 127 (10): 104710. https://doi.org/10.1063/1.2766957. https://doi.org/10.1063/1.2766957.

Pandey, S., M. Karakoti, D. Bhardwaj, G. Tatrari, R. Sharma, L. Pandey, M. J. Lee, and N. G. Sahoo. 2023. "Recent advances in carbon-based materials for high-performance perovskite solar cells: gaps, challenges and fulfillment." *Nanoscale Adv* 5 (6): 1492-1526. https://doi.org/10.1039/d3na00005b. https://www.ncbi.nlm.nih.gov/pubmed/36926580.

Paniel, N., A. Radoi, and J. L. Marty. 2010. "Development of an electrochemical biosensor for the detection of aflatoxin M1 in milk." *Sensors (Basel)* 10 (10): 9439-48. https://doi.org/10.3390/s101009439. https://www.ncbi.nlm.nih.gov/pubmed/22163418.

Panini, Nancy V., Eloy Salinas, Germán A. Messina, and Julio Raba. 2011. "Modified paramagnetic beads in a microfluidic system for the determination of zearalenone in feedstuffs samples." *Food chemistry* 125 (2): 791-796. https://doi.org/10.1016/j.foodchem.2010.09.035.

Parashar, Mritunjaya, Vivek Kumar Shukla, and Ranbir Singh. 2020. "Metal oxides nanoparticles via sol–gel method: a review on synthesis, characterization and applications." *Journal of Materials Science: Materials in Electronics* 31 (5): 3729-3749. https://doi.org/10.1007/s10854-020-02994-8. https://doi.org/10.1007/s10854-020-02994-8.

Park, S., and R. S. Ruoff. 2009. "Chemical methods for the production of graphenes." *Nat Nanotechnol* 4 (4): 217-24. https://doi.org/10.1038/nnano.2009.58. https://www.ncbi.nlm.nih.gov/pubmed/19350030.

Park, Young-Shin, Jeongkyun Roh, Benjamin T. Diroll, Richard D. Schaller, and Victor I. Klimov. 2021. "Colloidal quantum dot lasers." *Nature Reviews Materials* 6 (5): 382-401. https://doi.org/10.1038/s41578-020-00274-9. https://doi.org/10.1038/s41578-020-00274-9.

Pastucha, Matěj, Zdeněk Farka, Karel Lacina, Zuzana Mikušová, and Petr Skládal. 2019. "Magnetic nanoparticles for smart electrochemical immunoassays: a review on recent developments." *Mikrochimica acta (1966)* 186 (5): 312-312. https://doi.org/10.1007/s00604-019-3410-0.

Paukov, M., C. Kramberger, I. Begichev, M. Kharlamova, and M. Burdanova. 2023. "Functionalized Fullerenes and Their Applications in Electrochemistry, Solar Cells, and Nanoelectronics." *Materials (Basel)* 16 (3). https://doi.org/10.3390/ma16031276. https://www.ncbi.nlm.nih.gov/pubmed/36770286.

Pereira, Clara, André M. Pereira, Carlos Fernandes, Mariana Rocha, Ricardo Mendes, María Paz Fernández-García, Alexandra Guedes, Pedro B. Tavares, Jean-Marc Grenèche, João P. Araújo, and Cristina Freire. 2012. "Superparamagnetic MFe2O4 (M = Fe, Co, Mn) Nanoparticles: Tuning the Particle Size and Magnetic Properties through a Novel One-Step Coprecipitation Route." *Chemistry of materials* 24 (8): 1496-1504. https://doi.org/10.1021/cm300301c.

Perrotta, Patricio René, Fernando Javier Arévalo, Nelio Roberto Vettorazzi, María Alicia Zón, and Héctor Fernández. 2012. "Development of a very sensitive electrochemical magneto immunosensor for the direct determination of ochratoxin A in red wine." *Sensors and actuators. B, Chemical* 162 (1): 327-333. https://doi.org/10.1016/j.snb.2011.12.089.

Phopin, K., and T. Tantimongcolwat. 2020. "Pesticide Aptasensors-State of the Art and Perspectives." *Sensors* 20 (23). https://doi.org/10.3390/s20236809. <Go to ISI>://WOS:000597507700001.

Picheau, E., F. Hof, S. Amar, A. Derré, and A. Pénicaud. 2023. "Burning Graphite Faster than Carbon Black: A Case of Diffusion Control." *Angew Chem Int Ed Engl* 62 (20): e202303060. https://doi.org/10.1002/anie.202303060. https://www.ncbi.nlm.nih.gov/pubmed/37021794.

Pohanka, M., D. Jun, and K. Kuca. 2007. "Mycotoxin assays using biosensor technology: A review." *Drug and Chemical Toxicology* 30 (3): 253-261. https://doi.org/10.1080/01480540701375232. <Go to ISI>://WOS:000247602500008.

Police Patil, A. V., Y. S. Chuang, C. Li, and C. C. Wu. 2023. "Recent Advances in Electrochemical Immunosensors with Nanomaterial Assistance for Signal Amplification." *Biosensors (Basel)* 13 (1). https://doi.org/10.3390/bios13010125. https://www.ncbi.nlm.nih.gov/pubmed/36671960.

Ponnamma, D., Q. Guo, I. Krupa, M. A. Al-Maadeed, V. K T, S. Thomas, and K. K. Sadasivuni. 2015. "Graphene and graphitic derivative filled polymer composites as potential sensors." *Phys Chem Chem Phys* 17 (6): 3954-81. https://doi.org/10.1039/c4cp04418e. https://www.ncbi.nlm.nih.gov/pubmed/25585199.

Proença, Camila A., Thaísa A. Baldo, Tayane A. Freitas, Elsa M. Materón, Ademar Wong, Andrés A. Durán, Matias E. Melendez, Gustavo Zambrano, and Ronaldo C. Faria. 2019. "Novel enzyme-free immunomagnetic microfluidic device based on Co0.25Zn0.75Fe2O4 for cancer biomarker detection." *Analytica chimica acta* 1071: 59-69. https://doi.org/10.1016/j.aca.2019.04.047.

Puzyr', A.P., Purtov, K.V., Shenderova, O.A. et al. The adsorption of aflatoxin B1 by detonation-synthesis nanodiamonds. Dokl Biochem Biophys 417, 299–301 (2007). https://doi.org/10.1134/S1607672907060026

Pyrpassopoulos, S., D. Niarchos, G. Nounesis, N. Boukos, I. Zafiropoulou, and V. Tzitzios. 2007. "Synthesis and self-organization of Au nanoparticles." *Nanotechnology* 18 (48): 485604. https://doi.org/10.1088/0957-4484/18/48/485604. https://dx.doi.org/10.1088/0957-4484/18/48/485604.

Rajavel, K., C. R. Minitha, K. S. Ranjith, and R. T. Rajendra Kumar. 2012. "Recent progress on the synthesis and applications of carbon based nanostructures." *Recent Pat Nanotechnol* 6 (2): 99-104. https://doi.org/10.2174/187221012800270199. https://www.ncbi.nlm.nih.gov/pubmed/22292609.

Ramalingam, Saipriya, Abdallah Elsayed, and Ashutosh Singh. 2023. "An Aflatoxin-M1 biochip using graphene quantum dot-gold hybrid nanoparticles." *Food chemistry* 403: 134302-134302. https://doi.org/10.1016/j.foodchem.2022.134302.

Ramanathan, T., A. A. Abdala, S. Stankovich, D. A. Dikin, M. Herrera-Alonso, R. D. Piner, D. H. Adamson, H. C. Schniepp, X. Chen, R. S. Ruoff, S. T. Nguyen, I. A. Aksay, R. K. Prud'Homme, and L. C. Brinson. 2008. "Functionalized graphene sheets for polymer nanocomposites." *Nat Nanotechnol* 3 (6): 327-31. https://doi.org/10.1038/nnano.2008.96. https://www.ncbi.nlm.nih.gov/pubmed/18654541.

Rangel de Melo Rodrigues, Makson, Rayse Machado Ferreira, Fellipe dos Santos Pereira, Felipe Anchieta e Silva, Augusto César Azevedo Silva, Hector Aguilar Vitorino, Jaldyr de Jesus Gomes Varela Júnior, Auro Atsushi Tanaka, Marco Aurélio Suller Garcia, and Thenner Silva Rodrigues. 2022. "Application of AgPt Nanoshells in Direct Methanol Fuel Cells: Experimental and Theoretical Insights of Design Electrocatalysts over Methanol Crossover Effect." *ChemCatChem* 14 (23): e202200605. https://doi.org/https://doi.org/10.1002/cctc.202200605. https://doi.org/10.1002/cctc.202200605.

Reina, A., X. Jia, J. Ho, D. Nezich, H. Son, V. Bulovic, M. S. Dresselhaus, and J. Kong. 2009. "Large area, few-layer graphene films on arbitrary substrates by chemical vapor deposition." *Nano Lett* 9 (1): 30-5. https://doi.org/10.1021/nl801827v. https://www.ncbi.nlm.nih.gov/pubmed/19046078.

Reiss, Peter, Myriam Protière, and Liang Li. 2009. "Core/Shell Semiconductor Nanocrystals." *Small* 5 (2): 154-168. https://doi.org/https://doi.org/10.1002/smll.200800841. https://doi.org/10.1002/smll.200800841.

Ribeiro, José A., Cátia A. Carreira, Hye Jin Lee, Fernando Silva, Ana Martins, and Carlos M. Pereira. 2010. "Voltammetric determination of paraquat at DNA–gold nanoparticle composite electrodes." *Electrochimica Acta* 55 (27): 7892-7896. https://doi.org/https://doi.org/10.1016/j.electacta.2010.03.058. https://www.sciencedirect.com/science/article/pii/S0013468610004603.

Rogach, Andrey L., Thomas A. Klar, John M. Lupton, Andries Meijerink, and Jochen Feldmann. 2009. "Energy transfer with semiconductor nanocrystals." *Journal of Materials Chemistry* 19 (9): 1208-1221. https://doi.org/10.1039/B812884G. http://dx.doi.org/10.1039/B812884G.

Rosado, Taíssa F., Isael P. Costa, Juliana Nadier, Roberto R. de Avillez, Yutao Xing, Guilhermo Solórzano, Augusto C. A. Silva, André H. B. Dourado, Clenilton C. dos Santos, Vinícius W. Faria, Marco A. Fraga, Jaldyr Júnior, Auro A. Tanaka, Marco A. S. Garcia, and Anderson G. M. da Silva. 2023. "Beyond surface: Correlating CuI /CuII and O-vacancy surface sites in CuxO nanocubes with their activities as noble metal-free anodes for fuel cells." *Surfaces and Interfaces* 40: 102889. https://doi.org/https://doi.org/10.1016/j.surfin.2023.102889. https://www.sciencedirect.com/science/article/pii/S2468023023002596.

Roy, Nidhija, Archana Gaur, Aditi Jain, Susinjan Bhattacharya, and Vibha Rani. 2013. "Green synthesis of silver nanoparticles: An approach to overcome toxicity." *Environmental Toxicology and Pharmacology* 36 (3): 807-812. https://doi.org/https://doi.org/10.1016/j.etap.2013.07.005. https://www.sciencedirect.com/science/article/pii/S138266891300152X.

Ruhunage, C., V. Dhawan, C. P. Nawarathne, A. Hoque, X. T. Cui, and N. T. Alvarez. 2023. "Evaluation of Polymer-Coated Carbon Nanotube Flexible Microelectrodes for Biomedical Applications." *Bioengineering (Basel)* 10 (6). https://doi.org/10.3390/bioengineering10060647. https://www.ncbi.nlm.nih.gov/pubmed/37370578.

Sarter, S., and N. Zakhia. 2004. "Chemiluminescent and bioluminescent assays as innovative prospects for mycotoxin determination in food and feed." *Luminescence* 19 (6): 345-51. https://doi.org/10.1002/bio.791. https://www.ncbi.nlm.nih.gov/pubmed/15558672.

Schladt, T. D., K. Schneider, H. Schild, and W. Tremel. 2011. "Synthesis and bio-functionalization of magnetic nanoparticles for medical diagnosis and treatment." *Dalton Trans* 40 (24): 6315-43. https://doi.org/10.1039/c0dt00689k. https://www.ncbi.nlm.nih.gov/pubmed/21359397.

Senellart, Pascale, Glenn Solomon, and Andrew White. 2017. "High-performance semiconductor quantum-dot single-photon sources." *Nature Nanotechnology* 12 (11): 1026-1039. https://doi.org/10.1038/nnano.2017.218. https://doi.org/10.1038/nnano.2017.218.

Senthilnathan, J., Y. F. Liu, K. S. Rao, and M. Yoshimura. 2014. "Submerged liquid plasma for the synchronized reduction and functionalization of graphene oxide." *Sci Rep* 4: 4395. https://doi.org/10.1038/srep04395. https://www.ncbi.nlm.nih.gov/pubmed/24637779.

Shen, H., L. Zhang, M. Liu, and Z. Zhang. 2012. "Biomedical applications of graphene." *Theranostics* 2 (3): 283-94. https://doi.org/10.7150/thno.3642. https://www.ncbi.nlm.nih.gov/pubmed/22448195.

Shirasaki, Yasuhiro, Geoffrey J. Supran, Moungi G. Bawendi, and Vladimir Bulović. 2013. "Emergence of colloidal quantum-dot light-emitting technologies." *Nature Photonics* 7 (1): 13-23. https://doi.org/10.1038/nphoton.2012.328. https://doi.org/10.1038/nphoton.2012.328.

Shrestha, L. K., R. G. Shrestha, J. P. Hill, and K. Ariga. 2013. "Self-assembled fullerene nanostructures." *J Oleo Sci* 62 (8): 541-53. https://doi.org/10.5650/jos.62.541. https://www.ncbi.nlm.nih.gov/pubmed/23985483.

Siddiqi, K. S., A. Ur Rahman, Tajuddin, and A. Auid-Orcid Husen. "Biogenic Fabrication of Iron/Iron Oxide Nanoparticles and Their Application." (1931-7573 (Print)).

Singh, Chandan, Saurabh Srivastava, Md Azahar Ali, Tejendra K. Gupta, Gajjala Sumana, Anchal Srivastava, R. B. Mathur, and Bansi D. Malhotra. 2013. "Carboxylated multiwalled carbon nanotubes based biosensor for aflatoxin detection." *Sensors and actuators. B, Chemical* 185: 258-264. https://doi.org/10.1016/j.snb.2013.04.040.

Singh, J., and A. Mehta. 2020. "Rapid and sensitive detection of mycotoxins by advanced and emerging analytical methods: A review." *Food Sci Nutr* 8 (5): 2183-2204. https://doi.org/10.1002/fsn3.1474. https://www.ncbi.nlm.nih.gov/pubmed/32405376.

Song, Hai-Zhi. 2020. "The Development of Quantum Emitters Based on Semiconductor Quantum Dots." In *Quantum Dot Optoelectronic Devices*, edited by Peng Yu and Zhiming M. Wang, 83-106. Cham: Springer International Publishing.

Song, J., W. Han, S. Dong, C. Fang, Y. Cheng, D. Liu, and X. Zhang. 2020. "Constructing hydrothermal carbonization coatings on carbon fibers with controllable thickness for achieving

tunable sorption of dyes and oils via a simple heat-treated route." *J Colloid Interface Sci* 559: 263-272. https://doi.org/10.1016/j.jcis.2019.10.047. https://www.ncbi.nlm.nih.gov/pubmed/31634670.

Speranza, G. 2021. "Carbon Nanomaterials: Synthesis, Functionalization and Sensing Applications." *Nanomaterials (Basel)* 11 (4). https://doi.org/10.3390/nano11040967. https://www.ncbi.nlm.nih.gov/pubmed/33918769.

Srivastava, Saurabh, Vinod Kumar, Kamal Arora, Chandan Singh, Md Azahar Ali, Nitin K. Puri, and Bansi D. Malhotra. 2016. "Antibody conjugated metal nanoparticle decorated graphene sheets for a mycotoxin sensor." *RSC Advances* 6 (61): 56518-56526. https://doi.org/10.1039/C6RA04469G. http://dx.doi.org/10.1039/C6RA04469G.

Stankovich, S., D. A. Dikin, G. H. Dommett, K. M. Kohlhaas, E. J. Zimney, E. A. Stach, R. D. Piner, S. T. Nguyen, and R. S. Ruoff. 2006. "Graphene-based composite materials." *Nature* 442 (7100): 282-6. https://doi.org/10.1038/nature04969. https://www.ncbi.nlm.nih.gov/pubmed/16855586.

Stevenson, C. D., C. V. Rice, P. M. Garland, and B. K. Clark. 1997. "Thermal and Laser Pyrolysis of Hydrocarbon Anion Radicals." *J Org Chem* 62 (7): 2193-2197. https://doi.org/10.1021/jo961487q. https://www.ncbi.nlm.nih.gov/pubmed/11671528.

Su, L., Y. Song, C. Fu, and D. Tang. 2019. "Etching reaction-based photoelectrochemical immunoassay of aflatoxin B(1) in foodstuff using cobalt oxyhydroxide nanosheets-coating cadmium sulfide nanoparticles as the signal tags." *Anal Chim Acta* 1052: 49-56. https://doi.org/10.1016/j.aca.2018.11.059. https://www.ncbi.nlm.nih.gov/pubmed/30685041.

Su, L., P. Tong, L. Zhang, Z. Luo, C. Fu, D. Tang, and Y. Zhang. 2019. "Photoelectrochemical immunoassay of aflatoxin B(1) in foodstuff based on amorphous TiO(2) and CsPbBr(3) perovskite nanocrystals." *Analyst* 144 (16): 4880-4886. https://doi.org/10.1039/c9an00994a. https://www.ncbi.nlm.nih.gov/pubmed/31298669.

Sugawara, M., H. Ebe, N. Hatori, M. Ishida, Y. Arakawa, T. Akiyama, K. Otsubo, and Y. Nakata. 2004. "Theory of optical signal amplification and processing by quantum-dot

semiconductor optical amplifiers." *Physical Review B* 69 (23): 235332. https://doi.org/10.1103/PhysRevB.69.235332. https://link.aps.org/doi/10.1103/PhysRevB.69.235332.

Sun, Y., B. Mayers, and Y. Xia. 2003. "Metal Nanostructures with Hollow Interiors." *Advanced Materials* 15 (7-8): 641-646. https://doi.org/https://doi.org/10.1002/adma.200301639. https://doi.org/10.1002/adma.200301639.

Sutter, P. W., J. I. Flege, and E. A. Sutter. 2008. "Epitaxial graphene on ruthenium." *Nat Mater* 7 (5): 406-11. https://doi.org/10.1038/nmat2166. https://www.ncbi.nlm.nih.gov/pubmed/18391956.

Swetha, P. D. Priya, A. Nikitha, M. Manjunath Shenoy, Yoon-Bo Shim, and K. Sudhakara Prasad. 2023. "Ni/Ni(OH) 2 -rGO nanocomposites sensor for the detection of long forgotten mycotoxin, xanthomegnin." *Talanta (Oxford)* 253: 123953. https://doi.org/10.1016/j.talanta.2022.123953.

Tajik, Somayeh, Hadi Beitollahi, Fariba Garkani Nejad, Zahra Dourandish, Mohammad A. Khalilzadeh, Ho Won Jang, Richard A. Venditti, Rajender S. Varma, and Mohammadreza Shokouhimehr. 2021. "Recent Developments in Polymer Nanocomposite-Based Electrochemical Sensors for Detecting Environmental Pollutants." *Industrial & Engineering Chemistry Research* 60 (3): 1112-1136. https://doi.org/10.1021/acs.iecr.0c04952. https://doi.org/10.1021/acs.iecr.0c04952.

Tang, J., P. Xiong, Y. Cheng, Y. Chen, S. Peng, and Z. Q. Zhu. 2019. "Enzymatic oxydate-triggered AgNPs etching: A novel signal-on photoelectrochemical immunosensing platform based on Ag@AgCl nanocubes loaded RGO plasmonic heterostructure." *Biosens Bioelectron* 130: 125-131. https://doi.org/10.1016/j.bios.2019.01.014. https://www.ncbi.nlm.nih.gov/pubmed/30735945.

Teja, Amyn S., and Pei-Yoong Koh. 2009. "Synthesis, properties, and applications of magnetic iron oxide nanoparticles." *Progress in Crystal Growth and Characterization of Materials* 55

(1): 22-45. https://doi.org/https://doi.org/10.1016/j.pcrysgrow.2008.08.003. https://www.sciencedirect.com/science/article/pii/S0960897408000168.

Thakkar, Kaushik N., Snehit S. Mhatre, and Rasesh Y. Parikh. 2010. "Biological synthesis of metallic nanoparticles." *Nanomedicine: Nanotechnology, Biology and Medicine* 6 (2): 257-262. https://doi.org/https://doi.org/10.1016/j.nano.2009.07.002. https://www.sciencedirect.com/science/article/pii/S1549963409001154.

Thambidurai, M., N. Muthukumarasamy, S. Agilan, N. Murugan, S. Vasantha, R. Balasundaraprabhu, and T. S. Senthil. 2010. "Strong quantum confinement effect in nanocrystalline CdS." *Journal of Materials Science* 45 (12): 3254-3258. https://doi.org/10.1007/s10853-010-4333-7. https://doi.org/10.1007/s10853-010-4333-7.

Thanh, Nguyen T. K., N. Maclean, and S. Mahiddine. 2014. "Mechanisms of Nucleation and Growth of Nanoparticles in Solution." *Chemical Reviews* 114 (15): 7610-7630. https://doi.org/10.1021/cr400544s. https://doi.org/10.1021/cr400544s.

Thong, N. M., T. C. Ngo, D. Q. Dao, T. Duong, Q. T. Tran, and P. C. Nam. 2016. "Functionalization of fullerene via the Bingel reaction with α-chlorocarbanions: an ONIOM approach." *J Mol Model* 22 (5): 113. https://doi.org/10.1007/s00894-016-2981-5. https://www.ncbi.nlm.nih.gov/pubmed/27114364.

Tothill, I. E. 2011. "Biosensors and nanomaterials and their application for mycotoxin determination." *World Mycotoxin Journal* 4 (4): 361-374. https://doi.org/10.3920/wmj2011.1318. <Go to ISI>://WOS:000297061900002.

Toyos-Rodríguez, C., A. Llamedo-González, D. Pando, S. García, J. A. García, F. J. García-Alonso, and A. de la Escosura-Muñiz. 2022. "Novel magnetic beads with improved performance for Alzheimer's disease biomarker detection." *Microchemical journal* 175: 107211. https://doi.org/10.1016/j.microc.2022.107211.

Tran, T. Q., R. J. Headrick, E. A. Bengio, S. Myo Myint, H. Khoshnevis, V. Jamali, H. M. Duong, and M. Pasquali. 2017. "Purification and Dissolution of Carbon Nanotube Fibers Spun

from the Floating Catalyst Method." *ACS Appl Mater Interfaces* 9 (42): 37112-37119. https://doi.org/10.1021/acsami.7b09287. https://www.ncbi.nlm.nih.gov/pubmed/28959881.

Umer, Asim, Shahid Naveed, Naveed Ramzan, and Muhammad Shahid Rafique. 2012. "SELECTION OF A SUITABLE METHOD FOR THE SYNTHESIS OF COPPER NANOPARTICLES." *Nano* 07 (05): 1230005. https://doi.org/10.1142/S1793292012300058. https://doi.org/10.1142/S1793292012300058.

Urusov, Alexandr E., Alina V. Petrakova, Maxim V. Vozniak, Anatoly V. Zherdev, and Boris B. Dzantiev. 2014. "Rapid Immunoenzyme Assay of Aflatoxin B1 Using Magnetic Nanoparticles." *Sensors (Basel, Switzerland)* 14 (11): 21843-21857. https://doi.org/10.3390/s141121843.

Valera, Enrique, Raül García-Febrero, Christopher T. Elliott, Francisco Sánchez-Baeza, and M. P. Marco. 2019. "Electrochemical nanoprobe-based immunosensor for deoxynivalenol mycotoxin residues analysis in wheat samples." *Analytical and bioanalytical chemistry* 411 (9): 1915-1926. https://doi.org/10.1007/s00216-018-1538-0.

Varanda, Laudemir C., Caio G. S. Souza, Daniel A. Moraes, Herbert R. Neves, JoÃO B. Souza Junior, Monica F. Silva, Rafael A. Bini, Rebecca F. Albers, Tiago L. Silva, and Watson Beck Junior. 2019. "Size and shape-controlled nanomaterials based on modified polyol and thermal decomposition approaches. A brief review." *Anais da Academia Brasileira de Ciências* 91 (4). https://doi.org/10.1590/0001-3765201920181180.

Vernardou, D., C. Drosos, A. Kafizas, M. E. Pemble, and E. Koudoumas. 2020. "Towards High Performance Chemical Vapour Deposition V." *Molecules* 25 (23). https://doi.org/10.3390/molecules25235558. https://www.ncbi.nlm.nih.gov/pubmed/33256209.

Vidal, J. C., L. Bonel, A. Ezquerra, P. Duato, and J. R. Castillo. 2012. "An electrochemical immunosensor for ochratoxin A determination in wines based on a monoclonal antibody and paramagnetic microbeads." *Anal Bioanal Chem* 403 (6): 1585-93.

https://doi.org/10.1007/s00216-012-5951-5.
https://www.ncbi.nlm.nih.gov/pubmed/22466259.

Wagner, Angela M., Jennifer M. Knipe, Gorka Orive, and Nicholas A. Peppas. 2019. "Quantum dots in biomedical applications." *Acta Biomaterialia* 94: 44-63. https://doi.org/https://doi.org/10.1016/j.actbio.2019.05.022. https://www.sciencedirect.com/science/article/pii/S1742706119303393.

Wang, H., Y. H. Zhang, Y. G. Chu, H. M. Ma, Y. Li, D. Wu, B. Du, and Q. Wei. 2016a. "Disposable competitive-type immunoassay for determination of aflatoxin B1 via detection of copper ions released from Cu-apatite." *Talanta* 147: 556-560. https://doi.org/10.1016/j.talanta.2015.10.040. <Go to ISI>://WOS:000366078200078.

Wang, Huan, Yihe Zhang, Yanguang Chu, Hongmin Ma, Yan Li, Dan Wu, Bin Du, and Qin Wei. 2016b. "Disposable competitive-type immunoassay for determination of aflatoxin B1 via detection of copper ions released from Cu-apatite." *Talanta* 147: 556-560. https://doi.org/https://doi.org/10.1016/j.talanta.2015.10.040. https://www.sciencedirect.com/science/article/pii/S0039914015304070.

Wang, J., R. Liang, and W. Qin. 2020. "Thin polymeric membrane ion-selective electrodes for trace-level potentiometric detection." *Anal Chim Acta* 1139: 1-7. https://doi.org/10.1016/j.aca.2020.09.024. https://www.ncbi.nlm.nih.gov/pubmed/33190691.

Wang, Ru, Kang-Qiang Lu, Zi-Rong Tang, and Yi-Jun Xu. 2017. "Recent progress in carbon quantum dots: synthesis, properties and applications in photocatalysis." *Journal of Materials Chemistry A* 5 (8): 3717-3734. https://doi.org/10.1039/C6TA08660H. http://dx.doi.org/10.1039/C6TA08660H.

Wang, Xu, Reinhard Niessner, and Dietmar Knopp. 2014. "Magnetic Bead-Based Colorimetric Immunoassay for Aflatoxin B1 Using Gold Nanoparticles." *Sensors (Basel, Switzerland)* 14 (11): 21535-21548. https://doi.org/10.3390/s141121535.

Wang, Y., Z. Li, J. Wang, J. Li, and Y. Lin. 2011. "Graphene and graphene oxide: biofunctionalization and applications in biotechnology." *Trends Biotechnol* 29 (5): 205-12.

https://doi.org/10.1016/j.tibtech.2011.01.008.
https://www.ncbi.nlm.nih.gov/pubmed/21397350.

Wang, Zhihua, Jinshu Li, Lijuan Xu, Yanjun Feng, and Xiaoquan Lu. 2014. "Electrochemical sensor for determination of aflatoxin B1 based on multiwalled carbon nanotubes-supported Au/Pt bimetallic nanoparticles." *Journal of solid state electrochemistry* 18 (9): 2487-2496. https://doi.org/10.1007/s10008-014-2506-z.

Wei, D., and J. Kivioja. 2013. "Graphene for energy solutions and its industrialization." *Nanoscale* 5 (21): 10108-26. https://doi.org/10.1039/c3nr03312k. https://www.ncbi.nlm.nih.gov/pubmed/24057074.

Wood, Vanessa, and Vladimir Bulović. 2010. "Colloidal quantum dot light-emitting devices." *Nano Reviews* 1 (1): 5202. https://doi.org/10.3402/nano.v1i0.5202. https://doi.org/10.3402/nano.v1i0.5202.

Wu, Wei, Zhaohui Wu, Taekyung Yu, Changzhong Jiang, and Woo-Sik Kim. 2015. "Recent progress on magnetic iron oxide nanoparticles: synthesis, surface functional strategies and biomedical applications." *Science and Technology of Advanced Materials* 16 (2): 023501-23543. https://doi.org/10.1088/1468-6996/16/2/023501.

Wu, Xia, Gao Qing Lu, and Lianzhou Wang. 2011. "Shell-in-shell TiO2 hollow spheres synthesized by one-pot hydrothermal method for dye-sensitized solar cell application." *Energy & Environmental Science* 4 (9): 3565-3572. https://doi.org/10.1039/C0EE00727G. http://dx.doi.org/10.1039/C0EE00727G.

Wu, Zhengzong, Deyun He, and Bo Cui. 2018. "A fluorometric assay for staphylococcal enterotoxin B by making use of platinum coated gold nanorods and of upconversion nanoparticles." *Microchimica Acta* 185 (11): 516. https://doi.org/10.1007/s00604-018-3058-1. https://doi.org/10.1007/s00604-018-3058-1.

Xiang, Q. 2011. "The Development and Application of Electrochemical Biosensor." *Information and Management Engineering, Pt V* 235: 215-220. <Go to ISI>://WOS:000310717900036.

Xiao, Y., Y. X. Pang, Y. Yan, P. Qian, H. Zhao, S. Manickam, T. Wu, and C. H. Pang. 2023. "Synthesis and Functionalization of Graphene Materials for Biomedical Applications: Recent Advances, Challenges, and Perspectives." *Adv Sci (Weinh)* 10 (9): e2205292. https://doi.org/10.1002/advs.202205292. https://www.ncbi.nlm.nih.gov/pubmed/36658693.

Xie, Yan-Jun, Ying Yang, Wei-Jun Kong, Shi-Hai Yang, and Mei-Hua Yang. 2015. "Application of Nanoparticle Probe-based Lateral Flow Immunochromatographic Assay in Mycotoxins Detection." *Chinese Journal of Analytical Chemistry* 43 (4): 618-628. https://doi.org/https://doi.org/10.1016/S1872-2040(15)60821-0. https://www.sciencedirect.com/science/article/pii/S1872204015608210.

Xing, Ke-Yu, Shan Shan, Dao-Feng Liu, and Wei-Hua Lai. 2020. "Recent advances of lateral flow immunoassay for mycotoxins detection." *TrAC, Trends in analytical chemistry (Regular ed.)* 133: 116087. https://doi.org/10.1016/j.trac.2020.116087.

Xu, Guoli, Danqun Huo, Jingzhou Hou, Chao Zhang, Yanan Zhao, Changjun Hou, Jing Bao, Xin Yao, and Mei Yang. 2021. "An electrochemical aptasensor of malathion based on ferrocene/DNA-hybridized MOF, DNA coupling-gold nanoparticles and competitive DNA strand reaction." *Microchemical Journal* 162: 105829. https://doi.org/https://doi.org/10.1016/j.microc.2020.105829. https://www.sciencedirect.com/science/article/pii/S0026265X20337711.

Xuan, Z., H. Liu, J. Ye, L. Li, W. Tian, and S. Wang. 2020. "Reliable and disposable quantum dot-based electrochemical immunosensor for aflatoxin B." *Anal Bioanal Chem* 412 (27): 7615-7625. https://doi.org/10.1007/s00216-020-02897-x. https://www.ncbi.nlm.nih.gov/pubmed/32856110.

Xuan, Zhihong, Jin Ye, Bing Zhang, Li Li, Yu Wu, and Songxue Wang. 2019. "An Automated and High-Throughput Immunoaffinity Magnetic Bead-Based Sample Clean-Up Platform for the Determination of Aflatoxins in Grains and Oils Using UPLC-FLD." *Toxins* 11 (10): 583. https://www.mdpi.com/2072-6651/11/10/583.

Yadav, P., P. K. Rai, S. Mallick, and P. Kumar. 2022. "External electric field to control the Diels-Alder reactions of endohedral fullerene." *Phys Chem Chem Phys* 24 (18): 11131-11136. https://doi.org/10.1039/d2cp01267g. https://www.ncbi.nlm.nih.gov/pubmed/35475483.

Yang, G., F. Cheng, S. Zuo, J. Zhang, Y. Xu, Y. Hu, and X. Hu. 2023. "Growing Carbon Nanotubes In Situ Surrounding Carbon Fiber Surface via Chemical Vapor Deposition to Reinforce Flexural Strength of Carbon Fiber Composites." *Polymers (Basel)* 15 (10). https://doi.org/10.3390/polym15102309. https://www.ncbi.nlm.nih.gov/pubmed/37242883.

Yang, W., S. Akhtar, K. Leifer, and H. Grennberg. 2013. "Noncovalent functionalization of graphene in suspension." *ISRN Org Chem* 2013: 656185. https://doi.org/10.1155/2013/656185. https://www.ncbi.nlm.nih.gov/pubmed/24052867.

Yao, S., X. Yuan, L. Jiang, T. Xiong, and J. Zhang. 2020. "Recent Progress on Fullerene-Based Materials: Synthesis, Properties, Modifications, and Photocatalytic Applications." *Materials (Basel)* 13 (13). https://doi.org/10.3390/ma13132924. https://www.ncbi.nlm.nih.gov/pubmed/32629789.

Yeo, Sang Young, and Sung Hoon Jeong. 2003. "Preparation and characterization of polypropylene/silver nanocomposite fibers." *Polymer International* 52 (7): 1053-1057. https://doi.org/https://doi.org/10.1002/pi.1215. https://doi.org/10.1002/pi.1215.

Yu, Yanyang, Jie Han, Jiaqi Yin, Jingcheng Huang, Jing Liu, Lingjun Geng, Xia Sun, and Wenping Zhao. 2022. "Dual-Target Electrochemical Sensor Based on 3D MoS2-rGO and Aptamer Functionalized Probes for Simultaneous Detection of Mycotoxins." *Frontiers in chemistry* 10: 932954-932954. https://doi.org/10.3389/fchem.2022.932954.

Yun, Y., V. Shanov, Y. Tu, S. Subramaniam, and M. J. Schulz. 2006. "Growth mechanism of long aligned multiwall carbon nanotube arrays by water-assisted chemical vapor deposition." *J Phys Chem B* 110 (47): 23920-5. https://doi.org/10.1021/jp057171g. https://www.ncbi.nlm.nih.gov/pubmed/17125359.

Yáñez-Sedeño, Paloma, Susana Campuzano, and José M. Pingarrón. 2016. "Magnetic Particles Coupled to Disposable Screen Printed Transducers for Electrochemical Biosensing." *Sensors* 16 (10): 1585. https://doi.org/10.3390/s16101585.

Zaman, Gaffar Sarwar, Ibrahem Waleed, Ruaa Ali Obeid, Shaymaa Abdulhameed Khudair, Saafa Abaas Abd Al-Kahdum, Kadhum Al-Majdi, Ahmed S. Abed, Ali Alsalamy, Maytham T. Qasim, and Ahmed Hussien Radie Alawadi. 2023. "Electrochemical determination of zearalenone in agricultural food samples using a flower like nanocomposite-modified electrode." *Materials chemistry and physics* 305. https://doi.org/10.1016/j.matchemphys.2023.127986.

Zamfir, Lucian-Gabriel, Irina Geana, Sondes Bourigua, Lucian Rotariu, Camelia Bala, Abdelhamid Errachid, and Nicole Jaffrezic-Renault. 2011. "Highly sensitive label-free immunosensor for ochratoxin A based on functionalized magnetic nanoparticles and EIS/SPR detection." *Sensors and actuators. B, Chemical* 159 (1): 178-184. https://doi.org/10.1016/j.snb.2011.06.069.

Zamolo, V. A., E. Vazquez, and M. Prato. 2014. "Carbon nanotubes: synthesis, structure, functionalization, and characterization." *Top Curr Chem* 350: 65-109. https://doi.org/10.1007/128_2012_403. https://www.ncbi.nlm.nih.gov/pubmed/23408276.

Zhang, Hui, Zhaoqiang Shi, Shuting Cheng, Qingqing Yang, Xia Sun, and Yemin Guo. 2019. "Ultrasensitive Immunosensor for Aflatoxin B1 Detection Based on Screen-Printed Carbon Electrode Modified by Ferrocene @Multi-Walled Carbon Nanotubes." *International journal of electrochemical science* 14 (9): 9170-9180. https://doi.org/10.20964/2019.09.61.

Zhang, J., X. Liu, R. Blume, A. Zhang, R. Schlögl, and D. S. Su. 2008. "Surface-modified carbon nanotubes catalyze oxidative dehydrogenation of n-butane." *Science* 322 (5898): 73-7. https://doi.org/10.1126/science.1161916. https://www.ncbi.nlm.nih.gov/pubmed/18832641.

Zhang, Songbai, Youming Shen, Guangyu Shen, Sha Wang, Guoli Shen, and Ruqin Yu. 2016. "Electrochemical immunosensor based on Pd–Au nanoparticles supported on functionalized PDDA-MWCNT nanocomposites for aflatoxin B1 detection." *Analytical Biochemistry* 494: 10-

15. https://doi.org/https://doi.org/10.1016/j.ab.2015.10.008. https://www.sciencedirect.com/science/article/pii/S0003269715004972.

Zhang, X., Z. Wang, H. Xie, R. Sun, T. Cao, N. Paudyal, W. Fang, and H. Song. 2018. "Development of a Magnetic Nanoparticles-Based Screen-Printed Electrodes (MNPs-SPEs) Biosensor for the Quantification of Ochratoxin A in Cereal and Feed Samples." *Toxins (Basel)* 10 (8). https://doi.org/10.3390/toxins10080317. https://www.ncbi.nlm.nih.gov/pubmed/30082606.

Zhou, Binbin, Hao Xie, Sisi Zhou, Xingxin Sheng, Liang Chen, and Ming Zhong. 2023. "Construction of AuNPs/reduced graphene nanoribbons co-modified molecularly imprinted electrochemical sensor for the detection of zearalenone." *Food chemistry* 423: 136294-136294. https://doi.org/10.1016/j.foodchem.2023.136294.

Zhou, D. B., X. Sheng, F. Han, Y. Y. Hu, L. Ding, Y. L. Lv, W. Song, and P. Zheng. 2018. "Magnetic solid-phase extraction based on [60]fullerene functionalization of magnetic nanoparticles for the determination of sixteen polycyclic aromatic hydrocarbons in tea samples." *J Chromatogr A* 1578: 53-60. https://doi.org/10.1016/j.chroma.2018.10.010. https://www.ncbi.nlm.nih.gov/pubmed/30337166.

Zhou, Qian, and Dianping Tang. 2020. "Recent advances in photoelectrochemical biosensors for analysis of mycotoxins in food." *TrAC, Trends in analytical chemistry (Regular ed.)* 124: 115814. https://doi.org/10.1016/j.trac.2020.115814.

Zhou, S. Y., L. G. Xu, H. Kuang, J. Xiao, and C. L. Xu. 2020. "Immunoassays for rapid mycotoxin detection: state of the art." *Analyst* 145 (22): 7088-7102. https://doi.org/10.1039/d0an01408g. <Go to ISI>://WOS:000587582800001.

Zhu, Shoujun, Yubin Song, Joy Wang, Hao Wan, Yuan Zhang, Yang Ning, and Bai Yang. 2017. "Photoluminescence mechanism in graphene quantum dots: Quantum confinement effect and surface/edge state." *Nano Today* 13: 10-14. https://doi.org/https://doi.org/10.1016/j.nantod.2016.12.006. https://www.sciencedirect.com/science/article/pii/S1748013216302614.

Zhuang, Shiqiang, Eon Soo Lee, Lin Lei, Bharath Babu Nunna, Liyuan Kuang, and Wen Zhang. 2016. "Synthesis of nitrogen-doped graphene catalyst by high-energy wet ball milling for electrochemical systems." *International Journal of Energy Research* 40 (15): 2136-2149. https://doi.org/https://doi.org/10.1002/er.3595. https://doi.org/10.1002/er.3595.

Zijlstra, Peter, Michel Orrit, and A. Femius Koenderink. 2014. "Metal Nanoparticles for Microscopy and Spectroscopy." In *Nanoparticles: Workhorses of Nanoscience*, edited by Celso de Mello Donegá, 53-98. Berlin, Heidelberg: Springer Berlin Heidelberg.

Zinoubi, Khaoula, Amani Chrouda, Raya Soltane, Youssef O. Al-Ghamdi, Sami Garallah Almalki, Gamal Osman, Houcine Barhoumi, and Nicole Jaffrezic Renault. 2021. "Highly Sensitive Impedimetric Biosensor Based on Thermolysin Immobilized on a GCE Modified with AuNP-decorated Graphene for the Detection of Ochratoxin A." *Electroanalysis* 33 (1): 136-145. https://doi.org/https://doi.org/10.1002/elan.202060247. https://doi.org/10.1002/elan.202060247.

Zoppas, F. M., T. F. Beltrame, F. A. Sosa, A. M. Bernardes, E. Miró, and F. A. Marchesini. 2020. "Superficial properties of activated carbon fiber catalysts produced by green synthesis and their application in water purification." *Environ Sci Pollut Res Int* 27 (32): 40405-40420. https://doi.org/10.1007/s11356-020-10012-x. https://www.ncbi.nlm.nih.gov/pubmed/32666447.

Zuo, H., J. Duan, B. Lyu, W. Lyu, Y. Li, X. Mei, and Y. Liao. 2023. "Carbon Nanotube Template-Assisted Synthesis of Conjugated Microporous Polytriphenylamine with High Porosity for Efficient Supercapacitive Energy Storage." *Macromol Rapid Commun*: e2300238. https://doi.org/10.1002/marc.202300238. https://www.ncbi.nlm.nih.gov/pubmed/37335809.

ARTIGO 3

Artigo submetido na revista Journal of Materials Chemistry A.

Flow injection analysis of hydroquinone using amperometric sensor modified with nanomaterials

Roberta Castro Martins, Mateus Aquino Gonçalves, Adelir Aparecida Saczk, Zuy Maria Magriotis, Teodorico Castro Ramalho, Lúcio Angnes, Tássia Regina de Oliveira and Fabiana S. Felix

Abstract

Carbon paste electrode (CPE) has been widely used in diverse applications, such as environmental analysis, pharmaceutical analysis, food analysis, electrocatalysis, and others. In order to improve the performance of electrochemical sensors, surface modification processes are carried out. Thus, the objective of this work was to develop an amperometric sensor modified with functionalized multi-walled carbon nanotubes (fMWCNT) and HY-type zeolite (ZEO-HY) for the analysis of hydroquinone (HQ) in pharmaceutical products. Practical and theoretical studies were carried out regarding the contribution of the modifiers used, as well as the characterization of the developed material. There was no chemical bond in the interaction between the modifiers and the analyte, and the equilibrium distances could be calculated. Furthermore, it was possible to elucidate the contribution of fMWCNT in the improvement of the peak current. Regarding the characterization processes, the results were consistent with the literature. Amperometry in association with flow injection analysis (FIA) was chosen to analyze commercial samples containing HQ. A sample rate of 100 injections per hour was achieved, and the limit of quantification (LQ) was 8.99 x 10^{-7} mol L^{-1}. The pharmaceutical samples analyzed showed results in agreement with those values found on the cream labels, as well as the High-Performance Liquid Chromatography (comparative technique).

Keywords:

Introduction

Since its introduction in electrochemical measurements, carbon paste electrode (CPE) has been widely used in diverse applications, such as environmental analysis, pharmaceutical analysis, food analysis, electrocatalysis, and others [1 – 5]. Its simplest form requires just carbon powder and a binder (unmodified carbon paste) [6]. The use of CPE has grown and become more and more common in laboratories since it can be prepared simply by hand mixing, and the

analyst himself can choose the proportions and what materials will be incorporated into the carbon paste [7].

The first modification of carbon paste is dated between 1964 and 1965 [8]. Its base continued to be the mixture of graphite powder and organic liquid, but here a modifying agent was added [7]. As a recommendation, 10 to 30% (w/w) of the modifying agent can be incorporated into the mixture, and it can be made by dissolving it in the binder or mixing it mechanically with the paste [8]. By modifying the carbon paste, the analyst can improve the sensitivity and selectivity of the electroanalytical methods [9]. Examples of modifying agents are humic substances, silica, and silica-containing matrices, substrates from living organisms, ion exchangers, and clay minerals. In the last ones, metallic nanoparticles, graphene, carbon nanotubes, and zeolites can be highlighted, respectively [8, 10-18].

Carbon nanotubes (CNTs) are carbon-based nanostructures that present exceptional electrical, thermal, and mechanical properties [19]. CNTs possess a large number of functional groups on their surface, such as carboxylic, hydroxyl, and amino groups, which can interact with ions in solution through electrostatic interactions. Therefore, it can be widely used in electrochemical systems as an ion exchanger for the detection and determination of ions in solution [8].

Zeolites (ZEO) are aluminosilicates that can be either natural or synthetic. Its structure is formed by a three-dimensional network of tetrahedral units composed of silicon, aluminum, and oxygen atoms [20]. These units form cages, channels, and pores within the crystal lattice. ZEO can also be applied as ion-exchange materials, due the presence of exchangeable cations within their structure (H^+, Na^+, K^+, Ca^{2+}, NH_4^+) [8, 21]. Therefore, its application in sensing has been growing [22 – 32].

In this work, an amperometric sensor modified with HY-type zeolite (ZEO-HY) and functionalized multi-walled carbon nanotubes (fMWCNT) was built for later application in the FIA system for determination of hydroquinone (HQ) in pharmaceutical samples. HQ (1,4-benzenediol) is an aromatic organic compound and its quantification becomes important since in some countries of the American continent its use is not allowed or is controlled in concentrations higher than 4%, because this can cause some kind of risk to consumer, as long-term carcinogenic and genotoxic effects [33 – 36]. Simultaneously, theoretical investigations at the

Density Functional Theory (DFT) level, the Quantum Theory of Atoms in Molecules (QTAIM) calculations, and Spin Density calculations were explored, aiming to elucidate the interactions and contributions of the modifiers used to assemble the modified carbon paste.

Experimental

Materials and methods

All solutions used throughout this study were prepared with purified water obtained from a Millipore Milli-Q system with resistivity ≥18.2 MΩ cm (Bedford, MA, USA). The monobasic and bibasic sodium phosphate used to prepare the buffer solution were purchased from Dinâmica Química Contemporânea Ltda® (São Paulo/Brazil). Mineral oil was purchased from Nujol® (São Paulo/ Brazil). Graphite powder was purchased from Synth (Brazil) and the HY-type zeolite (faujasite structure - FAU) used in this work was supplied by Zeochem (reference n V1148.4). Multi-walled carbon nanotubes with dimensions of 6-9 nm in diameter and 5 μm in length, with 95% purity, were obtained from Sigma-Aldrich (Missouri, USA). The HQ standard was purchased from NEON Analytical Reagents Ltda® (São Paulo/ Brazil). Potassium chloride was purchased from Sigma-Aldrich (Missouri, USA). Potassium ferri/ferrocyanide was purchased from Sigma-Aldrich (Missouri, USA). Pharmaceutical formulations of HQ cream were purchased at a local drugstore.

Instrumentation

Cyclic voltammetry. For all electrochemical experiments, a Metrohm Autolab potentiostat (Herisau, Switzerland) was used, coupled to a computer with the NOVA 2.1 software and an electrochemical cell composed of an arrangement of three electrodes, the working electrode being a Teflon rod (7 cm) and an orifice of 0.262 mm in diameter and 0.300 mm in depth, the auxiliary electrode a platinum wire and the reference electrode Ag|AgCl (KClsat). Scanning electromicrographs were obtained on a LEO EVO 40XVP scanning electron microscope and an Ultra-High Resolution STEM-FEG Field Free Analytical TESCAN/CLARA. Fourier transform infrared spectroscopy was carried out in a Bruker spectrophotometer, model Vertex 70v.

Scanning electron microscopy (SEM). Samples were prepared following the methodology proposed by Alves *et al*., 2012 [37]. The fMWCNT and the CP-ZEO-CNT carbon paste were fixed with the aid of carbon tape on the stubs and went directly to the

analysis. After fixation in the stub, the ZEO-HY was sputtered into a gold bath and subsequently taken for analysis.

Fourier transform infrared spectroscopy (FTIR). The experiments were carried out in a DLaTGS detector, and the beam splitter was KBr. The brand and model of the ATR reading unit was Bruker Praying Mantis Platinum. The resolution used was $4cm^{-1}$, 32 scans were performed and the measurement range was mid-infrared (between 4000 and 400 cm^{-1}).

Amperometry-FIA. For the experiments in amperometry-FIA, the system shown in Figure 1 was set up. The working electrode CP-ZEO-CNT was used and the auxiliary and reference electrodes were made of platinum wire and Ag|AgCl (KClsat), respectively. For the optimization of this system, a univariate study was carried out with values of working potential (0.0 – 0.3 V *vs.* Ag/AgCl), flow rate (1.72 – 4.69 mL min^{-1}), and injection volume (15 – 130 µL).

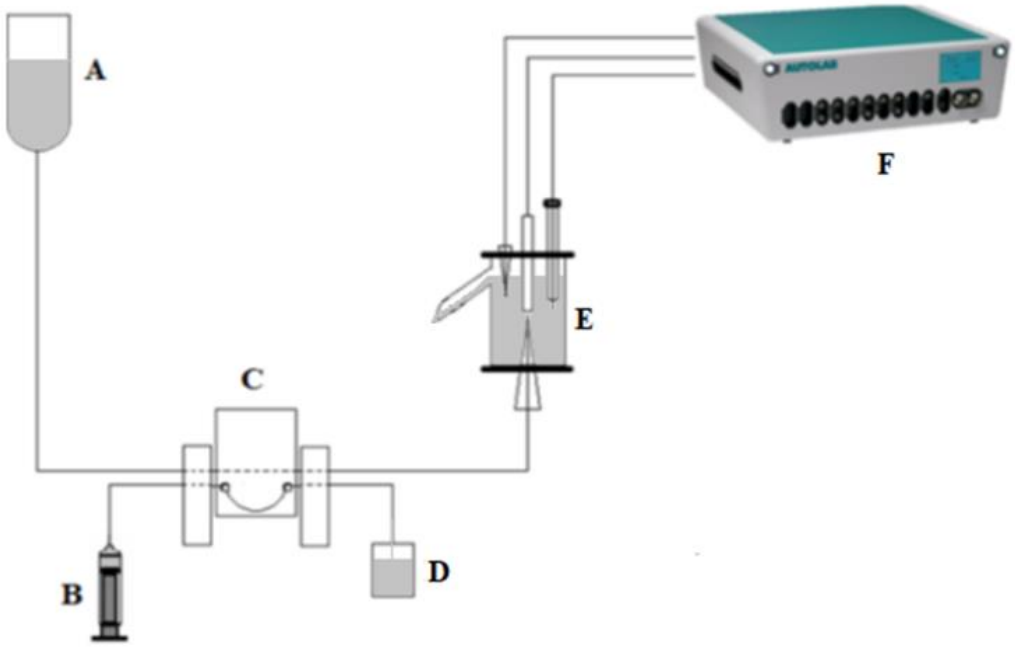

Figure 1: Representative scheme of the amperometry-FIA system. A: reservoir and electrolyte, B: syringe, C: sample loop, D: sample reservoir, E: wall-jet cell, F: potentiostat.

Comparative method. HPLC measurements were performed using a Shimadzu LC-10VP chromatograph equipped with UV/VIS detector (SPD-10AV), LC column (Lychrispher 100 A° RP18-C18, 250 x 4.6 mm, 5 µm), column oven (CTO-20A), degasser (DGU-20A5), autosampler and pump (LC-10AD-VP). The mobile phase was composed of acetonitrile and water (75:25 v/v) with pH 2.1 (adjusted with phosphoric acid before mixing with acetonitrile) and the flow rate was 1.0 mL min^{-1}. The wavelength of the UV/VIS detector was set at 293 nm. Samples were simply diluted in the mobile phase before injections [38].

Sample preparation. Pharmaceutical creams were purchased at a local pharmacy in the city of Lavras (MG-Brazil) and used as samples for HQ determination. Its concentration was determined using the electrochemical sensor in the amperometry-FIA. Sample preparation was carried out by weighing up an amount of 1.5 g of pharmaceutical cream sample, which was dissolved in 40 mL of phosphate buffer 0.1 mol L^{-1}, pH 6.5, and kept stirring until complete dissolution, the solution was then placed in an ultrasonic bath for 10 minutes. After this process, the volume was adjusted with the same buffer solution in a 50 mL volumetric flask. Then, 55 µL were transferred to a 10 mL volumetric flask.

Computational calculations. For computational methods, the zeolite structure was exported following the following parameters: Space Group: Fd-3m; network parameters: a = 24.3450 Å, b = 24.3450 Å, c = 24.3450 Å [39,40]. The carbon nanotube structure was built using the TubeGen website [41]. After the construction of the structures, both geometries were optimized in the Gaussian 09 program [42] with the B3LYP functional and the base functions 6–311g for all atoms. Then, single-point calculations were performed, approximating every 0.5 Å of the zeolite molecule to the carbon nanotube. For QTAIM calculations [43,44] were performed using AIMALL program package, calculations were performed using QTAIMQB program [45] and the analysis of these results was performed using the AIMSTUDIO program.

Results and discussion

Construction of the carbon paste electrode. For the construction of the carbon paste electrode, three carbon pastes with different compositions were prepared:

i. Graphite powder and mineral oil (CP);
ii. Graphite powder, mineral oil, and ZEO-HY (CP-ZEO);
iii. Graphite powder, mineral oil, ZEO-HY, and fMWCNT according to Felix *et al*., 2016 [46] (CP-ZEO-CNT).

The composition of the carbon paste was optimized through voltammetric measurements of an HQ concentration of 5.0 x 10^{-4} mol L^{-1}, in a potential range of -0.29 to 0.15 V, and a scan rate of 50 mV s^{-1}. Two steps were performed, the first being the development of the CP-ZEO paste and the second the CP-ZEO-CNT paste. For this, the ranges of values shown in Table 1 were studied.

Table 1: Value ranges for each component used for the carbon paste optimization step.

Component	**Range (%(m/m))**
Step 1	
Graphite powder	50 – 80
Mineral oil	20 – 30
ZEO-HY	0 – 30
Step 2	
Graphite powder	20 – 50
Mineral oil	20
ZEO-HY	30
fMWCNT	0 – 30

For the optimization step of the modified carbon paste electrode (step 1), a solution of 5.0 x 10^{-4} mol L^{-1} of HQ was used. In the case of the system studied under the conditions proposed in this work, the results obtained for the CP electrode in 80% graphite powder + 20% mineral oil were unfavorable, since it was not possible to visualize the peak current within the studied potential range.

For the CP-ZEO system (50% graphite powder + 20% mineral oil + 30% ZEO-HY), also in step 1, there was better sensor performance in smaller proportions of

mineral oil, and this result may be related to the fact that mineral oil acts as an insulator [47]. About graphite powder *vs*. ZEO-HY, the current response was improved at higher proportions of zeolite. This result can be explained due to the conductive properties of zeolite added to its large surface area [48, 49]. Thus, after analysing the results and the interactions of the variables, it was decided to proceed with the fixed proportion of ZEO-HY at 30% and mineral oil at 20% for step 2.

In the second optimization step, the contribution of fMWCNT in the current response was studied. For the CP-ZEO-CNT system, the condition with the most favorable current response was 30% graphite powder, 20% mineral oil, 30% ZEO-HY, and 20% fMWCNT. The addition of fMWCNT to the system containing ZEO-HY caused an increase in the current signal, and this effect can be explained by the properties of the nanotubes, mainly high electrical conductivity [50, 51].

Cyclic voltammograms were obtained to visualize the contribution profile of the carbon paste components during the redox process of HQ, as shown in Figure 2.

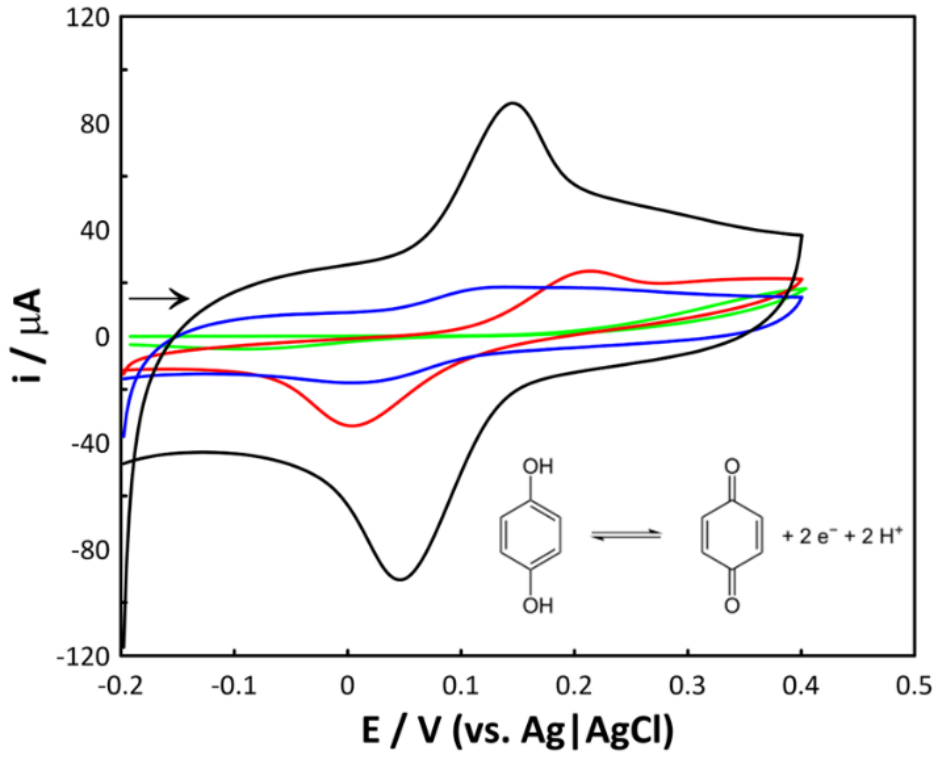

Figure 2: Cyclic voltammograms of a 1.0 x 10^{-3} mol L^{-1} HQ solution in 0.1 mol L^{-1} phosphate buffer, pH 6.5, using different working electrodes: (–) CP (80 % graphite

powder + 20% mineral oil), (–) CP-ZEO (50% graphite powder + 20% mineral oil + 30% ZEO-HY), (–) CP-CNT (50% graphite powder graphite + 20% mineral oil + 30% fMWCNT) and (–) CP-ZEO-CNT (30% graphite powder + 20% mineral oil + 30% ZEO-HY + 20% fMWCNT). v = 100 mV s^{-1}.

The oxidation current response of the CP-ZEO electrode was 1.36 times greater than the CP-CNT electrode. However, it can be seen that the peak oxidation potential value of the CP-CNT electrode (0.127 V) occurs at a lower value than that of the CP-ZEO electrode (0.205 V). Thus, when both modifiers (ZEO and fMWCNT) were used, it was possible to notice a significant improvement in the anodic current and also an improvement in the peak potential value. The current response of the CP-ZEO-CNT electrode was 4.66 and 6.35 times greater than the CP-ZEO and CP-CNT electrodes, respectively. In terms of peak potential, for the CP-ZEO-CNT electrode, there was a displacement of the oxidation peak to 0.144 V. This significant improvement in this analytical signal was also observed during the cathodic process.

The signal improvement that was observed with the modification of the carbon paste using ZEO-HY and fMWCNT can also be justified by the increase in the effective area of the voltammetric sensors produced, which was estimated using the Randles-Sevcik equation [52] and 0.1 mol L^{-1} potassium ferrocyanide stock solution in 0.1 mol L^{-1} KCl (voltammetric experiments not shown here). The effective areas of the electrodes CP, CP-ZEO, and CP-ZEO-CNT were 0.015 cm^2, 0.252 cm^2, and 0.321 cm^2, respectively. When comparing the effective areas of the CP with CP-ZEO and CP-ZEO-CNT, an increase of 16.80 and 21.40 times, respectively, were found. However, the comparison of the effective areas between both CP-ZEO and CP-ZEO-CNT electrodes showed only an increase of 1.27 times. The result obtained with the ZEO-HY modifier can be justified, as already mentioned, by the large surface area of this material [48, 49]. It was possible to see in both electrochemical and surface area response the influence of the zeolitic material addition. However, when the fMWCNT was added to the CP electrode, it showed an important improvement in the electrochemical response but not as significant as was observed in ZEO-HY.

For a better understanding of the observations obtained with cyclic voltammetry experiments involving different carbon paste electrode constructions, some theoretical studies were made. In this regard, theoretical calculations were conducted to assess the molecular interaction between zeolite, carbon nanotube, and analyte. Our theoretical findings indicate that the nature of the molecular interaction between zeolite, carbon nanotube, and analyte does not involve any chemical bonding (Figure S1). Additionally, the equilibrium distance for adsorption between zeolite and the carbon nanotube and zeolite and analyte was found to be 3.5 Å and 3.0 Å, respectively (Figure S2 and S3). To investigate and confirm these molecular interactions, QTAIM calculations were performed (Table S1, S2, and S3).

Furthermore, spin density calculations were carried out to depict the probability density of locating a particle with a specific spin orientation, namely the majority spin (α) and the minority spin (β), at a given spatial point. Consequently, the distribution of spin density in a given molecule reveals contributions from electrons with different orientations [53, 54].

In general, α spin density signifies the regions where electrons are originating from, while β spin density indicates the regions where the electrons are heading. Figure 3 illustrates these regions with blue (spin α) and green (spin β) colors, allowing observation of the spin density for zeolite (Figure 3A) and zeolite with carbon nanotube (Figure 3B).

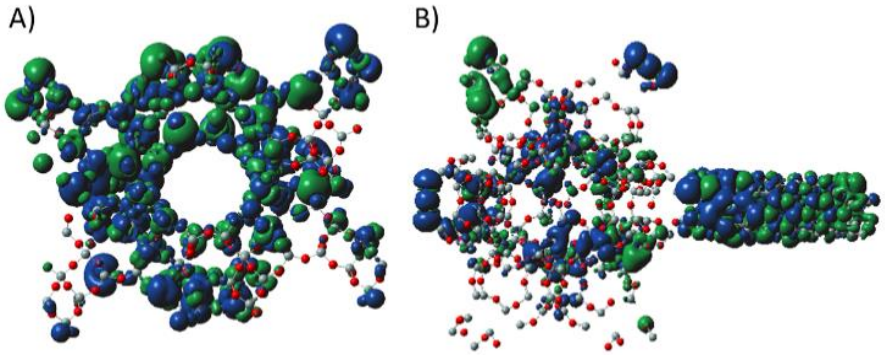

Figure 3: Spin-density map of the compounds (the isosurface contour value is 0.0004 a.u). A) zeolite, B) zeolite with carbon nanotube

When the carbon nanotube was added to the CP-ZEO electrode, part of the spin density of the zeolite was transferred to the carbon nanotube (a decrease in the spin density of the zeolite was observed). Thus, it was possible to notice that there was a transfer of electrons from the zeolite to the carbon nanotube, which can explain another factor that influences the gain in the electrochemical response that was observed in the CP-ZEO-CNT electrode.

Due to the results obtained during this study, it was decided to follow the voltammetric studies with the carbon paste composed of 30% graphite powder, 20% mineral oil, 30% ZEO-HY, and 20%CNT.

Scanning electron microscopy studies. Scanning electromicrographs of fMWCNT (Figure 4A), ZEO-HY (Figure 4B), and CP-ZEO-CNT (Figure 4C/D) were performed in order to have an understanding of how the materials that make up the carbon paste were arranged after the homogenization process.

It was possible to observe that the interaction that occurs between the two modifiers used is superficial, that is, the ZEO-HY adheres to the surface of the fMWCNT. In addition to also being able to observe the lumpy characteristic of the zeolite material, characterized by the porosity of the material and the expected superficial characteristic of the fMWCNT [55, 56].

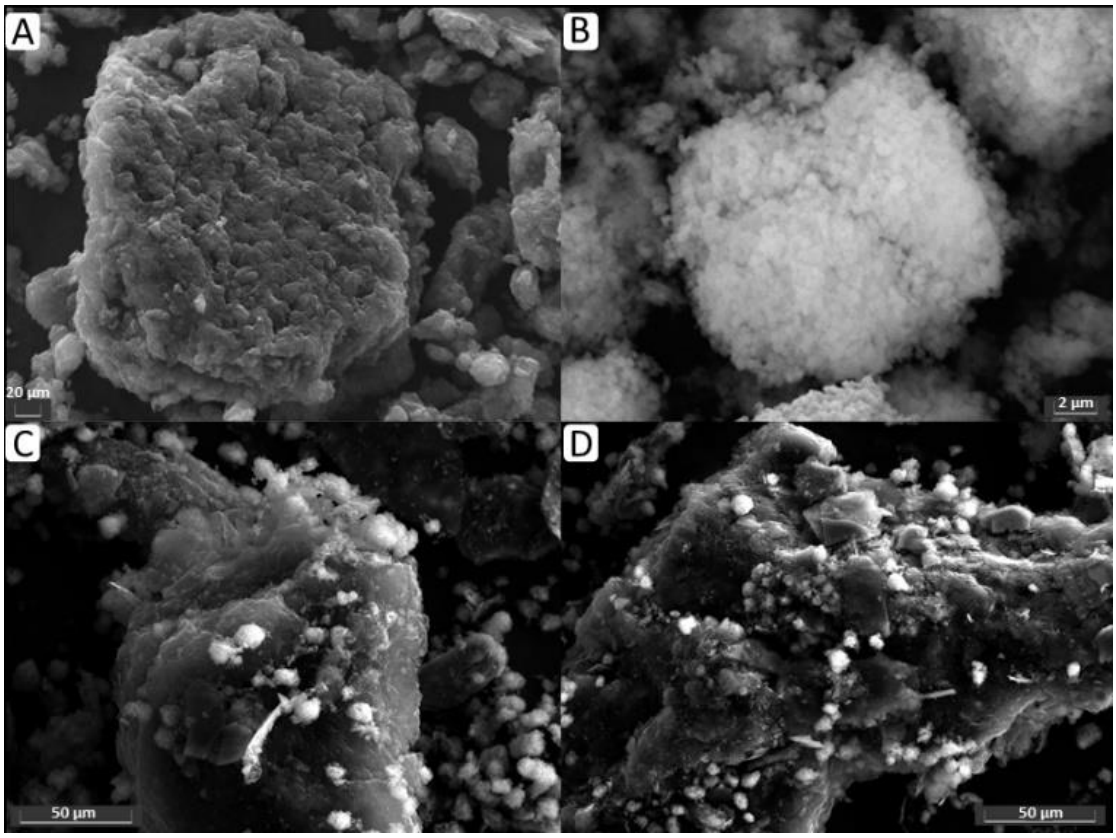

Figure 4: Electromicrographs of A) fMWCNT, magnitude of 531x, B) ZEO-HY, magnitude of 9.76 kx, C) CP-ZEO-CNT, magnitude of 2.14 kx, D) CP-ZEO-CNT, magnitude of 1.59 kx.

Fourier transform infrared spectroscopy studies. Vibrational spectroscopy in the infrared region was used as a complementary technique in the characterization of the sensors. In FTIR studies (Figure 5), the expected bands according to the literature were visualized [56 – 60].

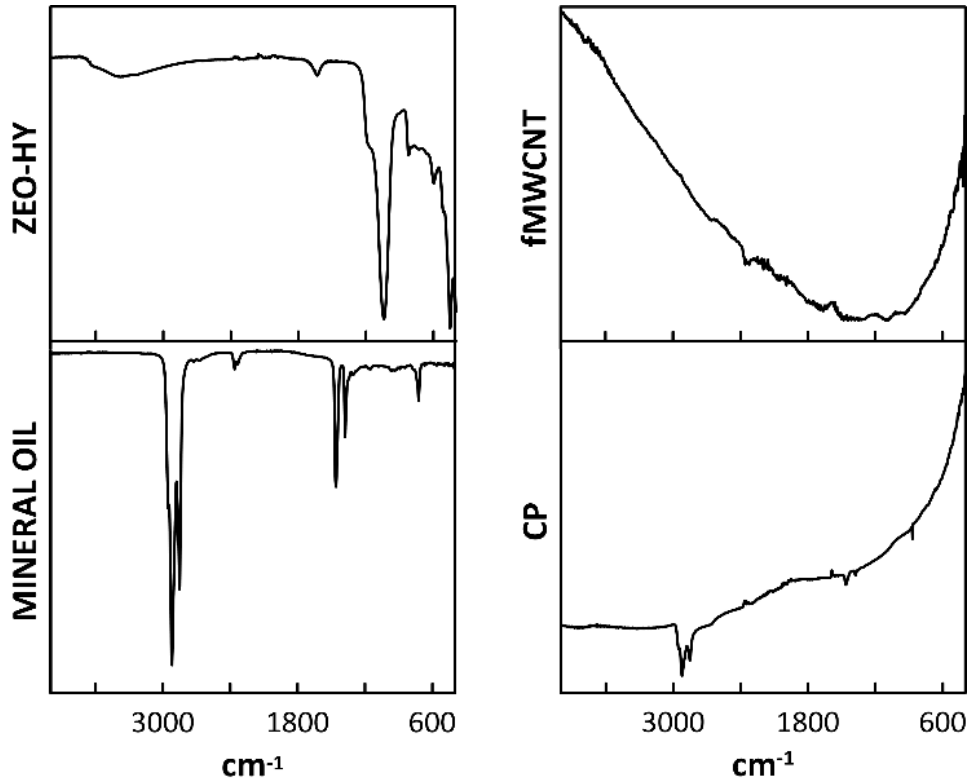

Figure 5: FTIR spectra of ZEO-HY, fMWCNT, mineral oil, and CP.

In the spectrum resulting from the ZEO-HY analyses (Figure 5), bands around 1630 cm^{-1} referring to water molecules present in the material can be seen. Bands related to the Y-type of the zeolite formation were observed around 526, 620, 834, and 950 cm^{-1}. The hydroxyl groups Si–OH, Si–OH–Al, and OH were responsible for the bands around 3410 cm^{-1}. At about 574 cm^{-1}, the double-ring external linkage band was observed. Symmetrical and asymmetrical stretching vibrations referring to the internal TO4 structure (T=Si, Al) appear at around 982 cm^{-1}, while at around 1146 cm^{-1} it was possible to observe asymmetric vibrations of the external TO4 structure. As for the external double-ring bond associated with the FAU structure of ZEO-HY, a band was observed at around 1389 cm^{-1} [59].

In the spectrum resulting from the fMWCNT analysis (Figure 5), it was expected to find bands around 1617 and 1645 cm^{-1}, referring to the carboxylate and carboxylic acid groups, respectively, resulting from the functionalization performed on the multiwalled carbon nanotubes [60]. The results were satisfactory.

The characteristic bands of the spectrum referring to the mineral oil (Figure 5) were observed at around 2922.15, 1457.79, and 722.90 cm^{-1} referring to CH_3 and CH_2 symmetric and asymmetric stretches, CH_3 and CH_2 bending vibrations and $(CH2)_4$ rock vibrations, respectively [57, 61]. In the CP, the spectral behavior of the mineral oil can still be observed, showing its influence on the response, even if at a lower intensity (Figure 5).

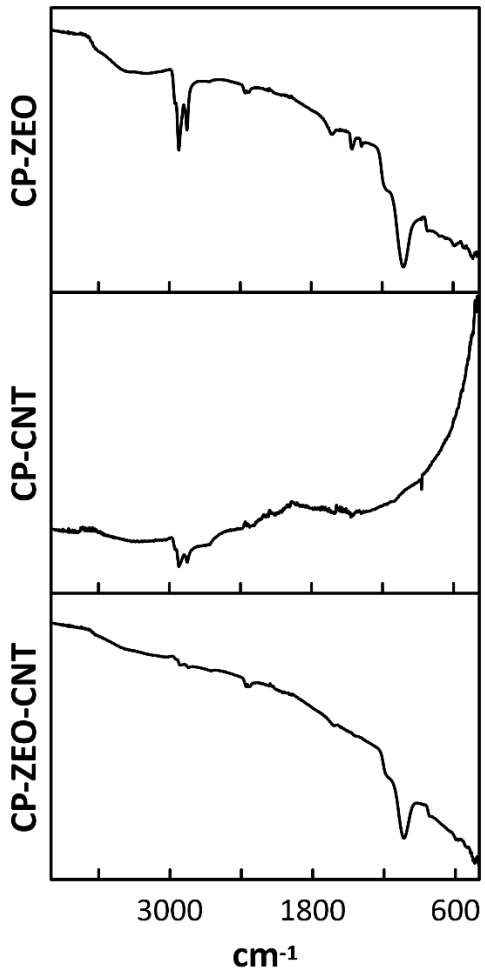

Figure 6: FTIR spectra of CP-ZEO, CP-CNT and CP-ZEO-CNT.

When the ZEO-HY was added to the CP system (Figure 6), that is, when we have the CP-ZEO, the bands referring to the zeolite structure, which have already been mentioned, can still be seen, and the presence of the band referring to the mineral oil spectrum was still present with considerable intensity. In the CP-CNT system (Figure

6), that is, with the addition of fMWCNT, a greater decrease in the bands referring to mineral oil can be seen.

Finally, in the CP-ZEO-CNT system used for the development of this work, it was possible to notice that when the components were all together, the decrease of the bands referring to the mineral oil was much less intense, and the characteristic behavior of the zeolitic material remains (Figure 6). Speculating, this fact of the decrease in the contribution of mineral oil in the system can perhaps be directly linked with the resistivity (next on calculated) presented by the sensor.

Electrochemical studies. The surface of the three different electrodes (only CP, CP-ZEO, and CP-ZEO-CNT) was investigated using electrochemical impedance spectroscopy (EIS). Figure 7 illustrates the Nyquist plots (−Z″ vs. Z′) using 1.0 x10^{-3} mol L^{-1} potassium ferri/ferrocyanide solution in 0.1 mol L^{-1} KCl. The alteration of the charge transfer resistance (Rct), corresponding to the diameter of the semicircle, caused by each step of modification of the electrode surface was investigated, as well as the carbon paste without modification (only CP) [62].

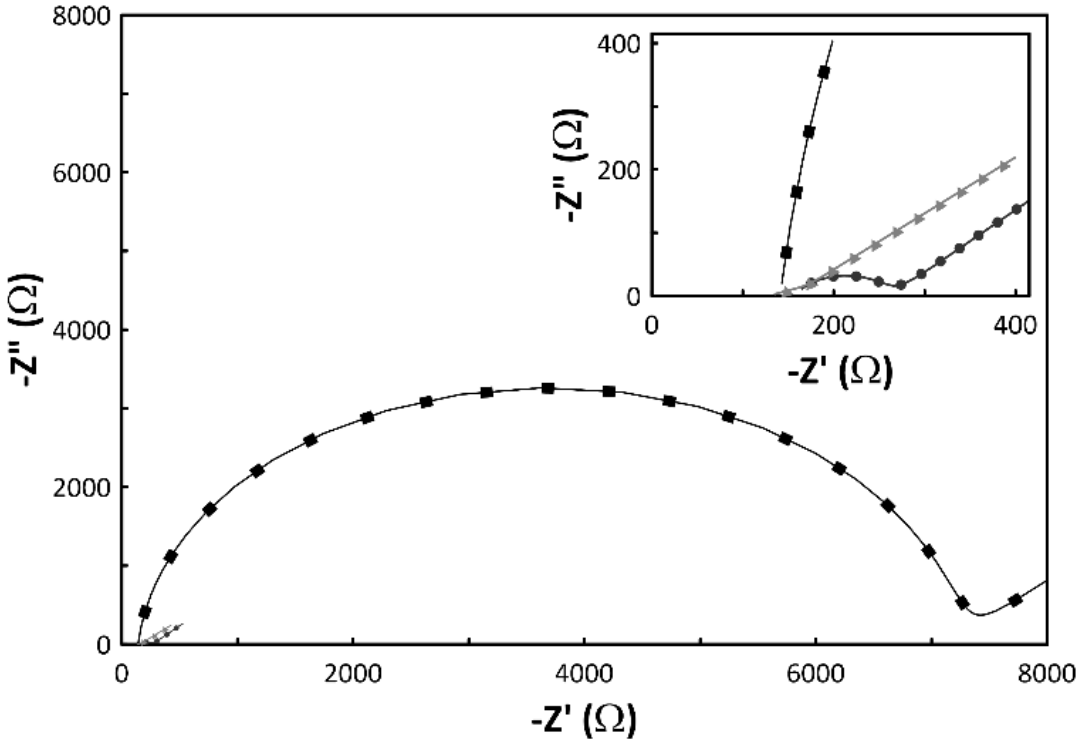

Figure 7: Impedance spectra using a 1.0 x 10^{-3} mol L^{-1} ferri/potassium ferrocyanide stock solution in 0.1 mol L-1 KCl for different electrodes: (■)CP, (●) CP- ZEO, (▲) CP-ZEO-CNT. Frequency range: 0.1-100,000 Hz (10 data points), amplitude: 0.01 V.

Before the modification, the Rct of the CP was around 7063 Ω. The addition of zeolite to the electrode (CP-ZEO) decreased the resistance (Rct = 109 Ω), attributed to the cation exchange properties of the zeolite [63]. The resistance slightly decreased with the addition of CNTs to the sensor (CP-ZEO-CNT), Rct = 48 Ω. This effect was attributed to the excellent conduction of CNTs, acting as a facilitator in the electron transfer process [64]. In this way, the CP-ZEO-CNT electrode proved to be adequate for the following voltammetric experiments.

The cyclic voltammograms of the CP-ZEO-CNT electrode in 1.0 x 10^{-3} mol L^{-1} solution containing 0.1 mol L^{-1} phosphate solution in different pH values (from 5.5 to 7.5) were performed because of the ease of preparation of phosphate solution. In all these conditions, the analyte showed oxidation and reduction peaks in the potential window of -0.2 to 0.6 V with a scan rate of 50 mV s^{-1} (not shown here). As a result, it was observed that at pH 5.5, 7.0, and 7.5 the results were not very satisfactory due to the lower current peaks, as well as a higher work potential in certain cases. For pH 6.0 and pH 6.5, a better response was observed, with peak currents greater than the other studied pH. According to Li *et al*., 2015 [65], at pH values between 3 and 7, HQ appears in its non-dissociated form, and at pH values greater than 7, its auto-oxidation happens instantly, and mono and dissociated anions may appear. This relationship between the dissociation pH of HQ and the way it appears in a solution can be seen in electrochemical experiments of pH values of the reaction medium.

At pH values of 7.0 and 7.5, the oxidation current was not as intense as at pH values of 6.0 and 6.5. This fact may be directly linked to the concentration of HQ species not yet oxidized, that is, the fact that at these higher pH values, possibly a good part of the HQ molecules had already undergone auto-oxidation.

At pH 5.5, it was noticed that even being within the HQ non-dissociation range, the result was not as satisfactory as the other pH 6.0 and 6.5. This fact may be related in some way to the point of zero charge (PZC) pH value of the zeolite used (pH PZC = 4.56). When the

supporting electrolyte has a pH value higher than the pH value of the PZC of the material studied, in this case, ZEO-HY, its surface will be negatively charged. Otherwise, that is, if the pH of the supporting electrolyte is lower than the pH of the PZC, the material will have a positive surface charge. Therefore, inferring that at pH 6.0 and 6.5 the zeolite surface is more negatively charged than at pH 5.5, perhaps one can expect greater facilitation in the cation exchange of the developed sensor.

The oxidation current values of the voltammograms of the studies carried out at pH 6.0 and pH 6.5 were very close. The current response of pH 6.0 was 1.04 times greater than that of pH 6.5. Therefore, the lowest value of work potential obtained was used as a criterion for choosing the pH of the reaction medium. When comparing the responses of pH 6.0 with pH 6.5, a work potential 1.07 times greater was observed. Therefore, we chose to work with a 0.1 mol L^{-1} phosphate buffer solution at pH 6.5 for the development of this work.

Figure 8 shows the variation of anodic and cathodic currents with a scan rate from 10 to 100 mVs^{-1}, using a 1.0 x 10^{-3} mol L^{-1} HQ solution in 0.1 mol L^{-1} phosphate buffer, pH 6.5. An increase in the anodic and cathodic currents occurred, as well as the peak potentials shifted toward more positive and negative values for oxidation and reduction processes, respectively. According to the linear variations of cathodic and anodic peak currents with the square root of the scan rate, there is an indication that the mass transport of HQ to the electrode surface is controlled by diffusion [66, 67].

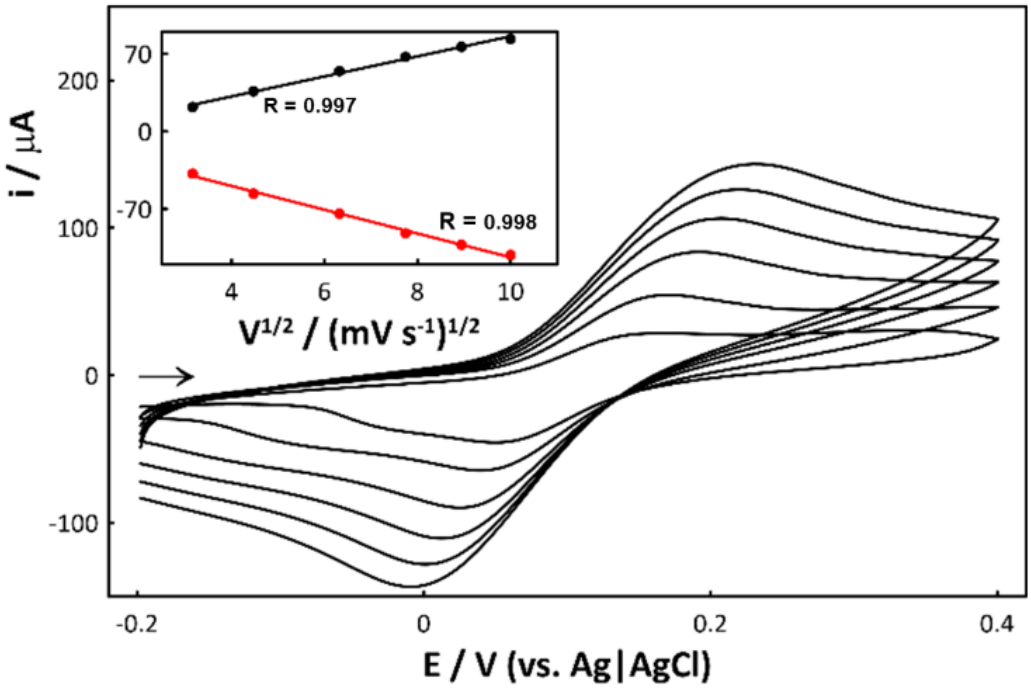

Figure 8: Cyclic voltammograms of a solution of 1.0 x 10^{-3} mol L^{-1} HQ in 0.1 mol L^{-1} phosphate buffer, pH 6.5, at different scanning speeds (10 – 100 mV s^{-1}). The detail shows the linear relationships between the anode and cathode currents with the square root of the scan rate.

In order to evaluate the stability of the modified working electrode, a CP-ZEO-CNT sensor was constructed and readings were taken on days 0, 3, 6, and 12. The RSD values of the oxidation current response were calculated at 0.91% (3 days), 1.99 % (6 days) and 7.66% (12 days).

Regarding the interference test performed (results not shown) in a 1:1 concentration proportion of HQ, ascorbic acid (AA), and citric acid (CA), the peak current response of HQ was 3.9 and 2.4 times greater than the AA and CA peak current, respectively. Thus, it was considered that there was no significant contribution of both compounds in the peak current response when the determination of hydroquinone was performed. Moreover, both AA and CA are excipients and are not in the same concentration as HQ in pharmaceutical creams.

Amperometry-FIA studies. To establish the best conditions for amperometric flow injection analysis of HQ, the influence of some parameters such as working potential (0.0 – 0.3 V *vs*. Ag/AgCl), flow rate (1.72 – 4.69 mL min^{-1}) and injection volume (15 – 130 µL) were evaluated in phosphate buffer 0.1 mol L^{-1}, pH 6.5. The main parameters for the determination of HQ have been optimized. The most favorable values were 0.1 V (*vs*. Ag/AgCl) for the working electrode, 4.69 mL min^{-1} for flow rate, and 65 µL for injection volume, considering the best relation between the current signal and sample rate. These optimized values were fixed for all measurements done during this work. Increasing concentrations of HQ in phosphate buffer 0.1 mol L^{-1}, pH 6.5 were added. The linearity between the anodic currents and the HQ concentrations was found in a concentration range from 1.0 x 10^{-6} to 1.0 x 10^{-3} mol L^{-1} (Figure 9).

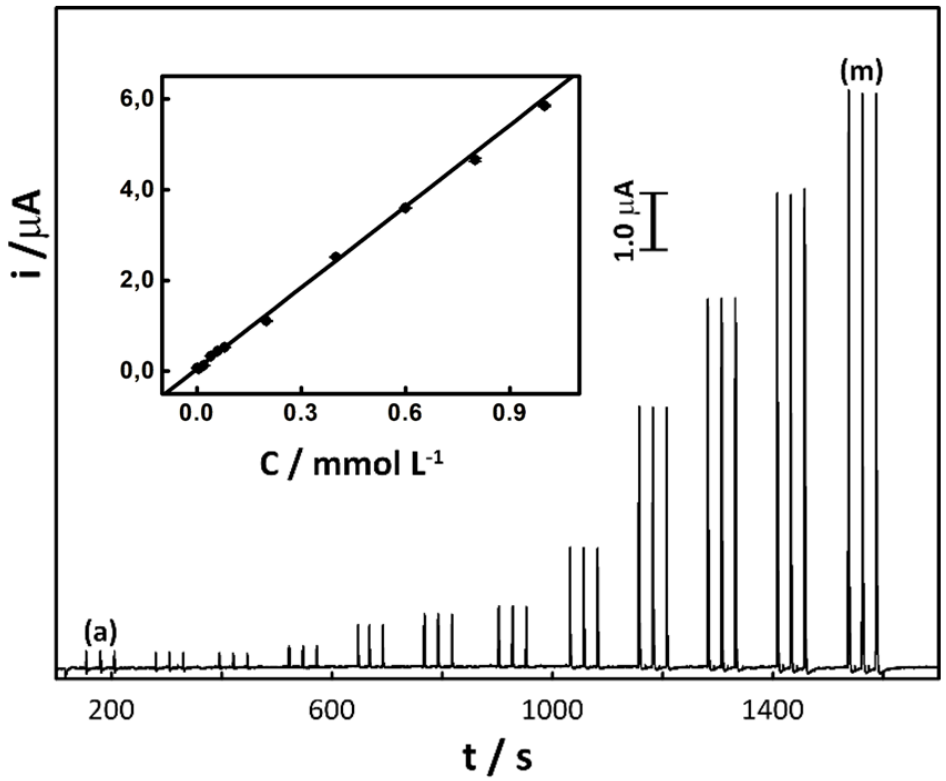

Figure 9: Amperometric responses of the CP-ZEO-CNT electrode to increasing concentrations of HQ in phosphate buffer 0.1 mol L^{-1}, pH 6.5: (a) 1.0; (b) 2.0; (c) 6.0 x 10^{-6}, (d) 2.0; (e) 4.0; (f) 6.0; (g) 8.0 x 10^{-5}, (h) 2.0; (i) 4.0; (j) 6.0; (k) 8.0; (l) 1.0 x 10^{-3}

mol L^{-1}. Working potential: 0.1 V, injection volume: 65 µL, and flow rate: 4.69 mL min^{-1}.

A linear regression equation of $i = 4.87 \times 10^{-8} + 0.00597\ C_{HQ}$ was obtained, with R = 0.997. A limit of detection (LD) of 2.69×10^{-7} mol L^{-1} (three times the standard deviation of the blank/curve slope) and a limit of quantification (LQ) of 8.99×10^{-7} mol L^{-1} (ten times the standard deviation of the blank/curve slope) [68] were found. As for the sampling rate, a value of 100 injections per hour was obtained.

Some works on modified sensors for HQ determination can be found in the literature. Mendonça *et al*., 2021 [69] used a photoelectrochemical flow system applying TiO_2 impregnated with Au nanoparticles, obtaining a LOD of 3.38×10^{-8} mol L^{-1}. Rahemi *et al*., 2020 [70] used TiO_2 impregnated with horseradish peroxidase to eliminate the need for H_2O_2 in the system, in their results the calculated LOD was 2.00 and 3.30×10^{-7} mol L^{-1}, for low and high HQ concentrations respectively. Therefore, the result found in this work (2.69×10^{-7} mol L^{-1}) was considered satisfactory.

For the repeatability studies, signals were recorded after 15 injections of 6.0×10^{-5} mol L^{-1} HQ in 0.1 mol L^{-1} phosphate buffer, pH 6.5, on the CP-ZEO-CNT. It was possible to calculate a relative standard deviation (RSD) of 1.44%.

For the HQ quantification step in commercial samples, analyses of pharmaceutical creams **S1** and **S2** were performed in 0.1 mol L^{-1} phosphate buffer, pH 6.5, on the CP-ZEO-CNT electrode (Figure 10).

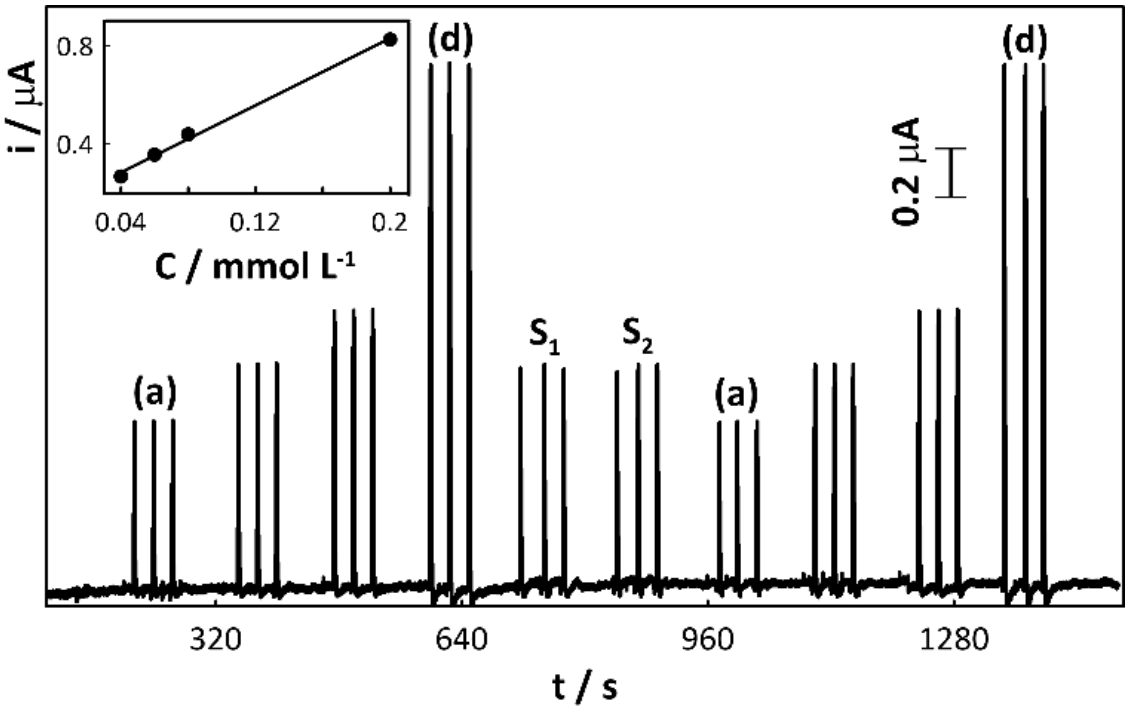

Figure 10: Analysis of commercial samples S1 and S2 in 0.1 mol L^{-1} phosphate buffer, pH 6.5, on the CP -ZEO-CNT electrode. Detail: analytical curve after consecutive injections of HQ standard solutions (a) 4.0; (b) 6.0; (c) 8.0 x 10^{-5}; (d) 2.0 x 10^{-4} mol L^{-1}. Working potential: 0.1 V, injection volume: 65 µL, and flow rate: 4.69 mL min^{-1}.

To compare the results obtained with the proposed method, the samples were also analyzed by HPLC. The results are presented in Table 2.

Table 2: Results obtained for HQ analysis in commercial samples using the proposed amperometric method. Nominal value: 40 mg/g.

Sample	**Composition**	**Amperometry-FIA ± S.D. (mg/g)**	**HPLC ± S.D. (mg/g)**
S1	Hydroquinone and excipient q.s.p.*	39.9 ± 0.5	35.60 ± 0.04
S2	Hydroquinone and excipient q.s.p.*	41 ± 1.5	37.7 ± 0.1

*Propylparaben, methylparaben, sodium metabisulfite, disodium edetate dihydrate, ascorbic acid, benzophenone, octinoxate, octisalate, citric acid, isopropyl palmitate, propylene glycol, cetostearyl alcohol, sodium lauryl sulfate, sodium myristyl sulfate, purified water.

The proposed method presented similar results to those obtained by HPLC. Considering the T-Student test, both methods did not present a significant difference at a confidence level of 95% (n=2), with p-value < α (0.05). Furthermore, the results were consistent with legislation, with a concentration of no more than 4%. We concluded that the proposed sensor is suitable for the determination of HQ in commercial samples and can be used as an alternative method for HQ determination.

Conclusions

With the voltammetric studies carried out in this work, it was possible to find that the best performance of the electrochemical sensor was with the composition of 20% mineral oil, 30% graphite powder, 30% HY zeolite, and 20% CNT. Moreover, it was also possible to understand the contribution of the zeolitic material as a modifier of the developed amperometric sensor, by calculating the areas of the electrodes.

Theoretical calculations showed that there was no chemical bond in the interaction between the modifiers and the analyte, and the equilibrium distances between the zeolite and the nanotube and the zeolite and the analyte could be calculated at 3.0 and 3.5 A, respectively. Furthermore, it was possible to perform the spin density calculation, essential data to elucidate the contribution of fMWCNT in the improvement of the peak current of the cyclic voltammogram of the developed amperometric sensor.

Regarding the characterization studies carried out in this work (MEV, FTIR, EIS, scan rate studies), it was possible to reach satisfactory and consistent results with the literature, as well as to verify the interaction between ZEO-HY and fMWCNT.

The amperometric sensor presented to be suitable with precise results and short analysis time (100 injections per hour) during flow injection analysis of HQ in pharmaceutical samples.

To confirm its reliability, hydroquinone quantification studies were carried out in the same samples by a comparative chromatographic method.

Conflicts of interest

There are no conflicts to declare.

Acknowledgments

This work was supported by the FAPEMIG, CNPq, CAPES (Finance code 001), EMBRAPA-CAFÉ (Notice 20/2018 and code 145), FAPESP and FINEP. We would like to thank the Laboratory of Electron Microscopy and Ultrastructural Analysis (LME) and the Multiuser Laboratory of Instrumental Analysis (LABMAI) of the Federal University of Lavras (UFLA).

Notes and references

1 V. Gautam, K.P. Singh and V.L. Yadav, *Analytical and Bioanalytical Chemistry*, 2018, **410**, 2173–2181;

2 R.F. Aglan, M.M. Hamed and H.M. Saleh, *Journal of Analytical Science and Technology*, 2019, **10**, 7;

3 A. Afkhami, H. Khoshsafar, H. Bagheri and T. Madrakian, *Sensors and Actuators B: Chemical*, 2014, **203**, 909-918;

4 H. Beitollahi, S. G. Ivari and M. Torkzadeh-Mahani, *Biosensors and Bioelectronics*, 2018, **110**, 97-102;

5 W. Sun, R. Gao, and K. Jiao, *The Journal of Physical Chemistry B*, 2007, **111 (17)**, 4560-4567;

6 K. Kalcher, J. M. Kauffmann, J. Wang, I. Svancara, K. Vytras, C. Neuhold and Z. Yang, *Electroanalysis*, 1995, **7 (1)**, 5-22;

7 I. Švancara, K. Vytřas, K. Kalcher, A. Walcarius and J. Wang, *Electroanalysis*, 2009, **21**, 7-28;

8 I. Švancara, K. Vytřas, J. Barek and J. Zima, *Critical Reviews in Analytical Chemistry*, 2001, **31 (4)**, 311-345;

9 N. Baig, M. Sajid and T. A. Saleh, *TrAC Trends in Analytical Chemistry*, 2019, **111**, 47-61;

10 S. S. M. Manickaraj, S. Pandiyarajan, A. H. Liao, A. R. P. Selvam, S. T. Huang, J. R. Vimala, K. Y. Lee and H. C. Chuang, *Chemosphere*, 2023, **328**, 138534;

11 A. Jeyaraman, B. Karuppaiah, S. M. Chen and Y. C. Huang, *Colloids and Surfaces A: Physicochemical and Engineering Aspects*, 2023, **666**, 131278;

12 S. Tajik, H. Beitollahi, F. G. Nejad, I. Sheikhshoaie, A. S. Nugraha, H. W. Jang, Y. Yamauchi and M. Shokouhimehr, *Journal of Materials Chemistry A*, 2021, **9**, 8195-8220;

13 K. Zinoubi, A. Chrouda, R. Soltane, Y. O. Al-Ghamdi, S. G. Almalki, G. Osman, H. Barhoumi, and N. J. Renault, *Electroanalysis*, 2020, **33(1)**, 136–145;

14 C. Liu, X. Chen, B. Zongab and S. Mao, *Journal of Materials Chemistry A*, 2019, **7**, 6616-6630;

15 H. Bhardwaj, G. Sumana and C. A. Marquette, *Food Chemistry*, 2020, **307**, 125530;

16 H. Nasrollahpour, B. Khalilzadeh, R. Rahbarghazi, N. Erk, M. R. Rashidi and A. Naseri, *Cancer Nano*, 2023, **14**, 45;

17 Z. Chen, C. Wu, Y. Yuan, Z. Xie, T. Li, H. Huang, S. Li, J. Deng, H. Lin, Z. Shi, C. Li, Y. Hao, Y. Tang, Y. You, O. A. Al-Hartomy, S. Wageh, A. G. Al-Sehemi, R. Lu, L. Zhang, X. Lin, Y. He, G. Zhao, D. Li and H. Zhang, *Journal of Nanobiotechnology*, 2023, **21**, 141;

18 D. K. Han, C. A. Li, S. H. Song, K. Cho, J. S. Choi, S. E. Son and G. H. Seong, *Journal of Analytical Science and Technology*, 2023, **14**, 9;

19 R. Kour, S. Arya, S. J. Young, V. Gupta, P. Bandhoria and A. Khosla, *Journal of The Electrochemical Society*, 2020, **167 (3)**, 037555;

20 L. Chen, J. Jansson, M. Skoglundh, and H. Grönbeck, *The Journal of Physical Chemistry C*, 2016, **120 (51)**, 29182–29189;

21 X. Chen, B. Shen, H. Sun and G. Zhan, *Microporous and Mesoporous Materials*, 2018, **261**, 227-236;

22 K. Fendrych, R. Porada, B. Baś, *Journal of Hazardous Materials*, 2023, **448**, 130953;

23 R. Porada, N. Wenninger, C. Bernhart, K. Fendrych, J. Kochana, B. Baś, K. Kalcher and A. Ortner, *Microchemical Journal*, 2023, **187**, 108455,

24 Y. Jiang, E. Yifeng P. Wei, J. Wang, P. Chen, L. Wang, T. F. Krenzel, K. Qian, Kun and T. Xiyuan, *RSC Advances*, 2023, **13 (5)**, 3364-3370;

25 A. H. Miller, H. T. T. Nguyen, J. G. Nery and A. J. Fielding, *Journal of Applied Electrochemistry*, 2023, **53**, 1715–1725;

26 R. Tan, P. Jiang, C. Pan, J. Pan, N. Gao, Z.i Cai, F. Wu, G. Chang, A. Xie and Y.He, *Microchimica Acta*, 2023, **190**, 30;

27 S. Y. Al-Nami, A. Hameed, O. A. Azher, N. A. Alamrani, E. Aljuhani, H. M. Abumelha and N. M. El-Metwaly, *Arabian Journal for Science and Engineering*, 2023, **48**, 539–549;

28 J. Feng, X. Liang, Z. Ma, *Biosensors and Bioelectronics*, 2021, **175**, 112853;

29 W. Zhang, C. Wang, M. Peng, G. Ren, K. Li and Y. Lin, *Chemical Communications*, 2020, **56 (47)**, 6436-6439;

30 S. Lv, K. Zhang, L. Zhu, D. Tang, R. Niessner, and D. Knopp, *Analytical Chemistry*, 2019, **91 (18)**, 12055–12062;

31 Y. Chen, Y. Zhao, and Y. Wang, *International Journal of Nanomedicine*, 2020, **15**, 6619-6629;

32 W. Ma, Q. Jiang, P. Yu, L. Yang and L. Mao, *Analytical Chemistry*, 2013, **85 (15)**, 7550–7557;

33 ANVISA. AGENCIA NACIONAL DE VIGILÂNCIA SANITÁRIA. Resolução da diretoria colegiada- RDC nº 529, de 04 de agosto de 2021;

34 U.S.A. Food & Drug Administration. Department of Health and Human Services. Hydroquinone: Nomination Profile. 21 May 2009;

35 U.S.A. Food & Drug Administration. Department of Health and human services. 21 CFR Part 300. August 29, 2006;

36 U.S.A. Food & Drug Administration. Department of Health and Human Services 21 CFR Part 310. April 1, 2015;

37 E. ALVES, presented in part at Introductory Course to Scanning Electron Microscopy and X-ray Microanalysis, Lavras, MG-Brazil, August, 2022;

38 R. R. Cunha, T. F. Tormin, E. M. Richter, R. A. A. Munoz. *Química Nova*, 2013, **36 (5)**, 663-668;

39 G. Bergerhoff, W.H. Baur, W. Nowacki, *Journal of Mineralogy and Geochemistry*, 1958, **198**, 193-200;

40 Database of Zeolite Structures, https://asia.iza-structure.org/IZA-SC/framework.php?STC=FAU, (accessed May 2023);

41 TubeGen Online, https://turin.nss.udel.edu/research/tubegenonline.html, (accessed May 2023);

42 R, M.J. Frisch, G.W. Trucks, H.B. Schlegel, G.E. Scuseria, M.A. Robb, J.R. Cheeseman, G. Scalmani, V. Barone, B. Mennucci, G.A. Petersson, H. Nakatsuji, M. Caricato, X. Li, H.P. Hratchian, A.F. Izmaylov, J. Bloino, G. Zheng, J.L. Sonnenberg, M. Hada, M. Ehara, K. Toyota, R. Fukuda, J. Hasegawa, M. Ishida, T. Nakajima, Y. Honda, O. Kitao, H. Nakai, T. Vreven, J.A. Montgomery Jr., J.E. Peralta, F. Ogliaro, M. Bearpark, J.J. Heyd, E. Brothers, K.N. Kudin, V.N. Staroverov, R. Kobayashi, J. Normand, K. Raghavachari, A. Rendell, J.C. Burant, S.S. Iyengar, J. Tomasi, M. Cossi, N. Rega, J.M. Millam, M. Klene, J.E. Knox, J.B. Cross, V. Bakken, C. Adamo, J. Jaramillo, R. Gomperts, R.E. Stratmann, O. Yazyev, A.J. Austin, R. Cammi, C. Pomelli, J.W. Ochterski, R.L. Martin, K. Morokuma, V.G. Zakrzewski, G.A. Voth, P. Salvador, J.J. Dannenberg, S. Dapprich, A.D. Daniels. Farkas, J.B. Foresman, J. V Ortiz, J. Cioslowski and D.J. Fox, Gaussian 09 software;

43 F. Cortesguzman and R.F.W. Bader, Coordination Chemistry Reviews, 2005, **249**, 633–662;

44 C.F. Matta, J. Hernández-Trujillo, T.-H. Tang and R.F.W. Bader, *Chemistry*, 2003, **9**, 1940–51;

45 T.A. Keith, AIM ALL. TK Gristmill Software, Overland Park KS., 2010;

46 J. Rouabeh, L. M'barki, A. Hammami, I. Jallouli and A. Driss, Heliyon, 2019, **5**, e01159;

47 F. S. Felix, D. Daniel, J. R. Matos, C. L. do Lago and L. Angnes, *Analytica Chimica Acta*, 2016, **928**, 32-38;

48 T. Wang, Y. Chu, X. Li, Y. Liu, H. Luo, D. Zhou, F. Deng, X. Song, G. Lu, and J. Yu, Journal of the American Chemical Society, 2023, **145**, 9, 5342–5352;

49 G. T.M. Kadja, N. T.U. Culsum, S. Mardiana, N. J. Azhari, A. T.N. Fajar, Irkham, *Materials Today Communications*, 2022, **33**, 104331;

50 K. Conley and A. J. Karttunen, *The Journal of Physical Chemistry C*, 2022, 126, **40**, 17266–17274;

51 A. M. Ashrafi and L. Richtera, *Molecules*, 2019, **24(12)**, 2215;

52 J.F. Rusling and K. Ito. *Analytica Chimica Acta*, 1991, **252**, 23-27;

53 D. Esteban-Gómez, A. de Blas, T. Rodríguez-Blas, L. Helm, C. Platas-Iglesias, *ChemPhysChem*, 2012, **13 (16)**, 3640–50;

54 B. T. L. Pereira, E. F. Silva, M. A. Gonçalves, D. T. Mancini, T. C. Ramalho, *Journal of Chemistry*, 2017, **2017**, 8102812;

55 L. B. Bortolatto, R. A. A. B. Santa, J. C. Moreira, D. B. Machado, M. A. P. M. Martins, M. A. Fiori, N. C. Kuhnen and H. G. Riella, *Microporous and Mesoporous Materials*, 2017, **248**, 214-221;

56 B. C. Janegitz, L. C. S. Figueiredo-Filho, L. H. Marcolino-Junior, S. P.N. Souza, E. R. Pereira-Filho and O. Fatibello-Filho, *Journal of Electroanalytical Chemistry*, 2011, **660(1)**, 209-216;

57 I. A. Hadialnashia, I. I. Mohamed, M. Almelian and M. A. Omran, *Journal of Telecommunication*, 2018, **10**, 81-85;

58 T. P. Teng, S. C. Chang, Z. Y. Chen, C. K. Huang, S. F. Tseng and C. Rong Yang, *The International Journal of Advanced Manufacturing Technology*, 2019, **104**, 2751–2760;

59 A. Mekki, A. Benmaati, A. Mokhtar, M. Hachemaoui, F. Zaoui, H. H. Zahmani, M. Sassi, S. Hacini and B. Boukoussa, *Journal of Inorganic and Organometallic Polymers and Materials*, 2020, **30**, 2323–2334;

60 B. C. Janegitz, L. H. Marcolino-Junior, S. P. Campana-Filho, R. C. Faria and O. Fatibello-Filho, *Sensors and Actuators B: Chemical*, 2009, **142**, 260–266;

61 LibreTexts™ Chemistry, https://chem.libretexts.org/Ancillary_Materials/Laboratory_Experiments/Wet_Lab_Experiments/Organic_Chemistry_Labs/Misc/IR_Spectra_of_Selected_Compounds, (accessed May 2023);

62 D. M. Guldi, G. M. A. Rahman, F. Zerbetto and M. Prato, *Accounts of Chemical Research*, 2005, **38(11)**, 871–878;

63 S. Cotchim, K. Promsuwan, M. Dueramae, S. Duerama, A. Dueraning, P. Thavarungkul, P. Kanatharana and W. Limbut, *Journal of The Electrochemical Society*, 2020, **167(15)**, 155528;

64 K. Ahmad, P. Kumara and S. M. Mobin, *Nanoscale Advances*, 2020, **2**, 502-511;

65 C. Li, L. Li, L. Sun, Z. Pei, J. Xie and S. Zhang, *Carbon*, 2015, **89**, 74-81;

66 D.V. RIBEIRO, C.A.C. SOUZA and J.C.C. ABRANTES, *IBRACON Structures and Materials Journal*, 2015, **8**, 4;

67 D. Thatikayala, M.T. Noori, B. Min, *Materials Today Chemistry*, 2023, **29**, 101412;

68 BRASIL. Agência Nacional de Vigilância Sanitária. Resolução RE nº 899, de 29 de maio de 2003;

69 C. D. Mendonça, S. U. Khan, V. Rahemi, S. W. Verbruggen, S. A.S. Machado, K. De Wael, *Electrochimica Acta*, 2021, **389**, 138734;

70 V. Rahemi, S. Trashin, Z. Hafideddine, S. Van Doorslaer, V. Meynen, L. Gorton, and K. De Wael, *Analytical Chemistry*, 2020, **92(5)**, 3643–3649.